Allpass-Based Analysis-Synthesis Filter-Banks: Design and Application

Von der Fakultät für Elektrotechnik und Informationstechnik
der Rheinisch-Westfälischen Technischen Hochschule Aachen
zur Erlangung des akademischen Grades eines
Doktors der Ingenieurwissenschaften genehmigte Dissertation

vorgelegt von

Diplom-Ingenieur

Heinrich Wilhelm Löllmann

aus Osnabrück

Berichter: Universitätsprofessor Dr.-Ing. Peter Vary
Universitätsprofessor Dr.-Ing. Ulrich Heute

Tag der mündlichen Prüfung: 1. Juni 2011

AACHENER BEITRÄGE ZU DIGITALEN NACHRICHTENSYSTEMEN

Herausgeber:

Prof. Dr.-Ing. Peter Vary
Institut für Nachrichtengeräte und Datenverarbeitung
Rheinisch-Westfälische Technische Hochschule Aachen
Muffeter Weg 3a
52074 Aachen
Tel.: 0241-80 26 956
Fax.: 0241-80 22 186

Bibliografische Information der Deutschen Bibliothek
Die Deutsche Bibliothek verzeichnet diese Publikation in der Deutschen Nationalbibliografie; detaillierte bibliografische Daten sind im Internet über http://dnb.ddb.de abrufbar

1. Auflage Aachen:
Wissenschaftsverlag Mainz in Aachen
(Aachener Beiträge zu digitalen Nachrichtensystemen, Band 30)
ISSN 1437-6768
ISBN 3-86130-308-6

Wissenschaftsverlag Mainz
Süsterfeldstr. 83, 52072 Aachen
Tel.: 02 41 / 2 39 48 oder 02 41 / 87 34 34
Fax: 02 41 / 87 55 77
www.Verlag-Mainz.de

Herstellung: Druckerei Mainz GmbH,
Süsterfeldstr. 83, 52072 Aachen
Tel.: 02 41 / 87 34 34; Fax: 02 41 / 87 55 77
www.Druckservice-Aachen.de

Gedruckt auf chlorfrei gebleichtem Papier

"D 82 (Diss. RWTH Aachen University, 2011)"

Acknowledgments

This PhD thesis has been written during my stay as research assistant at the *Institute of Communication Systems and Data Processing* of *RWTH Aachen University*. I would like to express my gratitude to those who contributed to the success of this work.

First of all, I would like to express my sincere gratitude to my supervisor Prof. Dr.-Ing. Peter Vary for the trustful collaboration and many helpful discussions. I highly appreciate his kindness and support. I also want to thank the co-referee Prof. Dr.-Ing. Ulrich Heute for his interest in the results of this thesis. The work of his former research group has provided a valuable impetus for this thesis.

Furthermore, I want to thank all my colleagues and permanent staff of the institute for providing a pleasant and enjoyable working environment. In particular, I am grateful to Dipl.-Ing. Bernd Geiser, Dipl.-Ing. Bastian Sauert, Dipl.-Ing. Thomas Esch, Dipl.-Ing. Magnus Schäfer, Dipl.-Ing. Christoph Nelke, Dipl.-Ing. Matthias Pawig, Dipl.-Ing. Aulis Telle and Dipl.-Ing. Birgit Schotsch for their proof-readings of parts of the manuscript as well as M. Sc. Marco Jeub for the good collaboration on the topic of speech dereverberation. I owe special thanks to Dr.-Ing. Hauke Krüger and Dr.-Ing. Christiane Antweiler for many valuable discussions and their friendship. I also want to thank Dipl.-Ing. Thomas Schlien and Andreas Welbers for their technical support as well as my former colleagues Dr.-Ing. Gerald Enzner, Dr.-Ing. Frank Mertz, Dr.-Ing. Christoph Erdmann and Dr.-Ing. Marc Adrat for the good collaboration.

Special thanks go to the students who contributed to this work. In particular, I am indebted to Dipl.-Ing. Guido Dartmann, Dipl.-Ing. Matthias Hildenbrand and Dipl.-Ing. Fabian Altenbach for their valuable contributions.

This work was accompanied by projects with Siemens, Munich and GN ReSound, Eindhoven and I want to thank our former project partners for the good collaboration.

Finally, I wish to express my deepest thanks to my family, especially my parents Gerd Heinz and Ilse Löllmann for their love and unbroken support.

Aachen, September 2011 *Heinrich Wilhelm Löllmann*

Abstract

Filter-banks are an essential component of many algorithms for digital signal processing, which are nowadays employed in a variety of ubiquitous devices. Filter-banks enable signal processing in the frequency-domain and their design has often a significant influence on the performance of a system with regard to its computational complexity, signal quality and delay. In this thesis, novel design approaches for different types of *allpass-based* analysis-synthesis filter-banks are devised. A substantial benefit of these recursive filter-banks is that they can achieve a high frequency selectivity and/or a non-uniform time-frequency resolution with a low signal delay.

One focus of this work is the design of allpass-based *quadrature-mirror filter-banks* (QMF-banks) with near-perfect reconstruction. New synthesis filter-banks are presented which consist of allpass polyphase filters. They are designed by simple analytical expressions such that the trade-off between reconstruction error and signal delay of the filter-bank can be controlled in a simple manner. The devised QMF-bank has been employed in a candidate proposal for a new ITU-T speech and audio codec and has helped to achieve a high speech and audio quality with a low signal delay.

A key issue in the design of allpass-based filter-banks is to compensate non-linear phase distortions caused by the recursive analysis filter-bank. Therefore, known as well as novel *phase equalizer* designs for this purpose are presented and analyzed.

Another focus of this work is the design of *allpass transformed* analysis-synthesis filter-banks. They can achieve a non-uniform time-frequency resolution similar to that of the human auditory system, which is beneficial for speech and audio processing systems. Novel closed-form and numerical designs for the synthesis filter-bank are introduced, which aim for different design objectives. A benefit of the closed-form designs is their simplicity, while the numerical designs allow the explicit control of specific properties of the filter-bank such as signal delay, reconstruction error, bandpass characteristic of the synthesis filters etc. The new numerical designs are all stated as a convex optimization problem which can be solved rather easily.

Finally, an efficient implementation for the special case of an allpass transformed filter-bank without subsampling is derived. This system, termed as *filter-bank equalizer,* allows to perform adaptive subband filtering with a low signal delay. It is shown how this filter-bank can be used for noise reduction, speech dereverberation, or speech intelligibility improvement in noisy environments. These low delay speech enhancement systems are of particular interest for applications within cell phones, hands-free devices, or digital hearing aids.

Kurzfassung

Filterbänke sind ein essentieller Bestandteil zahlreicher Algorithmen für die digitale Signalverarbeitung, die heutzutage in einer Vielzahl von unterschiedlichen Geräten eingesetzt werden. Filterbänke ermöglichen eine Signalverarbeitung im Frequenzbereich und deren Entwurf hat oft einen entscheidenden Einfluss auf die Leistungsfähigkeit eines Systems in Bezug auf dessen Rechenkomplexität, Signalqualität und Verzögerungszeit. In dieser Arbeit werden neuartige Entwurfsverfahren für unterschiedliche Klassen von *allpass-basierten* Filterbänken entwickelt. Ein wesentlicher Vorteil dieser rekursiven Filterbänke ist, dass sie eine hohe Frequenzselektivität und/oder eine nichtgleichförmige Zeit-Frequenzauflösung mit einer gleichzeitig geringen Signallaufzeit erreichen können.

Ein Schwerpunkt dieser Arbeit bildet der Entwurf von allpass-basierten *Quadrature-Mirror-Filterbänken* (QMF-Bänken) mit fast perfekter Signalrekonstruktion. Neuartige Synthese-Filterbänke werden vorgestellt, dessen Polyphasenkomponenten aus Allpassfiltern bestehen. Diese werden mittels einfacher geschlossener Formeln entworfen, wodurch der Zielkonflikt zwischen Rekonstruktionsfehler und Signalverzögerung der Filterbank in einfacher Weise kontrolliert werden kann. Die neu vorgestellte QMF-Bank war Bestandteil eines neuen Sprach- und Audiocodecs der im Rahmen einer ITU-T Standardisierung vorgeschlagen wurde, und hat dazu beigetragen eine hohe Sprach- und Audioqualität mit einer gleichzeitig geringen Signallaufzeit zu erreichen.

Ein zentrales Problem beim Entwurf allpass-basierter Filterbänke ist die Kompensation nichtlinearer Phasenverzerrungen, die durch die rekursive Analyse-Filterbank verursacht werden. Daher werden bekannte sowie neue Ansätze zur Lösung dieses *Phasenkompensationproblems* vorgestellt und analysiert.

Ein anderer Schwerpunkt dieser Arbeit ist der Entwurf von *allpass-transformierten* Analyse-Synthese-Filterbänken. Diese können eine Frequenzauflösung erreichen, die der des menschlichen Gehörs sehr ähnelt, was von besonderem Interesse für die Sprach- und Audiosignalverarbeitung ist. Neue geschlossene sowie numerische Entwurfsverfahren für die Synthese-Filterbank werden vorgestellt, die unterschiedliche Entwurfsziele verfolgen. Ein Vorteil der geschlossenen Entwurfsverfahren ist deren Einfachheit, wohingegen die numerischen Verfahren den Vorteil bieten, dass bestimmte Eigenschaften der Filterbank, wie dessen Rekonstruktionsfehler, Signalverzögerung, Bandpasscharakteristik der Synthese-Filter etc., explizit beeinflusst werden können. Die neuen numerischen Verfahren beruhen dabei auf konvexen Optimierungsproblemen, die relativ einfach zu lösen sind.

Schließlich wird in dieser Arbeit eine besonders effiziente Realisierung für den Spezialfall einer allpass-transformierten Filterbank ohne Unterabtastung entwickelt. Dieses als *Filter-Bank Equalizer* bezeichnete System ermöglicht eine adaptive Signalfilterung mit geringer Signallaufzeit. Es wird aufgezeigt, wie dieses Verfahren für

die Störgeräuschreduktion, die Enthallung von Sprachsignalen oder die Verständlichkeitsverbesserung in gestörten Umgebungen eingesetzt werden kann. Diese Sprachverbesserungssysteme mit geringer Latenz sind für den Einsatz in Mobilfunktelefonen, Freisprecheinrichtungen oder digitalen Hörgeräten von besonderem Interesse.

Contents

Chapter 1

Introduction

DIGITAL signal processing systems have replaced successively analog systems over the past decades and can be found today in a variety of different devices such as mobile communication systems, consumer and car electronics, or hearing aids. A decisive advantage of digital signal processing is that systems can be realized which cannot or only hardly be realized by analog processing. An essential component of many algorithms for digital signal processing are filters and their concatenation as *filter-banks.* Filter-banks are mainly used for the spectral analysis of signals [Boa03, SM05], as transmultiplexers [Fli93], or to process a time-domain signal in the subband- or frequency-domain [Vai93, AZ03]. The last mentioned application thereby requires an *analysis-synthesis filter-bank* (AS FB) to obtain a reconstructed time-domain signal. For many applications, it is necessary or at least beneficial to employ a filter-bank in order to process the signal in the frequency-domain instead of the time-domain (even though both approaches are often closely related). The variety of applications for digital (analysis-synthesis) filter-banks has fostered the exploration of different variants.

Many filter-banks can be described as *modulated* filter-banks, e.g., [Var78, CR83, Glu93, Vai93, Kli99]. The analysis and synthesis filters are obtained by a real or complex modulation of a prototype filter such that the filter-bank design reduces to that of a single prototype filter. Modulated filter-banks are based, for example, on the discrete Fourier transform (DFT) or discrete cosine transform (DCT). Such a DFT or DCT filter-bank can be efficiently implemented by means of a polyphase network (PPN). Hence, this class of filter-banks is of overriding importance and a variety of filter-banks – including those treated in this work – evolve thereof.

Most modulated filter-banks belong to the class of *uniform* AS FBs. Filter-banks with a uniform time-frequency resolution are more commonly used and studied than non-uniform filter-banks. Their design is easier and they have usually a lower computational complexity than comparable non-uniform filter-banks. An advantage of *non-uniform* filter-banks is that their frequency resolution can be adapted to a specific application. For example, auditory filter-banks which mimic the non-uniform frequency resolution of the human ear are of special interest for speech and audio processing.

The signal reconstruction error is another important property of a filter-bank. An AS FB with *perfect reconstruction* (PR) provides an exact replica of the input signal, if no subband processing takes place. For many applications, such as speech and audio processing, a small reconstruction error is often tolerable. Filter-banks with *near-perfect reconstruction* (NPR) can be of interest in such cases, which permit a low reconstruction error in order to obtain more degrees of freedom for the filter-bank design.

An analysis filter-bank can consist either of non-recursive filters with a finite impulse response (FIR) or recursive filters having an infinite impulse response (IIR). FIR filter-banks are much more popular and explored than IIR filter-banks, cf., [Glu93, Kli99, VK95]. A problem in the design of *recursive* AS FBs with perfect reconstruction is that the use of IIR analysis filters usually leads to unstable or non-causal synthesis filters, e.g., [Vai93, VK95]. Therefore, it is in general much more difficult to design and implement a filter-bank by means of IIR filters than by FIR filters. In addition, it is much easier to realize a linear-phase system by means of FIR filters than by IIR filters.

An advantage of recursive filter-banks over their non-recursive counterparts is that they can achieve a comparable frequency selectivity with a much lower filter degree, which implies a lower algorithmic complexity and signal delay. In addition, a perfect signal reconstruction or linear phase response is not required for many applications such as speech and audio processing where small reconstruction errors or phase distortions remain unnoticed. Therefore, IIR filter-banks are an attractive (and sometimes overlooked) alternative to FIR filter-banks, which motivates their further exploration.

1.1 Allpass-Based Filter-Banks

This thesis deals with IIR (analysis-synthesis) filter-banks which are based on *allpass filters*. The considered allpass-based filter-banks can be divided into two main classes:

- quadrature-mirror filter-banks (QMF-banks) and Pseudo QMF-banks
- allpass transformed filter-banks.

The considered allpass-based two-channel QMF-banks and M-channel Pseudo QMF-banks use an analysis filter-bank whose polyphase components consist of allpass filters, e.g., [Vai93]. These filter-banks have a *uniform* frequency resolution and perform critical subsampling, which is attractive for subband coding applications.

An allpass transformed filter-bank is obtained by replacing the delay elements of the underlying (uniform) filter-bank by allpass filters [OJS71, BO74]. This frequency warping provokes a *non-uniform* time-frequency resolution. One advantage of allpass transformed filter-banks is their ability to mimic the non-uniform frequency resolution of the human auditory system with great accuracy [SA99], which is exploited, e.g., for speech and audio processing.

A common property of these two filter-bank classes is that their allpass-based analysis filters possess a non-linear phase response. The compensation of these phase distortions by means of a *phase equalization* at the synthesis side is a central design issue for both filter-bank classes, which motivates their joint treatment.

1.2 Related Works & Open Problems

The considered allpass-based filter-banks are well-known and their design and application has already been explored in previous PhD works such as [Kap98, Eng98, Gül01, Gal02, dH04]. Nevertheless, the design of such filter-banks is yet challenging and there exists still a number of open (and neglected) problems which are addressed in this work.

In [Gal02], a closed-form FIR phase equalizer design is devised, which is employed for the construction of allpass-based (Pseudo) QMF-banks as well as allpass trans-

formed AS FBs with near-perfect reconstruction. A benefit of this design approach is its simplicity, but the obtained allpass transformed filter-banks exhibit a rather high signal delay and complexity, which motivates a thorough exploration of alternative phase equalizer designs for allpass-based filter-banks.

In [Kap98], a filter-bank design based on an allpass transformation of first and higher order is introduced. A closed-form solution for the synthesis filter-bank is derived, which achieves a perfect signal reconstruction with a low signal delay. However, a stable and causal synthesis filter-bank has only been found in case of an allpass transformation of first order and the devised design does not apply for a filter-bank where the degree of the prototype lowpass filter exceeds the number of channels. Another main problem of this approach is that the synthesis filters exhibit no bandpass characteristic. This can lead to severe signal distortions if subband processing takes place.

In [dH04], a numerical design approach for allpass transformed AS FBs is presented. The coefficients of the analysis and synthesis prototype filter are determined with the objective to obtain subband filters with a high frequency selectivity as well as a low reconstruction error. The obtained allpass transformed AS FB exhibits a lower delay than the filter-bank design of [Gal02]. However, a perfect aliasing cancellation or even perfect reconstruction cannot be achieved with this approach as well as related numerical designs [VN03, WdDC03]. This raises the question whether an allpass transformed filter-bank with such properties can be obtained by a numerical design at all.

In [Eng98, Gül01], the application of an allpass-transformed DFT AS FB and a tree-structured wavelet filter-bank to speech enhancement is presented and the benefits of such non-uniform filter-banks for noise reduction systems are elaborated. However, a problem of these AS FBs is their rather high signal delay, which excludes their use for applications with demanding signal delay constraints such as digital hearing aids. This motivates the search for a filter-bank structure which allows to exploit the benefits of a non-uniform frequency resolution while having a low signal delay.

1.3 Structure of the Thesis

This thesis tackles, amongst others, the outlined problems and presents different novel design approaches for allpass-based filter-banks. The structure of this work is as follows:

Chap. 2 reviews some fundamental terms and concepts about digital filter-banks and allpass filters as far as needed for this work.

In *Chap. 3*, an improved design approach for allpass-based QMF-banks and Pseudo QMF-banks is presented. The polyphase components of the synthesis filter-banks consist of allpass filters which are designed by simple closed-form expressions. These synthesis polyphase filters act as *phase equalizers* to account for the non-linear phase responses of the analysis filters. Since many design proposals for allpass-based filter-banks differ essentially by the way to solve this phase equalization problem, different phase equalizer designs for this purpose are analyzed in the last part of this chapter.

The results of this analysis are also of importance for the design of *allpass transformed* filter-banks, which is treated in *Chap. 4*. In the first part of this chapter, the allpass transformation of first and higher order is reviewed and opposed to related warping techniques to design a non-uniform filter-bank. In the second part, *closed-*

form synthesis filter-bank designs are examined. Similar as for allpass-based (Pseudo) QMF-banks, the synthesis filter-bank has to compensate the phase distortions introduced by the allpass transformed analysis filter-bank. For this purpose, an improved synthesis filter-bank design is developed and compared with previous approaches.

An advantage of closed-form designs is their simplicity, but it is very difficult to incorporate dedicated design objectives. This problem is addressed by a *numerical* design framework, which is developed in the third part of this chapter. A new mathematical description for allpass transformed AS FBs is introduced from which several synthesis filter-bank designs are derived. They strive for different design objectives such as a complete aliasing cancellation, a sparse design, or perfect reconstruction.

A frequent concern in the design of filter-banks is the signal delay, which is addressed in *Chap. 5*. The concept of the uniform *filter-bank equalizer* (FBE) is derived, which allows to perform adaptive subband filtering with a low signal delay. A generalization of this concept is provided by the allpass transformed FBE. It is shown how a nearly perfect signal reconstruction can be achieved and the concept of the FBE is contrasted to that of a common AS FB with subsampling. For applications with very demanding signal delay constraints, a modification of the FBE is proposed, which achieves a further reduced signal delay in a simple and flexible manner.

In *Chap. 6*, the *application* of the introduced filter-bank designs is discussed for some selected examples. In the first part of this chapter, the application of the new QMF-bank design of Chap. 3 for hierarchical speech and audio coding is elaborated. Important design and implementation aspects are discussed and the performance of the new IIR QMF-bank design is contrasted to that of a comparable FIR QMF-bank. In the second part, the application of the FBE for low delay speech enhancement is investigated. It is shown how this system can be used for noise reduction, speech dereverberation, or near-end listening enhancement, and the achieved performance is compared to that of commonly used AS FBs with subsampling.

Chap. 7 concludes this work and summarizes the main results.

App. A lists the abbreviations, nomenclature and mathematical notation that is used in this work. Supplementary proofs and derivations are provided in *App. B*. Some related filter-bank designs are discussed in *App. C*. An overview of the employed error norms and optimization methods is given in *App. D*. The instrumental measures which are used for the evaluation of noise reduction systems are described in *App. E*.

Publications

Some parts of this PhD thesis have been published by the author at international conferences [LV05a, LV05b, LV05c, LV06b, LV06c, LV06d, LV07c, LV07d, LDV08a, LDV08b, LV08c, LV08d, LV08e, LDV09, LV09b, LV09c, LV09d, LV09e, LYJV10, LV11, SBS+06, SLV08, GKL+09, JLV10, ALM10], as journal papers [LV07b, LV09a, LV10] and a book chapter [LV08a] (which is indicated by underlined references).[1]

This PhD work was accompanied by projects with Siemens, Munich, Germany [LV04a, LV04b] and GN ReSound, Eindhoven, The Netherlands [LV06a, LV07a, LV08b].

[1] An errata sheet is provided at `www.ind.rwth-aachen.de/~bib/loellmann11a`.

Chapter 2

Fundamentals of Digital Filter-Banks

FUNDAMENTAL terms and concepts of analysis-synthesis filter-banks are introduced in this chapter as far as needed for this work. The following treatment is partly based on [CR83, Vai93, Kli99] where a more comprehensive exploration of (uniform) filter-banks can be found.

2.1 Analysis-Synthesis Filter-Banks

A general representation of a digital *analysis-synthesis filter-bank* (AS FB) is shown in Figure 2.1. The real input sequence $x(k)$ with discrete time index (sample index) $k \in \mathbb{Z}$ is a digital signal with sampling frequency $f_\mathrm{s} = 1/T_\mathrm{s}$.[1] This sequence is assumed to be of finite energy so that its z-transform $\mathcal{Z}\{x(k)\} = X(z)$ exists. The (digital) signal[2] $x(k)$ is split into the subband signals $x_i(k)$ by means of an *analysis filter-bank,* which consists of M analysis filters with passband widths $\Delta\Omega_i$ and real or complex impulse responses $h_i(k)$ for $i \in \{0, 1, \ldots, M-1\}$. The limited bandwidths of the M subband

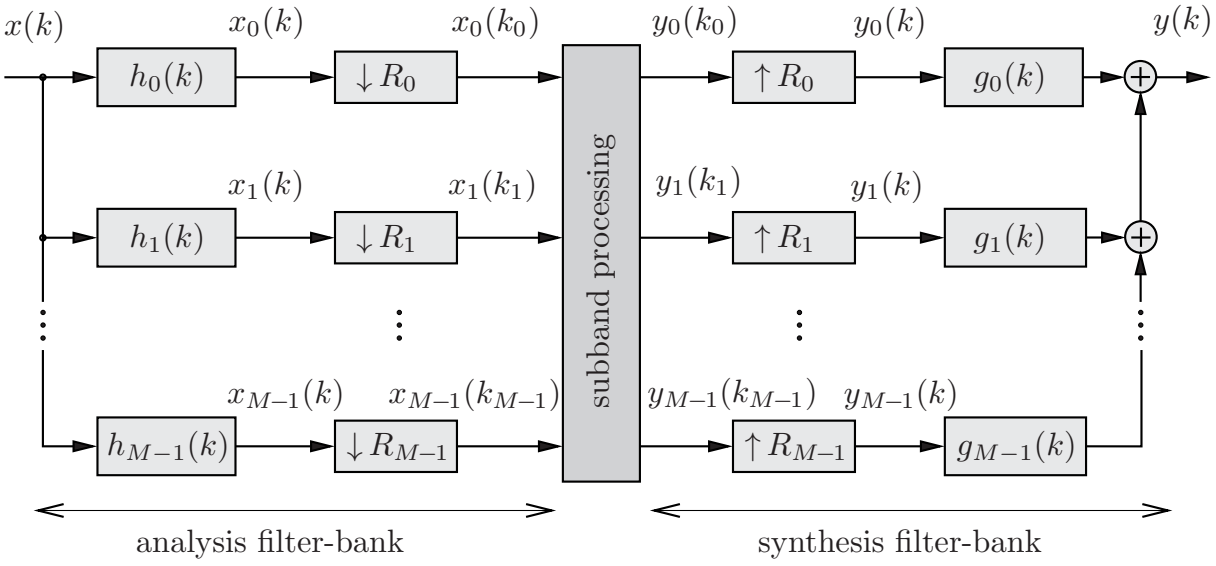

Figure 2.1: *General structure of an analysis-synthesis filter-bank (AS FB).*

[1] An overview of the used abbreviations and nomenclature can be found in App. A.

[2] The terms *signal* and *sequence* are used interchangeably as only digital signals are considered in this work.

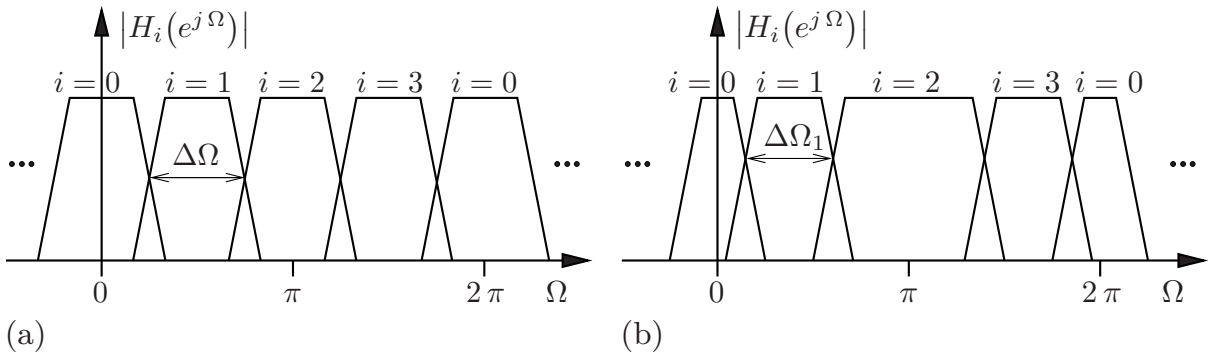

Figure 2.2: *Schematic of the magnitude responses of different filter-bank types for $M = 4$ subbands:*
(a) *uniform filter-bank*
(b) *non-uniform filter-bank.*

signals allow to perform a subsampling according to the rule [Mal92]

$$R_i \leq \frac{2\,\pi}{\Delta\Omega_i} \quad \text{for} \quad R_i \in \{1, 2 \ldots, M\} \quad \text{and} \quad \sum_{i=0}^{M-1} \Delta\Omega_i = 2\,\pi\,. \tag{2.1}$$

This leads to different sampling periods $T_{\mathrm{s}i} = T_{\mathrm{s}}\,R_i$, which is indicated by the discrete time index k_i in Figure 2.1.

A filter-bank with different passband widths $\Delta\Omega_i$ is termed as a *non-uniform* filter-bank. Accordingly, a filter-bank with equal passband widths $\Delta\Omega_i \equiv \Delta\Omega$ is denoted as a *uniform* filter-bank. The subband filters of such filter-banks are sketched schematically in Figure 2.2. For a uniform filter-bank, the same downsampling rate $R_i \equiv R$ is taken for each subband signal $x_i(k)$. In this case, *critical subsampling* is performed if $R = M$ and *non-critical subsampling* if $R < M$. This scenario of a single downsampling rate R is considered in the following, which is indicated by the notation $k_i \equiv k'$ for the discrete time index after downsampling.

In general, an $R-$fold *downsampler* or decimator converts an input sequence $x_{\mathrm{in}}(k)$ into the downsampled sequence

$$x_{\mathrm{d}}(k') = x_{\mathrm{in}}(k'R) \quad \text{for} \quad k' \in \mathbb{Z}\,. \tag{2.2}$$

This downsampling operation without zero filling leads to a different sampling period $T'_{\mathrm{s}} = T_{\mathrm{s}}\,R$ as indicated by the prime. The z-domain representation of Eq. (2.2) is given by

$$X_{\mathrm{d}}(z) = \frac{1}{R} \sum_{r=0}^{R-1} X_{\mathrm{in}}\left(z^{\frac{1}{R}}\,W_R^r\right) \tag{2.3}$$

where

$$W_R = e^{-j\,\frac{2\,\pi}{R}}\,. \tag{2.4}$$

It should be noted that the z-variable in Eq. (2.3) is based on the input sampling period T_s where the relation to the variable z', which is based on T_s', is given by $z' = z^R$. In this work, all z-domain expressions are related to the input sampling period T_s.

Eq. (2.3) reveals that the decimation leads to a superposition of the spectra $X_\mathrm{in}\left(e^{j\,\frac{1}{R}(\Omega - 2\pi r)}\right)$, which are frequency shifted and stretched versions (images) of $X_\mathrm{in}\left(e^{j\,\Omega}\right)$. These quantities are expressed in dependence of the *normalized frequency*

$$\Omega = \frac{2\,\pi\,f}{f_\mathrm{s}}, \tag{2.5}$$

which is simply termed as frequency, if there is no room for confusion. If the frequency spectrum $X_\mathrm{in}\left(e^{j\,\Omega}\right)$ is not perfectly bandlimited with $\Delta\Omega \leq 2\pi/R$, the superposition of its images causes an overlap effect called *aliasing*.[3]

The task of the *synthesis filter-bank* is to obtain the output signal $y(k)$ from the M subband signals $y_i(k')$. In a first step, an upsampling is performed. In general, an R-fold *upsampler* or expander inserts zeros according to

$$y_\mathrm{u}(k) = \begin{cases} y_\mathrm{in}(k') & \text{if } k = R\,k';\quad k' \in \mathbb{Z} \\ 0 & \text{otherwise.} \end{cases} \tag{2.6}$$

The corresponding description in the z-domain is given by

$$Y_\mathrm{u}(z) = Y_\mathrm{in}\left(z^R\right). \tag{2.7}$$

The upsampled signals $y_i(k)$ are interpolated by subsequent synthesis filters with impulse responses $g_i(k)$ for $i \in \{0, 1, \ldots M-1\}$ and finally added up to obtain the output signal $y(k)$ as depicted in Figure 2.1. Between analysis and synthesis filter-bank, the actual subband processing takes places. For example, the subband signals can be multiplied with spectral gain factors to perform speech enhancement (e.g., [Eng98]) or they might be quantized for subband coding applications (e.g., [Vai93]).

If no such subband processing takes place, $y_i(k') = x_i(k')\ \forall\ i$ and the filter-bank[4] provides the reconstructed input signal $y(k) = \hat{x}(k)$. In this case, it is straightforward to derive the following input-output relation by means of Eq. (2.3) and Eq. (2.7):

$$\widehat{X}(z) = \frac{1}{R}\sum_{r=0}^{R-1} X\left(z\,W_R^r\right)\ \sum_{i=0}^{M-1} H_i\left(z\,W_R^r\right)\cdot G_i(z) \tag{2.8}$$

$$= X(z)\ \underbrace{\frac{1}{R}\sum_{i=0}^{M-1} H_i(z)\cdot G_i(z)}_{=\,T_\mathrm{lin}(z)} + \underbrace{\frac{1}{R}\sum_{r=1}^{R-1} X\left(z\,W_R^r\right)\sum_{i=0}^{M-1} H_i\left(z\,W_R^r\right)\cdot G_i(z)}_{=\,\mathcal{D}_\mathrm{alias}(z)}. \tag{2.9}$$

[3] An illustration of this effect can be found in [Vai93, Chap. 5].

[4] The term filter-bank is simply used, if it is obvious from the context whether an analysis, synthesis, or analysis-synthesis filter-bank is meant.

The function $T_{\mathrm{lin}}(z)$ denotes the *linear transfer function* of the AS FB. Its frequency response and group delay are denoted by[5]

$$T_{\mathrm{lin}}\left(e^{j\,\Omega}\right) = \left|T_{\mathrm{lin}}\left(e^{j\,\Omega}\right)\right| \cdot e^{-j\,\varphi_{\mathrm{lin}}(\Omega)} \tag{2.10}$$

$$\tau_{\mathrm{lin}}(\Omega) = \mathrm{gdl}\left\{T_{\mathrm{lin}}\left(e^{j\,\Omega}\right)\right\}\ . \tag{2.11}$$

The function $\mathcal{D}_{\mathrm{alias}}(z)$ represents *aliasing distortions* caused by the subsampling. A frequency-domain measure for the maximal aliasing distortions is given by the *peak aliasing distortions* [Vai93]

$$\mathcal{D}_{\mathrm{peak}}(\Omega) = \sqrt{\sum_{r=1}^{R-1}\left|\frac{1}{R}\sum_{i=0}^{M-1} H_i\left(e^{j\,(\Omega-2\pi r/R)}\right)\cdot G_i\left(e^{j\,\Omega}\right)\right|^2}\ . \tag{2.12}$$

If no subband processing takes place, the filter-bank should provide an output signal $y(k) = \hat{x}(k)$ which is – at least approximately – a replica of the input signal $x(k)$. An AS FB achieves *perfect reconstruction* (PR), if the output signal is only a scaled and delayed copy of the input signal

$$\hat{x}(k) = c_{\mathrm{s}} \cdot x(k - D_{\mathrm{o}}) \quad \text{for} \quad D_{\mathrm{o}} \in \mathbb{N}_0\,; \quad c_{\mathrm{s}} \in \mathbb{R}_+\ . \tag{2.13a}$$

The value of D_{o} refers to the (overall) *signal delay* of the filter-bank. The set of all positive integer numbers including zero is denoted by $\mathbb{N}_0$ and $\mathbb{R}_+$ marks the set of all real numbers being greater than zero. If Eq. (2.13a) applies, the linear transfer function and aliasing distortions of Eq. (2.9) are given by

$$T_{\mathrm{lin}}(z) = c_{\mathrm{s}} \cdot z^{-D_{\mathrm{o}}} \quad \wedge \quad \mathcal{D}_{\mathrm{alias}}(z) \equiv 0\ . \tag{2.13b}$$

A filter-bank achieves perfect reconstruction in a strict sense, if Eq. (2.13) applies with $c_{\mathrm{s}} = 1$ and $D_{\mathrm{o}} = 0$. However, this can only be achieved by trivial systems without any practical relevance.

A filter-bank accomplishes *near-perfect reconstruction* (NPR), if

$$\hat{x}(k) \approx c_{\mathrm{s}} \cdot x(k - D_{\mathrm{o}}), \tag{2.14a}$$

which implies that

$$T_{\mathrm{lin}}(z) \approx c_{\mathrm{s}} \cdot z^{-D_{\mathrm{o}}} \quad \vee \quad \mathcal{D}_{\mathrm{alias}}(z) \approx 0\ . \tag{2.14b}$$

The tolerable deviations depend on the filter-bank design and the intended application, respectively. In general, the reconstruction error of a filter-bank with near-perfect reconstruction should be low enough such that no *noticeable* signal distortions occur, if no subband processing takes place.

[5] For this work, it is beneficial to define the phase response with a negative sign in the exponent, which differs to some definitions of the phase response in literature.

The filter-bank described by Eq. (2.9) is a *linear periodically time-varying* (LPTV) system with period R since $W_R^r = W_R^{r+m\,R}$ for $m \in \mathbb{Z}$. It becomes a *linear time-invariant* (LTI) system, if a complete *aliasing cancellation* is achieved, i.e., $\mathcal{D}_{\text{alias}}(z) \equiv 0$. The filter-bank causes no *linear magnitude distortions*, if

$$\left|T_{\text{lin}}\left(e^{j\,\Omega}\right)\right| = c_{\text{s}} \;\forall\; \Omega \tag{2.15}$$

where usually $c_{\text{s}} = 1$. Accordingly, the system causes no *linear phase distortions*, if the linear phase error

$$\Delta\varphi_{\text{lin}}(\Omega) = \varphi_{\text{lin}}(\Omega) - D_{\text{o}}\,\Omega \tag{2.16}$$

is identical to zero for all frequencies Ω.

Eq. (2.9) is commonly employed for the description and design of filter-banks, e.g., [Gal02, dH04]. For this work, a different representation is used in addition. The considered AS FBs with subsampling by R are LPTV systems with period R. This behavior is taken into account by determining the response of the filter-bank for R time-shifted unit sample sequences as input, i.e., $X(z) = z^{-\nu}$ for $\nu \in \{0, 1, \ldots, R-1\}$. This results in the new *overall transfer function* given by[6]

$$T_\nu(z) = \frac{\widehat{X}_\nu(z)}{z^{-\nu}} \quad \text{for} \quad \nu \in \{0, 1, \ldots, R-1\}\,. \tag{2.17}$$

The z-domain expression $\widehat{X}_\nu(z)$ represents the output signal of an AS FB without subband processing for an input signal given by $X(z) = z^{-\nu}$. Frequency response and group delay of the new overall transfer function read

$$T_\nu\left(e^{j\,\Omega}\right) = \left|T_\nu\left(e^{j\,\Omega}\right)\right| \cdot e^{-j\,\varphi_\nu(\Omega)} \tag{2.18}$$

$$\tau_\nu(\Omega) = \text{gdl}\left\{T_\nu\left(e^{j\,\Omega}\right)\right\}\,. \tag{2.19}$$

The evaluation of this overall transfer function at $\nu = 0$ is used for the analysis of filter-banks by calculating its logarithmic magnitude response

$$\left|T_0\left(e^{j\,\Omega}\right)\right| / \text{dB} = 20\log_{10}\left|T_0\left(e^{j\,\Omega}\right)\right| \tag{2.20}$$

and the (overall) phase error

$$\Delta\varphi_0(\Omega) = \varphi_0(\Omega) - D_{\text{o}}\,\Omega\,. \tag{2.21}$$

It should be noted that the overall transfer function $T_0(z)$ becomes equal to the linear transfer function $T_{\text{lin}}(z)$ for a filter-bank with perfect aliasing cancellation (or if no subsampling is performed). The introduced transfer function of Eq. (2.17) is not only used for the analysis of filter-banks, but also for their numerical design later in Chap. 4.

[6] In literature, the function $T_{\text{lin}}\left(e^{j\,\Omega}\right)$ is also referred to as overall transfer function (of the alias-free) system, e.g., [Vai93, AZ03]. This nomenclature is not adopted here to achieve a more clear distinction between the linear transfer function and overall transfer function of an AS FB.

2.2 Modulated Filter-Banks

This thesis deals exclusively with *modulated* filter-banks, especially AS FBs based on the *discrete Fourier transform* (DFT) and inverse discrete Fourier transform (IDFT), respectively. The M analysis filters are obtained by complex modulation according to

$$H_i(z) = H\left(z\, W_M^i\right) \tag{2.22}$$

$$= \sum_{l=0}^{L_\mathrm{a}-1} h(l) \cdot W_M^{-i\,l} \cdot z^{-l} \;\forall\; i \in \{0, 1, \ldots, M-1\} \tag{2.23}$$

with $W_M = e^{-j\,\frac{2\,\pi}{M}}$, e.g., [Vai93]. A causal filter with finite impulse response (FIR)

$$h(k) = 0 \quad \text{for} \quad k \geq L_\mathrm{a} \quad \text{and} \quad k < 0 \tag{2.24}$$

is taken as analysis *prototype (lowpass) filter* from which the other $M-1$ bandpass filters are obtained by complex modulation. This modulation causes a frequency shift according to

$$H_i\left(e^{j\,\Omega}\right) = H\left(e^{j\,(\Omega - \frac{2\,\pi}{M}\,i)}\right) \quad \text{for} \quad i \in \{0, 1, \ldots, M-1\}, \tag{2.25}$$

which results in a uniform analysis filter-bank as sketched schematically in Figure 2.2-a.

The synthesis filters are also obtained by complex modulation of an FIR synthesis prototype lowpass filter $g(k)$ according to[7]

$$G_i(z) = G\left(z\, W_M^i\right) \cdot W_M^{-i} \tag{2.26}$$

$$= \sum_{l=0}^{L_\mathrm{s}-1} g(l) \cdot W_M^{-i\,(l+1)} \cdot z^{-l}\,. \tag{2.27}$$

It should be noted that for the considered DFT AS FB $H(z) = H_0(z)$ and $G(z) = G_0(z)$ which, however, does not for apply for all transformation kernels as, for example, the oddly-stacked generalized discrete Fourier transform (GDFT) as shown in Sec. 5.1.1. If not mentioned otherwise, it is assumed that the lengths of analysis and synthesis prototype filter are identical

$$L = L_\mathrm{a} = L_\mathrm{s}\,. \tag{2.28}$$

The prototype lowpass filters are designed with the goal to achieve a high stopband attenuation in order to minimize or even eliminate aliasing distortions. The overall transfer function of Eq. (2.9) is then approximately or even exactly equal to its linear transfer function. It follows from Eq. (2.23) and Eq. (2.27) that the linear transfer

[7] This complex modulation scheme is not the only possibility, but beneficial for the later treatment in Sec. 2.3.

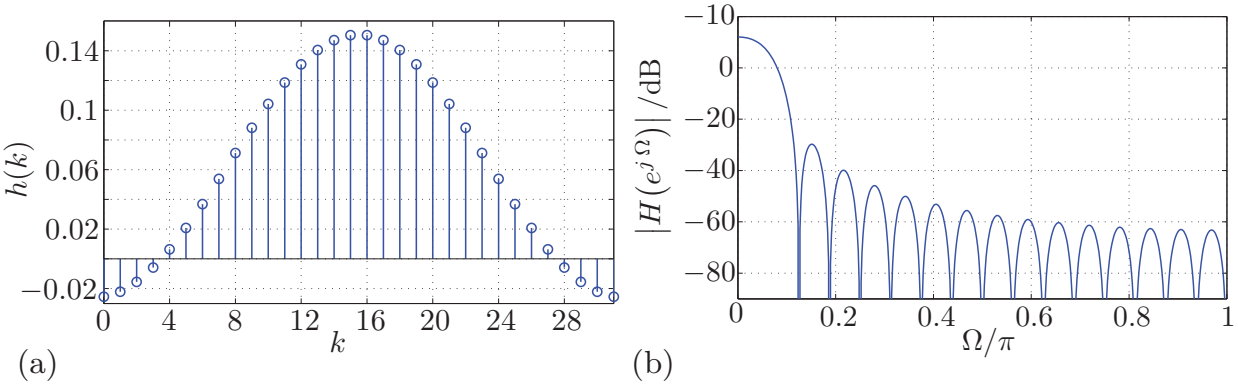

Figure 2.3: *ELT prototype filter of Eq.* (2.33) *for* $R = M/4 = 4$ *and* $L = 32$*:*
(a) *impulse response*
(b) *magnitude response.*

function of the considered DFT AS FB is given by

$$T_{\text{lin}}(z) = \frac{1}{R} \sum_{i=0}^{M-1} \sum_{l=0}^{L-1} \sum_{m=0}^{L-1} h(l) \cdot g(m) \cdot e^{j \frac{2\pi}{M} i\,(l+m+1)} \cdot z^{-(l+m)} \tag{2.29}$$

$$= \frac{M}{R} \sum_{\lambda \in \mathbb{Z}} \sum_{l=0}^{L-1} h(l) \cdot g(\lambda\, M - 1 - l) \cdot z^{-(\lambda\, M-1)}\,. \tag{2.30}$$

Thus

$$T_{\text{lin}}(z) = z^{-(L-1)}, \tag{2.31}$$

if the condition

$$\frac{M}{R} \sum_{l=0}^{L-1} h(l) \cdot g(\lambda\, M - l - 1) = \begin{cases} 1 & \text{if } \lambda\, M = L \\ 0 & \text{if } \lambda\, M \in \mathbb{Z} \backslash \{L\} \end{cases} \tag{2.32}$$

is met. This means that the convolution of analysis and synthesis prototype filter should provide an impulse response corresponding to an Mth band filter. The design of prototype filters to fulfill this requirement is treated in several publications, e.g., [Wac86, Vai93, Fli93, Kli99]. A closed-form solution for Eq. (2.32) is given by

$$h(l) = g(l) = \frac{\sqrt{R}}{L} \left(1 - \sqrt{2}\, \cos\!\left(\frac{\pi}{M}\, (l + 0.5) \right) \right)$$
$$\text{for} \quad l \in \{0, 1, \ldots, L-1\} \quad \text{and} \quad L = 2\,M\,. \tag{2.33}$$

These filters are termed as *ELT prototype filters* since they have been originally developed for cosine modulated filter-banks known as extended lapped transform (ELT) [Mal92, Kli99]. Impulse response and magnitude response of an ELT prototype filter are plotted in Figure 2.3. The ELT prototype filters of Eq. (2.33) achieve *perfect*

reconstruction for an oversampled DFT filter-bank and are considered primarily for the design examples in this work. If $L = M$, a rectangular prototype filter with

$$h(l) = g(l) = \frac{\sqrt{R}}{M} \;\forall\; l \in \{0, 1, \ldots, M-1\} \tag{2.34}$$

is used for the design examples. It should be noted that perfect reconstruction cannot be achieved with a DFT AS FB for critical subsampling, if $L > M$, e.g., [Kli99].

2.3 Polyphase Representation

The polyphase decomposition of FIR filters is introduced in [BBC76] and extended to IIR filters in [Var79]. This concept is of fundamental importance for the design as well as the efficient implementation of digital filter-banks, e.g., [Var78, VW83, Vai90, Vai93, Glu93, Kli99].

The type 1 polyphase representation for the analysis filters of Eq. (2.23) is obtained as follows

$$\begin{aligned} H_i(z) &= \sum_{\lambda=0}^{M-1} \sum_{m=0}^{l_M-1} h(Mm+\lambda) \cdot z^{-(Mm+\lambda)} \cdot W_M^{-i\,(Mm+\lambda)} \\ &= \sum_{\lambda=0}^{M-1} H_{0,\lambda}^{(M)}\left(z^M\right) \cdot z^{-\lambda} \cdot W_M^{-i\,\lambda} \end{aligned} \tag{2.35a}$$

with the type 1 polyphase components

$$H_{0,\lambda}^{(M)}(z) = \sum_{m=0}^{l_M-1} h(Mm+\lambda) \cdot z^{-m} \tag{2.35b}$$

and

$$l_M = \left\lceil \frac{L}{M} \right\rceil . \tag{2.36a}$$

If Eq. (2.32) applies

$$l_M = \frac{L}{M} \in \mathbb{N} . \tag{2.36b}$$

The operation $\lceil . \rceil$ returns the lowest integer which is greater or equal to the argument and $\mathbb{N}$ marks the set of all positive integers excluding zero. The type 2 polyphase representation of the synthesis filters of Eq. (2.27) reads

$$\begin{aligned} G_i(z) &= \sum_{\lambda=0}^{M-1} \sum_{m=0}^{l_M-1} g\Big(M\,(m+1) - \lambda - 1\Big) \cdot z^{-(M\,(m+1)-\lambda-1)} \cdot W_M^{-i\,(M\,(m+1)-\lambda)} \\ &= \sum_{\lambda=0}^{M-1} \bar{G}_{0,\lambda}^{(M)}\left(z^M\right) \cdot z^{-(M-\lambda-1)} \cdot W_M^{i\,\lambda} \end{aligned} \tag{2.37a}$$

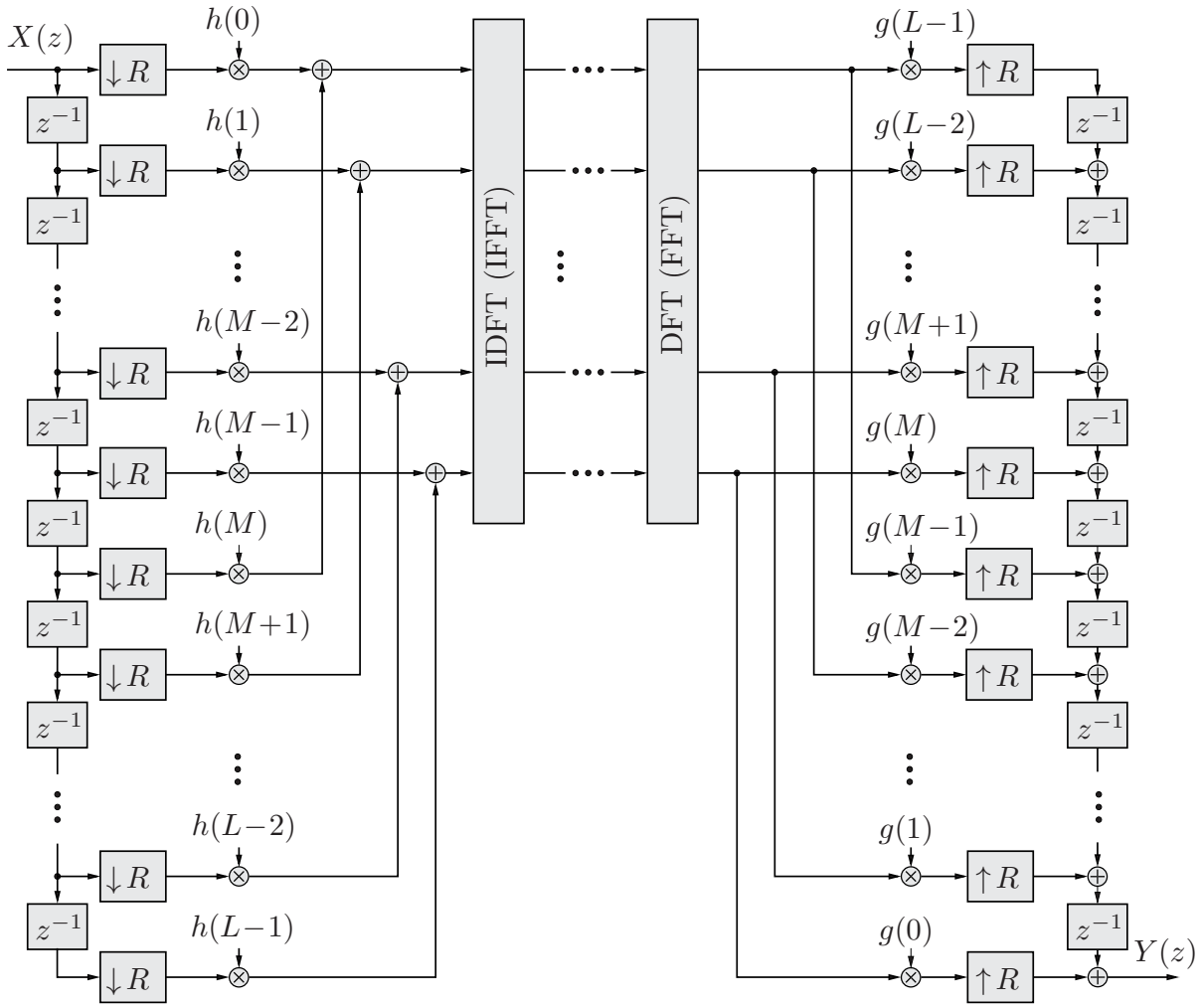

Figure 2.4: *Polyphase network (PPN) implementation of a DFT AS FB with subsampling by R and $L = 2\,M$ (without subband processing).*

with the type 2 polyphase components

$$\bar{G}_{0,\lambda}^{(M)}(z) = \sum_{m=0}^{l_M-1} g\big(M\,(m+1) - \lambda - 1\big) \cdot z^{-m}\,. \tag{2.37b}$$

There exists also a type 3 polyphase representation [CR83, Fli93] which, however, is not considered in this work.

Figure 2.4 shows the derived *polyphase network* (PPN) implementation of a DFT AS FB. It should be noted that for the introduced DFT filter-bank neither the DFT nor the IDFT perform here a scaling by $1/M$, which is implicitly considered by the choice for the prototype filter coefficients. The subsampling operations can be moved towards the delay elements due to the Noble identities depicted in Figure 2.5 [Vai93]. The IDFT and DFT, respectively, can be computed efficiently by the fast Fourier transform (FFT), e.g., [OSB99]. Hence, this PPN filter-bank implementation possesses only a low computational complexity. The processing scheme of Figure 2.4 can also be interpreted as *weighted overlap-add method* [Cro80, CR83]: The delay chains buffer the

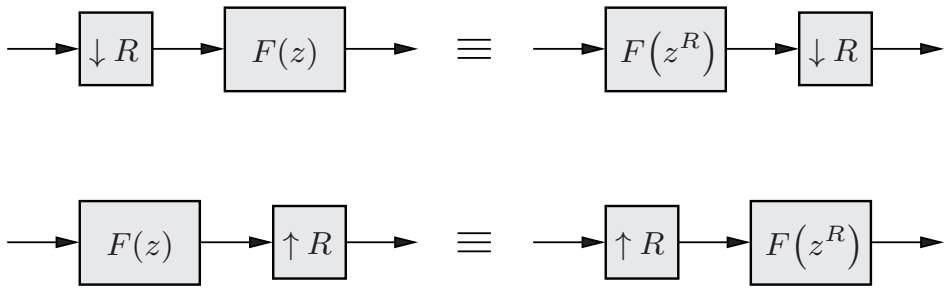

Figure 2.5: *The Noble identities for multi-rate processing.*

samples of the input and output frames whose overlap is determined by the subsampling rate R. The weighting coefficients are given by the coefficients of the FIR prototype filters. A 'zero-padding' can be achieved by setting some of these coefficients equal to zero.

Another common description of PPN filter-banks is based on a matrix representation, e.g., [Vai93, Glu93, Kli99] which, however, is of less importance for this work.

2.4 Spectral Representation of Multi-Rate Systems

An analysis-synthesis filter-bank is a *multi-rate* system due to the subsampling operations. Such a system can be described by its *system response* $t_{\mathrm{bi}}(k_2, k_1)$, which is the response of the system at instant k_2 to a unit sample sequence at instant k_1 where the sampling rates for k_1 and k_2 can be different [CR83, Sch08].

This work deals exclusively with uniform and non-uniform AS FBs which apply the same subsampling rate R in each subband. Such filter-banks are LPTV systems with period R according to Sec. 2.1. As a consequence, the system response has the property

$$t_{\mathrm{bi}}(k_2, k_1) = t_{\mathrm{bi}}(k_2 + m\,R, k_1 + m\,R) \;\forall\; k_2, k_1, m \in \mathbb{Z} \tag{2.38}$$

where the sampling times for k_1 and k_2 are identical. In addition, the considered filter-banks are causal systems such that $t_{\mathrm{bi}}(k_2, k_1) = 0$ for $k_1 > k_2$.

The representation of the system response in the frequency-domain reads

$$T_{\mathrm{bi}}\left(e^{j\,\Omega_2}, e^{j\,\Omega_1}\right) = \frac{1}{2\,\pi} \sum_{k_1=-\infty}^{\infty} \sum_{k_2=-\infty}^{\infty} t_{\mathrm{bi}}(k_2, k_1) \cdot e^{j\,(\Omega_1\,k_1 - \Omega_2\,k_2)}\,. \tag{2.39}$$

A general treatment of this *bifrequency system function* (BSF) can be found in [CR83, Sch08]. The following derivation differs slightly as only systems with the property of Eq. (2.38) are considered whose BSF is calculated for *discrete* frequencies

$$\Omega_1 = \frac{2\,\pi}{N_{\mathrm{bi}}}\,i_1 \quad \text{and} \quad \Omega_2 = \frac{2\,\pi}{N_{\mathrm{bi}}}\,i_2 \quad \text{with} \quad i_1, i_2 \in \{0, 1, \ldots, N_{\mathrm{bi}} - 1\}\,. \tag{2.40}$$

The frequency sampled version for the BSF of Eq. (2.39) is given by

$$T_{\mathrm{bi}}\left(e^{j\,\frac{2\,\pi}{N_{\mathrm{bi}}}\,i_2}, e^{j\,\frac{2\,\pi}{N_{\mathrm{bi}}}\,i_1}\right) = \frac{1}{N_{\mathrm{bi}}^2} \sum_{k_1=0}^{N_{\mathrm{bi}}-1} \sum_{k_2=0}^{N_{\mathrm{bi}}-1} t_{\mathrm{bi}}(k_2, k_1) \cdot e^{j\,\frac{2\,\pi}{N_{\mathrm{bi}}}\,(k_1\,i_1 - k_2\,i_2)}\,. \tag{2.41}$$

As shown in App. B.1, this expression can be converted to

$$T_{\mathrm{bi}}\left(e^{j\frac{2\pi}{N_{\mathrm{bi}}}i_2}, e^{j\frac{2\pi}{N_{\mathrm{bi}}}\left(i_2+l\frac{N_{\mathrm{bi}}}{R}\right)}\right) = \begin{cases} \dfrac{1}{R\,N_{\mathrm{bi}}}\displaystyle\sum_{k_1=0}^{R-1}\sum_{k=0}^{N_{\mathrm{bi}}-1} t_{\mathrm{bi}}(k_1+k,k_1)\cdot e^{j\frac{2\pi}{R}k_1 l}\cdot e^{-j\frac{2\pi}{N_{\mathrm{bi}}}k\,i_2} & \text{if } \; l\in\mathbb{Z} \\ 0 & \text{if } \; l\notin\mathbb{Z} \end{cases} \tag{2.42}$$

where it is sufficient to consider only the values for $l \in \{0, \pm 1, \pm 2, \ldots \pm (R-1)\}$ due to the $2\,\pi$-periodicity. For a *linear time-invariant* (LTI) system

$$t_{\mathrm{bi}}(k_1+k,k_1) = t_{\mathrm{bi}}(k,0) \tag{2.43}$$

so that the discrete BSF of Eq. (2.42) reduces to

$$T_{\mathrm{bi}}\left(e^{j\frac{2\pi}{N_{\mathrm{bi}}}i_2}, e^{j\frac{2\pi}{N_{\mathrm{bi}}}i_2}\right) = \frac{1}{N_{\mathrm{bi}}}\sum_{k=0}^{N_{\mathrm{bi}}-1} t_{\mathrm{bi}}(k,0)\cdot e^{-j\frac{2\pi}{N_{\mathrm{bi}}}k i_2}\,. \tag{2.44}$$

In this case, the discrete BSF represents the *linear transfer function* of the filter-bank $T_{\mathrm{lin}}\left(e^{j\,\Omega}\right)$ calculated by the DFT or FFT, respectively.

Since the allpass-based filter-banks treated in this work are recursive systems, the transformation length N_{bi} is determined in dependence of the individual system response $t_{\mathrm{bi}}(k_2,k_1)$ by the rule

$$\left|t_{\mathrm{bi}}(k_2,k_1)\right| \le \epsilon_{\mathrm{bi}} \quad \text{for} \quad k_2 \ge N_{\mathrm{bi}} \quad \text{and} \quad k_1 \in \{0,1,\ldots,R-1\} \tag{2.45}$$

to avoid (noticeable) spectral aliasing while keeping the length N_{bi} as short as possible. The value taken for the threshold ϵ_{bi} is equal to $2\cdot 10^{-16}$ (which is below the relative floating-point accuracy of MATLAB).

The properties of the BSF should be exemplified by means of Figure 2.6. It shows the magnitude of the BSF for two different AS FBs with the same subampling rate.[8] Only the frequency range of $\Omega_1, \Omega_2 \in [0, 2\,\pi]$ is considered due to the $2\,\pi$-periodicity of $T_{\mathrm{bi}}\left(e^{j\,\Omega_2}, e^{j\,\Omega_1}\right)$. The BSF $T_{\mathrm{bi}}\left(e^{j\,\Omega_2}, e^{j\,\Omega_1}\right)$ can have non-zero values only at the frequency lines

$$\Omega_1 = \Omega_2 + \frac{2\,\pi}{R}\,l \quad \text{for} \quad l \in \{0, \pm 1, \ldots \pm (R-1)\} \tag{2.46}$$

according to Eq. (2.42). The values on the main diagonal at $\Omega_1 = \Omega_2$ correspond to the magnitude response of the linear transfer function $T_{\mathrm{lin}}\left(e^{j\,\Omega_1}\right)$ according to Eq. (2.44). The BSFs in Figure 2.6 suggest both a low amount of linear magnitude distortions as their main diagonals at $\Omega_1 = \Omega_2$ are constant (at this resolution for the plots). The magnitude of the BSF is symmetric to this main diagonal. Hence, there are at

[8] The actual design of these filter-banks is not important for this discussion and explained in Sec. 4.3.3 in connection with Example 4.3 and Example 4.4.

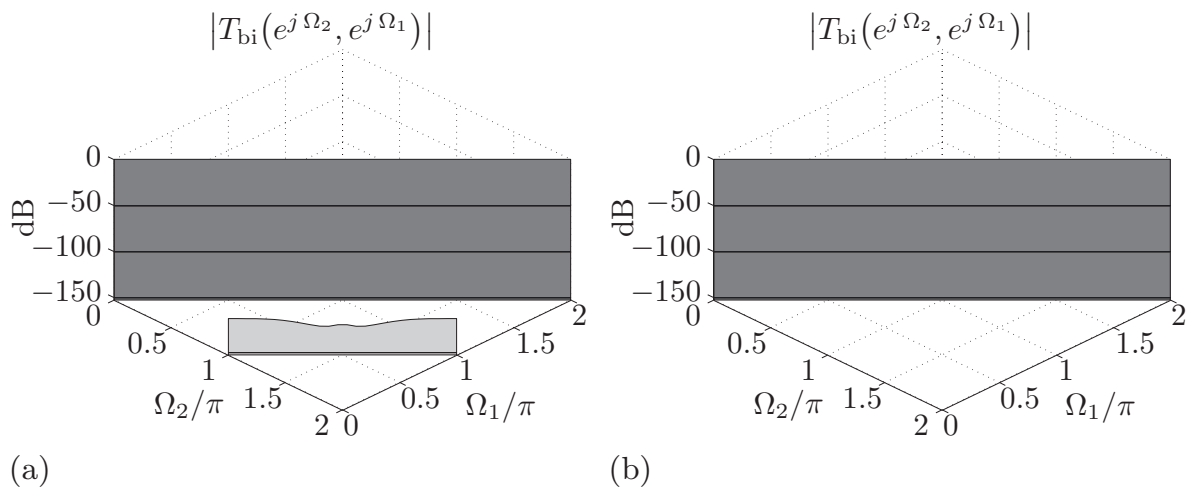

Figure 2.6: *Magnitude of the bifrequency system function (BSF) for two different AS FBs with a subsampling rate of $R = 2$ achieving a partial aliasing cancellation* (a) *and a perfect aliasing cancellation (b).*

most $R - 1$ unique elements on the side diagonals determined by Eq. (2.46), e.g., for $l \in \{1, 2, \ldots, R-1\}$. They show the number and magnitude of non-canceled alias components. This can be observed in Figure 2.6-a where an alias component occurs on the side diagonal $\Omega_1 = \Omega_2 + \pi$ since Eq. (2.46) applies here with $R = 2$.

It should be noted that if the peak alias distortions according to Eq. (2.12) are (almost) zero for all frequencies Ω, this does imply a BSF without alias components on its side diagonals. However, a BSF without alias components does not ensure in general that $\mathcal{D}_{\mathrm{peak}}(\Omega) \equiv 0$. Therefore, the peak aliasing distortions indicate to some extend how good (or bad) the aliasing cancellation works, if a modification of the subband signals takes place. The representation by the BSF has the advantage that the suppression of individual alias components becomes visible together with the linear magnitude distortions. Therefore, both representation are used in this work for the assessment of the achieved aliasing cancellation.

2.5 Allpass Filters

A common building block of all the filter-banks treated in this thesis are allpass filters. Besides IIR filter-banks, these filters are also part of many other signal processing systems and intensively treated, e.g., in [Vai93, RMV88, Sch08]. In the following, the main properties of allpass filters are described as far as needed for the later treatment.

The system function of a causal stable allpass filter of degree K in its *direct (filter) form* is given by

$$A^{[K]}(z) = \frac{\sum_{m=0}^{K} c^*(K-m) \cdot z^{-m}}{\sum_{m=0}^{K} c(m) \cdot z^{-m}}; \quad c(m) \in \mathbb{C}; \quad K \in \mathbb{N}\,. \tag{2.47}$$

The asterisk marks the complex conjugate value and $\mathbb{C}$ the set of all complex numbers. An alternative representation, which is primarily considered in this work, is the *cascade form*

$$A^{[K]}(z) = \prod_{m=1}^{K} A_m^{[1]}(z) \tag{2.48a}$$

$$= \prod_{m=1}^{K} \frac{1 - a^*(m) \cdot z}{z - a(m)}; \quad a(m) \in \left\{ \mathbb{C} \,\middle|\, \max_m \{|a(m)|\} < 1 \right\} \tag{2.48b}$$

with region of convergence

$$\mathcal{R}_\mathrm{c} = \left\{ z \in \mathbb{C} \,\middle|\, \max_m \{|a(m)|\} < |z| \right\} . \tag{2.48c}$$

The complex allpass poles are denoted by[9]

$$a(m) = \alpha(m) \cdot e^{j\,\gamma(m)}; \quad \alpha(m) \in \mathbb{R}; \quad \gamma(m) \in \{\, \mathbb{R} \,|\, 0 \le \gamma(m) \le 2\,\pi \,\} . \tag{2.49}$$

The allpass filter becomes identical to a mere delay element

$$A^{[K]}(z) = z^{-K} \quad \text{if} \quad a(m) = 0 \;\forall\; m, \tag{2.50}$$

which is a *trivial* allpass filter. As indicated by its name, a (unit-magnitude) allpass filter has the property

$$\left| A^{[K]}\left(e^{j\,\Omega}\right) \right| = 1 \;\forall\; \Omega\,. \tag{2.51}$$

As a consequence, allpass filters are *lossless* such that the (causal) input signal $x(k)$ and the output signal $y(k)$ of an allpass filter have the same energy

$$\sum_{k=0}^{\infty} |x(k)|^2 = \sum_{k=0}^{\infty} |y(k)|^2 .$$

An allpass filter of *first order* features the system function

$$A(z) = A^{[1]}(z) = \frac{1 - a^* z}{z - a} \quad \text{with} \quad a = \alpha \cdot e^{j\,\gamma}; \quad \alpha, \gamma \in \mathbb{R}\,. \tag{2.52}$$

Its frequency response is denoted by

$$A\left(e^{j\,\Omega}\right) = \frac{1 - a^* e^{j\,\Omega}}{e^{j\,\Omega} - a} = e^{-j\,\varphi_a(\Omega)} . \tag{2.53}$$

[9] It should be noted that $\alpha = \mathrm{sign}\{\Re\{a\}\} \cdot |a|$ and not $\alpha = |a|$ to simplify the later treatment.

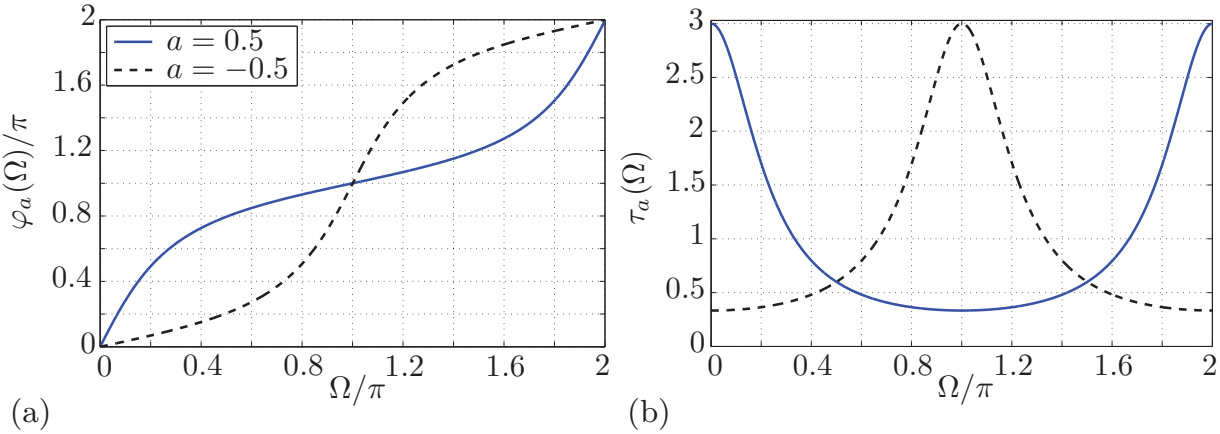

Figure 2.7: *Frequency responses of allpass filters of first order with real poles:*
(a) *phase response*
(b) *group delay.*

The phase response can be expressed as follows

$$\varphi_a(\Omega) = \Omega + 2\,\arctan\!\left(\frac{\alpha\,\sin(\Omega-\gamma)}{1-\alpha\,\cos(\Omega-\gamma)}\right) + 2\,\pi\,\chi(\Omega) \tag{2.54a}$$

$$= -\Omega + 2\,\arctan\!\left(\frac{\sin\Omega - \alpha\,\sin\gamma}{\cos\Omega - \alpha\,\cos\gamma}\right) + 2\,\pi\,\chi(\Omega)\,. \tag{2.54b}$$

Calculating the angle of a complex number by the inverse tangent function yields the principal value, which is within the range $-\pi$ to π. This can cause phase jumps of $2\,\pi$, which lead to discontinuities. This effect is avoided by the function $\chi(\Omega) \in \mathbb{Z}$, which ensures that the phase response is a continuous function for all frequencies (see also [OSB99]). This *unwrapped* phase response is considered in this work to ease the treatment. The group delay can be obtained by the derivative of the phase response

$$\tau_a(\Omega) = \frac{\partial\,\varphi_a(\Omega)}{\partial\,\Omega} = \frac{1-\alpha^2}{1-2\,\alpha\,\cos(\Omega-\gamma)+\alpha^2}\,. \tag{2.55}$$

The group delay is always positive and has extrema given by

$$\tau_{\max} = \max_{\Omega}\{\tau_a(\Omega)\} = \frac{1+|\alpha|}{1-|\alpha|} \quad \text{for} \quad \Omega = \gamma + \frac{\pi}{2}\Big(1-\operatorname{sign}(\alpha)\Big) \tag{2.56a}$$

$$\tau_{\min} = \min_{\Omega}\{\tau_a(\Omega)\} = \frac{1-|\alpha|}{1+|\alpha|} \quad \text{for} \quad \Omega = \gamma + \frac{\pi}{2}\Big(1+\operatorname{sign}(\alpha)\Big)\,. \tag{2.56b}$$

For allpass filters with real pole $a = \alpha$, the above equations apply with $\gamma = 0$. Phase response and group delay of such allpass filters are exemplified in Figure 2.7.

There exist different structures to implement an allpass filter, which becomes important, among others, w.r.t. a (fixed-point) implementation on a digital signal processor (DSP), e.g., [Mit98]. If not mentioned otherwise, the allpass filter implementation of Figure 2.8 is considered henceforth.

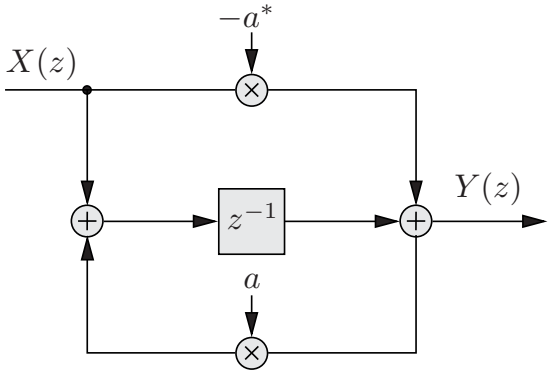

Figure 2.8: *Implementation of an allpass filter of first order in a direct form.*

The frequency response of an allpass filter of higher order according to Eq. (2.48) reads

$$A^{[K]}\left(e^{j\,\Omega}\right) = e^{-j\,\varphi_{\boldsymbol{a}}^{[K]}(\Omega)} \tag{2.57}$$

with phase response and group delay given by

$$\begin{aligned}\varphi_{\boldsymbol{a}}^{[K]}(\Omega) &= \sum_{m=1}^{K} \varphi_{a(m)}(\Omega) \\ &= K\,\Omega + 2\,\sum_{m=1}^{K} \arctan\left(\frac{\alpha(m)\,\sin\left(\Omega-\gamma(m)\right)}{1-\alpha(m)\,\cos\left(\Omega-\gamma(m)\right)}\right)\end{aligned} \tag{2.58}$$

$$\begin{aligned}\tau_{\boldsymbol{a}}^{[K]}(\Omega) &= \sum_{m=1}^{K} \tau_{a(m)}(\Omega) \\ &= \sum_{m=1}^{K} \frac{1-\alpha^2(m)}{1-2\,\alpha(m)\,\cos\left(\Omega-\gamma(m)\right)+\alpha^2(m)}\,.\end{aligned} \tag{2.59}$$

The unwrapped phase response of an allpass filter is monotonically increasing so that the group delay is always positive, which follows from Eq. (2.54) and Eq. (2.55).

An allpass filter which consists of a cascade of L_{ac} identical allpass filters of first order is termed as *allpass (filter) chain*. The system function for a chain of $K = L_{\mathrm{ac}}$ allpass filters is written

$$A^{L_{\mathrm{ac}}}(z) = \left(A^{[1]}(z)\right)^{L_{\mathrm{ac}}} \tag{2.60}$$

such that Eq. (2.58) and Eq. (2.59) reduce to

$$\varphi_{\boldsymbol{a}}^{[L_{\mathrm{ac}}]}(\Omega) = L_{\mathrm{ac}} \cdot \varphi_a(\Omega) \tag{2.61}$$

$$\tau_{\boldsymbol{a}}^{[L_{\mathrm{ac}}]}(\Omega) = L_{\mathrm{ac}} \cdot \tau_a(\Omega)\,. \tag{2.62}$$

A more comprehensive treatment of allpass chains can be found in [Kap98]. The design of filter-banks by means of allpass filters is treated in the following chapter(s).

Chapter 3

Recursive QMF-Banks

The design of filter-banks by means of *quadrature-mirror filters* (QMFs) is a well-known approach, e.g., [CR83, Vai93, Fli93]. A QMF-bank is a critically subsampled two-channel filter-bank originally proposed in [CEG76, EG77]. QMF-banks and variants thereof are used for a variety of applications such as subband coding or signal compression, e.g., [VK95, SPA07]. Most design proposals for QMF-banks consider FIR filters, cf., [VK95]. The main advantage of FIR QMF-banks over their IIR counterparts is that a system with linear-phase filters or perfect reconstruction can be realized more easily. However, IIR filter-banks are an attractive alternative as they can achieve a similar frequency selectivity as FIR filter-banks but with a much lower filter degree, which implies a lower signal delay and a lower computational complexity.

A common approach to realize a recursive QMF-bank is to use *allpass polyphase filters* [Weg79, Sar85]. Allpass polyphase filters can also be employed for the construction of a critically subsampled M-channel DFT filter-bank [HR90, RS87] also termed as *Pseudo QMF-bank*. A decisive advantage of such allpass-based analysis filter-banks is that they require only a low number of filter coefficients. A perfect signal reconstruction can be achieved by a synthesis filter-bank whose polyphase components are given by the inverse system functions of the allpass polyphase filters of the analysis filter-bank. However, such synthesis filters are either stable and anti-causal or causal and unstable. There exist different approaches to tackle this problem.

One scheme to realize anti-causal synthesis filters is to buffer the input samples in order to perform a 'time-reversed' filtering. Such a technique is proposed in [Ram88, HR90] for signals of finite length such as digital images. For the processing of signals of 'infinite' length, such as speech or audio signals, the anti-causal filtering can be realized by a double-buffering schemes [MCB92, CM96]. The Pseudo QMF-bank of [MCB92] achieves perfect reconstruction, but requires the transmission of filter states to the synthesis filter-bank. This transmission is avoided by the NPR design of [CM96] which, however, requires a rather high signal delay in order to avoid noticeable signal distortions.

These problems can be circumvented by approximating the needed anti-causal IIR filters by causal FIR filters, which results in an IIR/FIR (Pseudo) QMF-bank with near-perfect reconstruction. One approach to calculate the FIR filter coefficients is to solve this approximation problem numerically, e.g., by linear programming [ZAS98, LJW00, KDL00, KD02]. Another main approach is to determine the coefficients of the FIR synthesis filters by analytical expressions [GK01a, KB06]. Such a closed-form design can be applied to two-channel QMF-banks as well as Pseudo QMF-banks [GK01b, Gal02].

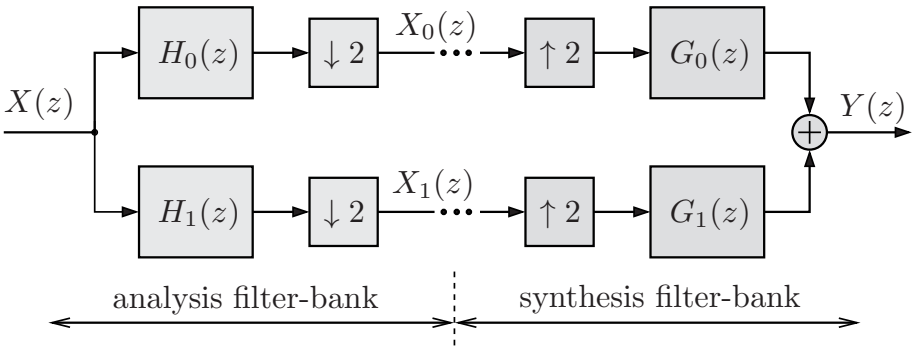

Figure 3.1: *General structure of a two-channel QMF-bank without spectral processing.*

The QMF-banks presented in this work are also derived by a closed-form design similar to the approach of [Gal02], but use allpass filters instead of FIR filters. A benefit of such an IIR/IIR QMF-bank is that amplitude distortions can be completely avoided and a lower algorithmic complexity is achieved in comparison to the related IIR/FIR QMF-bank designs of [GK01a, KB06, KDL00, KD02]. The new QMF-bank designs can also be extended to Pseudo QMF-banks similar to the designs of [Gal02].

The remainder of this chapter is organized as follows: The considered allpass-based QMF-banks are introduced in Sec. 3.1.1. The new QMF-bank designs are presented in Sec. 3.1.2. The extension of these designs to Pseudo QMF-banks is treated in Sec. 3.2. A central issue in the design of allpass-based filter-banks is to perform a phase equalization at the synthesis side. Therefore, different phase equalizer designs for this purpose are discussed in Sec. 3.3. The results of this chapter are finally summarized in Sec. 3.4.

3.1 Two-Channel QMF-Bank

The general structure of a critically subsampled two-channel quadrature-mirror filter-bank (QMF-bank) is shown in Figure 3.1, e.g., [Vai93]. This filter-bank is obtained from the general AS FB of Figure 2.1 for $M = 2$ and $R_i \equiv 2$. The input-output relation of Eq. (2.9) is now given by

$$\widehat{X}(z) = X(z) \cdot T_{\text{lin}}(z) + X(-z) \cdot T_{\text{alias}}(z) \tag{3.1}$$

with *linear transfer function*

$$T_{\text{lin}}(z) = \frac{1}{2}\Big(H_0(z) \cdot G_0(z) + H_1(z) \cdot G_1(z)\Big) \tag{3.2}$$

and *aliasing transfer function*

$$T_{\text{alias}}(z) = \frac{1}{2}\Big(H_0(-z) \cdot G_0(z) + H_1(-z) \cdot G_1(z)\Big)\,. \tag{3.3}$$

Thus, *perfect reconstruction* according to Eq. (2.13) is achieved if $T_{\mathrm{lin}}(z) = c_{\mathrm{s}} \cdot z^{-D_{\mathrm{o}}}$ and $T_{\mathrm{alias}}(z) \equiv 0$. If the analysis filters are related by

$$H_1(z) = H_0(-z), \tag{3.4}$$

they exhibit the property $\left|H_1\left(e^{j\,\Omega}\right)\right| = \left|H_0\left(e^{j\,(\pi-\Omega)}\right)\right|$ for FIR filters with real coefficients, which led to the term *quadrature-mirror filters* (QMFs) [EG77, Vai93]. Such an analysis filter-bank can be seen as special case of a DFT analysis filter-bank with $M = 2$ channels, cf., Sec. 2.2. The choice

$$G_0(z) = H_1(-z) \quad \text{and} \quad G_1(z) = -H_0(-z) \tag{3.5}$$

ensures complete *aliasing cancellation* ($T_{\mathrm{alias}}(z) \equiv 0$) and a linear transfer function given by

$$T_{\mathrm{lin}}(z) = \frac{1}{2}\left(H_0^2(z) - H_0^2(-z)\right). \tag{3.6}$$

Thus, the idea is to tolerate aliasing due to critical subsampling and to compensate these distortions by the synthesis filter-bank so that analysis filters with a limited stopband attenuation and non-zero transition bandwidth can be used. Due to Eq. (3.4) and Eq. (3.5), only a *single* prototype lowpass filter has to be designed.

The analysis filters can be represented by a type 1 *polyphase network* (PPN) according to Eq. (2.35) as follows

$$H_0(z) = H_{0,0}^{(2)}\left(z^2\right) + z^{-1}\, H_{0,1}^{(2)}\left(z^2\right) \tag{3.7a}$$

$$H_1(z) = H_{1,0}^{(2)}\left(z^2\right) + z^{-1}\, H_{1,1}^{(2)}\left(z^2\right) = H_{0,0}^{(2)}\left(z^2\right) - z^{-1}\, H_{0,1}^{(2)}\left(z^2\right) \tag{3.7b}$$

due to Eq. (3.4). Inserting Eq. (3.7) into Eq. (3.5) yields the following PPN representation for the synthesis filters

$$G_0(z) = H_{0,0}^{(2)}\left(z^2\right) + z^{-1}\, H_{0,1}^{(2)}\left(z^2\right) \tag{3.8a}$$

$$G_1(z) = -H_{0,0}^{(2)}\left(z^2\right) + z^{-1}\, H_{0,1}^{(2)}\left(z^2\right). \tag{3.8b}$$

The resulting PPN implementation is depicted in Figure 3.2 and termed as *standard* QMF-bank, cf., [Fli93, GG04].[1] The linear transfer function of Eq. (3.6) is now given by

$$T_{\mathrm{lin}}(z) = 2\, z^{-1}\, H_{0,0}^{(2)}\left(z^2\right) \cdot H_{0,1}^{(2)}\left(z^2\right). \tag{3.9}$$

For FIR filters, perfect reconstruction can be achieved, if and only if the polyphase components of Eq. (3.9) are given by [Vai93]

$$H_{0,0}^{(2)}(z) = h_0(l_0) \cdot z^{-l_0} \quad \text{and} \quad H_{0,1}^{(2)}(z) = h_0(l_1) \cdot z^{-l_1}. \tag{3.10}$$

However, this trivial solution does not permit filters with a high frequency selectivity.

There are different approaches to overcome this problem, e.g., [CR83, Vai93, Fli93]. One is to relax the PR constraint while another main approach is to strive for perfect reconstruction by giving up the condition of Eq. (3.4). These two approaches to design an FIR/FIR QMF-bank are briefly described in App. C.1.

[1] The term *standard* QMF-bank is not consistently used in literature.

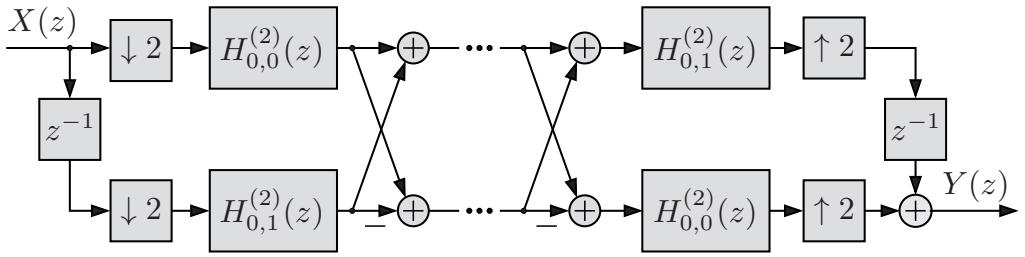

Figure 3.2: *PPN implementation of a two-channel standard QMF-bank.*

3.1.1 Allpass-Based QMF-Banks

Common design concepts for allpass-based QMF-banks are briefly described, which form the basis (and motivation) for the new design approach.

A wide family of rational system functions can be represented as sum of two allpass filters, e.g., [AL85, Sar85, VMN86, Vai93]. A Butterworth, Chebyshev, or elliptic *lowpass filter* is considered whose system function is given by

$$H_0(z) = \frac{A_I^{[K_I]}(z) + A_{II}^{[K_{II}]}(z)}{2} \,. \tag{3.11}$$

If the filter degree $D_\mathrm{f} = K_I + K_{II}$ of $H_0(z)$ is even, the allpass filters with system functions $A_I^{[K_I]}(z)$ and $A_{II}^{[K_{II}]}(z)$ have complex coefficients for their direct form implementation. The coefficients of $A_I^{[K_I]}(z)$ are complex conjugate to those of $A_{II}^{[K_{II}]}(z)$ and the filter degrees are related by $K_I = K_{II} = D_\mathrm{f}/2$.

If the filter degree D_f is *odd*, which is considered here, the coefficients of the two allpass filters are *real* and $D_\mathrm{f} = K_I + K_{II}$. The properties of these allpass-based filters follow from the *allpass decomposition theorem* [Vai93]:

The irreducible rational system functions $H_0(z)$ and $H_1(z)$ of two stable IIR filters with odd degree $D_\mathrm{f} = K_I + K_{II}$ can be expressed by the sum of two allpass filters with degrees K_I and K_{II} and real coefficients according to

$$H_0(z) = \frac{C_I(z)}{D_\mathrm{com}(z)} = \frac{\sum\limits_{m=0}^{D_\mathrm{f}} c_I(m) \cdot z^{-m}}{\sum\limits_{m=0}^{D_\mathrm{f}} d(m)} = \frac{A_I^{[K_I]}(z) + A_{II}^{[K_{II}]}(z)}{2} \tag{3.12a}$$

$$H_1(z) = \frac{C_{II}(z)}{D_\mathrm{com}(z)} = \frac{\sum\limits_{m=0}^{D_\mathrm{f}} c_{II}(n) \cdot z^{-m}}{\sum\limits_{m=0}^{D_\mathrm{f}} d(m)} = \frac{A_I^{[K_I]}(z) - A_{II}^{[K_{II}]}(z)}{2} \tag{3.12b}$$

if the following conditions are satisfied:

- The rational system functions of $H_0(z)$ and $H_1(z)$ have real coefficients and their magnitude responses are bounded by unity, i.e., $\left|H_i\left(e^{j\,\Omega}\right)\right| \leq 1$ for $i \in \{0, 1\}$.

- The polynomial $C_I(z)$ is symmetric and $C_{II}(z)$ is anti-symmetric such that

$$c_I(m) = c_I(D_\mathrm{f} - m) \;\wedge\; c_{II}(m) = -c_{II}(D_\mathrm{f} - m) \tag{3.13}$$

  for $m \in \{\,0, 1, \ldots, D_\mathrm{f}\,\}$ and $c_I(m), c_{II}(m) \in \mathbb{R}$.

- $H_0(z)$ and $H_1(z)$ are *power complementary*, i.e., $\left|H_0\left(e^{j\,\Omega}\right)\right|^2 + \left|H_1\left(e^{j\,\Omega}\right)\right|^2 = 1$.

Due to the last property, this class of subband filters is also referred to as *power symmetric* filters. Such filters can be used to construct an IIR QMF-bank, e.g., [RMV88, Vai93]. The choice

$$A_I^{[K_I]}(z) = A_0^{[K_0]}\left(z^2\right) \quad \text{and} \quad A_{II}^{[K_{II}]}(z) = z^{-1}\, A_1^{[K_1]}\left(z^2\right) \tag{3.14}$$

$$\text{with} \quad A_i^{[K_i]}(z) = \prod_{m=1}^{K_i} \frac{1 - a_i^*(m)\cdot z}{z - a_i(m)}; \quad i \in \{\,0, 1\,\} \tag{3.15}$$

for the two allpass filters of Eq. (3.12) yields the analysis filters

$$H_0(z) = \frac{1}{2}\left(A_0^{[K_0]}\left(z^2\right) + z^{-1}\, A_1^{[K_1]}\left(z^2\right)\right) \tag{3.16a}$$

$$H_1(z) = \frac{1}{2}\left(A_0^{[K_0]}\left(z^2\right) - z^{-1}\, A_1^{[K_1]}\left(z^2\right)\right). \tag{3.16b}$$

These *allpass-based* analysis filters of a QMF-bank are related by Eq. (3.4). Applying Eq. (3.5) to Eq. (3.16) yields the synthesis filters

$$G_0(z) = \frac{1}{2}\left(A_0^{[K_0]}\left(z^2\right) + z^{-1}\, A_1^{[K_1]}\left(z^2\right)\right) \tag{3.17a}$$

$$G_1(z) = \frac{1}{2}\left(-A_0^{[K_0]}\left(z^2\right) + z^{-1}\, A_1^{[K_1]}\left(z^2\right)\right). \tag{3.17b}$$

The filter degree of these subband filters is odd and amounts to $D_\mathrm{f} = 2\,(K_0 + K_1) + 1$. The polyphase components of the standard QMF-bank of Figure 3.2 now read

$$H_{0,0}^{(2)}(z) = \frac{1}{2}\, A_0^{[K_0]}(z) \quad \text{and} \quad H_{0,1}^{(2)}(z) = \frac{1}{2}\, A_1^{[K_1]}(z)\,. \tag{3.18}$$

This realization of the standard QMF-bank is referred to as *classical* allpass-based QMF-bank in this work.[2] The linear transfer function of Eq. (3.9) is now given by

$$T_\mathrm{lin}(z) = \frac{1}{2}\, z^{-1}\, A_0^{[K_0]}\left(z^2\right) \cdot A_1^{[K_1]}\left(z^2\right) \tag{3.19}$$

so that $\left|T_\mathrm{lin}\left(e^{j\,\Omega}\right)\right| = 1/2 \;\forall\; \Omega$. Therefore, this IIR filter-bank design causes only phase distortions, but no amplitude and aliasing distortions. The amount of phase distortions depends on the allpass sub-filters. For example, the choice $A_1^{[K_1]}(z) = z^{-K_1}$ is proposed in [ZI95], which yields the linear transfer function

$$T_\mathrm{lin}(z) = \frac{1}{2}\, A_0^{[K_0]}\left(z^2\right) \cdot z^{-(2\,K_1+1)}\,. \tag{3.20}$$

[2] There exists no common term for this type of QMF-bank in literature.

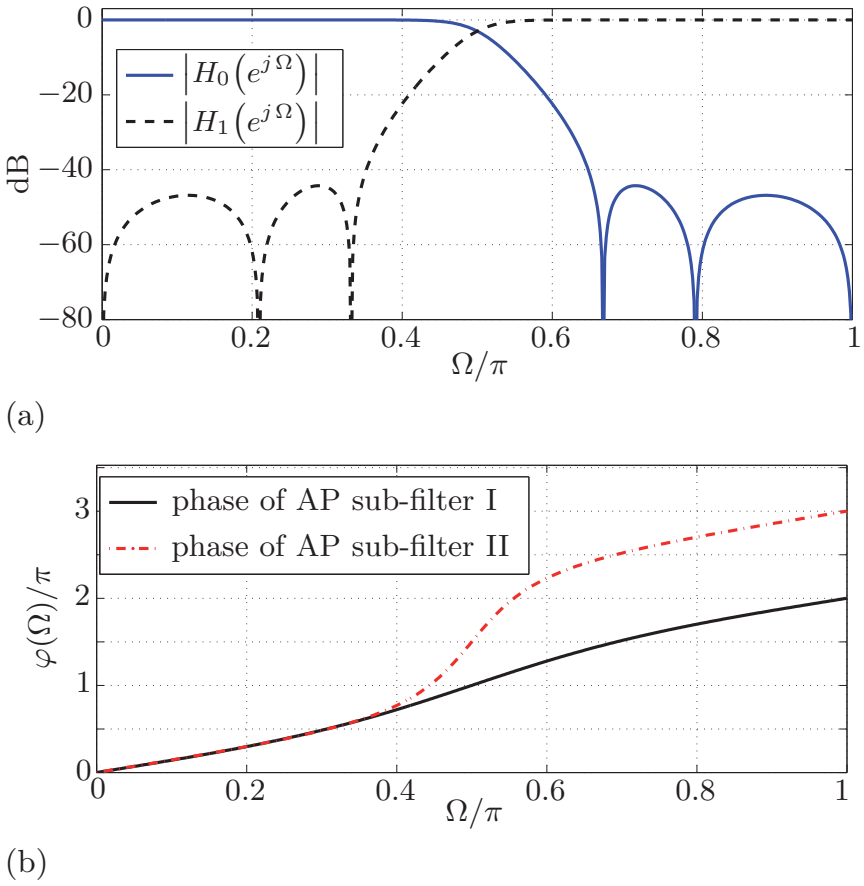

Figure 3.3: *Allpass-based analysis filters with coefficients* $a_0 = -0.1806$ *and* $a_1 = -0.6485$ *obtained by an LS error design for* $\Omega_s = 0.64\,\pi$*:*
(a) *magnitude responses of the analysis filters*
(b) *phase responses of the allpass sub-filters of the prototype lowpass filter.*

By this, lower phase distortions can be achieved than for the classical QMF-bank and the subband filters have an almost linear phase response in the passband, cf., [ZI95]. A drawback of this approach is that the degrees of freedom to design the prototype lowpass filter are reduced such that it is more difficult to achieve a desired filter characteristic regarding stopband attenuation, transition bandwidth etc.

The coefficients of the prototype lowpass filter can be determined by a least-squares (LS) error design approach, e.g., [Vai93]. The allpass filter coefficients are determined by minimizing the stopband energy of the prototype lowpass filter

$$E_{\mathrm{S}} = \int_{\Omega_{\mathrm{s}}}^{\pi} \left| H_0\left(e^{j\,\Omega}\right) \right|^2 \,\mathrm{d}\,\Omega\,. \tag{3.21}$$

This approach yields, for example, the allpass poles $a_0 = -0.1806$ and $a_1 = -0.6485$ for a stopband frequency of $\Omega_{\mathrm{s}} = 0.64\,\pi$ and allpass filters of first order, i.e., $K_0 = K_1 = 1$. The corresponding analysis filters of degree $D_{\mathrm{f}} = 5$ are examined in Figure 3.3. The phase responses $\varphi_{K_I}(\Omega)$ and $\varphi_{K_{II}}(\Omega)$ of the allpass sub-filters according to Eq. (3.12a) are also plotted to demonstrate the design principle of such filters: In the passband

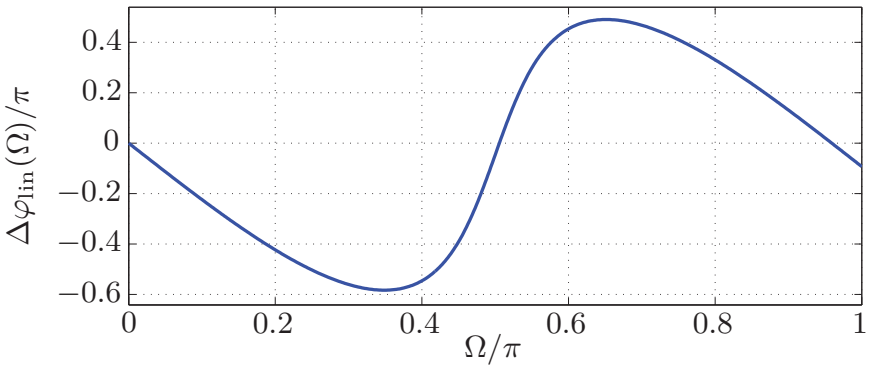

Figure 3.4: *Phase error $\Delta\varphi_{lin}(\Omega) = \varphi_{lin}(\Omega) - 18\,\Omega$ for the classical QMF-bank with allpass-based subband filters according to Figure 3.3.*

$0 \leq \Omega \leq \Omega_{\mathrm{p}}$, the phase responses of the two allpass filters are approximately equal so that $\left|H_0\left(e^{j\,\Omega}\right)\right| \approx 1$ in this region. In the stopband $\Omega_{\mathrm{s}} \leq \Omega \leq \pi$, the phase responses differ approximately by π so that $\left|H_0\left(e^{j\,\Omega}\right)\right| \approx 0$ in this region. The plot of the magnitude responses reveals that it is possible to achieve a stopband attenuation of 43 dB with a filter degree of 5 only, which cannot be accomplished by an FIR filter with such a low filter degree (cf., Sec. C.1).

It is obvious from Eq. (3.19) that the overall phase response of the classical allpass-based QMF-bank is non-linear. This is exemplified in Figure 3.4 where the phase error according to Eq. (2.16) is plotted. Hence, the classical allpass-based QMF-bank has the advantages that it possesses a low signal delay and a low computational complexity. In addition, it achieves a complete aliasing cancellation and causes no amplitude distortions. However, the main problem of this approach are the considerable phase distortions, which become even stronger if allpass sub-filters of higher degrees are used in order to achieve an increased stopband attenuation and a lower transition bandwidth, respectively.

The considered allpass-based analysis filters according to Eq. (3.12) are not the only way to construct an IIR QMF-bank. The use of the *lifting scheme* is an important alternative to design an allpass-based QMF-bank with perfect reconstruction [PKVA95, CMH00]. The system functions of the analysis filters are given by

$$H_0(z) = z^{-2\,d_0} + z^{-1}\,\mathcal{A}_0\left(z^2\right) \tag{3.22a}$$

$$H_1(z) = -\mathcal{B}_1\left(z^2\right) \cdot H_0(z) + z^{-2\,d_1-1}\,. \tag{3.22b}$$

The analysis and synthesis filters are related by Eq. (3.5) and the linear transfer function of this filter-bank reads

$$T_{\mathrm{lin}}(z) = 2\,z^{-2\,d_0-2\,d_1-1}\,. \tag{3.23}$$

One option is to use an allpass filter for $\mathcal{A}_0(z)$ and a linear-phase FIR filter for $\mathcal{B}_1(z)$ [CMH00]. An alternative, purely *allpass-based* design is considered in [PKVA95]. The choice $\mathcal{A}_0(z) = \mathcal{B}_1(z) = A^{[K]}(z)$, $d_0 = K$ and $d_1 = 2K - 1$ for Eq. (3.22) leads to the filter-bank shown in Figure 3.5. The filter coefficients can be obtained by minimization

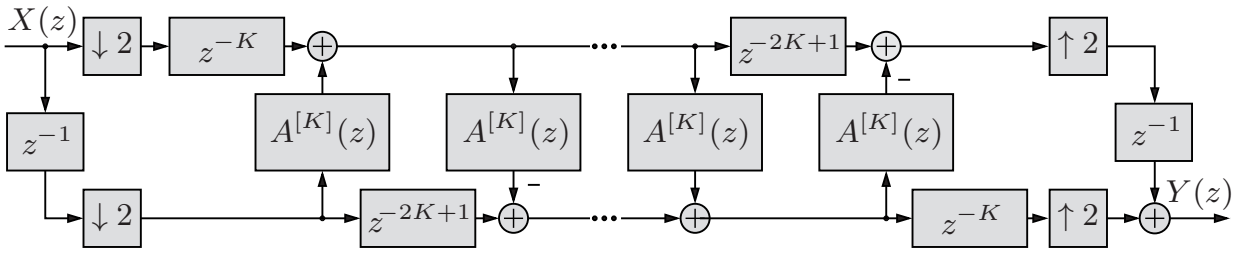

Figure 3.5: *Realization of an allpass-based QMF-bank with perfect reconstruction by means of the lifting scheme.*

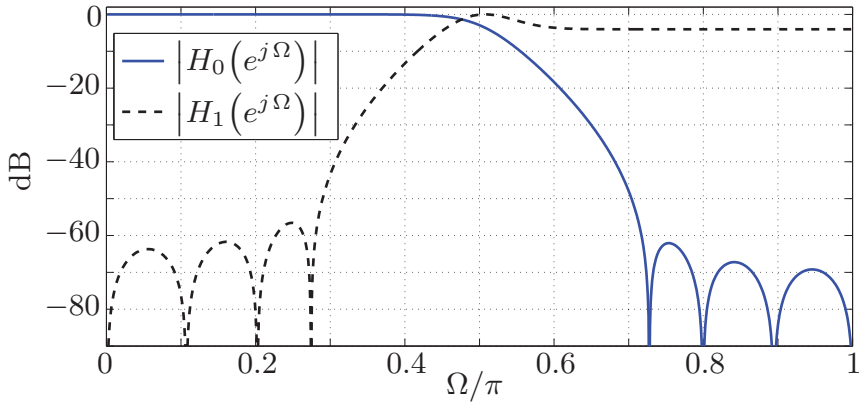

Figure 3.6: *Magnitude responses of the analysis filters for the allpass-based IIR QMF-bank of Figure 3.5 with* $K = 3$ *and allpass poles* $a(1) = 0.4551$, $a(2) = -0.0688$ *and* $a(3) = 0.0114$.

of the stopband energy of the analysis filters [PKVA95]. A drawback of such designs based on the lifting scheme is that it is more difficult to obtain subband filters with a high frequency selectivity due to the PR constraint being structurally imposed on the design process. This is exemplified in Figure 3.6. The analysis filters are designed by means of an LS error minimization of the stopband energy of Eq. (3.21) for a stopband frequency of $\Omega_s = 0.7\,\pi$. It can be observed that the analysis filters exhibit a high transition bandwidth and a 'superelevation' in the transition band.[3]

Hence, the design of allpass-based QMF-banks with perfect reconstruction is possible, but the constraint for perfect reconstruction can be overly restrictive for some applications. An example are speech and audio processing systems where small signal distortions remain mostly unnoticed. For such applications, it is beneficial to tolerate a small signal reconstruction error in order to obtain more degrees of freedom for the filter-bank design. These degrees of freedom might be used, for instance, to obtain subband filters with an improved frequency selectivity in order to reduce the cross-talk. Another option can be to trade the signal reconstruction error against a reduced signal delay and computational complexity, respectively. An allpass-based QMF-bank design which pursues this concept is presented in the following.

[3] A discussion of further QMF-bank designs which, for example, avoid a 'superelevation' in the transition band can be found in [SB02, Bre03].

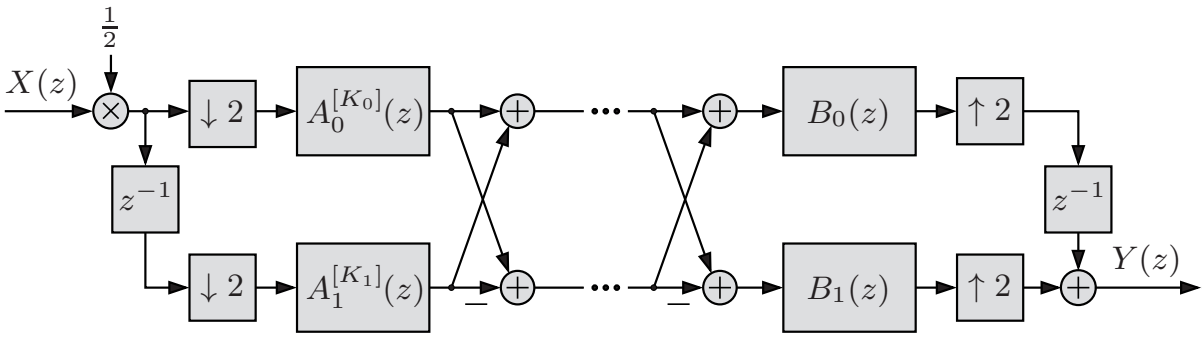

Figure 3.7: *General PPN implementation of a two-channel QMF-bank with allpass-based analysis filters.*

3.1.2 New IIR/IIR QMF-Bank Designs

Different closed-form designs for a purely allpass-based QMF-bank are now presented based on [LV08c]. The presented designs achieve either a partial or complete aliasing cancellation in the same manner as the IIR/FIR QMF-bank designs of [Gal02, GK01a, KB06], where the synthesis polyphase components consist now of allpass filters instead of FIR filters, which leads to filter-banks with very different properties.

3.1.2.1 Concept

The PPN representation of the considered QMF-bank is shown in Figure 3.7, e.g., [Gal02, KD02]. The analysis filters comply with Eq. (3.16), but the synthesis filters are now given by

$$G_0(z) = B_1\left(z^2\right) + z^{-1}\, B_0\left(z^2\right) \tag{3.24a}$$

$$G_1(z) = -B_1\left(z^2\right) + z^{-1}\, B_0\left(z^2\right) \tag{3.24b}$$

instead of Eq. (3.17). The linear transfer function of Eq. (3.2) and aliasing transfer function of Eq. (3.3) turn into

$$T_{\text{lin}}(z) = \frac{z^{-1}}{2}\left(A_0^{[K_0]}\left(z^2\right)\cdot B_0\left(z^2\right) + A_1^{[K_1]}\left(z^2\right)\cdot B_1\left(z^2\right)\right) \tag{3.25}$$

$$T_{\text{alias}}(z) = \frac{z^{-1}}{2}\left(A_0^{[K_0]}\left(z^2\right)\cdot B_0\left(z^2\right) - A_1^{[K_1]}\left(z^2\right)\cdot B_1\left(z^2\right)\right)\,. \tag{3.26}$$

Thus, a complete aliasing cancellation is achieved if

$$A_0^{[K_0]}(z)\cdot B_0(z) = A_1^{[K_1]}(z)\cdot B_1(z)\,. \tag{3.27}$$

The more demanding condition for perfect reconstruction reads

$$A_i^{[K_i]}(z)\cdot B_i(z) \stackrel{!}{=} z^{-\bar{\psi}} \quad \text{for} \quad \bar{\psi}\geq 0;\quad i\in\{\,0,1\,\}\,. \tag{3.28}$$

This requirement states a *phase equalization* problem: The non-linear phase response of the allpass filter shall be equalized by a phase equalizer to obtain an (almost) linear

overall phase response and a constant magnitude response. The trivial solution

$$B_i(z) = \left(A_i^{[K_i]}(z) \right)^{-1} \tag{3.29}$$

yields either an anti-causal or unstable IIR filter dependent on the region of convergence. This problem is avoided by the following allpass phase equalizer

$$\mathcal{P}_{i,1}^{\mathrm{ap}}(z) = \prod_{n=0}^{J_i-1} \frac{1 + (a_i^* z)^{2^n}}{z^{2^n} + a_i^{2^n}}; \quad J_i \in \mathbb{N}_0 \quad \text{for} \quad i \in \{\,0, 1\,\} \tag{3.30}$$

designed for an allpass filter of *first order* according to Eq. (2.52)

$$A_i(z) = \frac{1 - a_i^* z}{z - a_i}\,. \tag{3.31}$$

It should be noted that Eq. (3.30) includes the empty product

$$\mathcal{P}_{i,1}^{\mathrm{ap}}(z) \equiv 1 \quad \text{for} \quad J_i = 0 \tag{3.32}$$

as special case. The transfer function of allpass filter and phase equalizer

$$A_i(z) \cdot \mathcal{P}_{i,1}^{\mathrm{ap}}(z) = \frac{1 - (a_i^* z)^{2^{J_i}}}{z^{2^{J_i}} - a_i^{2^{J_i}}}; \quad i \in \{0, 1\} \tag{3.33}$$

is an allpass filter of degree 2^{J_i}. For allpass filters of *higher order* according to Eq. (3.15), the equalization can be accomplished by cascading the phase equalizer of Eq. (3.30):

$$\mathcal{P}_{i,K_i}^{\mathrm{ap}}(z) = \prod_{m=1}^{K_i} \prod_{n=0}^{J_i(m)-1} \frac{1 + (a_i^*(m) \cdot z)^{2^n}}{z^{2^n} + (a_i(m))^{2^n}}; \quad J_i(m) \in \mathbb{N}_0\,. \tag{3.34}$$

Such a kind of phase equalizer is referred to as *cascaded phase equalizer* in this work. The filter degree of this allpass phase equalizer amounts to

$$N_i^{\mathrm{ap}} = \sum_{m=1}^{K_i} \left(2^{J_i(m)} - 1 \right)\,. \tag{3.35}$$

The transfer function of an allpass filter of degree K_i and its phase equalizer

$$\Psi_i^{\mathrm{ap}}(z) = A_i^{[K_i]}(z) \cdot \mathcal{P}_{i,K_i}^{\mathrm{ap}}(z) \tag{3.36a}$$

$$= \prod_{m=1}^{K_i} \frac{1 - (a_i^*(m) \cdot z)^{I(i,m)}}{z^{I(i,m)} - (a_i(m))^{I(i,m)}}; \quad I(i,m) = 2^{J_i(m)} \tag{3.36b}$$

is an allpass filter of degree

$$d_i = \sum_{m=1}^{K_i} I(i,m) \;\forall\; i \in \{\,0, 1\,\}\,. \tag{3.37}$$

The allpass filter of Eq. (3.36) is always stable since $|a_i(m)| < 1$ and tends to z^{-d_i} for growing values of $I(i,m)$. It should be noted that the allpass property is maintained even for quantized allpass coefficients and that the poles of the allpass phase equalizer of Eq. (3.36) are closer to the origin than those of the allpass filter $A_i^{[K_i]}(z)$.

A more comprehensive treatment of the proposed allpass phase equalizer as well as a comparison with alternative phase equalizer designs for allpass-based filter-banks is conducted later in Sec. 3.3.

3.1.2.2 Design I

The first design follows from Eq. (3.28), which can be approximately fulfilled by the following choice for the synthesis polyphase filters

$$B_0(z) = \mathcal{P}_{0,K_0}^{\mathrm{ap}}(z) \cdot z^{-(d_1-d_0)} \tag{3.38a}$$

$$B_1(z) = \mathcal{P}_{1,K_1}^{\mathrm{ap}}(z) \tag{3.38b}$$

with allpass phase equalizer given by Eq. (3.34). The linear transfer function is obtained by inserting Eq. (3.38) into Eq. (3.25) such that

$$T_{\mathrm{lin}}(z) = \frac{z^{-1}}{2}\left(\Psi_0^{\mathrm{ap}}\left(z^2\right) \cdot z^{-2\,(d_1-d_0)} + \Psi_1^{\mathrm{ap}}\left(z^2\right)\right) \tag{3.39}$$

due to Eq. (3.36). The delay element $z^{-2\,(d_1-d_0)}$ accounts for the different signal delays of $\Psi_0^{\mathrm{ap}}\left(z^2\right)$ and $\Psi_0^{\mathrm{ap}}\left(z^2\right)$ where it is assumed that $d_1 \geq d_0$ w.l.o.g. Thus, the transfer function of Eq. (3.39) tends to $z^{-(2\,d_1+1)}$, if the values for d_0 and d_1 are increased. If allpass polyphase filters of first order are used for the analysis filters, Eq. (3.36) reduces to Eq. (3.33) such that Eq. (3.39) is given by

$$T_{\mathrm{lin}}(z) = \frac{z^{-2\,(d_1-d_0)-1}}{2}\,\frac{1-\left(a_0^* z^2\right)^{d_0}}{z^{2\,d_0}-a_0^{d_0}} + \frac{z^{-1}}{2}\,\frac{1-\left(a_1^* z^2\right)^{d_1}}{z^{2\,d_1}-a_1^{d_1}}\,. \tag{3.40}$$

The aliasing transfer function is obtained by inserting Eq. (3.38) into Eq. (3.26):

$$T_{\mathrm{alias}}(z) = \frac{z^{-1}}{2}\left(\Psi_0^{\mathrm{ap}}\left(z^2\right) \cdot z^{-2\,(d_1-d_0)} - \Psi_1^{\mathrm{ap}}\left(z^2\right)\right) \tag{3.41}$$

which evaluates for allpass polyphase filters of first order to

$$T_{\mathrm{alias}}(z) = \frac{z^{-2\,(d_1-d_0)-1}}{2}\,\frac{1-\left(a_0^* z^2\right)^{d_0}}{z^{2d_0}-a_0^{d_0}} - \frac{z^{-1}}{2}\,\frac{1-\left(a_1^* z^2\right)^{d_1}}{z^{2d_1}-a_1^{d_1}}\,. \tag{3.42}$$

If $d_0 = d_1$, the transfer functions of Eq. (3.40) and Eq. (3.42) simplify to

$$T_{\mathrm{lin}}(z) = \frac{z^{-1}}{2}\left(\frac{1-\left(a_0^* z^2\right)^{d_0}}{z^{2d_0}-a_0^{d_0}} + \frac{1-\left(a_1^* z^2\right)^{d_0}}{z^{2d_0}-a_1^{d_0}}\right) \tag{3.43}$$

$$T_{\mathrm{alias}}(z) = \frac{z^{-1}}{2}\left(\frac{1-\left(a_0^* z^2\right)^{d_0}}{z^{2d_0}-a_0^{d_0}} - \frac{1-\left(a_1^* z^2\right)^{d_0}}{z^{2d_0}-a_1^{d_0}}\right)\,. \tag{3.44}$$

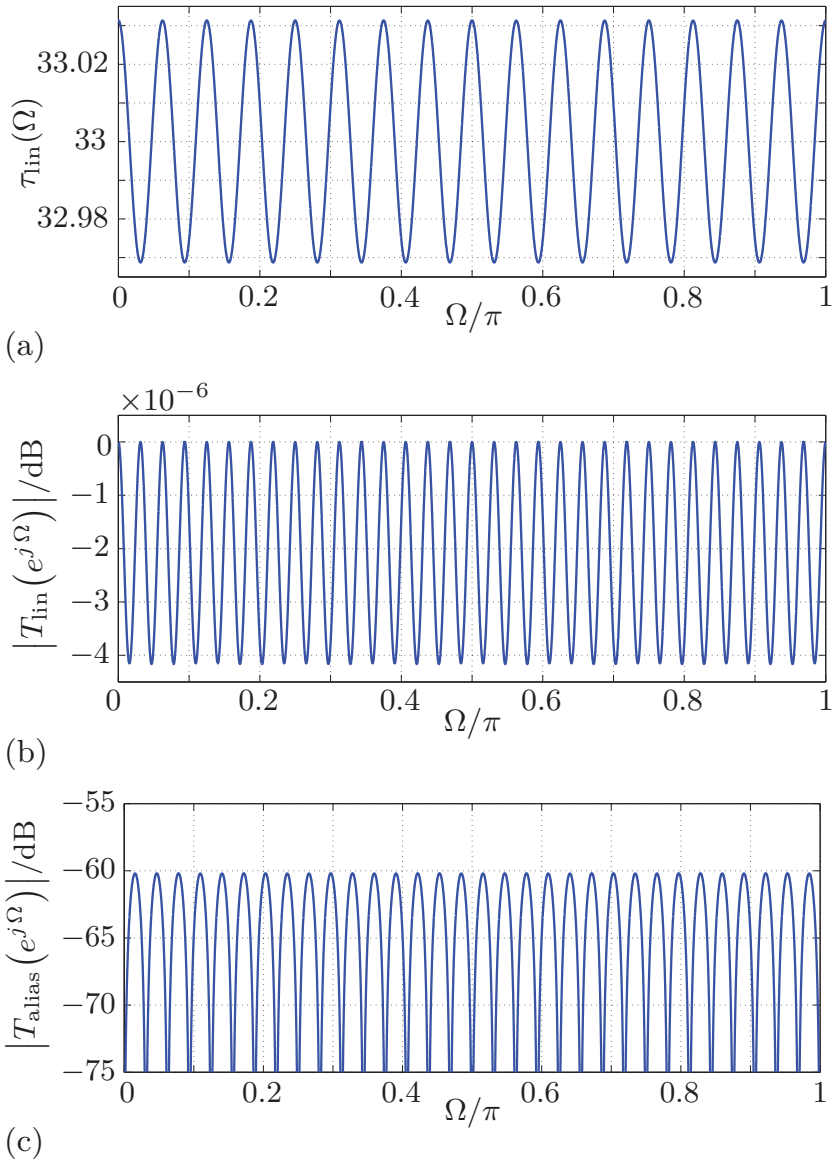

Figure 3.8: *Transfer functions for IIR QMF-bank design I with parameters* $d_0 = 8$, $d_1 = 16$ *and analysis filters according to Figure 3.3:*
(a) *linear group delay*
(b) *magnitude response of the linear transfer function*
(c) *magnitude response of the aliasing transfer function.*

Example 3.1: An allpass-based QMF-bank with $K_0 = K_1 = 1$ is considered. Figure 3.3-a shows the magnitude responses of the employed analysis filters, which are almost identical to those of the synthesis filters (hence not plotted). The parameters $d_0 = 8$ and $d_1 = 16$ are used for the synthesis filter-bank design according to Eq. (3.38). Figure 3.8 shows group delay and magnitude response of the linear transfer function according to Eq. (3.40) as well as the magnitude response of the aliasing transfer function given by Eq. (3.42). The new design causes almost no amplitude distortions and only a low amount of aliasing and group delay distortions. The amount of signal distortions can thereby be easily traded against delay and complexity by the choice for d_0 and d_1.

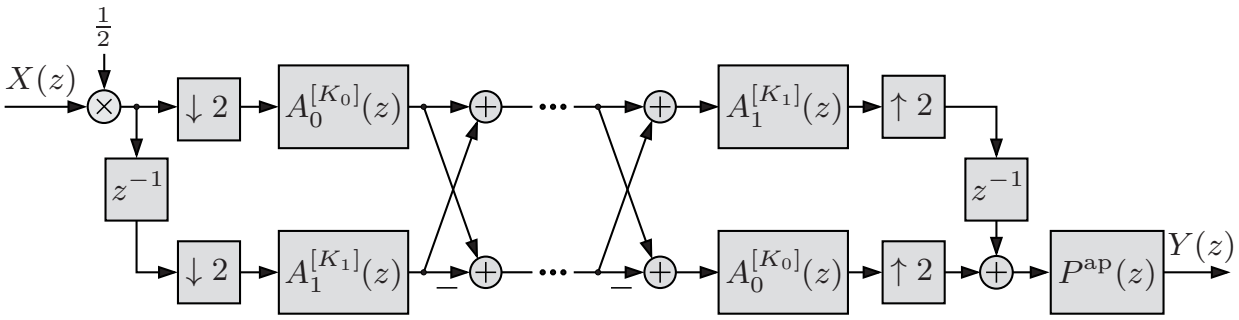

Figure 3.9: *Implementation of IIR QMF-bank design II as a cascade of the classical allpass-based QMF-bank and a subsequent allpass phase equalizer.*

3.1.2.3 Design II

The condition of Eq. (3.27) for complete aliasing cancellation can be met by the following synthesis polyphase filters

$$B_0(z) = \mathcal{P}^{\mathrm{ap}}_{0,K_0}(z) \cdot \Psi^{\mathrm{ap}}_1(z) \tag{3.45a}$$

$$B_1(z) = \mathcal{P}^{\mathrm{ap}}_{1,K_1}(z) \cdot \Psi^{\mathrm{ap}}_0(z) \tag{3.45b}$$

with allpass phase equalizers and transfer functions given by Eq. (3.34) and Eq. (3.36), respectively. The linear transfer function of Eq. (3.25) is now given by

$$T_{\mathrm{lin}}(z) = z^{-1}\, \Psi^{\mathrm{ap}}_0\left(z^2\right) \cdot \Psi^{\mathrm{ap}}_1\left(z^2\right) \tag{3.46}$$

which is an *allpass* filter of degree $2\,(d_0 + d_1) + 1$. The linear transfer function reads

$$T_{\mathrm{lin}}(z) = z^{-1}\, \frac{1 - \left(a_0^* z^2\right)^{d_0}}{z^{2d_0} - a_0^{d_0}}\, \frac{1 - \left(a_1^* z^2\right)^{d_1}}{z^{2d_1} - a_1^{d_1}}, \tag{3.47}$$

if allpass filters of first order are used for the analysis polyphase components.

Due to Eq. (3.36a), the linear transfer function of Eq. (3.46) can be decomposed into the linear transfer function of the classical allpass-based QMF-bank according to Eq. (3.19) and a subsequent allpass phase equalizer

$$T_{\mathrm{lin}}(z) = 2 \cdot \underbrace{\frac{1}{2}\, z^{-1}\, A_0^{[K_0]}\left(z^2\right) \cdot A_1^{[K_1]}\left(z^2\right)}_{\text{Eq. (3.19)}} \cdot \underbrace{\mathcal{P}^{\mathrm{ap}}_{0,K_0}\left(z^2\right) \cdot \mathcal{P}^{\mathrm{ap}}_{1,K_1}\left(z^2\right)}_{= P^{\mathrm{ap}}(z)}\,. \tag{3.48}$$

The corresponding QMF-bank is shown in Figure 3.9. Hence, the classical allpass-based QMF-bank is a *special case* of the new design and obtained if Eq. (3.32) applies. This generalization allows to make the remaining phase distortions arbitrarily small in dependence of the values for d_0 and d_1, but without introducing amplitude distortions.

Example 3.2: Example 3.1 is now repeated with the new synthesis filter-bank design II according to Eq. (3.45). The group delay of the linear transfer function of

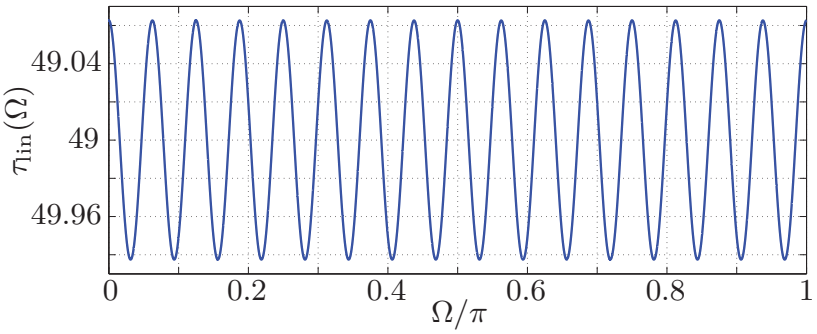

Figure 3.10: *Overall group delay for IIR QMF-bank design II with parameters* $d_0 = 8$, $d_1 = 16$ *and analysis filters according to Figure 3.3.*

Eq. (3.47) is plotted in Figure 3.8. A comparison with Figure 3.8-a shows that the group delay is higher and exhibits greater ripples as for the previous design I, but the design II avoids aliasing and magnitude distortions for the reconstructed signal.

For practical applications, such as speech or audio processing, a higher signal reconstruction error than for these design examples can usually be tolerated while subband filters with a higher stopband attenuation are desirable. Such aspects are discussed later in Sec. 6.1.

3.1.2.4 Design III

A more linear phase characteristics for the subband filters can be achieved by means of the following modification of the analysis filters

$$H_0'(z) = \frac{1}{2}\left(\Psi_0^{\mathrm{ap}}\left(z^2\right) + z^{-1}\, A_1^{[K_1]}\left(z^2\right) \cdot \mathcal{P}_{0,K_0}^{\mathrm{ap}}\left(z^2\right)\right) \tag{3.49a}$$

$$H_1'(z) = \frac{1}{2}\left(\Psi_0^{\mathrm{ap}}\left(z^2\right) - z^{-1}\, A_1^{[K_1]}\left(z^2\right) \cdot \mathcal{P}_{0,K_0}^{\mathrm{ap}}\left(z^2\right)\right) \tag{3.49b}$$

and synthesis filters

$$G_0'(z) = z^{-1}\, \Psi_1^{\mathrm{ap}}\left(z^2\right) + A_0^{[K_0]}\left(z^2\right) \cdot \mathcal{P}_{1,K_1}^{\mathrm{ap}}\left(z^2\right) \tag{3.50a}$$

$$G_1'(z) = z^{-1}\, \Psi_1^{\mathrm{ap}}\left(z^2\right) - A_0^{[K_0]}\left(z^2\right) \cdot \mathcal{P}_{1,K_1}^{\mathrm{ap}}\left(z^2\right). \tag{3.50b}$$

The relations to the subband filters of the classical QMF-bank according to Eq. (3.16) and Eq. (3.17) are given by

$$H_i'(z) = H_i(z) \cdot \mathcal{P}_{0,K_0}^{\mathrm{ap}}\left(z^2\right) \tag{3.51}$$

$$G_i'(z) = 2\, G_i(z) \cdot \mathcal{P}_{1,K_1}^{\mathrm{ap}}\left(z^2\right) \quad \text{with} \quad i \in \{0,1\}\,. \tag{3.52}$$

It follows from these relations and Eq. (3.19) that the overall transfer function for this design is given by Eq. (3.48). Hence, the reconstruction error is the same as for the previous design II, but the algorithmic complexity of the QMF-bank is higher. As for design II, the magnitude responses of the subband filters are *exactly* the same as for the classical allpass-based QMF-bank in contrast to the original approach of [Gal02]

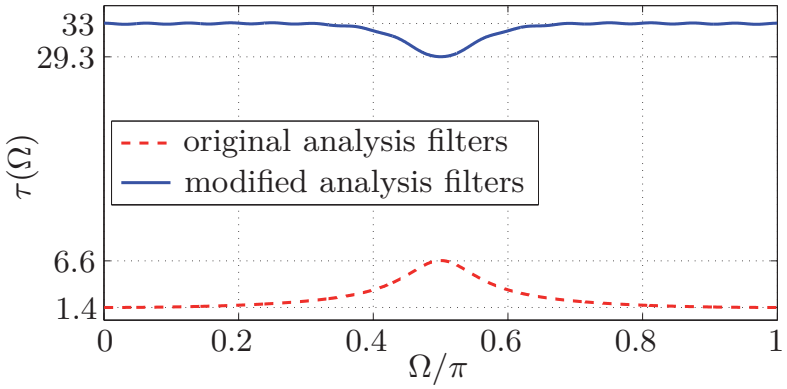

Figure 3.11: *Group delay $\tau(\Omega)$ of the original analysis filter $H_0\left(e^{j\,\Omega}\right)$ according to Figure 3.3 and modified analysis filter $H_0'\left(e^{j\,\Omega}\right)$ with linearized phase response for $K_0 = K_1 = 1$ and $d_0 = 16$. (The curves for the highpass and lowpass analysis filter are identical.)*

where FIR phase equalizers are used. The phase responses of the modified subband filters become more linear because of the multiplication with $\mathcal{P}_{i,K_i}^{\mathrm{ap}}\left(z^2\right)$, which leads to a partial phase compensation as exemplified in the following.

Example 3.3: The new design III is applied to the analysis filters of Figure 3.3. The plots of Figure 3.11 show that the group delay of the new analysis filters is more constant than for the original subband filters. The corresponding curves for the synthesis filters are not plotted as they are similar to those of the analysis filters.

3.1.2.5 Evaluation

The proposed IIR/IIR QMF-bank designs I and II are now compared with the related IIR/FIR QMF-bank designs of [GK01a, KDL00]. These designs can also achieve either a partial or complete aliasing cancellation, but use FIR phase equalizers instead of allpass phase equalizers. In addition, the para-unitary QMF Lattice design of [VH88] is considered to include an FIR/FIR QMF-bank with perfect reconstruction.[4] The different filter-banks are designed in such a manner that they have all approximately the same overall signal delay D_{o} and achieve a similar aliasing cancellation.

Table 3.1 contrasts the resulting reconstruction errors of the different filter-banks. In addition, their algorithmic complexity is also listed, which comprises here the number of real multiplications and summations per sample instant as well as the number of delay elements.[5] The considered NPR designs use the same allpass-based analysis filters

[4] A brief description of this FIR/FIR QMF-bank design is provided by App. C.1. A comparison of the proposed IIR/IIR QMF-bank design with the FIR/FIR QMF-bank design of Johnston [Joh80] is conducted in Sec. 6.1.

[5] This algorithmic complexity is a very general and common measure for the assessment of the complexity of a system. This measure can (only) serve as a rough estimate for the actual computational complexity of a system if implemented, e.g., on a DSP where the computational load depends on the specific chip architecture, the instruction set etc. However, such a specific analysis exceeds the scope of this work where the terms algorithmic complexity and computational complexity are used interchangeably.

Table 3.1: *Comparison of different QMF-bank designs regarding the minimum stopband attenuation (MSA), maximal aliasing distortions (MALD) for* $\left|T_{alias}\left(e^{j\,\Omega}\right)\right|$*, maximal amplitude distortions (MAMD) for* $\left|T_{lin}\left(e^{j\,\Omega}\right)\right| - 1$ *and maximal group delay deviations (MGDD) for* $\tau_{lin}(\Omega) - D_o$*. The last column contains the overall number of real multipliers (*$\mathcal{M}$*), real adders (*$\mathcal{A}$*) and the number of delay elements (*$\mathcal{D}$*). A value of approximately zero lies within the floating-point accuracy of MATLAB.*

QMF-bank	MSA [dB]	MALD [dB]	MAMD	MGDD [samples]	$\mathcal{M}/\mathcal{A}/\mathcal{D}$
signal delay $D_\mathrm{o} = 33$					
new design I	-43	-60.2	$+4.8 \cdot 10^{-7}$	$\pm 3.1 \cdot 10^{-2}$	9/12/24
NPR FB [GK01a]	-43	-66.2	$\pm 5 \cdot 10^{-4}$	$\pm 1.6 \cdot 10^{-2}$	15/17/36
NPR FB [KDL00]	-43	-61.9	$\pm 8 \cdot 10^{-4}$	$\pm 2.3 \cdot 10^{-2}$	15/17/36
PR FB [VH88]	-68	none	≈ 0	≈ 0	36/35/37
signal delay $D_\mathrm{o} = 49$					
new design II	-43	none	≈ 0	$\pm 6.3 \cdot 10^{-2}$	11/14/40
NPR FB [GK01a]	-43	none	$\pm 9.8 \cdot 10^{-4}$	$\pm 3.1 \cdot 10^{-2}$	16/18/52
NPR FB [KDL00]	-43	none	$\pm 16 \cdot 10^{-4}$	$\pm 4.6 \cdot 10^{-2}$	27/29/52
PR FB [VH88]	-88	none	≈ 0	≈ 0	52/51/52

of degree $D_\mathrm{f} = 5$ as shown in Figure 3.3 so that the minimum stopband attenuation (as defined in [Vai93]) is equal for these filter-banks. In contrast, the considered para-unitary QMF-bank uses analysis filters of degrees 32 and 49, respectively, which explains the better stopband attenuation and higher algorithmic complexity.

The QMF-banks with near-perfect reconstruction achieve a similar aliasing cancellation and have a significantly lower complexity than the para-unitary FIR QMF-bank with perfect reconstruction at the expense of small reconstruction errors. The new IIR/IIR QMF-bank causes no or negligible magnitude distortions and features the lowest algorithmic complexity of all considered designs at the expense of slightly higher group delay distortions. Due to these properties, the proposed design is of special interest for speech and audio processing since the human auditory systems is rather insensitive towards phase or group delay distortions, respectively. Such an application of the new QMF-bank is elaborated in Chap. 6.

3.2 M-Channel Pseudo QMF-Bank

The concept of the two-channel QMF-bank can be generalized, which leads to a modulated M-channel AS FB. Therefore, modulated M-channel filter-banks are also termed

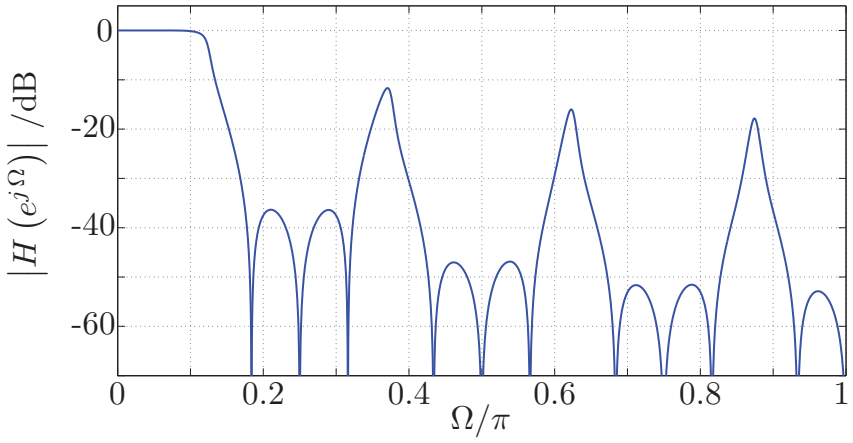

Figure 3.12: *Magnitude response of an IIR analysis prototype filter obtained by the non-linear phase design of [RS87] for $M = 8$ and $\Omega_p = 0.6\,\pi/M$.*

as *Pseudo QMF-banks,* cf., [Fli93].[6] As for the two-channel IIR QMF-bank treated before, it is also possible to construct such filter-banks by means of allpass polyphase filters [Ram88, HR90]. Accordingly, synthesis filter-bank designs for allpass-based QMF-banks can also be extended to such M-channel Pseudo QMF-banks [Gal02]. Similar to the approach of [Gal02], the use of the new allpass phase equalizer for such filter-banks is treated in the following based on [LV09e].

3.2.1 Filter-Bank Structure

A critically subsampled DFT AS FB with M channels is considered whose analysis filters are given by

$$H_i(z) = H\left(z\,W_M^i\right) \quad \text{for} \quad i \in \{\,0, 1, \ldots, M-1\,\}\,. \tag{2.22}$$

In contrast to the DFT filter-bank treated in Sec. 2.3, a *recursive* prototype lowpass filter is now taken whose type 1 polyphase representation reads

$$H(z) = \frac{1}{M} \sum_{\lambda=0}^{M-1} A_\lambda^{[K_\lambda]}\left(z^M\right) \cdot z^{-\lambda}\,. \tag{3.53}$$

The M analysis polyphase filters are now allpass filters according to Eq. (2.48) [HR90]. The real poles of the allpass filters $A_\lambda^{[K_\lambda]}(z)$ can be determined by the algorithms presented in [RS87].

An example for such a prototype lowpass filter is provided by Figure 3.12, which is determined by the non-linear phase design of [RS87] for a passband edge frequency of $\Omega_\mathrm{p} = 0.6\,\pi/M$ and allpass filter degrees $K_\lambda = 1$ for $\lambda \in \{0, 1, \ldots, M-2\}$ and $K_{M-1} = 0$ with $M = 8$. The corresponding allpass coefficients $a_0, \ldots, a_{M-1}$ are equal to 0.1038, 0.2078, 0.3144, 0.4260, 0.5458, 0.6774, 0.8263 and 0.

[6] It is also common to name such AS FBs simply as M-channel QMF-banks and/or to term only M-channel cosine modulated filter-banks as Pseudo QMF-banks.

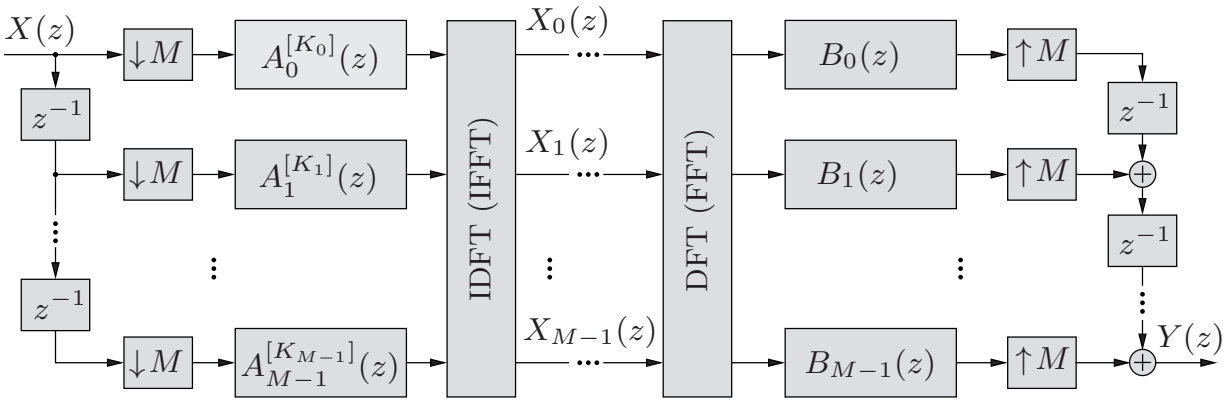

Figure 3.13: *PPN implementation of a critically subsampled DFT AS FB with allpass polyphase filters (without spectral processing).*

The width of the inevitable side-lobes and the transition-band can be reduced at the expense of a diminished stopband attenuation and vice versa. The side-lobes are caused by so-called 'don't care bands' and can be avoided by the design of [RNM86] at the price of an increased algorithmic complexity and signal delay. However, this approach is not considered here as the proposed synthesis filter-bank design can also be applied to this filter-bank in a straightforward fashion, cf., [Hil08].

Eq. (3.53) and Eq. (2.35a) lead to the following type 1 polyphase representation of the analysis filters

$$H_i(z) = \frac{1}{M} \sum_{\lambda=0}^{M-1} A_\lambda^{[K_\lambda]}\left(z^M\right) \cdot z^{-\lambda} \cdot W_M^{-i\lambda}; \quad i \in \{0, 1, \ldots, M-1\}\,. \tag{3.54}$$

The type 2 polyphase representation of the synthesis filters according to Eq. (2.37a) is now given by

$$G_i(z) = \sum_{\lambda=0}^{M-1} B_\lambda\left(z^M\right) \cdot z^{-(M-1-\lambda)} \cdot W_M^{i\lambda}\,. \tag{3.55}$$

The corresponding PPN implementation of this allpass-based DFT AS FB is shown in Figure 3.13. The QMF-bank of Figure 3.7 is included as special case of this Pseudo QMF-bank for $M = 2$. Accordingly, the following synthesis filter-bank designs can be seen as *generalization* of the previous QMF-bank designs I and II.

3.2.2 New Synthesis Filter-Bank Designs

Inserting Eq. (3.54) and Eq. (3.55) into Eq. (2.8) leads (after some steps) to the relation

$$\widehat{X}(z) = \frac{z^{-(M-1)}}{M} \sum_{r=0}^{M-1} X\left(z\, W_M^r\right) \sum_{\lambda=0}^{M-1} A_\lambda^{[K_\lambda]}\left(z^M\right) \cdot B_\lambda\left(z^M\right) \cdot W_M^{-\lambda\, r} \tag{3.56}$$

$$= X(z) \underbrace{\frac{z^{-(M-1)}}{M} \sum_{\lambda=0}^{M-1} A_\lambda^{[K_\lambda]}\left(z^M\right) \cdot B_\lambda\left(z^M\right)}_{= T_{\mathrm{lin}}(z)}$$

$$+ \sum_{r=1}^{M-1} X\left(z\, W_M^r\right) \underbrace{\frac{z^{-(M-1)}}{M} \sum_{\lambda=0}^{M-1} A_\lambda^{[K_\lambda]}\left(z^M\right) \cdot B_\lambda\left(z^M\right) \cdot W_M^{-\lambda\, r}}_{= U_r(z)} . \tag{3.57}$$

The function $T_{\mathrm{lin}}(z)$ represents the linear transfer function of the AS FB introduced in Eq. (2.9). The peak aliasing distortions of Eq. (2.12) are now determined by the alias components $U_r(z)$ as follows

$$\mathcal{D}_{\mathrm{peak}}(\Omega) = \sqrt{\sum_{r=1}^{M-1} \left|U_r(e^{j\,\Omega})\right|^2} . \tag{3.58}$$

Eq. (3.57) reveals that a filter-bank with perfect reconstruction according to Eq. (2.13) is obtained, if

$$A_\lambda^{[K_\lambda]}(z) \cdot B_\lambda(z) \stackrel{!}{=} z^{-\bar{\psi}} \;\forall\; \lambda \in \{0, 1, \ldots, M-1\} . \tag{3.59}$$

This phase equalization problem is similar to that of Eq. (3.28) and can be approximately solved with the allpass phase equalizer of Eq. (3.34). Accordingly, the transfer function of Eq. (3.36) is now given by

$$\Psi_\lambda^{\mathrm{ap}}(z) = A_\lambda^{[K_\lambda]}(z) \cdot \mathcal{P}_{\lambda,K_\lambda}^{\mathrm{ap}}(z) \tag{3.60a}$$

$$= \prod_{m=1}^{K_\lambda} \frac{1 - \left(a_\lambda^*(m) \cdot z\right)^{I(\lambda,m)}}{z^{I(\lambda,m)} - \left(a_\lambda(m)\right)^{I(\lambda,m)}}; \quad I(\lambda,m) = 2^{J_\lambda(m)} \tag{3.60b}$$

which represents an allpass filter with filter degree

$$d_\lambda = \sum_{m=1}^{K_\lambda} I(\lambda, m) \;\forall\; \lambda \in \{0, 1, \ldots, M-1\} . \tag{3.61}$$

3.2.2.1 Design I

Similar to QMF-bank design I of Sec. 3.1.2.2, near-perfect reconstruction can be accomplished by means of the following allpass polyphase filters at the synthesis side

$$B_\lambda(z) = \mathcal{P}^{\mathrm{ap}}_{\lambda,K_\lambda}(z) \cdot z^{-(d_{\max}-d_\lambda)} \quad \text{with} \quad d_{\max} = \max_\lambda \{d_\lambda\} \tag{3.62}$$

where $\mathcal{P}^{\mathrm{ap}}_{\lambda,K_\lambda}(z)$ and d_λ are given by Eq. (3.34) and Eq. (3.61). Inserting Eq. (3.62) into Eq. (3.57) yields the linear transfer function

$$T_{\mathrm{lin}}(z) = z^{-(1+d_{\max})M+1} \, \frac{1}{M} \sum_{\lambda=0}^{M-1} \Psi^{\mathrm{ap}}_\lambda\left(z^M\right) \cdot z^{Md_\lambda} \tag{3.63}$$

and alias components

$$U_r(z) = z^{-(1+d_{\max})M+1} \, \frac{1}{M} \sum_{\lambda=0}^{M-1} \Psi^{\mathrm{ap}}_\lambda\left(z^M\right) \cdot z^{Md_\lambda} \cdot W_M^{-\lambda\, r} \tag{3.64}$$

with $\Psi^{\mathrm{ap}}_\lambda(z)$ given by Eq. (3.60). The overall signal delay of this filter-bank amounts to

$$D_{\mathrm{o}} = (1 + d_{\max}) \cdot M - 1 \tag{3.65}$$

sample instants. For the special case $d_\lambda \equiv d_{\max}$, the signal reconstruction error can be reduced at the price of an increased computational complexity, but without increasing the signal delay D_{o}.

Example 3.4: The design of a DFT Pseudo QMF-bank with $M = 8$ subbands is considered whose analysis prototype lowpass filter is shown in Figure 3.12. For the synthesis filter-bank, the filter degrees d_λ of Eq. (3.61) are equal to $[2, 4, 4, 8, 8, 16, 16, 0]$. The zero value indicates an 'identity branch' for $\lambda = M - 1$ where $A^{[K_{M-1}]}_{M-1}(z) \equiv 1$ and $B_{M-1}(z) = z^{-d_{\max}}$. The magnitude response of the obtained synthesis prototype filter is not plotted as it is almost identical to that of Figure 3.12. The linear transfer function and peak aliasing distortions according to Eq. (3.57) and Eq. (3.58) are analyzed in Figure 3.14. A lower signal reconstruction error can be achieved by using higher filter degrees d_λ at the price of an increased signal delay D_{o}. An alternative design, which avoids amplitude and aliasing distortions, is presented in the following.

3.2.2.2 Design II

Inspection of Eq. (3.57) reveals that a complete aliasing cancellation is accomplished, if the product $A^{[K_\lambda]}_\lambda(z) \cdot B_\lambda(z)$ is identical for all $\lambda \in \{0, 1, \ldots, M-1\}$. This can be achieved by a synthesis filter-bank whose polyphase filters are given by

$$B_\lambda(z) = \prod_{\rho=0}^{\lambda-1} \Psi^{\mathrm{ap}}_\rho(z) \cdot \mathcal{P}^{\mathrm{ap}}_{\lambda,K_\lambda}(z) \prod_{\mu=\lambda+1}^{M-1} \Psi^{\mathrm{ap}}_\mu(z)\,. \tag{3.66}$$

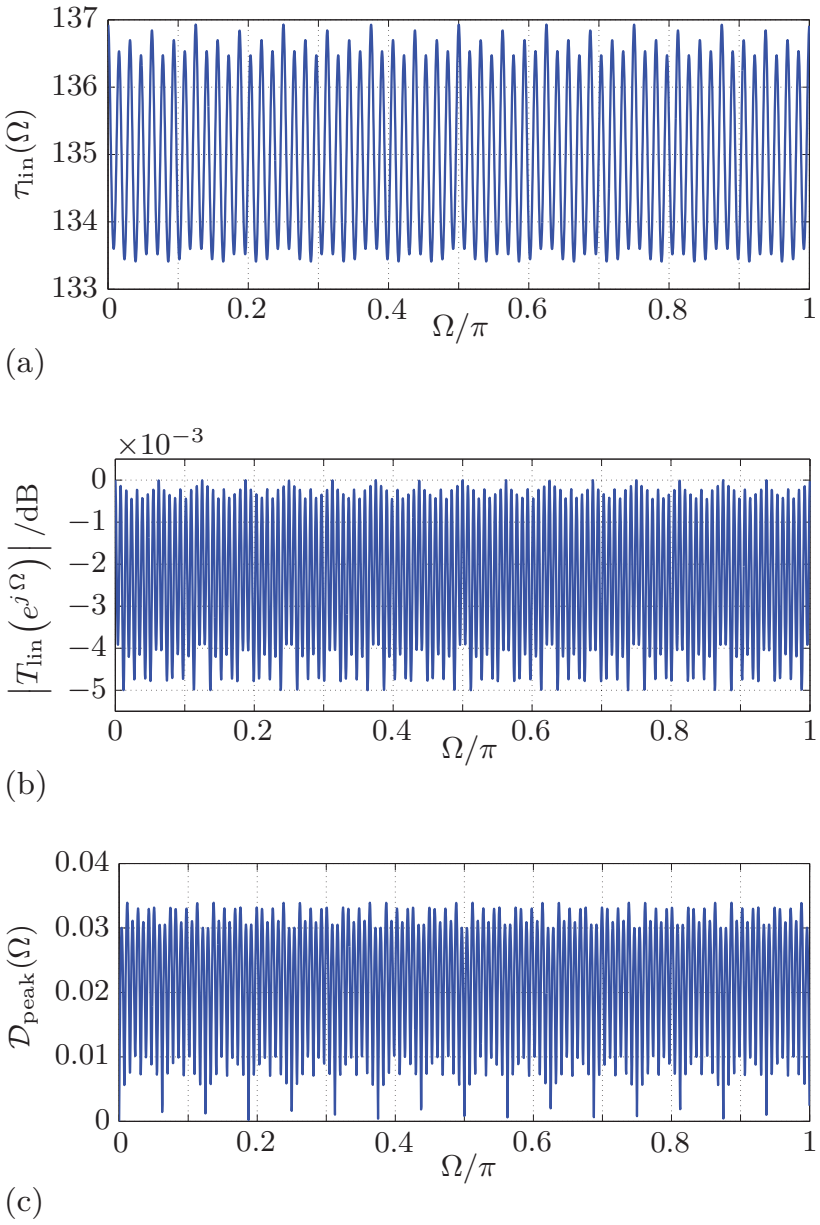

Figure 3.14: *Analysis of the reconstruction error for Pseudo QMF-bank design I with $M = 8$ channels and analysis prototype filter according to Figure 3.12:*
(a) *group delay of the linear transfer function*
(b) *magnitude response of the linear transfer function*
(c) *peak aliasing distortions.*

The resulting linear transfer function

$$T_{\mathrm{lin}}(z) = z^{-(M-1)}\,\frac{1}{M}\prod_{\lambda=0}^{M-1}\Psi_{\lambda}^{\mathrm{ap}}\left(z^{M}\right) \tag{3.67}$$

is an allpass filter such that no amplitude distortions occur. The remaining phase and group delay distortions, respectively, can be made arbitrarily small in dependence of

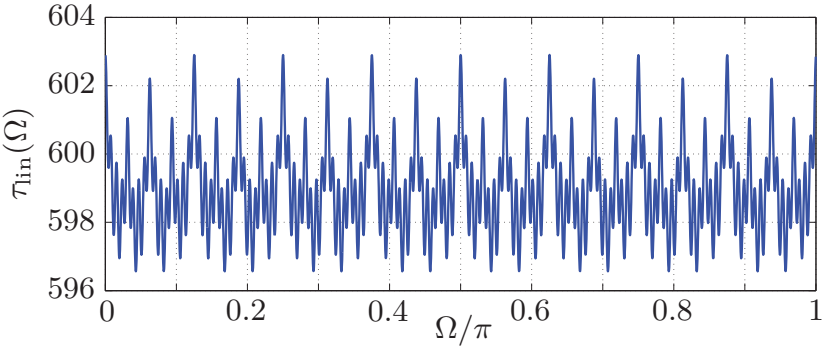

Figure 3.15: *Group delay of the overall transfer function for Pseudo QMF-bank design II with $M = 8$ channels and analysis prototype filter according to Figure 3.12.*

the tolerable signal delay, which amounts to

$$D_{\mathrm{o}} = M - 1 + M \sum_{\lambda=0}^{M-1} d_\lambda \tag{3.68}$$

sample instants according to Eq. (3.67) with d_λ given by Eq. (3.61).

Example 3.5: As for Example 3.4, a critically subsampled DFT Pseudo QMF-bank with $M = 8$ subbands is considered whose analysis prototype filter is shown in Figure 3.12. The filter degrees d_λ of Eq. (3.67) are now equal to $[2, 4, 4, 8, 8, 16, 32, 0]$. The overall group delay for this design is plotted in Figure 3.15. The Pseudo QMF-bank design II achieves complete aliasing cancellation and causes no amplitude distortions at the price of a higher group delay and a higher computational complexity in comparison to the previous design. The trade-off between signal delay and reconstruction error (phase distortions) can be easily adjusted by the choice of the filter degrees d_λ.

A comparison of the presented Pseudo QMF-bank design with the original approach of [GK01b] can be found in [LV09e, Hil08]. As for the previous QMF-bank designs, it turns out that the proposed IIR/IIR Pseudo QMF-bank designs exhibit higher phase distortions, similar aliasing distortions, but lower magnitude distortions in comparison to the corresponding IIR/FIR Pseudo QMF-bank designs of [GK01b]. In addition, the new filter-banks have also a lower algorithmic complexity. These different properties are reasoned by the fact that the proposed designs are based on allpass phase equalizers where the original designs of [GK01b, Gal02] are based on FIR phase equalizers. A detailed analysis of these two phase equalizer designs is performed in the following.

3.3 Phase Equalizer Design

The previous treatment has shown that solving the phase equalization problem as stated by Eq. (3.28) or Eq. (3.59) is a central issue in the design of allpass-based QMF-banks and Pseudo QMF-banks, respectively. This is also true for allpass transformed filter-banks, which are treated in the subsequent chapters. Actually, many design proposals for allpass-based filter-banks differ basically by the employed phase equalizer design,

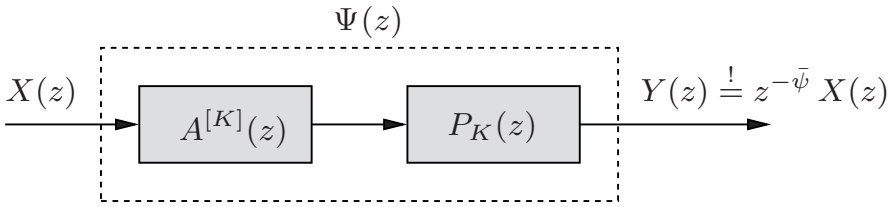

Figure 3.16: *General phase equalization problem for allpass-based filter-banks.*

which has a major impact on the performance of a filter-bank. This motivates to elaborate different phase equalizer designs for allpass-based filter-banks in more detail.

3.3.1 Design Problem

The filtering of a signal $x(k)$ by an allpass filter causes no magnitude distortions but phase distortions, which should be compensated by a subsequent *phase equalizer.* The formulation of this problem in the z-domain is depicted in Figure 3.16. The *transfer function* $\Psi(z)$ of degree D for the cascade of an allpass filter of degree K and a corresponding phase equalizer of degree N shall be equal to a delay element

$$\Psi(z) = A^{[K]}(z) \cdot P_K(z) \stackrel{!}{=} z^{-\bar{\psi}}; \quad \bar{\psi} \geq 0\,. \tag{3.69}$$

The *actual* transfer function $\Psi(z)$ should approximate the *desired* transfer function

$$\Psi_{\mathrm{d}}(z) = z^{-\bar{\psi}}\,. \tag{3.70}$$

Eq. (3.69) implies that the frequency response of the actual transfer function

$$\Psi\left(e^{j\,\Omega}\right) = \left|\Psi\left(e^{j\,\Omega}\right)\right| \cdot e^{-j\,\varphi_\Psi(\Omega)} \tag{3.71}$$

should have a linear phase response and constant group delay

$$\varphi_\Psi(\Omega) \stackrel{!}{=} \bar{\psi}\,\Omega \tag{3.72}$$

$$\tau_\Psi(\Omega) = \mathrm{gdl}\left\{\Psi\left(e^{j\,\Omega}\right)\right\} \stackrel{!}{=} \bar{\tau}\ \forall\ \Omega\,. \tag{3.73}$$

Thus, the above stated phase equalization problem can also be seen as *group delay equalization* problem.

The performance of a phase equalizer depends on the deviations between actual and desired transfer function. This difference is captured by the following *approximation errors* for magnitude response, phase response and group delay

$$\Delta\left|\Psi\left(e^{j\,\Omega}\right)\right| = \left|\Psi\left(e^{j\,\Omega}\right)\right| - \bar{c} \tag{3.74a}$$

$$\Delta\varphi_\Psi(\Omega) = \varphi_\Psi(\Omega) - \bar{\psi}\,\Omega \tag{3.74b}$$

$$\Delta\tau_\Psi(\Omega) = \tau_\Psi(\Omega) - \bar{\tau}\,. \tag{3.74c}$$

It is important to notice that the nominal group delay $\bar{\tau}$ is not necessarily equal to the nominal phase factor $\bar{\psi}$ which, in turn, is not necessarily equal to the degree D of the transfer function $\Psi(z)$ of Eq. (3.69). If a phase equalizer is designed in such a manner that the approximation error for a desired phase response is minimal with regard to a certain error norm, this does in general not ensure that the corresponding group delay error is also minimal for the same error norm, cf., [Lan93, Chap. 2]. Accordingly, the values for $\bar{\tau}$ and $\bar{\psi}$ depend not only on the filter degree D, but also on the considered error norm (cf., App. D.1).

In case of an *allpass chain* of length L_{ac} according to Eq. (2.60), the statement of Eq. (3.69) turns into the equation

$$\Psi(z) = A^{L_{\mathrm{ac}}}(z) \cdot P_{L_{\mathrm{ac}}}(z) \stackrel{!}{=} z^{-\bar{\psi}} \,. \tag{3.75}$$

This design problem is also considered as it plays an important role for the construction of the later treated *allpass transformed* filter-banks.

One possible strategy to solve the general phase equalization problem of Eq. (3.69) is to design a phase equalizer for a *single* allpass filter of first order by the requirement

$$\Psi_{\mathrm{s}}(z) = A(z) \cdot \underbrace{P_1(z)}_{=\mathcal{P}(z)} \stackrel{!}{=} z^{-\bar{\psi}_{\mathrm{s}}} \,. \tag{3.76}$$

This phase equalizer design can then be extended to allpass filters of higher order in a straightforward fashion as an allpass filter can always be represented in a cascade form according to Eq. (2.48).[7] For such a *cascaded phase equalization,* the design problem of Eq. (3.69) turns into the statement

$$\Psi(z) = \prod_{m=1}^{K} A_m(z) \cdot \mathcal{P}_m(z) \stackrel{!}{=} z^{-\sum_{m=1}^{K} \bar{\psi}_{\mathrm{s}}(m)} \,. \tag{3.77}$$

The proposed allpass phase equalizer design of Eq. (3.30) belongs to this category as well as the FIR phase equalizer design of [Gal02].

For the special case of an allpass chain, Eq. (3.77) simplifies to

$$\Psi(z) = \Big(A(z) \cdot \mathcal{P}(z)\Big)^{L_{\mathrm{ac}}} \stackrel{!}{=} z^{-L_{\mathrm{ac}}\bar{\psi}_{\mathrm{s}}} \,. \tag{3.78}$$

A straightforward solution for the general phase equalization problem of Eq. (3.69) is obtained by

$$P_K^{\mathrm{ideal}}(z) = \Big(A^{[K]}(z)\Big)^{-1} = \breve{A}^{[K]}(z) \tag{3.79}$$

where $\breve{A}^{[K]}(z)$ marks the para-conjugate system function of an allpass filter.[8] However, this 'ideal' phase equalizer is either causal and unstable for a region of convergence given by $\max\{|a(m)|\} < |z|$ or stable and anti-causal for a region of convergence given by $\max\{|a(m)|\} > |z|$. More advanced phase equalizer designs, which circumvent this problem, are elaborated in the following.

[7] If not mentioned otherwise, only this cascade form is considered for $A^{[K]}(z)$ in the following and the terms allpass *coefficient* and allpass *pole* are used interchangeably.

[8] The used nomenclature for filters is described in App. A.2.

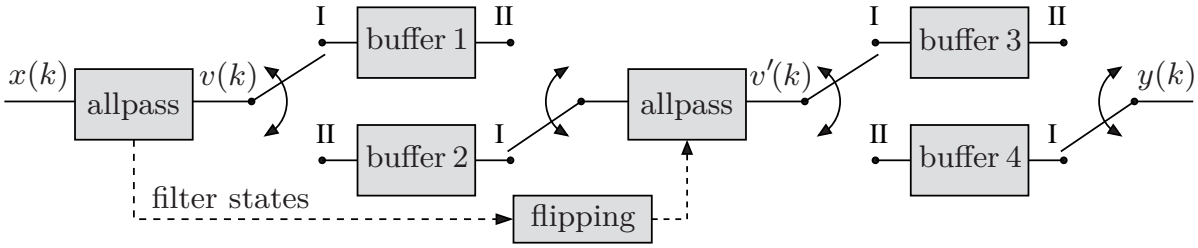

Figure 3.17: *Implementation of a non-causal allpass filter as phase equalizer with non-overlapping buffering according to [MCB92].*

3.3.2 Non-Causal Filtering

One approach to solve the considered phase equalization problem is to seek for a direct realization of the anti-causal phase equalizer given by Eq. (3.79). The implementation of non-causal IIR filters is treated already in [Cza82]. A non-causal filter can be realized by buffering the input samples in order to perform a 'time-reversed' filtering. Such a technique is employed in [Ram88, HR90] to implement an allpass-based Pseudo QMF-bank with perfect reconstruction which, however, relies on input signals of finite length such as digital images. The IIR Pseudo QMF-bank designs proposed in [MCB92, CM96] realize also non-causal allpass filters, but these filter-banks can also process signals of 'infinite' length such as speech and audio signals. The allpass-based Pseudo QMF-bank design of [MCB92] is extended in [CV92, CV93] to account for a more general class of PR filter-banks and time-varying filter-banks, respectively.

The proposal of [MCB92] achieves a perfect phase equalization so that Eq. (3.69) is exactly fulfilled. This scheme is illustrated in Figure 3.17. At each simultaneous shift of the four switches, the initial filter states of the second allpass filter are obtained from the final filter states of the first allpass filter by means of a 'flipping' operation (exchange matrix) [MCB92]. When all switches are at position I at sample instant k, the output $v(k)$ of the first allpass filter is fed into buffer 1 of length L_{buf} and the L_{buf} values of the previous frame $v(k-1), \ldots, v(k-L_{\text{buf}}+1)$ stored in buffer 2 are read-out in time-reversed order and fed into the second allpass filter. The output of this second allpass filter $v'(k)$ goes into buffer 3 and the output of the second allpass filter for the previous frame is read-out from buffer 4 in time-reversed order at the same time. Afterwards, all switches change to position II to process the next L_{buf} values and so on. The overall signal delay of this scheme is equal to $2\,L_{\text{buf}}$ sample instants.

Applying this approach to the IIR Pseudo QMF-bank of Figure 3.13 treated in Sec. 3.2.1 yields a filter-bank with perfect reconstruction and a delay of $2\,M\,L_{\text{buf}}+1$ sample instants. A disadvantage of this solution is the memory consumption due to the buffering and the transmission of the allpass filters states, especially if this filter-bank is applied for subband coding. However, a more severe drawback (which is not reported in the corresponding publications) is that even a slight modification of the subband signals can cause huge signal distortions. For the system of Figure 3.17 with an allpass of first order ($a = 0.5$) and buffer length $L_{\text{buf}} = 20$, a multiplication of the signal $v(k)$ with a factor of $1 + 10^{-13}$ can lead already to filter instability.

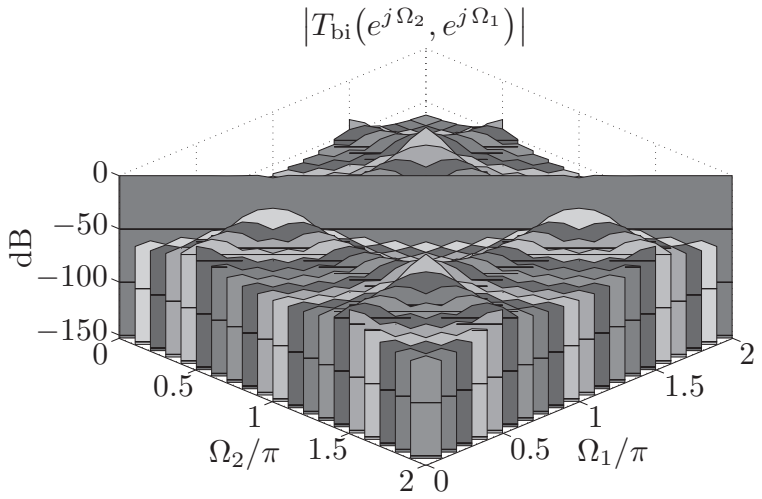

Figure 3.18: *Magnitude of the bifrequency system function* $T_{bi}\left(e^{j\,\Omega_2}, e^{j\,\Omega_1}\right)$ *for a QMF-bank with synthesis polyphase filters realized by time-reversed non-causal filtering with overlap buffering according to [CM96].*

The authors propose a modification of their scheme in [CM96], which avoids the transmission of filter states. The main structural difference to that of Figure 3.17 is that the buffers 1 and 2 are now of length $L_{\mathrm{buf}} + L_{\mathrm{ov}}$ where L_{ov} marks the number of samples that adjacent frames overlap. (The buffers 3 and 4 are still of length L_{buf}.) The processing of the additional L_{ov} overlapping samples achieves that the filter states of the second allpass filter converge to their correct values for the current block [CM96]. In contrast to the previous scheme, the transmission of filter states is avoided and the system is more robust towards signal modifications in between at the expense of a higher algorithmic complexity and a higher signal delay, which is now equal to $2\,L_{\mathrm{buf}} + L_{\mathrm{ov}} + 1$ sample instants. This modified scheme for non-causal filtering achieves no perfect phase equalization, but the equalization error can be made arbitrarily small by increasing the overlap L_{ov} which, in turn, increases signal delay and algorithmic complexity. Another drawback of this scheme is that the phase equalizer constitutes a *linear periodically time-varying* (LPTV) system. This effect is exemplified for a QMF-bank design according to Figure 3.7, which uses this non-causal filtering approach on the synthesis side with buffer length $L_{\mathrm{buf}} = L_{\mathrm{ov}} = 10$. (The used allpass coefficients are identical to those of Eq. (6.2).) Figure 3.18 shows a plot of the bifrequency system function (BSF) introduced in Sec. 2.4. There are $L_{\mathrm{buf}} + L_{\mathrm{ov}} - 1 = 19$ alias components on the side diagonals instead of one alias component as it occurs in case of a QMF-bank with *linear time-invariant* (LTI) synthesis filters and imperfect aliasing cancellation. Hence, the number of alias components increases with the buffer length. The alias components become of course even greater, if spectral modifications of the subband signals are performed. This creation of additional alias components (which is not reported in the corresponding publications) is avoided by the use of LTI phase equalizers, which are treated in the following.

3.3.3 Numerical Designs

The stated phase equalization problem can be solved by means of numerical design methods for allpass filters with prescribed phase response or group delay, respectively. Numerous publications deal with this issue, e.g., [SS90, Lan92, LL94, NLK94, ITK94, Lan98, MI03]. An advantage of such *general* phase equalizer designs is that they can be applied to very different phase equalization problems. Examples are the phase equalization of IIR filters, the design of lowpass filters consisting of allpass sub-filters (as described in Sec. 3.1.1), or the construction of recursive Hilbert transformers, cf., [Lan93]. The coefficients of the phase equalizer can be determined by minimizing the (weighted) error norm between prescribed and achieved phase response for the frequency range of interest. This is mostly done by employing either the least-squares (LS) norm (L_2-norm), e.g., [NLK94, CL94, LL94] or the Chebyshev norm (L_∞-norm), e.g., [Lan92, ITK94, Lan98]. This leads in both cases to a non-linear optimization problem, which is mostly solved by iterative schemes. A problem is that not all algorithms converge to a unique solution and that the design of phase equalizers of high degrees can cause numerical difficulties. Besides, it is rather cumbersome to incorporate the constraint for filter stability, cf., [Lan98]. A more comprehensive treatment of such general numerical phase equalizer designs can be found, e.g., in [Lan93, Lan98]. The focus of this work is on phase equalizers which are designed more specifically for allpass-based filter-banks.

3.3.4 Closed-Form Designs

In this section, different approaches are presented which address the *specific* phase equalization problem stated in Sec. 3.3.1. These designs have the following benefits in comparison to the above mentioned general numerical designs:

- The filter coefficients are given by analytical closed-form expression such that no (involved) numerical optimization is needed.
- The design of phase equalizers with high filter degrees poses no numerical problems.
- The approximation error can be described by simple analytical expressions. This allows to evaluate the trade-off between the remaining phase (or group delay) distortions versus signal delay in an easy manner.
- Filter stability is inherently ensured.
- The algorithmic complexity of these equalizers is often lower than for phase equalizers obtained by a numerical design.

The following treatment is partly based on [LV06d] where this class of phase equalizers is denoted as *parametric phase equalizers*.

3.3.4.1 LS FIR Phase Equalizer

The 'ideal' IIR phase equalizer of Eq. (3.79) can be approximated by a causal FIR filter in a simple fashion. For this, the anti-causal infinite impulse response

$$p_K^{\text{ideal}}(k) \;\circ\!\!-\!\!\bullet\; P_K^{\text{ideal}}(z) = \breve{A}^{[K]}(z) \quad \text{for} \quad \mathcal{R}_{\text{c}} = \Big\{ z \in \mathbb{C} \,\Big|\, \max\{|a(m)|\} > |z| \Big\} \tag{3.80}$$

is truncated and shifted by N samples. This leads to an FIR phase equalizer of length $N+1$ whose impulse response is given by

$$p_K^{\text{ls}}(k) = \begin{cases} p_K^{\text{ideal}}(k-N) & \text{if } 0 \le k \le N \\ 0 & \text{otherwise.} \end{cases} \tag{3.81}$$

An FIR filter obtained by truncating the infinite impulse response of the original IIR filter provides a least-squares (LS) error approximation, e.g., [KK98]. The $\mathcal{L}_2$-norm of the error between the frequency response of the time-shifted ideal phase equalizer and its approximation by an arbitrary FIR phase equalizer of degree N according to

$$\Big\| \Delta P_K\big(e^{j\,\Omega}\big) \Big\|_2 = \Big\| P_K^{\text{ideal}}\big(e^{j\,\Omega}\big) \cdot e^{-j\,\Omega\,N} - \widehat{P}_K\big(e^{j\,\Omega}\big) \Big\|_2 \tag{3.82}$$

becomes minimal for the filter of Eq. (3.81):

$$\widehat{P}_K\big(e^{j\,\Omega}\big) = P_K^{\text{ls}}\big(e^{j\,\Omega}\big)\,. \tag{3.83}$$

Therefore, this phase equalizer is termed as *LS FIR phase equalizer* in the following.

The phase equalizer degree N can be determined from the infinite impulse response $p_K^{\text{ideal}}(k)$ by exploiting the fact that there exists an integer N_ϵ where

$$\Big| p_K^{\text{ideal}}(-k) \Big| \le \epsilon_{\text{ls}} \quad \text{for} \quad k \ge N_\epsilon\,; \quad \epsilon_{\text{ls}} \in \mathbb{R}_+\,. \tag{3.84}$$

For a chosen threshold ϵ_{ls}, the phase equalizer degree N is then given by the minimal value of N_ϵ where this statement holds. The filter degree N controls the inherent trade-off between a low nominal group delay $\bar{\tau} = N$ and a low algorithmic complexity on the one hand, and a low amount of magnitude and phase distortions on the other hand.

3.3.4.2 Equiripple FIR Phase Equalizer

A cascaded FIR phase equalizer and its application to the design of different allpass-based filter-banks is presented in [Gal02]. The transfer function of an allpass filter of first order and a single FIR phase equalizer of filter length $N_{\text{s}}+1$ is given by

$$\underbrace{\frac{1-a^*z}{z-a}}_{=A(z)} \cdot \underbrace{(z-a)\sum_{l=0}^{N_{\text{s}}-1} z^{l-N_{\text{s}}} \cdot (a^*)^l}_{=\mathcal{P}^{\text{fir}}(z)} = \underbrace{z^{-N_{\text{s}}} - (a^*)^{N_{\text{s}}}}_{=\Psi_{\text{s}}^{\text{fir}}(z)}\,; \quad N_{\text{s}} \in \mathbb{N}\,. \tag{3.85}$$

The 'error term' $(a^*)^{N_\mathrm{s}}$ can be made arbitrarily small by increasing the phase equalizer degree N_s since $|a| < 1$. The degree of the transfer function $\Psi_\mathrm{s}^\mathrm{fir}(z)$ equals that of the FIR phase equalizer, i.e., $D_\mathrm{s} = N_\mathrm{s}$.

If this approach is used for the phase equalization of an *allpass chain* of length L_ac, the transfer function of Eq. (3.78) turns into an FIR filter given by

$$\Psi^\mathrm{fir}(z) = \Big(A(z) \cdot \mathcal{P}^\mathrm{fir}(z)\Big)^{L_\mathrm{ac}} \tag{3.86a}$$

$$= \Big(z^{-D_\mathrm{s}} - (a^*)^{D_\mathrm{s}}\Big)^{L_\mathrm{ac}} \ . \tag{3.86b}$$

As shown in the following, an equiripple approximation error is achieved in this case, which reasons the naming as *equiripple FIR phase equalizer* introduced in [LV06d]. The analytical expressions for the approximation errors of Eq. (3.74) are only presented here where details of the derivations are provided by App. B.2.1.

The magnitude response of the actual transfer function of Eq. (3.86) is given by

$$\Big|\Psi^\mathrm{fir}\left(e^{j\,\Omega}\right)\Big| = \Big(1 - 2\,\alpha^{D_\mathrm{s}} \cos\Big(D_\mathrm{s} \cdot (\Omega - \gamma)\Big) + \alpha^{2\,D_\mathrm{s}}\Big)^{\frac{L_\mathrm{ac}}{2}} \ . \tag{3.87}$$

The magnitude error of Eq. (3.74a) can be written

$$\begin{aligned}\Delta\Big|\Psi^\mathrm{fir}\left(e^{j\,\Omega}\right)\Big| &= \Big|\Psi^\mathrm{fir}\left(e^{j\,\Omega}\right)\Big| - \bar{c} \\ &= \Big|\Psi^\mathrm{fir}\left(e^{j\,\Omega}\right)\Big| - \frac{1}{2}\bigg(\Big(1 - \alpha^{D_\mathrm{s}}\Big)^{L_\mathrm{ac}} + \Big(1 + \alpha^{D_\mathrm{s}}\Big)^{L_\mathrm{ac}}\bigg) \ .\end{aligned} \tag{3.88}$$

This error function has the extrema

$$\Delta\Big|\Psi^\mathrm{fir}\left(e^{j\,\Omega_\mu}\right)\Big| = \frac{(-1)^\mu}{2}\left(\Big(1 - \alpha^{D_\mathrm{s}}\Big)^{L_\mathrm{ac}} - \Big(1 + \alpha^{D_\mathrm{s}}\Big)^{L_\mathrm{ac}}\right) \tag{3.89a}$$

for the extremal frequencies

$$\Omega_\mu = \frac{\mu\,\pi}{D_\mathrm{s}} + \gamma; \quad \mu \in \{0, 1, \ldots, 2D_\mathrm{s}\} \ . \tag{3.89b}$$

Hence, this error function possesses alternating extrema of equal magnitude

$$\Delta\Big|\Psi^\mathrm{fir}\left(e^{j\,\Omega_\mu}\right)\Big| = -\Delta\Big|\Psi^\mathrm{fir}\left(e^{j\,\Omega_{\mu+1}}\right)\Big|; \quad \mu = 0, 1, \ldots, 2D_\mathrm{s} - 1 \tag{3.90}$$

within the frequency interval $\Omega \in [\gamma, 2\pi + \gamma]$. These $2D_\mathrm{s} + 1$ extrema at Ω_μ constitute an *alternate* such that[9]

$$\begin{aligned}\max_\Omega\left\{\bigg|\,\Delta\Big|\Psi^\mathrm{fir}\left(e^{j\,\Omega}\right)\Big|\,\bigg|\right\} &= \bigg|\,\Delta\Big|\Psi^\mathrm{fir}\left(e^{j\,\Omega_\mu}\right)\Big|\,\bigg| \\ &= \Big\|\,\Delta\Big|\Psi^\mathrm{fir}\left(e^{j\,\Omega}\right)\Big|\,\Big\|_\infty \ .\end{aligned} \tag{3.91}$$

The phase response of the actual transfer function is given by

$$\varphi_\Psi^\mathrm{fir}(\Omega) = L_\mathrm{ac} \cdot \left(\arctan\left(\frac{\sin(D_\mathrm{s}\,\Omega) - \alpha^{D_\mathrm{s}} \sin(D_\mathrm{s}\,\gamma)}{\cos(D_\mathrm{s}\,\Omega) - \alpha^{D_\mathrm{s}} \cos(D_\mathrm{s}\,\gamma)}\right) + 2\,\pi\,\chi(D_\mathrm{s}\,\Omega)\right) \tag{3.92}$$

[9] The mathematical background is briefly explained in App. D.1.

with $\chi(\Omega)$ being introduced in Eq. (2.54). The phase error of Eq. (3.74b) reads

$$\Delta\varphi_{\Psi}^{\mathrm{fir}}(\Omega) = \varphi_{\Psi}^{\mathrm{fir}}(\Omega) - \bar{\psi}^{\mathrm{fir}}\,\Omega \tag{3.93}$$

$$= \varphi_{\Psi}^{\mathrm{fir}}(\Omega) - L_{\mathrm{ac}}\,D_{\mathrm{s}}\,\Omega\,. \tag{3.94}$$

It possesses the extrema

$$\Delta\varphi_{\Psi}^{\mathrm{fir}}(\Omega_{\mu}) = (-1)^{\mu+1} L_{\mathrm{ac}}\,\arctan\left(\frac{\alpha^{D_{\mathrm{s}}}\sin\left(\arccos\left(\alpha^{D_{\mathrm{s}}}\right)\right)}{1-\alpha^{2\,D_{\mathrm{s}}}}\right) \tag{3.95a}$$

$$\text{for}\;\; \Omega_{\mu} = \frac{1}{D_{\mathrm{s}}}\,\left(2\,\pi\left\lfloor\frac{\mu}{2}\right\rfloor - (-1)^{\mu}\,\arccos\left(\alpha^{D_{\mathrm{s}}}\right)\right) + \gamma \tag{3.95b}$$

where the operation $\lfloor x \rfloor$ provides the greatest integer which is equal to or smaller than x. Hence, the phase error function $\Delta\varphi_{\Psi}^{\mathrm{fir}}(\Omega)$ has $2D_{\mathrm{s}}+1$ alternating extrema

$$\Delta\varphi_{\Psi}^{\mathrm{fir}}(\Omega_{\mu}) = -\Delta\varphi_{\Psi}^{\mathrm{fir}}(\Omega_{\mu+1});\quad \mu = 0, 1, \ldots, 2\,D_{\mathrm{s}} - 1 \tag{3.96}$$

within the frequency interval $\Omega \in [\Omega_0, \Omega_{2D_{\mathrm{s}}}]$.

The group delay of the actual transfer function is obtained by differentiating the continuous (unwrapped) phase response of Eq. (3.92)

$$\tau_{\Psi}^{\mathrm{fir}}(\Omega) = L_{\mathrm{ac}}\,D_{\mathrm{s}}\,\frac{1-\alpha^{D_{\mathrm{s}}}\cos(D_{\mathrm{s}}\,(\Omega-\gamma))}{1-2\,\alpha^{D_{\mathrm{s}}}\cos(D_{\mathrm{s}}\,(\Omega-\gamma)) + \alpha^{2D_{\mathrm{s}}}}\,. \tag{3.97}$$

This group delay exhibits an equiripple approximation error for Eq. (3.74c)

$$\Delta\tau_{\Psi}^{\mathrm{fir}}(\Omega) = \tau_{\Psi}^{\mathrm{fir}}(\Omega) - \bar{\tau}^{\mathrm{fir}} \tag{3.98}$$

$$= \tau_{\Psi}^{\mathrm{fir}}(\Omega) - \frac{L_{\mathrm{ac}}\,D_{\mathrm{s}}}{1-\alpha^{2D_{\mathrm{s}}}} \tag{3.99}$$

with alternating extrema given by

$$\Delta\tau_{\Psi}^{\mathrm{fir}}(\Omega_{\mu}) = (-1)^{\mu}\,\frac{\alpha^{D_{\mathrm{s}}}}{1-\alpha^{2D_{\mathrm{s}}}}\,L_{\mathrm{ac}}\,D_{\mathrm{s}} \tag{3.100a}$$

$$\Omega_{\mu} = \frac{\pi\,\mu}{D_{\mathrm{s}}} + \gamma;\quad \mu = 0, 1, \ldots, 2D_{\mathrm{s}}\,. \tag{3.100b}$$

Thus, the approximation errors for magnitude response, phase response and group delay between actual and desired transfer function function according to Eq. (3.74) exhibit an equiripple behavior being characterized by Eq. (D.5) (which is not shown in [Gal02]). It should be noted that this property is established by analysis of a given filter, but not by numerically solving a Chebyshev approximation for a set of filters, cf., [Lan93].

3.3.4.3 Equiripple Allpass Phase Equalizer

A drawback of FIR phase equalizers is that they introduce magnitude distortions, which can be avoided by the use of allpass phase equalizers. A closed-form design for such a

phase equalizer is introduced by Eq. (3.30). This design approach for a cascaded phase equalization is originally proposed in [LV06d] for the design of allpass transformed filter-banks. As shown in the following, an equiripple approximation error for phase response and group delay is achieved for the phase equalization of allpass chains, which reasons the naming as *equiripple allpass phase equalizer.*

The allpass phase equalizer of Eq. (3.30) is considered (skipping the notation of the sub-indices). The actual transfer function of an allpass filter of first order and the corresponding allpass phase equalizer is given by

$$\underbrace{\frac{1-a^*z}{z-a}}_{=A(z)} \underbrace{\prod_{l=0}^{J-1} \frac{1+(a^*z)^{2^l}}{z^{2^l}+a^{2^l}}}_{=\mathcal{P}^{\mathrm{ap}}(z)} = \underbrace{\frac{1-(a^*z)^{D_\mathrm{s}}}{z^{D_\mathrm{s}}-a^{D_\mathrm{s}}}}_{=\Psi_\mathrm{s}^{\mathrm{ap}}(z)}; \quad D_\mathrm{s}=2^J; \quad J\in\mathbb{N}_0 \tag{3.101}$$

due to Eq. (3.33). The actual transfer function $\Psi_\mathrm{s}^{\mathrm{ap}}(z)$ represents an allpass filter, which tends to z^{-D_s} for an increasing filter degree D_s since $|a|<1$. The degree of the allpass phase equalizer N_s is related to the degree of the actual transfer function D_s by the relation

$$D_\mathrm{s} = 2^J = N_\mathrm{s}+1\,. \tag{3.102}$$

The restriction to values of 2^J can be avoided by expressing the system function of this allpass phase equalizer in its direct form

$$\mathcal{P}^{\mathrm{ap}}(z) = \frac{\sum\limits_{n=0}^{N_\mathrm{s}-1} (a^*)^{N_\mathrm{s}-1-n}\, z^{-n}}{\sum\limits_{n=0}^{N_\mathrm{s}-1} a^n\, z^{-n}} \tag{3.103}$$

with $N_\mathrm{s}\in\mathbb{N}$. The price for this increased flexibility for the allpass filter degree N_s is that this direct form implementation requires usually more multipliers and adders than the realization by the cascade form according to Eq. (3.101).

If the design of Eq. (3.101) is used for phase equalization of an allpass chain of length L_ac, the transfer function of Eq. (3.78) is given by

$$\Psi^{\mathrm{ap}}(z) = \Big(A(z)\cdot\mathcal{P}^{\mathrm{ap}}(z)\Big)^{L_\mathrm{ac}} \tag{3.104a}$$

$$= \left(\frac{1-(a^*z)^{D_\mathrm{s}}}{z^{D_\mathrm{s}}-a^{D_\mathrm{s}}}\right)^{L_\mathrm{ac}}\,. \tag{3.104b}$$

An interesting link between equiripple FIR phase equalizer and allpass phase equalizer can be established by decomposing the transfer function of Eq. (3.86) into an allpass filter given by Eq. (3.104) and a minimum-phase filter according to

$$\underbrace{\Big(z^{-D_\mathrm{s}}-(a^*)^{D_\mathrm{s}}\Big)^{L_\mathrm{ac}}}_{=\Psi^{\mathrm{fir}}(z)} = \underbrace{\left(\frac{1-(a^*z)^{D_\mathrm{s}}}{z^{D_\mathrm{s}}-a^{D_\mathrm{s}}}\right)^{L_\mathrm{ac}}}_{=\Psi^{\mathrm{ap}}(z)} \underbrace{\Big(1-a^{D_\mathrm{s}}z^{-D_\mathrm{s}}\Big)^{L_\mathrm{ac}}}_{=\Psi^{\mathrm{min}}(z)}\,. \tag{3.105}$$

This indicates already that the FIR phase equalizer achieves a lower phase and group delay error than the allpass phase equalizer at the price of magnitude distortions. The following analysis provides a more precise quantification of this result.

Calculating the phase response and group delay of the actual transfer function of Eq. (3.104) yields

$$\varphi_{\Psi}^{\mathrm{ap}}(\Omega) = L_{\mathrm{ac}} \cdot \left(2 \arctan \left(\frac{\sin(D_{\mathrm{s}}\,\Omega) - \alpha^{D_{\mathrm{s}}} \sin(D_{\mathrm{s}}\,\gamma)}{\cos(D_{\mathrm{s}}\,\Omega) - \alpha^{D_{\mathrm{s}}} \cos(D_{\mathrm{s}}\,\gamma)} \right) + 2\,\pi\,\chi(\Omega) - D_{\mathrm{s}}\,\Omega \right) \tag{3.106}$$

$$\tau_{\Psi}^{\mathrm{ap}}(\Omega) = L_{\mathrm{ac}}\,D_{\mathrm{s}}\,\frac{1-\alpha^{D_{\mathrm{s}}}}{1-2\,\alpha^{D_{\mathrm{s}}}\cos(D_{\mathrm{s}}\,(\Omega-\gamma)) + \alpha^{2\,D_{\mathrm{s}}}}\,. \tag{3.107}$$

As shown in App. B.2.2, the phase error of Eq. (3.74b) for the desired phase response can be written as follows

$$\begin{aligned} \Delta\varphi_{\Psi}^{\mathrm{ap}}(\Omega) &= \varphi_{\Psi}^{\mathrm{ap}}(\Omega) - \bar{\psi}^{\mathrm{ap}}\,\Omega && (3.108)\\ &= \varphi_{\Psi}^{\mathrm{ap}}(\Omega) - L_{\mathrm{ac}}\,D_{\mathrm{s}}\,\Omega && (3.109)\\ &= 2\,\Delta\varphi_{\Psi}^{\mathrm{fir}}(\Omega)\,. && (3.110) \end{aligned}$$

Thus, curve progression and extremal frequencies Ω_μ of the phase error are the same as for the equiripple FIR phase equalizer according to Eq. (3.95), but the magnitude of the error is twice as high.[10] A similar relation can be established for the group delay of Eq. (3.99)

$$\begin{aligned} \Delta\tau_{\Psi}^{\mathrm{ap}}(\Omega) &= \tau_{\Psi}^{\mathrm{ap}}(\Omega) - \bar{\tau}^{\mathrm{ap}} && (3.111)\\ &= \tau_{\Psi}^{\mathrm{ap}}(\Omega) - L_{\mathrm{ac}}\,D_{\mathrm{s}}\,\frac{1+\alpha^{2\,D_{\mathrm{s}}}}{1-\alpha^{2\,D_{\mathrm{s}}}} && (3.112)\\ &= 2\,\Delta\tau_{\Psi}^{\mathrm{fir}}(\Omega) && (3.113) \end{aligned}$$

which is proven in App. B.2.2.

It can be concluded that phase and group delay error of this allpass phase equalizer provide an equiripple error (which is characterized by Eq. (D.5)). The error functions of phase and group delay have the same curve progression and extremal frequencies Ω_μ as those of the corresponding FIR phase equalizer, but the extrema of phase and group delay error are twice as high as for the FIR phase equalizer. On the other hand, the analyzed FIR phase equalizer causes an equiripple magnitude error while the allpass phase equalizer introduces no magnitude distortions. A nice property of the derived analytical expressions for the approximation errors of Eq. (3.74) is that they allow to evaluate the *maximal* magnitude, phase and group delay error in dependence on the design parameters a, D_{s} and L_{ac} in a simple fashion. The magnitude of the error functions is thereby only dependent on the magnitude of the allpass pole α where the extremal frequencies Ω_μ depend only on its phase γ.

[10] The different values for the extrema are not contradictory to the alternation theorem (briefly explained in App. D.1), which states the existence of a unique solution, since the approximation errors for different transfer functions are considered.

The property of an equiripple error usually gets lost in case of a general cascaded phase equalization according to Eq. (3.77). The analysis of the approximation errors for this case is less insightful and hence not treated in more detail.

3.3.4.4 Evaluation & Design Examples

Some characteristic properties of the discussed closed-form designs are evaluated in the following. As a simple but instructive example, the phase equalization of an allpass filter of first order with either a real or complex pole is considered.[11] A filter degree of $N_\mathrm{s} = 7$ is used for the equiripple allpass phase equalizer and a filter degree of $N_\mathrm{s} = 8$ is taken for the equiripple FIR phase equalizer and LS FIR phase equalizer such that all systems have approximately the same overall signal delay with $\bar{\tau} \approx 8$.[12] The resulting error functions according to Eq. (3.74) are plotted in Figure 3.19. For the LS FIR phase equalizer, the values $\bar{c} = 1$, $\bar{\psi} = 7.9964$ and $\bar{\tau} = 8$ are used for the evaluation of Eq. (3.74). The corresponding values for the equiripple phase equalizers are determined by the formulas established in Sec. 3.3.4.2 and Sec. 3.3.4.3.

Figure 3.19 shows that the approximation errors for the LS FIR phase equalizer are of similar magnitude, but more frequency dependent than for the equiripple FIR phase equalizer.

The previous analysis of the equiripple FIR phase equalizer and equiripple allpass phase equalizer has revealed that the extremal frequencies Ω_μ for the phase error as well as the group delay error are the same for both phase equalizers and for an allpass pole $a = \alpha\, e^{j\,\gamma}$ only dependent on the value for γ (but not α). This can be observed in Figure 3.19 where the extremal frequencies for $a = 0.5$ and $a = 0.5\, e^{j\,\pi/8}$ differ by a frequency shift of $\pi/8 = 0.125\,\pi$.

The magnitudes of the alternating extrema are only dependent on the value for α (but not γ). Therefore, the extrema of the equiripple approximation errors are identical for both poles. The allpass phase equalizer causes no magnitude distortions, but the maximal phase and group delay error are (exactly) twice as high as for the corresponding equiripple FIR phase equalizer.

The algorithmic complexity of the different phase equalizers is finally compiled in Table 3.2. All phase equalizers are designed for a general allpass filter of K-th order and have filter degrees which are equal to the number of delay elements. The cascade form of an allpass filter is taken with its single allpass filters implemented according to Figure 2.8. A cascaded phase equalization according to Eq. (3.77) is considered where $D_\mathrm{s}(m)$ represents the filter degree of each single phase equalizer.

An advantage of the equiripple allpass phase equalizer in comparison to the other listed phase equalizers is its comparatively low algorithmic complexity for higher values of $D_\mathrm{s}(m)$, cf., Eq. (3.101). If $D_\mathrm{s}(m)$ is not a power of two, the closed-form design of Eq. (3.103) can be used. The algorithmic complexity of this phase equalizer corresponds to that of a general allpass phase equalizer obtained, e.g., by a numerical design.

[11] The phase equalization of an allpass chain according to Eq. (3.75) is discussed in Sec. 4.2.3 in connection with allpass transformed filter-banks.

[12] A comparison of the considered closed-form phase equalizer designs with the numerical allpass phase equalizer design of [LL94] is provided by [LV06d].

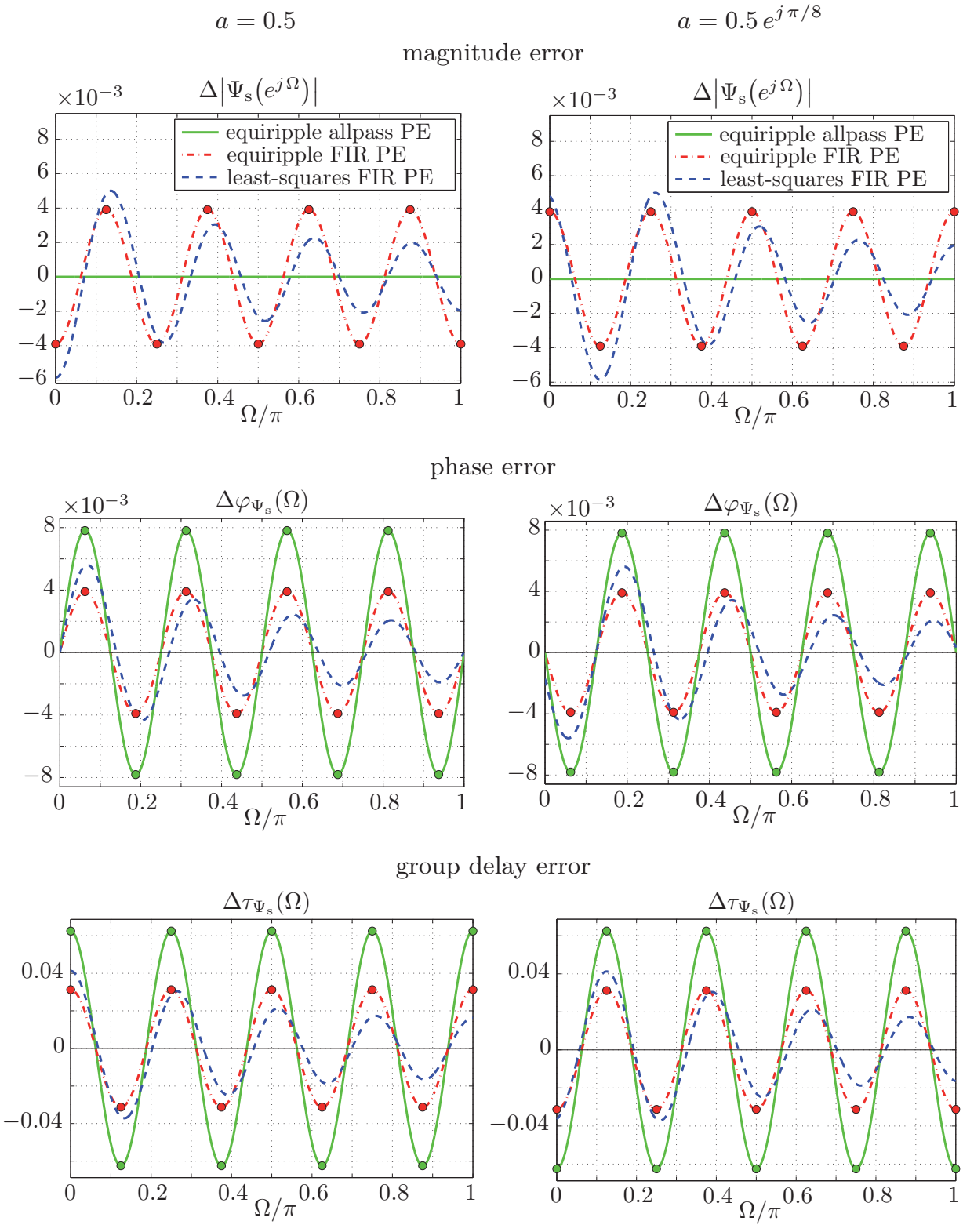

Figure 3.19: *Approximation errors of Eq.* (3.74) *for different closed-form phase equalizer designs applied to an allpass filter of first order with pole a such that* $\bar{\tau} \approx 8$ *in each case. The left column shows the plots for a real allpass pole* ($a = 0.5$) *and the right column the plots for a complex pole* ($a = 0.5\,e^{j\,\pi/8}$).

Table 3.2: *Algorithmic complexity of the least-squares FIR phase equalizer (LS FIR PE), equiripple FIR phase equalizer (ER FIR PE), equiripple allpass phase equalizer (ER AP PE) and general allpass phase equalizer (gen. AP PE) designed for an allpass of K-th order. The number of delay elements is equal to the filter degree of each phase equalizer.*

	multipliers	adders	delay elements
LS FIR PE	N	$N-1$	$N-1$
ER FIR PE	$\sum_{m=1}^{K} D_{\mathrm{s}}(m)$	$\sum_{m=1}^{K} \big(D_{\mathrm{s}}(m)-1\big)$	$\sum_{m=1}^{K} \big(D_{\mathrm{s}}(m)-1\big)$
ER AP PE	$2\sum_{m=1}^{K} \log_2 D_{\mathrm{s}}(m)$	$2\sum_{m=1}^{K} \log_2 D_{\mathrm{s}}(m)$	$\sum_{m=1}^{K} \big(D_{\mathrm{s}}(m)-1\big)$
gen. AP PE	$2\sum_{m=1}^{K} (D_{\mathrm{s}}(m)-1$	$2\sum_{m=1}^{K} (D_{\mathrm{s}}(m)-1)$	$\sum_{m=1}^{K} \big(D_{\mathrm{s}}(m)-1\big)$

It follows from Table 3.2 that the LS FIR phase equalizer and equiripple FIR phase equalizer of this example with $K = 1$ require each 8 multipliers, 7 adders and 7 delay elements, where the equiripple allpass phase equalizer needs 6 multipliers, 6 adders and 7 delay elements. In contrast, a general allpass phase equalizer of the same degree would require 14 adders, 14 multipliers and 7 delay elements. The differences between the phase equalizers become of course even more pronounced in case of a phase equalization for an allpass filter of higher order ($K > 1$).

3.4 Conclusions

The design of allpass-based QMF-banks and Pseudo QMF-banks with near-perfect reconstruction is treated in this chapter. The analysis filters of these critically subsampled AS FBs consist of allpass polyphase filters. This approach facilitates a high frequency selectivity with a low filter degree. The proposed synthesis filter-banks have in common that they consist only of *allpass* polyphase filters, which are designed by simple analytical expressions. This allows to adjust the trade-off between signal delay and reconstruction error in a simple and flexible manner.

The presented QMF-bank design I achieves a minimization of amplitude, phase and aliasing distortions with a low algorithmic complexity. The proposed QMF-bank design II has a higher algorithmic complexity and signal delay than design I, but achieves a complete aliasing cancellation and introduces no amplitude distortions. This design can be seen as a generalization of the classical allpass-based QMF-bank where the remaining phase distortions are now reduced by a subsequent phase equalizer. An extension of this second design is discussed, which allows to obtain subband filters with a more linear phase response at the price of an increased algorithmic complexity.

The main difference to the related IIR/FIR QMF-bank designs of [GK01a, KDL00, KD02, KB06] is that the proposed IIR/IIR QMF-bank designs cause higher phase distortions, but they possess a lower algorithmic complexity and cause no or negligible amplitude distortions. Due to these properties, the devised QMF-bank designs are

of special interest for speech and audio applications as the human auditory system is rather insensitive towards phase distortions. One possible application are speech and audio coding systems, which is elaborated in Chap. 6.

The devised QMF-bank designs I and II can be extended to a critically subsampled M-channel DFT AS FB. The analysis filters of this Pseudo QMF-bank consist of allpass polyphase filters. One option is to design the synthesis allpass polyphase in such a manner that amplitude, phase and aliasing distortions are minimized. Alternatively, aliasing and amplitude distortions can be avoided at the expense of an increased algorithmic complexity and signal delay.

The construction of allpass-based filter-banks relies essentially on solving a *phase equalization problem*. Therefore, different phase equalizer designs for allpass-based filter-banks are elaborated in more detail.

A general problem in the design of allpass-based filter-banks with perfect reconstruction is that the required synthesis polyphase filters, which can be regarded as phase equalizers, are anti-causal. One approach to solve this problem is to perform a 'time-reversed' filtering and to transmit initial filter states to the synthesis filter-bank [MCB92]. It turns out that this PR filter-bank design is very susceptible towards modifications of the subband signals and, hence, less suitable for practical applications.

The NPR design of [CM96] relies also on a time-reversed filtering, but requires no transmission of the filter states at the price of an increased signal delay and a higher algorithmic complexity. However, the investigation of this approach reveals that it constitutes a linear periodically time-varying (LPTV) system, which creates alias components whose number grows with the length of the buffers used for the time-reversed filtering. Hence, the use of this approach for the phase equalization within allpass-based filter-banks causes additional aliasing distortions in contrast to the use of linear time-invariant (LTI) phase equalizers.

A main approach to construct LTI phase equalizers is to approximate the 'ideal' non-causal phase equalizer by a causal FIR or IIR filter. These phase equalizers can be designed by closed-form expression, which avoids the difficulties of a general numerical (allpass) phase equalizer design.

The analysis of the closed-form FIR phase equalizer design of [Gal02] shows that the phase, group delay and magnitude error function exhibit an equiripple behavior, if the phase response of an allpass filter of first order or an allpass chain is equalized. In this case, the proposed closed-form allpass phase equalizer design exhibits an equiripple behavior for the phase and group delay error as well. The alternating extrema are twice as high as for the equiripple FIR phase equalizer and located at the same frequency points, while the equiripple allpass phase equalizer causes no amplitude distortions and has a lower complexity. This reasons the above mentioned differences of the proposed IIR/IIR (Pseudo) QMF-bank designs to the corresponding IIR/FIR (Pseudo) QMF-bank designs of [Gal02].

Chapter 4

Allpass Transformed Analysis-Synthesis Filter-Banks

The allpass transformation is a well-known technique to design a digital filter-bank with non-uniform time-frequency resolution [OJS71, OJ72, BO74, Var78, Var80]. This transformation provides a *frequency warped* filter-bank by substituting the delay elements of the analysis filters by allpass filters of first order. An advantage of this approach is that the frequency resolution of the filter-bank is merely adjusted by the choice for a single allpass pole such that an individual redesign of the analysis filters is not required.

The allpass transformation allows to design a filter-bank whose frequency bands provide a very good approximation of the so-called Bark frequency bands, which model the non-uniform frequency resolution of the human auditory system [SA99]. Non-uniform filter-banks with such an auditory frequency resolution are of interest for speech and audio processing and are used, e.g., for (perceptual) speech enhancement [Eng98, GEH98, dHCG03, Coh01, PPB04, DMFB07]. An advantage of frequency warped AS FBs is thereby their lower signal delay and lower computational complexity in comparison to a corresponding tree-structured QMF-bank or wavelet packets, respectively.

The design of allpass transformed AS FBs is comprehensively treated in different works such as [Kap98, Gal02, dH04]. Despite significant progress, the construction of such filter-banks is still a challenging problem. As for other non-uniform AS FBs [HV89, AV99], it is more difficult to achieve an (almost) perfect signal reconstruction in comparison to uniform filter-banks. The allpass transformation of an FIR analysis filter-bank results in an IIR analysis filter-bank such that a linear phase response is converted into a non-linear one. These phase modifications must be (partly) compensated by the synthesis filter-bank. Another main problem is that the aliasing cancellation does not function in the same manner as for the underlying uniform AS FB due to the non-uniform bandwidths of the warped analysis filters. As a consequence, the synthesis filter-bank design for allpass transformed filter-banks is more demanding than for their uniform counterparts.

In this chapter, the main design approaches for allpass transformed AS FBs are reviewed. This analysis reveals some shortcomings of existing approaches, which leads to the development of several improved and novel designs.

In Sec. 4.1, the concept of the allpass transformation is revisited and compared with alternative frequency warping techniques to design a non-uniform filter-bank. Based

on that, the design of allpass transformed AS FBs by means of analytical closed-form expressions is treated in Sec. 4.2. A benefit of the closed-form designs is their simplicity, but they are less suitable if specific design constraints should be incorporated. This issue is tackled by a new numerical design framework presented in Sec. 4.3. A discussion and summary of the different design approaches is finally provided by Sec. 4.4.

4.1 Frequency Warping by Allpass Transformation

The design of tunable digital filters by means of an allpass transformation is a well-know method [Con67, Con68, Con70, Sch68, SW70]. In the process, the delay elements of a lowpass filter are replaced by identical allpass filters of first order. This bilinear transformation allows to tune stopband and passband frequency of a lowpass filter by simply varying a single allpass coefficient. An advantage of this frequency warping is that characteristic properties of the original lowpass filter, such as the number of ripples in the passband, the number of poles in the stopband, the passband and stopband attenuation etc., are not altered. Besides this lowpass-to-lowpass transformation, it is also possible to transform a lowpass filter into a highpass, bandpass, or bandstop filter by an appropriate choice for the employed allpass filter [SW70, Mit98].

The allpass transformation can also be exploited to perform short-term spectral analysis with a non-uniform frequency resolution and to construct non-uniform digital filter-banks [OJS71, OJ72, BO74, Var78, Var80, Dob91]. This design approach for warped filter-banks is further generalized in [KSV96, Kap98] where the allpass transformation of higher order is introduced.

In the following, the concept of the allpass transformation is reviewed and contrasted to related techniques to construct a non-uniform filter-bank.

4.1.1 Allpass Transformation of First Order

A common approach to design a frequency warped filter-bank is to replace the delay elements of the analysis filters by allpass filters of first order

$$z^{-1} \rightarrow A(z) \tag{4.1}$$

with $A(z)$ given by Eq. (2.52) [OJS71, OJ72]. This transformation provides a conformal mapping from the unit disk onto another unit disk in the z-plane. Applying this *allpass transformation of first order* to the analysis filters of a (uniform) DFT filter-bank given by

$$H_i(z) = \sum_{l=0}^{L-1} h(l) \cdot W_M^{-i\,l} \cdot z^{-l}; \quad i \in \{0, 1, \ldots, M-1\} \tag{2.23}$$

yields the allpass transformed system functions

$$\widetilde{H}_i(z) = \sum_{l=0}^{L-1} h(l) \cdot W_M^{-i\,l} \cdot A^l(z)\,. \tag{4.2}$$

The tilde-notation is used in this work to mark system functions which are altered by frequency warping (see also App. A.2). Inserting Eq. (2.53) into Eq. (4.2) yields the following relation between allpass transformed and original analysis filters

$$\widetilde{H}_i\left(e^{j\,\Omega}\right) = \sum_{l=0}^{L-1} h(l) \cdot W_M^{-i\,l} \cdot e^{-j\,l\,\varphi_a(\Omega)} \tag{4.3}$$

$$= H_i\left(e^{j\,\varphi_a(\Omega)}\right); \quad i \in \{0, 1, \ldots, M-1\}\,. \tag{4.4}$$

Hence, the allpass transformation causes a *frequency warping* where a frequency interval of $\Delta\Omega = 2\,\pi$ is mapped onto an interval of $2\,\pi$ on the warped frequency scale

$$[0, 2\,\pi] \rightarrow [0, 2\,\pi] \quad : \quad \Omega \mapsto \varphi_a(\Omega)\,. \tag{4.5}$$

The warping characteristic is thereby controlled by the phase response $\varphi_a(\Omega)$ as given by Eq. (2.54). The mechanism of this frequency transformation is demonstrated by Figure 4.1. For a real and positive allpass coefficient[1] $a > 0$, a higher frequency resolution is achieved for the lower frequency bands and vice versa for the higher frequency bands. The opposite applies if $a < 0$. Thus, the frequency resolution can be adjusted by a single allpass coefficient, also referred to as *warping coefficient*. Hence, an individual subband filter design, as needed, e.g., for the construction of non-uniform filter-banks by means of 'transition filters' [Pri95, DZ96, CJ03, DBSN06], is not required.

Besides, allpass transformed filter-banks achieve a non-uniform time *and* frequency resolution. In contrast, the realization of a non-uniform filter-bank by means of a simple subband merging alters the frequency resolution but not the time resolution, i.e., the frequency resolution is decreased without improving the time resolution.

The allpass transformation allows to design a non-uniform filter-bank whose frequency bands approximate the *Bark frequency bands* with great accuracy [SA99]. The frequency resolution of the human auditory system is determined by so-called *critical bands*. The mapping between frequency and critical bands can be described by the critical band rate or Bark scale, respectively. An analytical expression for this relation is given by [ZF99]

$$\frac{\xi_{\mathrm{bark}}(f)}{\mathrm{Bark}} = 13 \arctan\left(\frac{0.76\,f}{\mathrm{kHz}}\right) + 3.5 \arctan\left(\left(\frac{f}{7.5\,\mathrm{kHz}}\right)^2\right)\,. \tag{4.6}$$

Figure 4.2 illustrates that such a frequency mapping can be well approximated by an allpass transformation. The relation between the real allpass pole $a = \alpha$ and sampling frequency f_s for such an approximation of the Bark scale is given by [SA99]

$$a_{\mathrm{bark}} = 1.0674 \sqrt{\frac{2}{\pi} \arctan\left(0.05683\,\frac{f_\mathrm{s}}{\mathrm{kHz}}\right)} - 0.1916\,. \tag{4.7}$$

A modification of the Bark frequency scale is given by the *equivalent rectangular bandwidth* (ERB) scale [MG96, Moo97]

$$\frac{\xi_{\mathrm{erb}}(f)}{\mathrm{ERB}} = 21.4\,\log_{10}\left(0.00437\,\frac{f}{\mathrm{Hz}} + 1\right)\,. \tag{4.8}$$

[1] The terms *allpass pole* and *allpass coefficient* are used interchangeably.

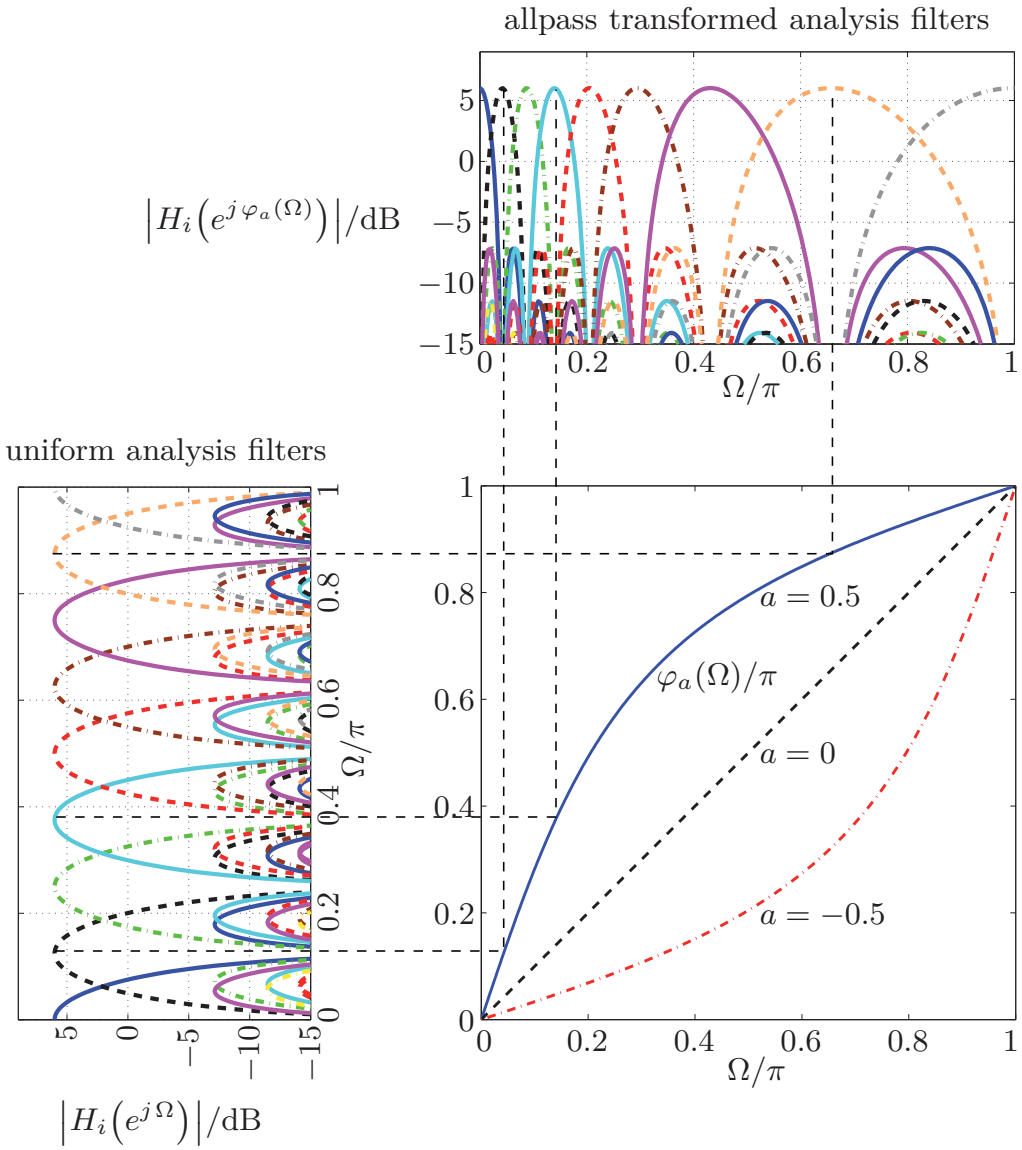

Figure 4.1: *Allpass transformation of first order applied to a DFT analysis filter-bank with rectangular prototype filter of length* $L = M = 16$.

As shown in [SA99], a good mapping for this scale is achieved by an allpass transformation of first order with an allpass coefficient determined by

$$a_{\mathrm{erb}} = 0.7446 \sqrt{\frac{2}{\pi} \arctan\left(0.4418 \, \frac{f_{\mathrm{s}}}{\mathrm{kHz}}\right)} + 0.03237 \,. \tag{4.9}$$

Due to the ability to approximate the Bark or ERB scale with great accuracy, allpass transformed filter-banks are proposed, amongst others, for noise reduction [GEH98], subband beamforming [dHGCN02], acoustic echo control [BP99], subband coding based on auditory modeling [FKK05], or reverberation time estimation [LV11].

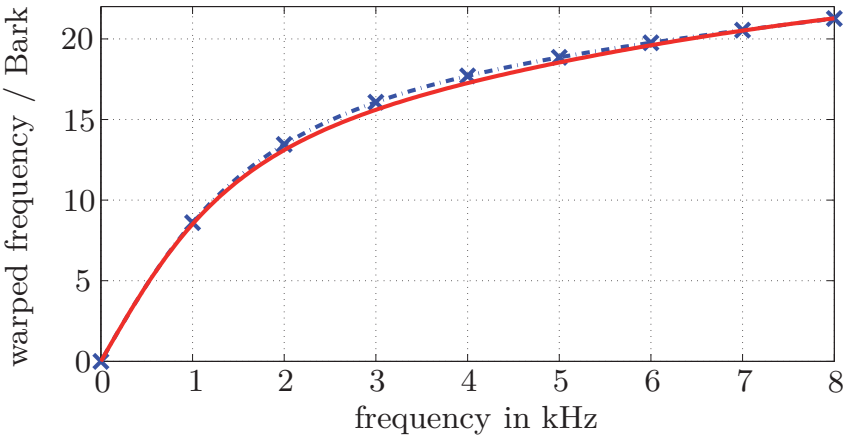

Figure 4.2: *Approximation of the Bark frequency scale: The solid line corresponds to the analytical expression of Eq.* (4.6)*. The dashed line marks the frequency warping for an allpass transformation with* $a = 0.576$ *and sampling frequency of* 16 *kHz.*

4.1.2 Allpass Transformation of Higher Order

The allpass transformation of first order can be extended to allpass filters of higher order [KSV96, Kap98]. The delay elements are now replaced by allpass filters of higher order according to

$$z^{-l} \rightarrow \left(A^{[K]}(z)\right)^{l} \cdot \left(B^{[K-1]}(z)\right)^{L-1-l} \quad \forall\ l \in \{\,0, 1, \ldots, L-1\,\} \tag{4.10}$$

where the system functions of the allpass filters are given by

$$A^{[K]}(z) = \prod_{m=1}^{K} \frac{1 - a^*(m) \cdot z}{z - a(m)}; \quad a(m) \in \left\{\mathbb{C}\middle|\, |a(m)| < 1\right\}; \quad \max_m \{|a(m)|\} < |z| \tag{4.11}$$

$$B^{[K-1]}(z) = \prod_{m=1}^{K-1} \frac{1 - b^*(m) \cdot z}{z - b(m)}; \quad b(m) \in \left\{\mathbb{C}\middle|\, |b(m)| < 1\right\}; \quad \max_m \{|b(m)|\} < |z|\,. \tag{4.12}$$

The frequency responses of these allpass filters are denoted by

$$A^{[K]}\left(e^{j\,\Omega}\right) = e^{-j\,\varphi_{\boldsymbol{a}}^{[K]}(\Omega)} \tag{4.13a}$$

$$B^{[K-1]}\left(e^{j\,\Omega}\right) = e^{-j\,\varphi_{\boldsymbol{b}}^{[K-1]}(\Omega)}\,. \tag{4.13b}$$

Applying the allpass transformation of Eq. (4.10) to the DFT analysis filters of Eq. (2.23) yields

$$\widetilde{H}_i(z) = \left(B^{[K-1]}(z)\right)^{L-1} \sum_{l=0}^{L-1} h(l) \cdot \left(\frac{A^{[K]}(z)}{B^{[K-1]}(z)}\right)^{l} \cdot W_M^{-i\,l} \tag{4.14}$$

$$= \Lambda(z) \sum_{l=0}^{L-1} h(l) \cdot \Theta^{l}(z) \cdot W_M^{-i\,l}; \;\; i \in \{\,0, 1, \ldots, M-1\,\} \tag{4.15}$$

$$\text{with} \quad \Lambda(z) = \left(B^{[K-1]}(z)\right)^{L-1} \quad \text{and} \quad \Theta(z) = \frac{A^{[K]}(z)}{B^{[K-1]}(z)} \tag{4.16}$$

to ease the notation. The common allpass transformation of *first order* is included as special case for $K = 1$ so that Eq. (4.16) is given by

$$\Lambda(z) = 1 \;\; \text{and} \;\; \Theta(z) = \frac{1 - a^* z}{z - a}\,. \tag{4.17}$$

An efficient PPN implementation of the analysis filter-bank is obtained by rewriting Eq. (4.15) as follows

$$\widetilde{H}_i(z) = \Lambda(z) \sum_{m=0}^{l_M-1} \sum_{\lambda=0}^{M-1} h(m\,M + \lambda) \cdot \left(\Theta(z)\right)^{m\,M+\lambda} \cdot W_M^{-i\lambda} \tag{4.18}$$

with l_M given by Eq. (2.36). Figure 4.3 illustrates this type 1 PPN implementation of the DFT analysis filter-bank for $l_M = 2$.

The frequency responses of the uniform analysis filters given by Eq. (2.23) and the non-uniform analysis filters of Eq. (4.14) are related by

$$\widetilde{H}_i\left(e^{j\,\Omega}\right) = e^{-j\,(L-1)\,\varphi_{\boldsymbol{b}}^{[K-1]}(\Omega)}\, H_i\left(e^{j\,\varphi_\Theta(\Omega)}\right); \;\; i \in \{0, 1, \ldots, M-1\} \tag{4.19a}$$

$$\varphi_\Theta(\Omega) = \varphi_{\boldsymbol{a}}^{[K]}(\Omega) - \varphi_{\boldsymbol{b}}^{[K-1]}(\Omega)\,. \tag{4.19b}$$

The phase difference of Eq. (4.19b) ensures that the property of Eq. (4.5) applies for the allpass transformation of higher order as well such that

$$[0, 2\,\pi] \to [0, 2\,\pi] \;\; : \;\; \Omega \mapsto \varphi_\Theta(\Omega)\,. \tag{4.20}$$

In contrast, the allpass transformation $z^{-l} \to \left(A^{[K]}(z)\right)^{l}$ maps the frequency interval of $[0, 2\,\pi]$ onto an interval of $\Delta\Omega = 2\,\pi\,K$, which causes an undesirable comb-filter effect for $K > 1$, cf., [KSV96].[2]

Eq. (4.19a) reveals that the warping characteristic is solely determined by the phase response $\varphi_\Theta(\Omega)$ and, thus, the system function $\Theta(z)$. However, dependent on the choice for $B^{[K-1]}(z)$, the filter with system function $\Theta(z)$ can become either unstable or anti-causal. Therefore, the additional filter with system function $\Lambda(z)$ is employed so that the warped analysis filters of Eq. (4.14) are always stable and causal.

[2] The exploitation of such an effect for the design of comb-filters is treated in [Sch75].

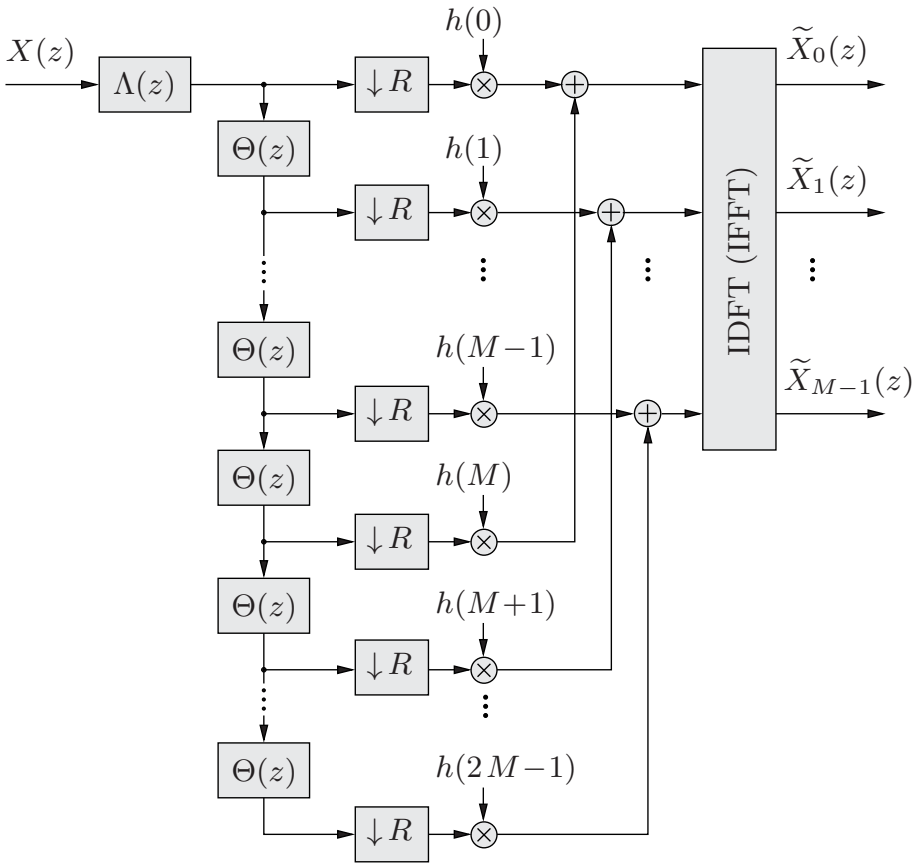

Figure 4.3: *PPN implementation of a warped DFT analysis filter-bank with downsampling by R and $L = 2\,M$ for an allpass transformation of higher order. The allpass transformation of first order is included as special case for $\Lambda(z) = 1$ and $\Theta(z) = A(z)$.*

The function of Eq. (4.20) is bijective, if the continuous (unwrapped) phase response $\varphi_\Theta(\Omega)$ is monotonically increasing, which is guaranteed by a positive group delay

$$\frac{\partial\,\varphi_\Theta(\Omega)}{\partial\,\Omega} > 0 \;\forall\; \Omega\,. \tag{4.21}$$

This property is required to ensure a *unique* frequency mapping such that a comb-filter effect is avoided. The choice

$$B^{[K-1]}(z) = z^{-(K-1)} \tag{4.22}$$

is of special interest as it reduces the implementation cost for the filter-bank and simplifies the design procedure. This choice is considered for the design examples in this work (while the derived designs still apply for the general case). With Eq. (4.22) and Eq. (2.59), the requirement of Eq. (4.21) can now be written

$$\sum_{m=1}^{K} \frac{1-\alpha^2(m)}{1-2\,\alpha(m)\,\cos\big(\Omega-\gamma(m)\big)+\alpha^2(m)} > K-1 \;\forall\; \Omega\,. \tag{4.23}$$

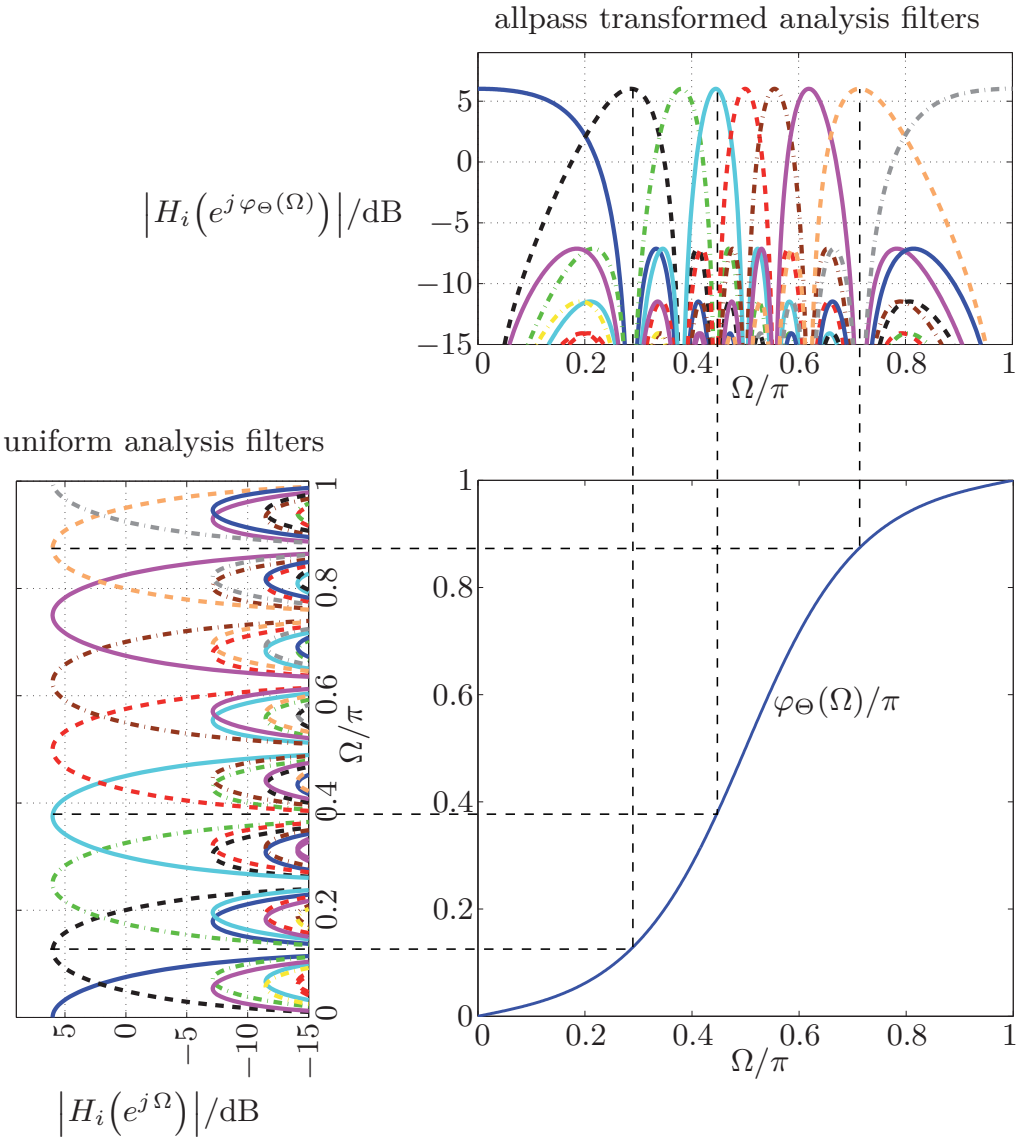

Figure 4.4: *Allpass transformation of second order applied to a DFT analysis filter-bank with rectangular prototype filter of length $L = M = 16$. The allpass coefficients are given by $a(1) = -j\,0.5$, $a(2) = j\,0.5$ and $b(1) = 0$.*

The effect of an allpass transformation of higher order is demonstrated in Figure 4.4. It is easily verified (and visible) that the phase response $\varphi_\Theta(\Omega)$ fulfills Eq. (4.20) and Eq. (4.21). The bandwidths of the non-uniform analysis filters decrease first and increase afterwards within the interval $\Omega \in [0, \pi]$ since the phase response $\varphi_\Theta(\Omega)$ has an inflection point within this region, which cannot be achieved by an allpass transformation of first order (see Figure 4.1). Thus, the allpass transformation of higher order can achieve a more flexible adjustment of the frequency resolution in contrast to the more common allpass transformation of first order at the expense of an increased computational complexity and delay.

4.1.3 Alternative Frequency Warping Techniques

Besides the allpass transformation, there are some other frequency warping techniques to design a non-uniform filter-bank, which have different pros and cons. In the following, the main alternatives are briefly discussed to point out their specific differences in comparison to the considered allpass transformed filter-banks.

4.1.3.1 Warped DFT

The *warped discrete Fourier transform* (WDFT) can be used to obtain a frequency warped filter-bank, e.g., [MM01]. Such filter-banks are proposed, e.g., for perceptual noise reduction [PPB04, BPP06] or frequency estimation [FMD03, VP06]. The WDFT is a special case of a non-uniform DFT. It is obtained from the DFT by the substitution

$$e^{-j\,\frac{2\,\pi}{M}\,i} \rightarrow A\left(e^{j\,\frac{2\,\pi}{M}\,i}\right) \tag{4.24}$$

such that the WDFT of a sequence $x(k)$ is given by

$$X_i^{(\mathrm{wdft})}(k) = \sum_{k=0}^{M-1} x(k) \cdot \left(\frac{e^{-j\,\frac{2\,\pi}{M}\,i} - a^*}{1 - a\,e^{-j\,\frac{2\,\pi}{M}\,i}}\right)^k \quad \text{for} \quad i \in \{\,0, 1, \ldots, M-1\,\}\,. \tag{4.25}$$

Hence, the frequency points of the WDFT are non-uniformly spaced on the unit circle according to the phase response of the employed allpass filter. The (uniform) DFT can be seen as special case obtained for $a = 0$. In [MM01], the WDFT based on allpass filters of first and second order is presented as well as an algorithm for its efficient calculation. However, the computational burden to calculate the WDFT is still significantly higher than for the DFT for which the efficient FFT can be applied.

A *WDFT filter-bank* evolves by replacing the DFT and IDFT of the AS FB according to Figure 2.4 by the WDFT and its inverse [MM01]. A benefit of this approach is that it alters the frequency resolution of the filter-bank without increasing its signal delay. The resulting analysis filters have the system functions

$$H_i^{(\mathrm{wdft})}(z) = \sum_{l=0}^{L-1} h(l) \cdot A^l\left(e^{-j\,\frac{2\,\pi}{M}\,i}\right) \cdot z^{-l} \quad \text{for} \quad i \in \{0, 1, \ldots, M-1\}\,. \tag{4.26}$$

Thus, the analysis filters of a WDFT filter-bank are obtained from Eq. (2.23) by the substitution of Eq. (4.24). In contrast, the analysis filters of an allpass transformed filter-bank are obtained by the substitution of Eq. (4.1). Hence, the center frequencies of the analysis filters of a WDFT filter-bank are shifted as for allpass transformed filters, but their bandwidths remain the same. This effect is illustrated in Figure 4.5. In comparison to an allpass transformed filter-bank as shown in Figure 4.1, the analysis filters of the WDFT filter-bank with $a = -0.5$ show a strong overlap of their pass-bands at lower frequencies where 'gaps' occur at higher frequencies, which results in a diminished spectral selectivity and complicates the signal reconstruction. This effect is reflected by an ill-conditioned WDFT matrix whose condition number can easily exceed

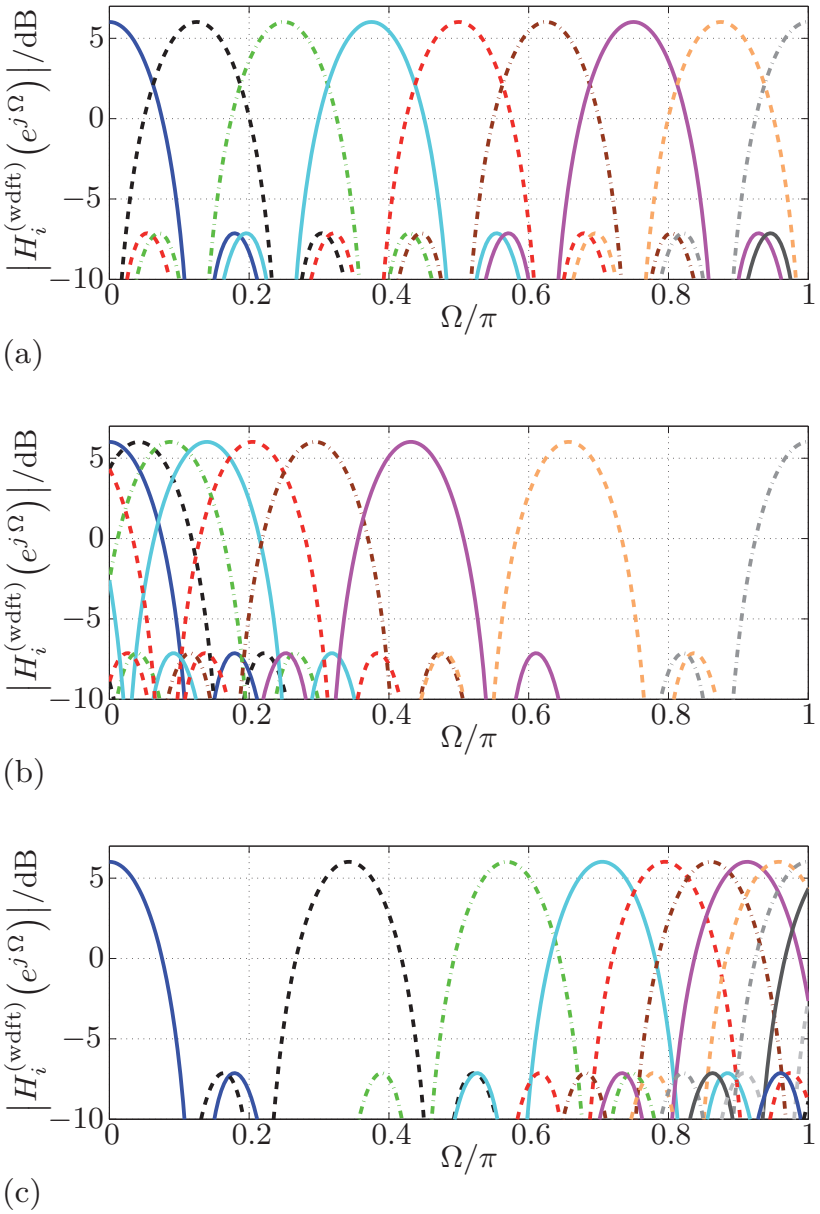

Figure 4.5: *Magnitude responses of the analysis filters of a WDFT filter-bank with $M = 16$ channels and rectangular prototype filter of length $L = M$ for different allpass coefficients:* (a) $a = 0$, (b) $a = -0.5$, (c) $a = 0.5$.

10^{12} for values of about $|a| > 0.3$ and $M > 50$ [FMSD02].[3] An approach to calculate approximately the inverse of an ill-conditioned WDFT matrix is to employ a singular value decomposition and to either reduce or set to zero the smallest singular values [FMSD02, PPB04]. This regularization, however, introduces some distortions to the reconstructed signal. The numerical difficulties for the computation of the inverse WDFT (matrix) become even more pronounced with regard to a practical implementation with limited arithmetic precision as, for example, on a (fixed-point) DSP.

[3]The DFT matrix has a condition number of one so that the calculation of its inverse matrix (IDFT matrix) causes no problems.

4.1.3.2 Non-Recursive Frequency Warping

The allpass transformation of a linear-phase filter leads not only to shifted passband and stopband frequencies, but also to a non-linear phase response according to Eq. (4.5). Such phase distortions, whose compensation is a central issue in the design of allpass transformed filter-banks, can be avoided by using a *non-recursive frequency warping* technique [OMM76, CR76, AR79, Var80].[4] An FIR lowpass filter with linear phase response is considered whose frequency response can be written [OMM76]

$$H_{\mathrm{lin}}\left(e^{j\,\Omega}\right) = e^{-j\,N_{\mathrm{lin}}\,\Omega} \sum_{l=0}^{N_{\mathrm{lin}}} h_{\mathrm{lin}}(l) \cdot (\cos\Omega)^l \ . \tag{4.27}$$

The substitution

$$\cos\Omega \rightarrow \sum_{\nu=0}^{K_c} h_c(\nu) \cdot (\cos\Omega)^\nu \tag{4.28}$$

yields a linear-phase FIR filter whose cutoff frequency is determined by the choice for the coefficients $h_c(\nu)$, cf., [OMM76, CR76]. This frequency transformation increases the length of the original impulse response of $2\,N_{\mathrm{lin}} + 1$ samples to $2\,K_c\,N_{\mathrm{lin}} + 1$ samples. The frequency warping of Eq. (4.28) can also be applied to bandpass filters [AR79].

The use of this non-recursive frequency warping for the design of a non-uniform analysis *filter-bank* requires that the conditions of Eq. (4.20) and Eq. (4.21) are fulfilled, i.e., a frequency interval of $2\,\pi$ is mapped bijectively onto a warped frequency interval of $2\,\pi$ to avoid a comb-filter effect.[5] The investigations in [Ber92] reveal that such a behavior can be achieved by the transformation of Eq. (4.28) for $K_c \geq 7$ which, however, would cause an unacceptable increase of filter length and signal delay, respectively. The later treatment shows that the realization of an allpass transformed filter-bank with an almost linear phase response requires a much lower filter degree and signal delay, respectively. Besides, the additional aliasing distortions due to the non-uniform analysis filters also need to be compensated by some means as for allpass transformed filter-banks. Therefore, this non-recursive frequency warping is apparently more attractive for the design of filters than for non-uniform AS FBs.

Besides frequency warped filter-banks, it is common to realize a non-uniform filter-bank with ERB or Bark-scaled frequency partitioning by means of gammatone filter-banks or tree-structured filter-banks. The characteristic differences of these filter-banks in comparison to allpass transformed filter-banks are discussed in App. C.2.

Henceforth, allpass transformed filter-banks are only considered and the terms *all-pass transformation* and *frequency warping* are therefore used interchangeably.

[4] There exists no common term for this kind of frequency warping in literature. It is referred to as *non-recursive* frequency warping in this work as an FIR filter is converted into an FIR filter. In contrast, the allpass transformation is considered to be a *recursive* frequency warping technique since it converts an FIR filter into an IIR filter.

[5] Such a unique mapping is not necessarily required for the design of a single lowpass or bandpass filter, if the 'ambiguities' occur in the stopband.

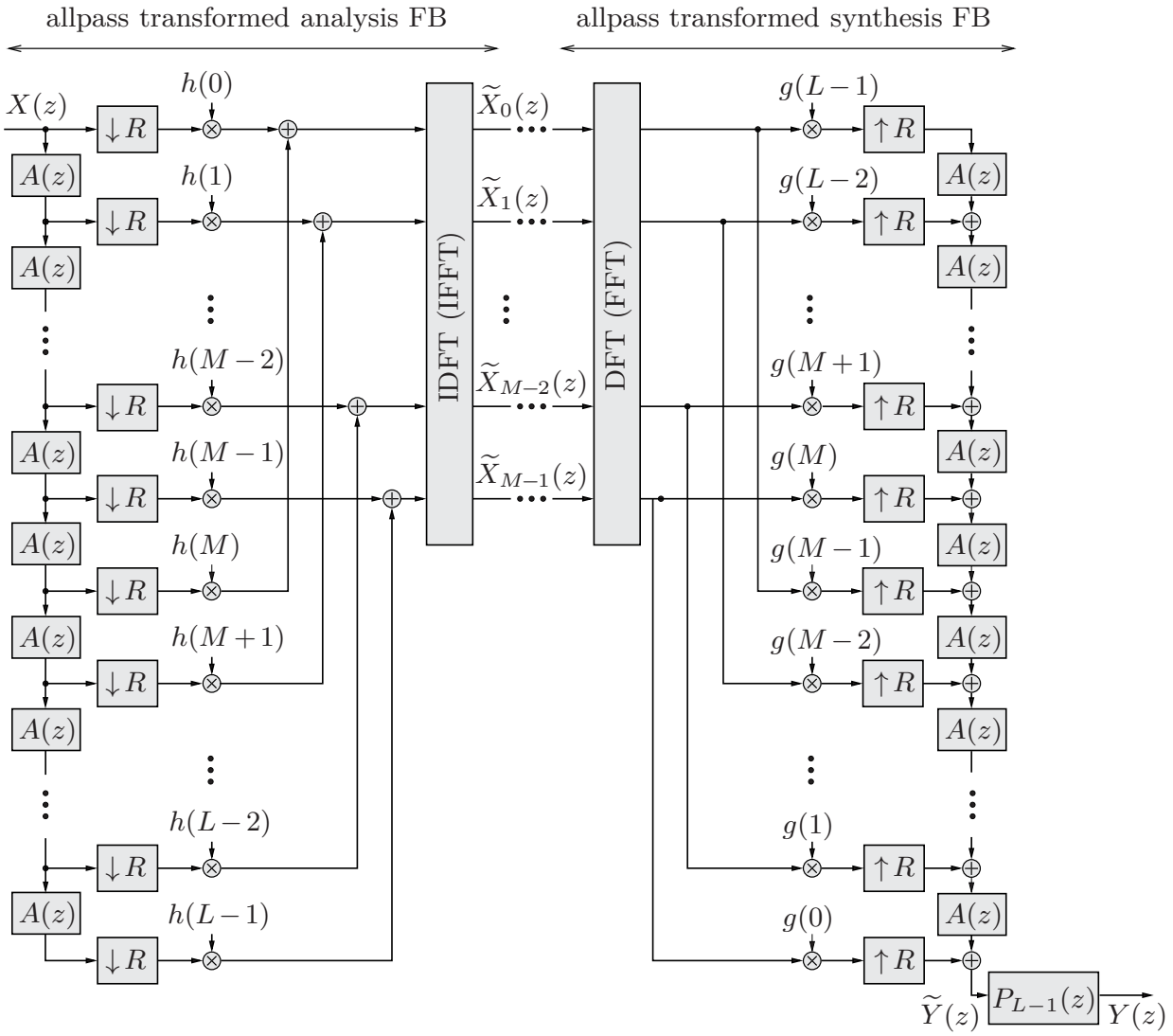

Figure 4.6: *PPN implementation of an allpass transformed DFT AS FB for a prototype filter of length $L = 2\,M$ with a warped synthesis filter-bank and a single phase equalizer.*

4.2 Closed-Form Filter-Bank Designs

Different approaches to design the synthesis filters for an allpass-transformed analysis filter-bank by means of analytical closed-form expressions are now treated.

4.2.1 Warped Synthesis Filter-Bank

A common approach to design an allpass transformed (DFT) AS FB is to replace the delay elements of the analysis filters *and* synthesis filters by allpass filters of first order and to process the output signal by a phase equalizer [Eng98, GEH98, PP03a, LV06d]. Figure 4.6 shows the PPN implementation of such a DFT filter-bank.[6] The *uniform*

[6] The term *closed-form design* does not exclude a numerical prototype filter design for the underlying uniform filter-bank.

DFT filter-bank of Figure 2.4 can be seen as a special case since the delay element z^{-1} is a trivial allpass filter.

Due to the allpass transformation, the input-output relation of the uniform AS FB according to Eq. (2.9) turns into

$$\widehat{\widetilde{X}}(z) = X(z) \underbrace{\frac{1}{R} \sum_{i=0}^{M-1} \widetilde{H}_i(z) \cdot \widetilde{G}_i(z)}_{= \widetilde{T}_{\mathrm{lin}}(z)} + \underbrace{\frac{1}{R} \sum_{r=1}^{R-1} X\left(z\, W_R^r\right) \sum_{i=0}^{M-1} \widetilde{H}_i\left(z\, W_R^r\right) \cdot \widetilde{G}_i(z)}_{= \widetilde{\mathcal{D}}_{\mathrm{alias}}(z)} . \tag{4.29}$$

The system functions of the warped analysis filters are given by Eq. (4.2). Accordingly, applying the allpass transformation of Eq. (4.1) to the uniform synthesis filters of Eq. (2.27) yields the (frequency) *warped* synthesis filters

$$\widetilde{G}_i(z) = \sum_{l=0}^{L-1} g(l) \cdot A^l(z) \cdot W_M^{-i(l+1)} \;\forall\; i \in \{0, 1, \ldots, M-1\} . \tag{4.30}$$

In general, this allpass transformed AS FB does not achieve perfect reconstruction, even if the underlying uniform filter-bank provides perfect reconstruction. One effect of the frequency warping is that the aliasing cancellation does not work as for the uniform filter-bank due to the non-uniform bandwidths of the warped subband filters, cf., [Gal02]. The (additional) aliasing distortions caused by the allpass transformation can be reduced by longer prototype filters ($L \gg M$) having a high stopband attenuation and by the use of a low subsampling rate ($R \ll M$), cf., [Eng98, GEH98]. The overall transfer function of the allpass transformed AS FB is then approximately equal to its linear transfer function according to Eq. (4.29). If the linear transfer function of the underlying uniform filter-bank fulfills Eq. (2.31), it is obvious that the linear transfer function of the warped filter-bank according to Eq. (4.29) is given by

$$\widetilde{T}_{\mathrm{lin}}(z) = \Big(A(z)\Big)^{L-1} . \tag{4.31}$$

Thus, the allpass transformation causes no linear magnitude distortions but *phase distortions*. As indicated in Figure 4.6, these linear phase distortions can be compensated by processing the output signal $\tilde{y}(k)$ by a phase equalizer designed for an allpass chain of length $L_{\mathrm{ac}} = L - 1$. A suitable phase equalizer design for this purpose is discussed later in Sec. 4.2.3.

It is important to notice that the considered filter-bank of Figure 4.6 does not use different subsampling rates R_i adapted to the non-uniform bandwidths of the warped analysis filters according to Eq. (2.1). The design of allpass transformed filter-banks with individual subsampling rates is treated, e.g., in [Gal02, dHCG03, PP03b]. An advantage of different subsampling rates is that a higher subsampling ratio and better aliasing cancellation can usually be achieved in total. A severe drawback is that the downsampling has to be performed after the IDFT and the upsampling before the DFT as the Noble identities of Figure 2.5 cannot be applied. As a consequence, all

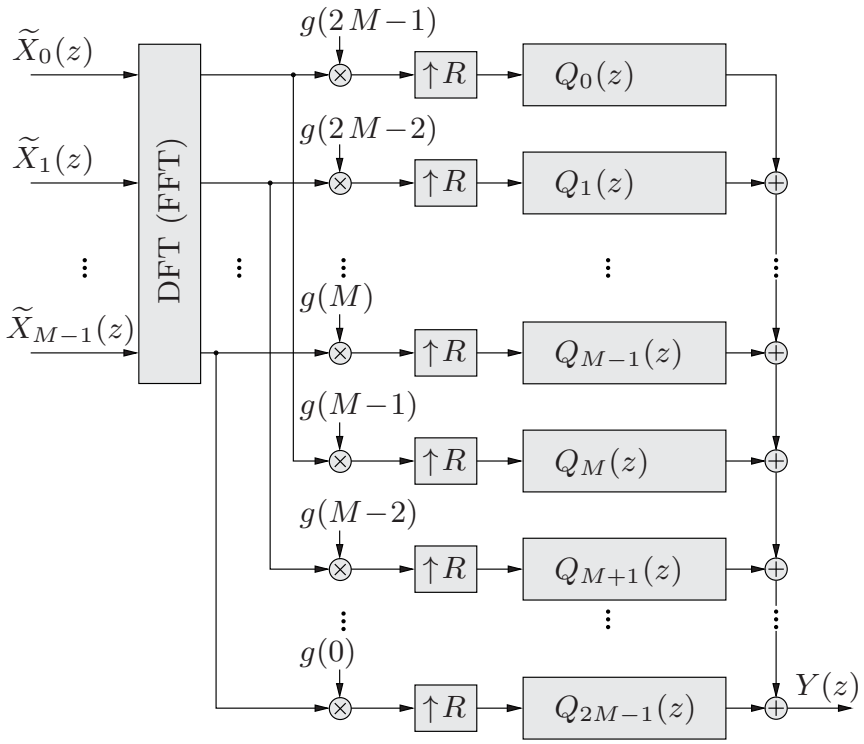

Figure 4.7: *General structure of an FIR synthesis filter-bank for an allpass transformed analysis filter-bank according to Figure 4.3 with* $L = 2\,M$.

arithmetic operations of analysis and synthesis filter-bank have to be performed at the non-decimated input sampling rate, which results in a high computational load.

Another approach is to combine frequency warping with subband merging as proposed in [PPW08]. This offers an enhanced flexibility for the adjustment of the frequency resolution at the price of an increased design complexity and can be exploited to implement a warped filter-bank efficiently by 'multiplierless' allpass filters [PP08].

4.2.2 FIR Synthesis Filter-Banks

The previously discussed filter-bank of Figure 4.6 uses allpass transformed FIR synthesis filters, which are IIR filters. Instead, it is also possible to use FIR synthesis filters. The general structure of such a synthesis filter-bank is shown in Figure 4.7. The synthesis filters are now given by

$$\bar{G}_i(z) = \sum_{l=0}^{L-1} g(l) \cdot Q_{L-1-l}(z) \cdot W_M^{-i(l+1)}; \quad i \in \{\,0, 1, \ldots, M-1\,\}\,. \tag{4.32}$$

The coefficients of the L FIR synthesis *sub-filters*

$$Q_l(z) = \sum_{\eta=0}^{L_\mathrm{q}-1} q_l(\eta) \cdot z^{-\eta} \quad \text{for} \quad l \in \{\,0, 1, \ldots, L-1\,\} \quad \text{and} \quad L_\mathrm{q} \geq L \tag{4.33}$$

can be determined in different ways.

One approach is to design these sub-filters as *phase equalizers* [Gal02, PP03a, LV07c]. With Eq. (4.2) and Eq. (4.32), the linear transfer function of Eq. (2.9) reads

$$\begin{aligned}\overline{T}_{\mathrm{lin}}(z) &= \frac{1}{R}\sum_{i=0}^{M-1}\widetilde{H}_i(z)\cdot\bar{G}_i(z) \qquad (4.34)\\ &= \frac{1}{R}\sum_{i=0}^{M-1}\sum_{l=0}^{L-1}\sum_{m=0}^{L-1} h(l)\cdot g(m)\cdot W_M^{-i(l+m+1)}\cdot A^l(z)\cdot Q_{L-1-m}(z)\\ &= \frac{M}{R}\sum_{\lambda\in\mathbb{Z}}\sum_{l=0}^{L-1} h(l)\cdot g(\lambda M-1-l)\cdot A^l(z)\cdot Q_{L-\lambda M+l}(z)\,. \qquad (4.35)\end{aligned}$$

The sub-filters are designed as phase equalizers with the requirement

$$A^l(z)\cdot Q_l(z) \stackrel{!}{=} z^{-D_{\mathrm{o}}} \;\forall\; l\in\{0,1,\ldots,L-1\}\,. \qquad (4.36)$$

Thus

$$\overline{T}_{\mathrm{lin}}(z) = z^{-D_{\mathrm{o}}}, \qquad (4.37)$$

if the conditions of Eq. (4.36) and Eq. (2.32) are met.

A synthesis filter-bank with a *cascaded phase equalization* as discussed in Sec. 3.3.4.2 is proposed in [GK00, GK02, Gal02]. Single FIR phase equalizers according to Eq. (3.85) are concatenated such that the FIR sub-filters of Eq. (4.33) are given by

$$Q_l(z) = \left(\mathcal{P}^{\mathrm{fir}}(z)\right)^l\cdot z^{-(L-1-l)\,N_{\mathrm{s}}} \quad\text{for}\quad l\in\{0,1,\ldots,L-1\}\,. \qquad (4.38)$$

The sub-filter length amounts to $L_{\mathrm{q}} = N_{\mathrm{s}}\,(L-1)+1$ and the synthesis filters of Eq. (4.32) have now the system functions

$$\bar{G}_i(z) = \sum_{l=0}^{L-1} g(l)\cdot\left(\mathcal{P}^{\mathrm{fir}}(z)\right)^{L-1-l}\cdot z^{-l\,N_{\mathrm{s}}}\cdot W_M^{-i(l+1)} \qquad (4.39)$$

with $i\in\{0,1,\ldots,M-1\}$. The efficient implementation of this synthesis filter-bank is shown in Figure 4.8. The single FIR phase equalizers with filter degree N_{s} are designed by the requirement of Eq. (4.36), which now reads

$$A^l(z)\cdot\left(\mathcal{P}^{\mathrm{fir}}(z)\right)^l\cdot z^{-(L-1-l)\,N_{\mathrm{s}}} \stackrel{!}{=} z^{-(L-1)\,N_{\mathrm{s}}} \quad\text{for}\quad l\in\{0,1,\ldots,L-1\}\,. \qquad (4.40)$$

The delay elements are needed to compensate the different delays of allpass chain and phase equalizers as shown in Figure 4.8. The linear transfer function is given by

$$\overline{T}_{\mathrm{lin}}(z) = z^{-(L-1)\,N_{\mathrm{s}}}\,, \qquad (4.41)$$

if the prototype filters fulfill Eq. (2.32) and the phase equalizers Eq. (4.40). The filter-bank has hence an overall signal delay of $D_{\mathrm{o}} = (L-1)\,N_{\mathrm{s}}$ sample instants. In practice,

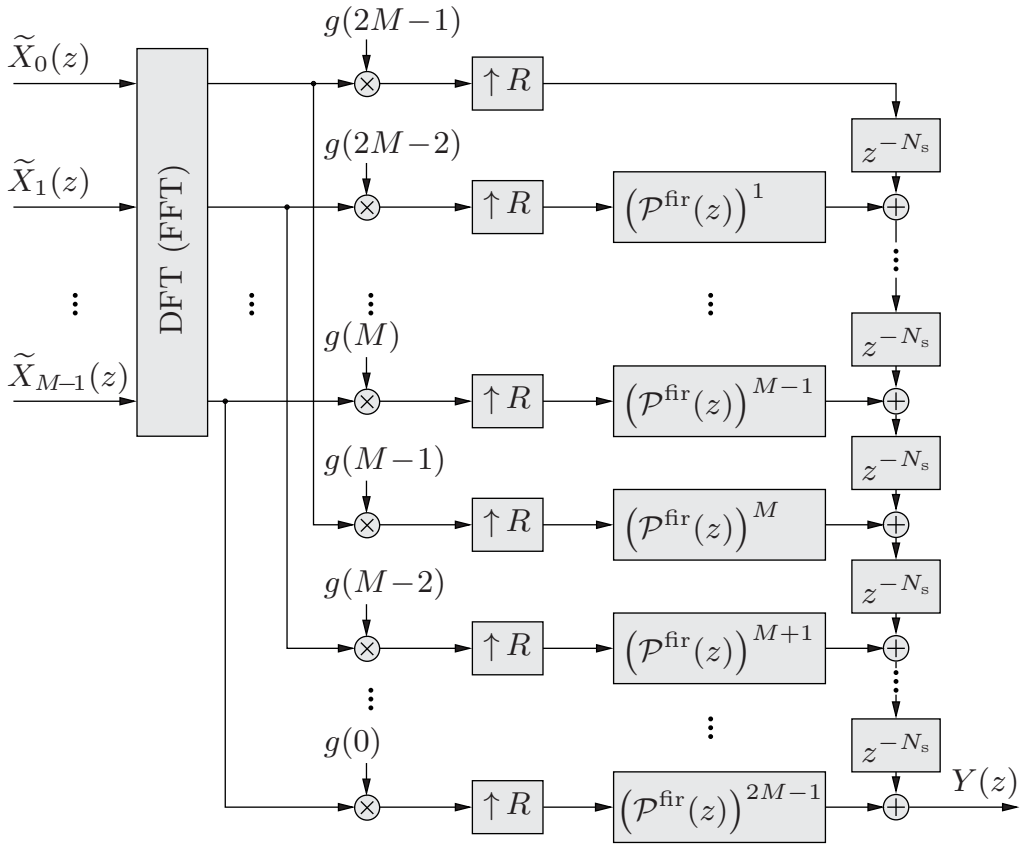

Figure 4.8: *FIR synthesis filter-bank with cascaded phase equalization according to [Gal02] for a prototype filter of length $L = 2\,M$ and analysis filter-bank given by Figure 4.6.*

a linear transfer function according to Eq. (4.41) can only be achieved approximately where the deviations are controlled by the filter degree N_{s}.

In [PP03a], it is shown that the synthesis filter-banks of Figure 4.8 and Figure 4.6 are equivalent but have a different complexity, if cascaded phase equalizers are used which fulfill Eq. (4.40) exactly. According to Eq. (4.30), the synthesis filters of an allpass transformed synthesis filter-bank with a cascaded phase equalizer at its output have the system functions

$$\widetilde{\widetilde{G}}_i\,(z) = \widetilde{G}_i(z) \cdot \left(\mathcal{P}^{\mathrm{fir}}(z)\right)^{L-1} \tag{4.42}$$

$$= \sum_{l=0}^{L-1} g(l) \cdot A^l(z) \cdot \left(\mathcal{P}^{\mathrm{fir}}(z)\right)^{L-1} \cdot W_M^{-i(l+1)}\,. \tag{4.43}$$

If Eq. (4.40) is fulfilled,

$$\begin{aligned} A^l(z) \cdot \left(\mathcal{P}^{\mathrm{fir}}(z)\right)^{L-1} &= A^l(z) \cdot \left(\mathcal{P}^{\mathrm{fir}}(z)\right)^{l} \cdot \left(\mathcal{P}^{\mathrm{fir}}(z)\right)^{L-1-l} \\ &= z^{-l\,N_{\mathrm{s}}} \cdot \left(\mathcal{P}^{\mathrm{fir}}(z)\right)^{L-1-l} \end{aligned} \tag{4.44}$$

such that Eq. (4.43) becomes equal to Eq. (4.39) in this case.

In [LV07c], it is proposed to employ the LS FIR phase equalizer of Sec. 3.3.4.1 for the sub-filters of Eq. (4.33)

$$Q_l(z) = P_l^{\mathrm{ls}}(z) \;\forall\; l \in \{\,0, 1, \ldots, L-1\,\} \tag{4.45}$$

such that the synthesis filter of Eq. (4.32) are given by

$$\bar{G}_i(z) = \sum_{l=0}^{L-1} g(l) \cdot P_{L-1-l}^{\mathrm{ls}}(z) \cdot W_M^{-i\,(l+1)}; \;\; i \in \{\,0, 1, \ldots, M-1\,\}\,. \tag{4.46}$$

The LS FIR phase equalizers have all the same filter degree $N = L_{\mathrm{q}} - 1$ and they are designed by the condition of Eq. (4.36), which now reads

$$A^l(z) \cdot P_l^{\mathrm{ls}}(z) \stackrel{!}{=} z^{-N} \;\forall\; l \in \{\,0, 1, \ldots, L-1\,\}\,. \tag{4.47}$$

If this requirement is (exactly) fulfilled, the linear transfer function is given by Eq. (4.37) with $D_{\mathrm{o}} = N$ (presuming that Eq. (2.32) is met). The 'ideal' phase equalizer to fulfill Eq. (4.47) is given by

$$P_l^{\mathrm{ideal}}(z) = z^{-N} \cdot A^{-l}(z) \;\forall\; l \in \{\,0, 1, \ldots, L-1\,\}\,. \tag{4.48}$$

Inserting this 'ideal' phase equalizer into Eq. (4.46) yields the magnitude responses

$$\begin{aligned}
\left|\bar{G}_i^{(\mathrm{ideal})}\left(e^{j\,\Omega}\right)\right| &= \left|e^{-j\,\Omega\,N} \sum_{l=0}^{L-1} g(l) \cdot \left(A\left(e^{j\,\Omega}\right)\right)^{-(L-1-l)} \cdot W_M^{-i\,(l+1)}\right| \\
&= \left|e^{-j\,\Omega\,N} \cdot W_M^{-i} \cdot e^{j\,(L-1)\,\varphi_a(\Omega)} \sum_{l=0}^{L-1} g(l) \cdot e^{-j\,l\,\varphi_a(\Omega)} \cdot W_M^{-il}\right| \\
&= \left|\sum_{l=0}^{L-1} g(l) \cdot e^{-j\,l\,\varphi_a(\Omega)} \cdot W_M^{-il}\right|\,.
\end{aligned} \tag{4.49}$$

If $g(l) = h(l)$, it follows from Eq. (4.49) and Eq. (4.3) that

$$\left|\bar{G}_i^{(\mathrm{ideal})}\left(e^{j\,\Omega}\right)\right| = \left|\widetilde{H}_i\left(e^{j\,\Omega}\right)\right| \;\forall\; i \in \{\,0, 1, \ldots, M-1\,\}\,. \tag{4.50}$$

Thus, the magnitude responses of the synthesis filters are identical to those of the allpass transformed analysis filters in case of a perfect phase equalization where Eq. (4.47) is exactly fulfilled. This result can be derived in the same manner for the synthesis filters of Eq. (4.39). In practice, the equality of Eq. (4.50) can only be achieved approximately as the 'ideal' phase equalizer of Eq. (4.48) is either unstable or non-causal. However, the derived relation reveals that the magnitude responses of the synthesis filters can be enhanced by improving the phase equalization. An illustration for this behavior is given later by Example 4.2 in Sec. 4.2.3.

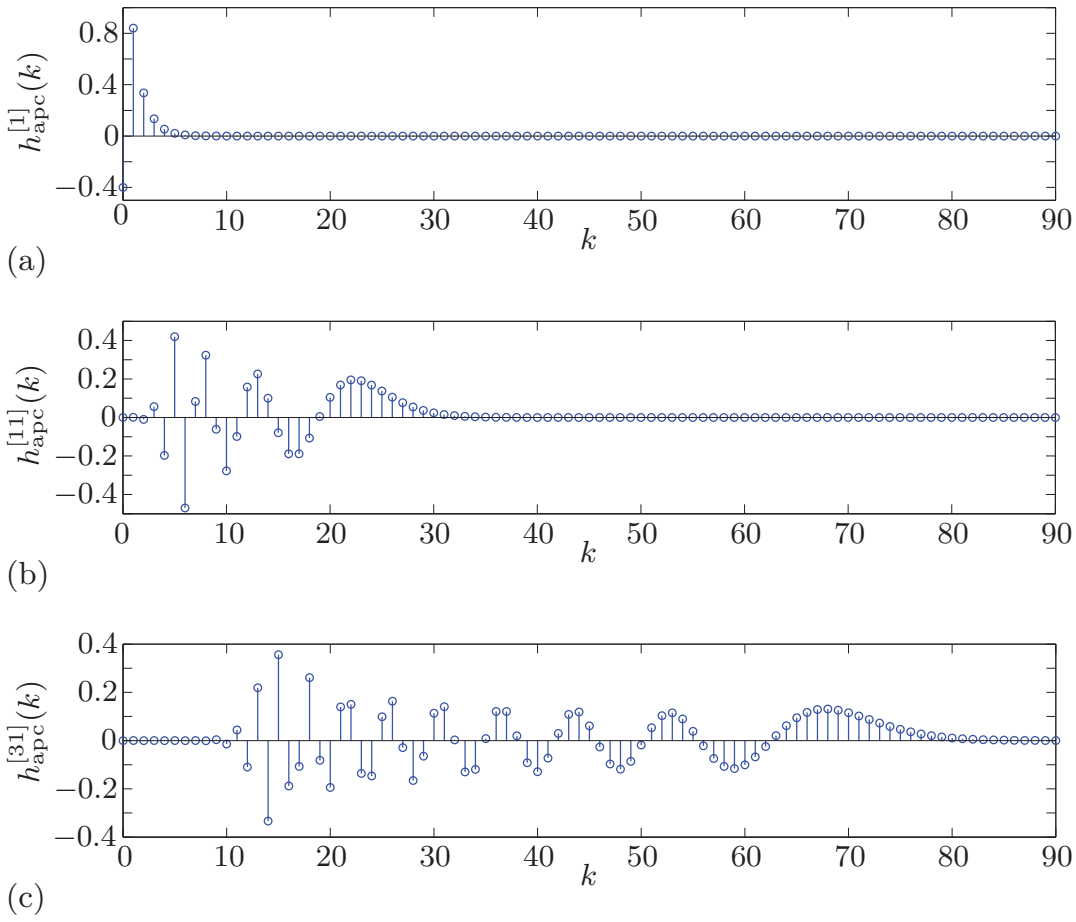

Figure 4.9: *Impulse responses of allpass chains with allpass coefficient* $a = 0.4$ *and different lengths:* (a) $L_{ac} = 1$, (b) $L_{ac} = 11$, (c) $L_{ac} = 31$.

The synthesis filter-bank with LS FIR phase equalizers can be implemented in a similar fashion as the synthesis filter-bank of Figure 4.8. The underlying concept is based on the rationale that the impulse response of a short allpass chain decreases more rapidly towards zero than that of a long allpass chain as exemplified by Figure 4.9. Hence, phase equalizers with different degrees N_l can be used such that Eq. (4.47) turns into the requirement

$$A^l(z) \cdot P_l^{\mathrm{ls}}(z) \stackrel{!}{=} z^{-N_l} \;\; \forall \;\; l \in \{\, 1, 2 \ldots, L-1 \,\} \,. \tag{4.51}$$

The different phase equalizer degrees N_l can be determined by means of Eq. (3.84) and the requirement

$$\Delta N_l = N_l - N_{l-1} \geq 0 \quad \text{for} \quad l = 2, 3, \ldots, L-1 \,. \tag{4.52}$$

This leads to the efficient synthesis filter-bank implementation depicted in Figure 4.10.

Another measure to reduce the complexity of the synthesis filter-bank of Figure 4.7 and it variants (such as the filter-bank of Figure 4.10) is to implement the sub-filters by an efficient *polyphase structure*. The L_{q} FIR sub-filters of Eq. (4.33) can be expressed

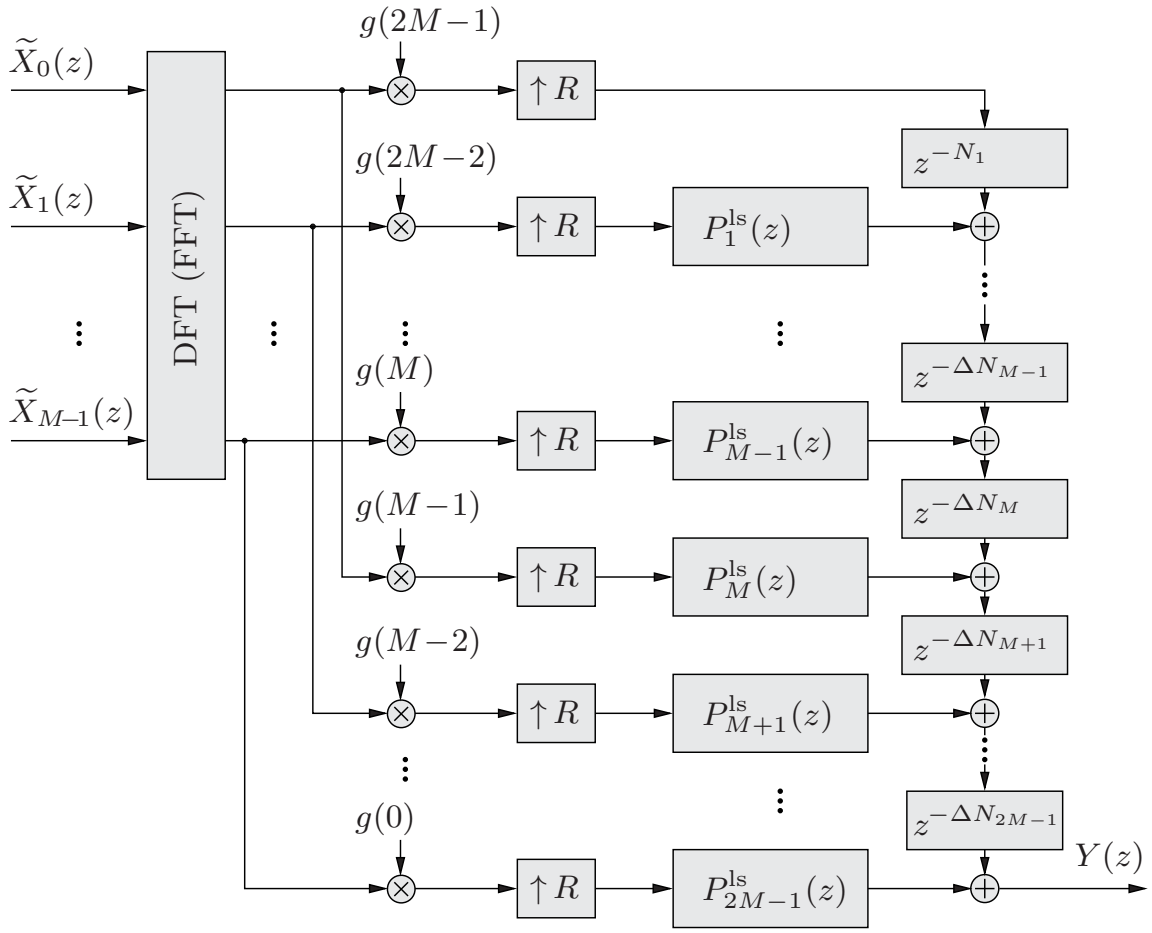

Figure 4.10: *Efficient implementation of a synthesis filter-bank with LS FIR phase equalizers of variable degree N_l for a prototype filter with $L = 2\,M$.*

in a polyphase representation similar to Eq. (2.35b):

$$Q_l(z) = \sum_{\eta=0}^{L_\mathrm{q}-1} q_l(\eta) \cdot z^{-\eta}; \quad l \in \{\,0, 1, \ldots, L-1\,\} \qquad [4.33]$$

$$= \sum_{r=0}^{R-1} \sum_{m=0}^{l_Q-1} q_l(m\,R + r) \cdot z^{-(m\,R+r)}$$

$$= \sum_{r=0}^{R-1} Q_{l,\,r}^{(R)}\left(z^R\right) \cdot z^{-r} \qquad (4.53)$$

with the (type 1) polyphase components

$$Q_{l,\,r}^{(R)}(z) = \sum_{m=0}^{l_Q-1} q_l(m\,R + r) \cdot z^{-m} \quad \text{for} \quad l_Q = \left\lceil \frac{L_\mathrm{q}}{R} \right\rceil . \qquad (4.54)$$

Exploiting the Noble identities of Figure 2.5 allows now to implement each sub-filter of the synthesis filter-bank by an efficient polyphase network (PPN) as shown in

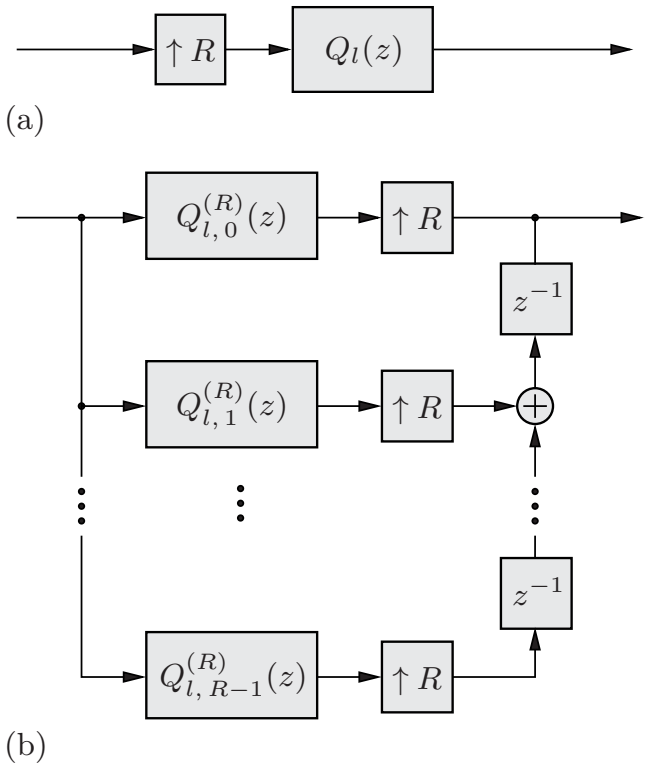

Figure 4.11: *Efficient implementation of upsampling and sub-filtering:*
(a) *original structure of branch l*
(b) *efficient implementation by a polyphase network.*

Figure 4.11. This polyphase implementation reduces the complexity of the sub-filters by a factor of R since $L_\mathrm{q} \gg R$ and is facilitated by the fact that the synthesis filter-bank uses an *identical* subsampling rate R for each subband as well as FIR sub-filters. For the following derivations, the synthesis filter-bank of Figure 4.7 is considered for the sake of simplicity, keeping in mind that the actual implementation can be done by an efficient PPN implementation, mostly in combination with the filter-bank structure of Figure 4.10.

Finally, it should be noted that the discussed synthesis filter-bank designs can be applied in a straightforward manner to an analysis filter-bank designed by an allpass transformation of higher order according to Sec. 4.1.2 so that this case is not treated in more detail.

4.2.3 Phase Equalizer Design for Warped Filter-Banks

As for the allpass-based (Pseudo) QMF-banks treated before, the phase equalizer design exerts a major influence on the performance of a warped filter-bank regarding its reconstruction error, signal delay and algorithmic complexity. However, there are two important differences between allpass-based (Pseudo) QMF-banks and allpass transformed AS FBs to be taken into account.

Firstly, a perfect phase equalization yields an allpass-based QMF-bank with perfect reconstruction which, however, does not apply for allpass transformed AS FBs. This is

due to the structural difference that allpass filters and phase equalizers of a QMF-bank or Pseudo QMF-bank are operated in the subsampled time-domain as opposed to allpass transformed filter-banks (compare, e.g., Figure 3.7 or Figure 3.13 with Figure 4.6).

Secondly, the equalization of mostly long allpass chains is required for a warped AS FB in contrast to allpass-based QMF-banks. In [LV07c], it is shown that the LS FIR phase equalizer of Sec. 3.3.4.1 is especially suitable for such purposes. As demonstrated in the following, this phase equalizer achieves a superior performance in comparison to cascaded phase equalizers as given by the equiripple phase equalizers treated in Sec. 3.3.4.2 and Sec. 3.3.4.3.

Example 4.1: The design problem of Eq. (3.75) is considered for an allpass chain of length $L_{\mathrm{ac}} = 31$ and allpass coefficient $a = 0.4$ whose impulse response is plotted in Figure 4.9-c. The phase equalization is performed by the proposed LS FIR phase equalizer and the equiripple FIR phase equalizer of [Gal02].[7] Figure 4.12 shows the plots of magnitude response and group delay of the transfer function $\Psi\left(e^{j\,\Omega}\right)$ given by Eq. (3.75) as well as the phase error defined by Eq. (3.74b). The equiripple FIR phase equalizer of [Gal02] achieves an equiripple error for the magnitude, group delay and phase error in accordance with the results of Sec. 3.3.4.2. The LS FIR phase equalizer of Sec. 3.3.4.1 achieves a significantly lower approximation error than the equiripple FIR phase equalizer for the *same* filter degree ($N = L_{\mathrm{ac}}\,N_{\mathrm{s}}$) and signal delay, respectively. It is also illustrated that the LS FIR phase equalizer can provide a comparable approximation error as the equiripple FIR phase equalizer, but with a considerably lower filter degree.

It is not contradictory to the alternation theorem (briefly explained in App. D.1) that the LS FIR phase equalizer achieves a lower approximation error than the equiripple FIR phase equalizer for the same filter degree. The equiripple phase equalizer leads to a transfer function $\Psi\left(e^{j\,\Omega}\right)$ which shows an equiripple approximation error for Eq. (3.74) with regard to the desired transfer function $\Psi_{\mathrm{d}}\left(e^{j\,\Omega}\right)$ as proven in Sec. 3.3.4.2. In contrast, the LS FIR phase equalizer achieves an LS error approximation for the desired phase equalizer according to Eq. (3.82). Hence, different approximation criteria are involved.

Example 4.2: The impact of the phase equalizer for the design of a warped DFT AS FB is now investigated. An allpass transformed analysis filter-bank according to Figure 4.6 is considered with $M = 32$ frequency channels and a subsampling rate of $R = 4$. An allpass coefficient of $a = 0.4$ is used for the allpass transformation, which yields a good approximation of the Bark scale for a sampling frequency of $f_{\mathrm{s}} = 8\,\mathrm{kHz}$ according to Eq. (4.7). The magnitude responses of the analysis filters are shown in Figure 4.13 where the prototype filters of analysis and synthesis filter-bank are given by Eq. (2.33). The FIR synthesis filter-bank of Figure 4.7 is used employing either equiripple FIR phase equalizers according to Eq. (4.38) or LS FIR phase equalizers according to Eq. (4.45) for the sub-filters of Eq. (4.33).

The transfer functions and synthesis filters of the two AS FBs are analyzed in Figure 4.14. The upper subplots show the progression of magnitude response and

[7] The use of the equiripple allpass phase equalizer of Sec. 3.3.4.3 yields similar results in this case due to its close relation to the equiripple FIR phase equalizer.

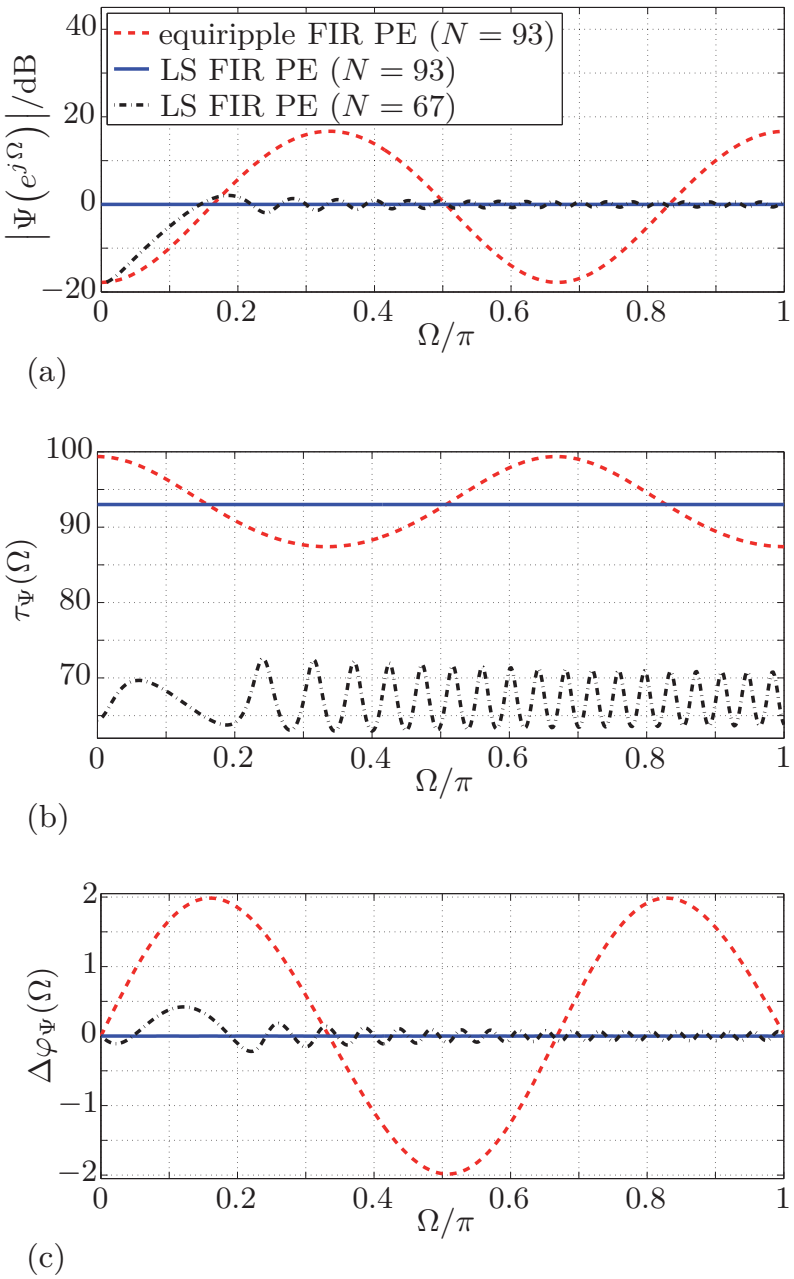

Figure 4.12: *Phase equalization of an allpass chain of length* $L_{ac} = 31$ *and allpass coefficient* $a = 0.4$ *by different FIR phase equalizers (PEs) of degree* N*:*
(a) *magnitude response of the transfer function* $\Psi\left(e^{j\,\Omega}\right)$
(b) *group delay of the transfer function* $\Psi\left(e^{j\,\Omega}\right)$
(c) *phase error of Eq.* (3.74b).

phase error for the overall and linear transfer function of the filter-bank (introduced in Sec. 2.1 and Sec. 4.2.2). Both filter-banks are designed for the *same* overall signal delay $D_\mathrm{o} = N = (L-1)\,N_\mathrm{s}$. It can be observed that the use of the LS FIR phase equalizer results in a significantly lower amount of amplitude and phase distortions in comparison to the equiripple FIR phase equalizer. The distortions for the overall transfer function $T_0\left(e^{j\,\Omega}\right)$ are higher than for the linear transfer function $\overline{T}_\mathrm{lin}\left(e^{j\,\Omega}\right)$

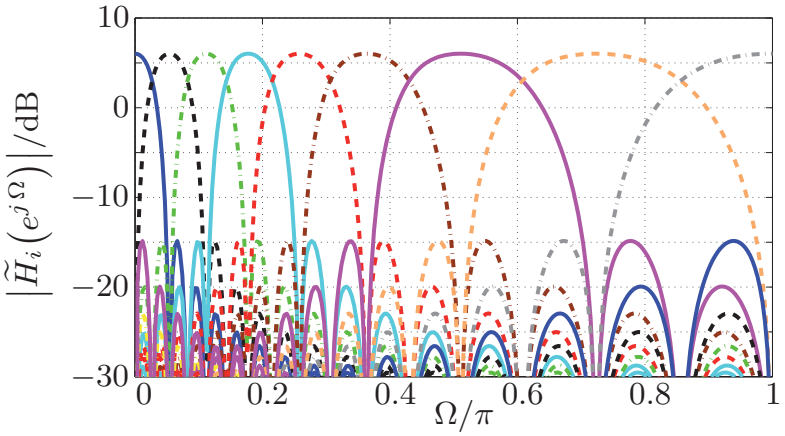

Figure 4.13: *Magnitude responses of an allpass transformed DFT analysis filter-bank with parameters* $L = 2\,M = 32$, $R = 4$ *and* $a = 0.4$.

due to non compensated alias components, which are illustrated by the plots of the BSF in Figure 4.14-c and Figure 4.14-d. The plots of the BSF show that both designs achieve a similar aliasing cancellation, but the design with LS FIR phase equalizers causes much lower linear magnitude distortions as indicated by the constant line on the main diagonal in Figure 4.14-d.

It is shown in the previous section that the magnitude responses of the synthesis filters become almost identical to those of the analysis filters, if a good phase equalization is achieved, cf., Eq. (4.50). This effect is demonstrated by the subplots of Figure 4.14-e and Figure 4.14-f, which show the magnitude responses of the synthesis filters for the two filter-bank designs. The low phase equalization error for the LS FIR phase equalizer results in synthesis filters whose magnitude responses are almost identical to those of the analysis filters shown in Figure 4.13. In contrast, the high phase error of the equiripple FIR phase equalizer yields synthesis filters with an insufficient bandpass characteristic.

The comparison of the two synthesis filter-bank designs is performed for the *same* overall system delay D_o to demonstrate and highlight the strong influence of the phase equalizer design. It is of course also possible to achieve the same reconstruction error and bandpass characteristic for the synthesis filters with the equiripple FIR phase equalizer as with the LS FIR phase equalizer, but this requires a significantly higher filter degree and signal delay, respectively, in case of the equiripple FIR phase equalizer.

Finally, it should be noticed that the filter-bank structure proposed in [GK00, GK02, Gal02] differs somewhat from the filter-bank of Figure 4.8. As mentioned before, the proposals in [GK00, GK02, Gal02] consider different subsampling rates R_i for the subbands. Another difference is that the lifting scheme[8] is employed to achieve an improved frequency selectivity for the prototype filters with a constrained signal delay [GK02, Gal02]. However, these differences are not relevant for this discussion as the proposed LS FIR phase equalizer can also be applied in this case in a straightforward fashion and provides the same benefits as pointed out before.

[8] An example for a filter-bank based on the lifting scheme is provided by Figure 3.5.

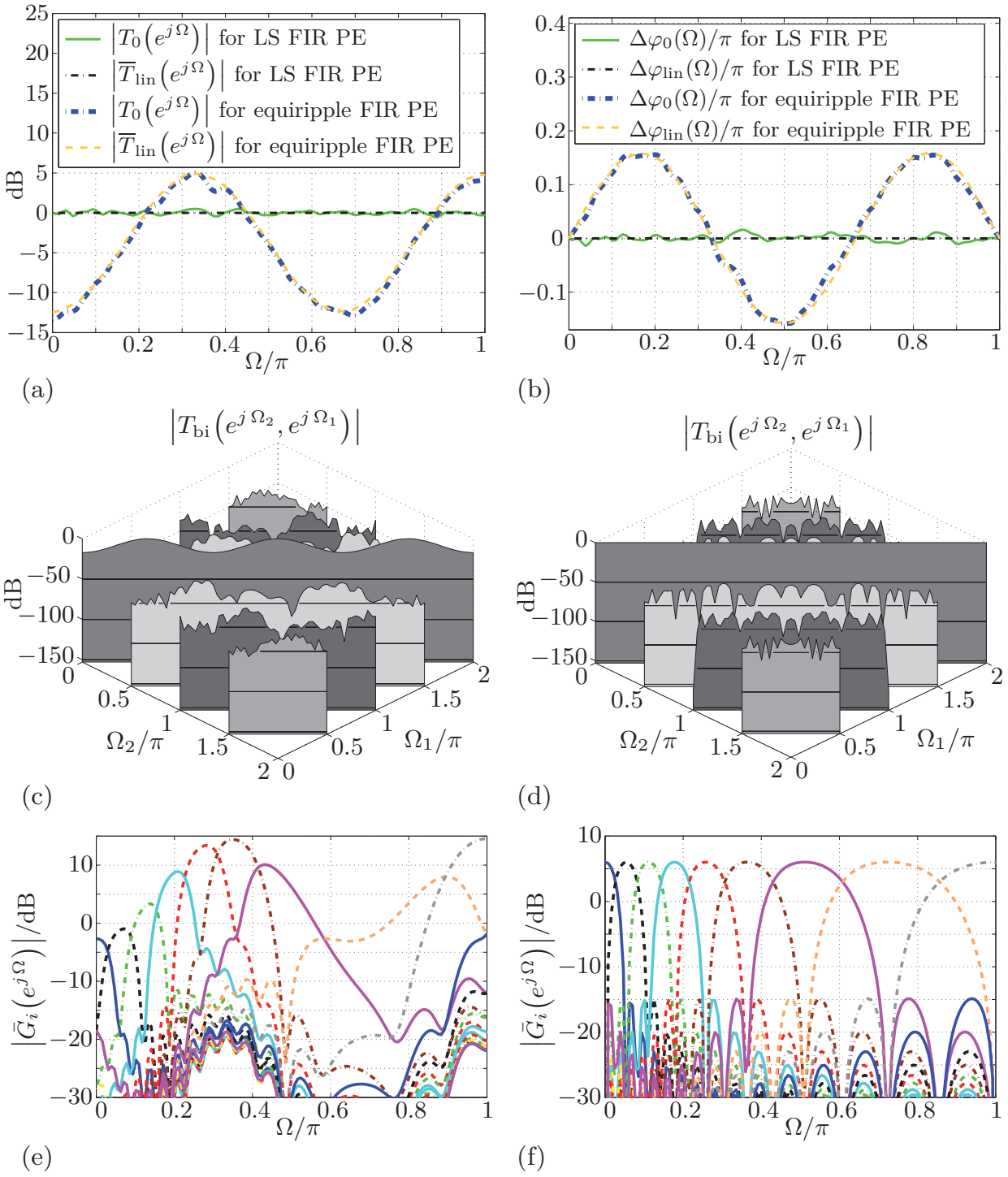

Figure 4.14: *Evaluation of a warped DFT AS FB with analysis filter-bank given by Figure 4.6 and parameters $L = 2\,M = 32$, $R = 4$, $a = 0.4$. The FIR synthesis filter-bank of Figure 4.7 is used with two different phase equalizers having a maximal degree of $N = (L-1)\,N_s = 93$ and delay $D_o = 93$:*
(a) *magnitude responses of linear and overall transfer function*
(b) *phase errors of linear and overall transfer function*
(c) *magnitude of BSF for filter-bank with equiripple FIR phase equalizers*
(d) *magnitude of BSF for filter-bank with LS FIR phase equalizers*
(e) *magnitude responses of synthesis filters with equiripple FIR phase equalizers*
(f) *magnitude responses of synthesis filters with LS FIR phase equalizers.*

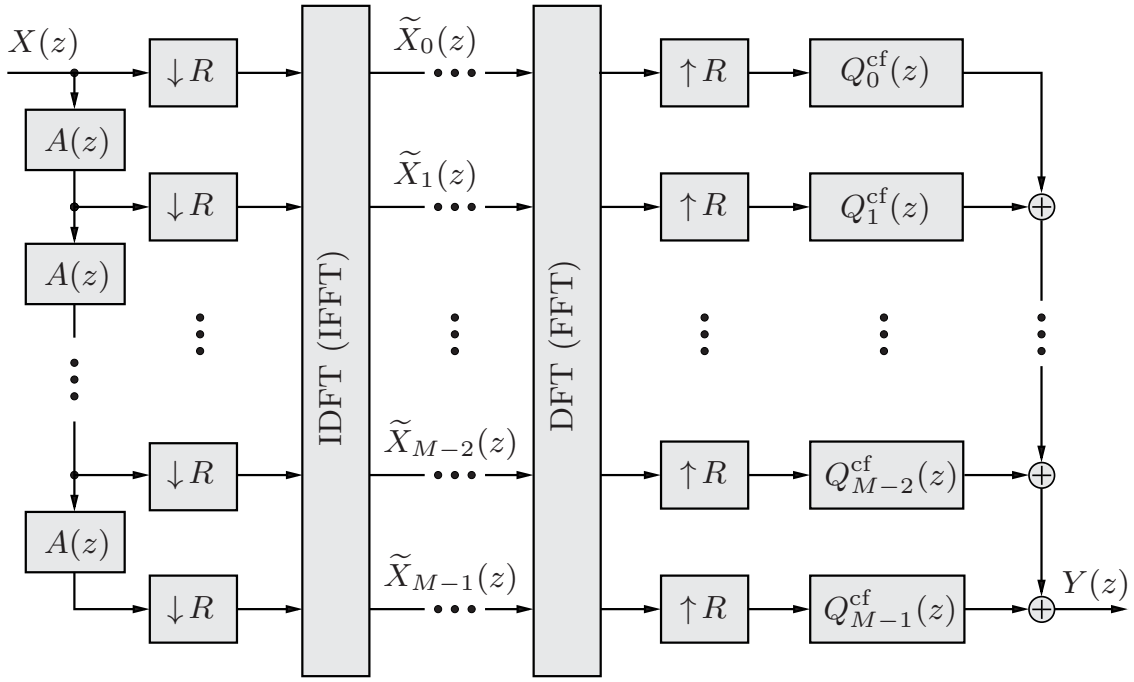

Figure 4.15: *Allpass transformed DFT AS FB for closed-form PR design.*

4.2.4 PR Designs

The filter-bank designs discussed so far achieve near-perfect reconstruction by means of phase equalization. Closed-form synthesis filter-bank designs to achieve a perfect signal reconstruction are proposed in [Kap98, Sha00, SM02a, FK03]. These designs follow actually the same design principle and have the same properties as shown in the following.

The considered AS FB is depicted in Figure 4.15 for an allpass transformation of first order. It can be regarded as special case of the analysis filter-bank of Figure 4.6 for $L = M$ and $h(l) \equiv 1$ and the synthesis filter-bank of Figure 4.7 for $L = M$, $g(l) \equiv 1$ and $Q_i(z) = Q_i^{\mathrm{cf}}(z)$ with $l, i \in \{\,0, 1, \ldots, M-1\,\}$. The use of Eq. (2.3) and Eq. (2.7) leads to the following representation for the reconstructed input signal in the z-domain

$$\widehat{X}(z) = \sum_{r=0}^{R-1} X\left(z\,W_R^r\right) \underbrace{\frac{1}{R} \sum_{i=0}^{M-1} A^i\left(z\,W_R^r\right) \cdot Q_i^{\mathrm{cf}}(z)}_{=\,\mathcal{S}_r(z)} \,. \tag{4.55}$$

Perfect reconstruction can be achieved if

$$\mathcal{S}_r(z) = \begin{cases} z^{-(R-1)} & \text{for } r = 0 \\ 0 & \text{for } r \in \{\,1, 2, \ldots, R-1\,\}\,. \end{cases} \tag{4.56}$$

This condition can be fulfilled by the restriction

$$Q_i^{\mathrm{cf}}(z) \equiv 0 \quad \text{for} \quad R \le i \le M-1 \tag{4.57a}$$

and if the system functions $Q_0^{\mathrm{cf}}(z),\ldots,Q_{R-1}^{\mathrm{cf}}(z)$ of the remaining sub-filters satisfy the following set of equations

$$\underbrace{\begin{bmatrix} 1 & A\big(z\big) & \ldots & A^{R-1}\big(z\big) \\ 1 & A\big(z\,W_R\big) & \ldots & A^{R-1}\big(z\,W_R\big) \\ \vdots & \vdots & \ddots & \vdots \\ 1 & A\big(z\,W_R^{R-1}\big) & \ldots & A^{R-1}\big(z\,W_R^{R-1}\big) \end{bmatrix}}_{= \boldsymbol{A}_{\mathrm{alias}}(z) \in \mathbb{C}^{R\times R}} \cdot \begin{bmatrix} Q_0^{\mathrm{cf}}(z) \\ Q_1^{\mathrm{cf}}(z) \\ \vdots \\ Q_{R-1}^{\mathrm{cf}}(z) \end{bmatrix} = \begin{bmatrix} R\,z^{-(R-1)} \\ 0 \\ \vdots \\ 0 \end{bmatrix} . \tag{4.57b}$$

The system functions of the resulting synthesis filters are given by

$$\bar{G}_i^{\mathrm{cf}}(z) = \sum_{l=0}^{M-1} Q_{M-1-l}^{\mathrm{cf}}(z) \cdot W_M^{-i(l+1)} \quad \text{for} \quad i \in \{\,0,1,\ldots,M-1\,\}\,. \tag{4.58}$$

Formally, these filters can be seen as a special case of Eq. (4.32) with $L = M$ and $g(l) \equiv 1$ where the sub-filters are now determined according to Eq. (4.57). The (warped) alias component matrix $\boldsymbol{A}_{\mathrm{alias}}(z)$ of Eq. (4.57b) has a Vandermonde structure, which allows to calculate its inverse by methods closely related to Lagrange's polynomial interpolation formula, e.g., [PTVF92, Chap. 2]. The obtained system functions $Q_i^{\mathrm{cf}}(z)$ represent FIR filters of degree $2\,(R-1)$ [FK03]. The overall signal delay of this filter-bank amounts to $D_{\mathrm{o}} = R-1$ due to Eq. (4.56). The closed-form PR solutions of [Kap98, Sha00, SM02a] are actually equivalent to that of [FK03] and hence not treated separately.[9]

A severe drawback of this closed-form PR design approach is that the synthesis filters have no distinctive bandpass characteristic, cf., [FK03]. For example, if no subsampling is performed ($R = 1$), Eq. (4.57) yields the synthesis sub-filters

$$Q_i^{\mathrm{cf}}(z) = \begin{cases} 1 & \text{for } i = 0 \\ 0 & \text{for } i \in \{\,1,2,\ldots,M-1\,\}\,. \end{cases} \tag{4.59}$$

The corresponding synthesis filters of Eq. (4.58) are given by $\bar{G}_i^{\mathrm{cf}}(z) \equiv 1$ in this case, which are trivial allpass filters but no bandpass filters. The corresponding filter-bank provides perfect reconstruction even in a strict sense, i.e., $\widehat{X}(z) = X(z)$, but such a design has of course no practical relevance.

The magnitude responses of $\bar{G}_0^{\mathrm{cf}}\big(e^{j\,\Omega}\big)$ for higher subsampling rates ($R > 1$) are plotted in Figure 4.16. It can be observed that the magnitude responses of $\bar{G}_0^{\mathrm{cf}}\big(e^{j\,\Omega}\big)$

[9] The solutions of [Sha00, SM02a, FK03] are all obtained by inversion of the warped alias component matrix where the derivation in [Kap98, Chap. 4] is based on a 'tree reconstruction network', which can be converted into the structure of Figure 4.15. In [Kap98, Sha00, SM02a], an explicit solution for a causal and stable synthesis filter-bank is only given for critically subsampling ($R = M$) where the solution of [FK03] considers a variable subsampling rate $R \in \{1,2,\ldots,M\}$.

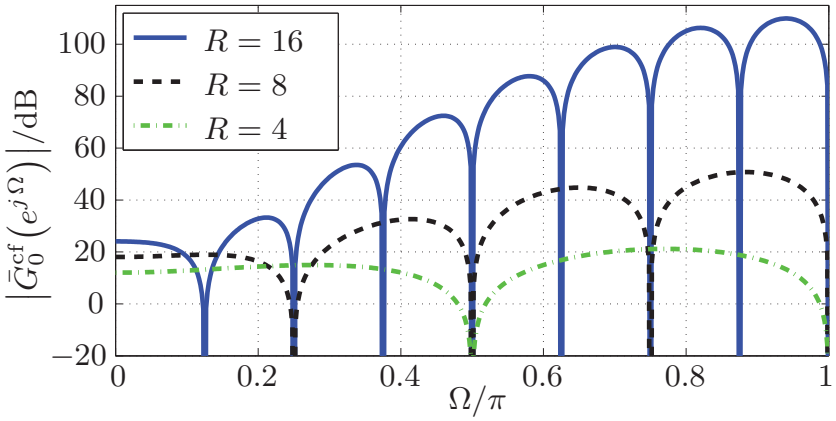

Figure 4.16: *Magnitude response of the synthesis lowpass filter for different subsampling rates R obtained by a closed-form PR design. The underlying AS FB is depicted by Figure 4.15. An allpass coefficient of $a = 0.4$ and $M = 16$ channels are considered.*

show no lowpass characteristic at all. (Similar observations can also be made for the other synthesis filters.) The missing bandpass characteristic of the synthesis filters can cause high signal distortions if spectral modifications of the subband signals, such as spectral weighting or quantization, are performed.

The synthesis filter-bank design according to Eq. (4.57b) can also be applied in case of an allpass transformation of higher order. In this case, the inversion of the Vandermonde matrix $\boldsymbol{A}_{\mathrm{alias}}(z)$ yields IIR filters for the system functions $Q_0^{\mathrm{cf}}(z), \ldots Q_{R-1}^{\mathrm{cf}}(z)$ which are not necessarily causal and stable [Sha00, SM02a, FK03]. The use of non-causal filtering techniques to solve this problem, as suggested in [Sha00, SM02a], has decisive drawbacks as shown in Sec. 3.3.2. This applies also for the design approach of [Kap98] where a causal and stable synthesis filter-bank is only found for the case of an allpass transformation of first order.

Another drawback of these closed-form synthesis filter-bank designs is that they do not provide a solution for an allpass transformed PPN analysis filter-bank where $L > M$, which makes it difficult to employ prototype filters with a high frequency selectivity. This general limitation is pointed out in [Sha00, Chap. 2] for closed-form designs which are based on inversion of the alias component matrix such as [SM02a, FK03]. Similar, the closed-form PR solution of [Kap98] applies also only for analysis prototype filters of filter length $L = M$. In contrast to the designs of [Sha00, SM02a, FK03], the analysis and synthesis prototype filters considered in [Kap98] are related by $h(l) = 1/g(l)$ for $l \in \{0, 1, \ldots, L-1\}$. However, such a choice is only feasible for (rectangular) prototype filters of length $L = M$.

It is important to notice that the derivation of a uniform filter-bank with perfect reconstruction by inversion of the alias component matrix is well established and does not cause the above mentioned problems, e.g., [Vai93]. This shows that the application of design approaches for uniform filter-banks to the more general case of allpass transformed filter-banks is not always straightforward and has to be done with care.

4.3 Numerical Filter-Bank Designs

All the closed-form designs discussed in the previous sections have the advantage that the synthesis filters are obtained by simple analytical expressions. In addition, a perfect or at least nearly perfect compensation of (linear) phase distortions can be achieved by this approach.

A drawback of these closed-form approaches is that they are rather inflexible: The synthesis filter-bank designs based on phase equalization lack the (explicit) design target to reduce the aliasing distortions caused by the warped analysis filter-bank. In contrast, the closed-form designs discussed in Sec. 4.2.4 achieve perfect reconstruction with a low signal delay, but these solutions apply only for the case $L = M$ and an allpass transformation of first order. A more severe shortcoming of these closed-form PR designs is that the obtained synthesis filters have no bandpass characteristic. This is due to the fact that synthesis filters with a bandpass characteristic are not (and cannot be) the design target of such an approach.

These drawbacks motivate to design the synthesis filter-bank by means of a *numerical* approach, which facilitates the incorporation of *specific* design targets. By this, the signal reconstruction error or bandpass characteristic of the synthesis filters can be better controlled. The aim is thereby to achieve an *optimal* design according to a given error criterion.

The numerical filter-bank designs presented in the following are all formulated as a *semi-definite program* (SDP) or special cases thereof.[10] This kind of mathematical programming[11] has gained increasing research interest over the past decades, e.g., [VB96, WSV00, BV04, AL07]. Algorithms such as the interior-point method have been developed, which facilitate an efficient solution of such convex optimization problems in polynomial time, e.g., [Wri97, Ye97, WSV00]. Due to these advances, convex optimization methods have become increasingly popular for various engineering applications, e.g., [VB96, LA00, LY06, AL07].

After a brief discussion of some known numerical design approaches for allpass transformed AS FBs, several new synthesis filter-bank designs are introduced, which pursue different design objectives.

4.3.1 Previous Designs

A common approach to reduce the reconstruction error of an allpass transformed DFT AS FB according to Figure 4.6 (without phase equalizer) is to design its *prototype filters* by numerical optimization, which can be done in a similar manner as for uniform filter-banks, cf., [dH04].

In [dHGCN02], a dedicated prototype filter design for the analysis and synthesis filter-bank is proposed. The FIR analysis prototype lowpass filter of length $L = M$ is designed by two requirements. The first requirement is that the LS error between the ideal lowpass filter with linear phase response and the actual (warped) lowpass filter

[10] An overview of these convex optimization problems is provided by App. D.2.

[11] The term *program* refers in this work to a (numerical) optimization problem or mathematical program, respectively.

should be minimized within the passband

$$\int_{-\Omega_\mathrm{p}}^{\Omega_\mathrm{p}} \left| \widetilde{H}\left(e^{j\,\Omega}\right) - e^{-j\,\Omega\,\tau_h} \right|^2 \,\mathrm{d}\,\Omega \;\rightarrow\; \min\,. \tag{4.60}$$

The second requirement is to minimize the so-called inband aliasing

$$\int_{-\pi}^{\pi} \sum_{\substack{r=0 \\ r \neq \frac{R}{2}}}^{R-1} \left| \widetilde{H}_{\frac{M}{2}}\left(e^{j\,\frac{\Omega}{R}}\, W_R^r\right) \right|^2 \,\mathrm{d}\,\Omega \;\rightarrow\; \min \tag{4.61}$$

with $\widetilde{H}_i\left(e^{j\,\Omega}\right)$ given by Eq. (4.2). Only the aliasing term in the subband $i = M/2$ is considered. This subband causes the highest aliasing distortions as it possesses the highest bandwidth for $a > 0$. The aliasing term for $r = R/2$ is omitted in Eq. (4.61) since it contains the desired spectral content of subband $i = M/2$ [dHGCN02]. For a set of discrete frequencies, the joint minimization according to Eq. (4.60) and Eq. (4.61) can be expressed in a matrix notation in dependence of the vector $\boldsymbol{h}$ which contains the coefficients of the analysis prototype filter. These coefficients are finally determined by an over-determined set of linear equations [dHGCN02].

The M coefficients of the synthesis prototype lowpass filter are also determined by two requirements. The first one is to minimize the LS error between the desired and actual so-called total response of the filter-bank

$$\int_{-\pi}^{\pi} \left| \mathcal{T}_\mathrm{des}\left(e^{j\,\Omega}\right) - \sum_{i=0}^{M-1} \sum_{r=0}^{R-1} \widetilde{H}_i\left(e^{j\,\Omega}\, W_R^r\right) \cdot \widetilde{G}_i\left(e^{j\,\Omega}\right) \right|^2 \,\mathrm{d}\,\Omega \;\rightarrow\; \min \tag{4.62}$$

with $\widetilde{G}_i\left(e^{j\,\Omega}\right)$ given by Eq. (4.30). The second requirement is to reduce the aliasing

$$\int_{-\pi}^{\pi} \sum_{i=0}^{M-1} \sum_{r=1}^{R-1} \left| \widetilde{H}_i\left(e^{j\,\Omega}\, W_R^r\right) \cdot \widetilde{G}_i\left(e^{j\,\Omega}\right) \right|^2 \,\mathrm{d}\,\Omega \;\rightarrow\; \min\,. \tag{4.63}$$

This joint minimization can be written in a matrix notation so that the vector with the coefficients of the synthesis prototype filter $\boldsymbol{g}$ is determined by a set of linear equations [dHGCN02].

A variant of this design approach is proposed in [VN03]. The analysis prototype filter is designed by minimizing the inband aliasing according to Eq. (4.61) while keeping the error of Eq. (4.60) below a certain threshold. Similarly, the coefficients of the synthesis prototype filter are determined by minimizing the aliasing according to Eq. (4.63) while keeping the error for the total response according to Eq. (4.62) below a threshold. In both cases, the prototype filter coefficients are determined by a quadratically constrained quadratic program (QCQP), which is formulated and solved by an equivalent semi-definite program (SDP) [VN03].

The design of [WdDC03] considers individual subsampling rates R_i for each subband and prototype filters of length $L \geq M$. The analysis prototype filter is obtained by an LS error minimization of its passband and stopband error (which reduces the inband aliasing implicitly). The synthesis prototype lowpass filter is obtained by a joint minimization similar to that of Eq. (4.62) and Eq. (4.63). As in [dHGCN02], the coefficients of analysis and synthesis prototype filter are finally determined by a set of linear equations [WdDC03].

An advantage of all these numerical prototype filter designs is that the reconstruction properties of the filter-bank are improved without a (noteworthy) increase of signal delay and algorithmic complexity of the original allpass transformed AS FB according to Figure 4.6. On the other hand, only a very limited reduction of linear distortions and aliasing distortions can be achieved as the $2\,L$ prototype filter coefficients offer only a very restricted number of 'degrees of freedoms'. A complete aliasing cancellation or even a perfect signal reconstruction is not achieved by these design approaches. Therefore, a novel numerical design framework is devised in the following to tackle these shortcomings.

4.3.2 New Matrix Representation

The allpass transformed DFT analysis filter-bank of Figure 4.3 and the FIR synthesis filter-bank of Figure 4.7 are considered. In contrast to Sec. 4.2.2, the coefficients of the FIR sub-filters according to Eq. (4.33) are now determined by a numerical design approach. Basis for *all* the following designs is a matrix representation of the new overall transfer function introduced in Eq. (2.17). Following Eq. (2.8), the input-output relation of the considered warped AS FB can now be written

$$\widehat{X}(z) = \frac{1}{R} \sum_{r=0}^{R-1} X\left(z\,W_R^r\right) \sum_{i=0}^{M-1} \widetilde{H}_i\left(z\,W_R^r\right) \cdot \bar{G}_i(z)\,. \tag{4.64}$$

The analysis filters are given by Eq. (4.15) and the synthesis filters by Eq. (4.32). Applying Eq. (2.17) to Eq. (4.64) results in

$$\begin{aligned} T_\nu(z) &= \frac{\widehat{X}_\nu(z)}{z^{-\nu}} \\ &= \frac{1}{R} \sum_{r=0}^{R-1} W_R^{-r\,\nu} \sum_{i=0}^{M-1} \widetilde{H}_i\left(z\,W_R^r\right) \cdot \bar{G}_i(z) \quad \text{for} \quad \nu \in \{\,0, 1, \ldots, R-1\,\}\,. \end{aligned} \tag{4.65}$$

For a numerical design approach, a matrix formulation of $T_\nu(z)$ in dependence of the unknown $L_\mathrm{q}\,L$ coefficients $q_l(\eta)$ of the L synthesis sub-filters is required. Some manip-

ulations of Eq. (4.32) lead to the representation

$$\begin{aligned}\bar{G}_i(z) &= \sum_{l=0}^{L-1} g(l)\cdot W_M^{-i\,(l+1)}\cdot Q_{L-1-l}(z) \qquad [4.32]\\ &= \sum_{l=0}^{L-1} g(l)\cdot W_M^{-i\,(l+1)} \sum_{\eta=0}^{L_\mathrm{q}-1} q_{L-1-l}(\eta)\cdot z^{-\eta}\\ &= \boldsymbol{v}_i^T\cdot\boldsymbol{D}^T(z)\cdot\boldsymbol{p} \quad \text{for} \quad i\in\{\,0,1,\ldots,M-1\,\} \qquad (4.66a)\end{aligned}$$

with

$$\begin{aligned}\boldsymbol{v}_i &= \Big[\, g(L-1)\cdot W_M^{-Li},\, g(L-2)\cdot W_M^{-(L-1)i},\,\ldots\\ &\qquad\qquad \ldots,\, g(1)\cdot W_M^{-2i},\, g(0)\cdot W_M^{-i}\,\Big]^T \qquad (4.66b)\\ \boldsymbol{D}(z) &= \boldsymbol{I}_L\otimes\boldsymbol{d}_{L_\mathrm{q}}(z) \qquad (4.66c)\\ \boldsymbol{d}_{L_\mathrm{q}}(z) &= \Big[\,1,\, z^{-1},\,\ldots,\, z^{-(L_\mathrm{q}-1)}\,\Big]^T \qquad (4.66d)\\ \boldsymbol{p} &= \Big[\,\boldsymbol{q}_0^T,\,\boldsymbol{q}_1^T,\,\ldots,\,\boldsymbol{q}_{L-1}^T\,\Big]^T \qquad (4.66e)\\ \boldsymbol{q}_l &= \Big[\,q_l(0), q_l(1),\ldots,q_l(L_\mathrm{q}-1)\,\Big]^T \;\forall\; l\in\{\,0,1,\ldots,L-1\,\}\,. \qquad (4.66f)\end{aligned}$$

The operator $\otimes$ marks the Kronecker product of two matrices, $\boldsymbol{I}_L$ an identity-matrix of size $L\times L$ and the superscript T denotes the transpose of a matrix or vector.

As a simple example, the matrix representation of Eq. (4.32) for $L=M=2$ and $L_\mathrm{q}=2$ is given by

$$\begin{aligned}\bar{G}_i(z) &= \begin{bmatrix} g(1)\cdot W_2^{-2i}\\ g(0)\cdot W_2^{-i}\end{bmatrix}^T \cdot \begin{bmatrix} 1 & z^{-1} & 0 & 0\\ 0 & 0 & 1 & z^{-1}\end{bmatrix}\cdot\begin{bmatrix} q_0(0)\\ q_0(1)\\ q_1(0)\\ q_1(1)\end{bmatrix}\\ &= \begin{bmatrix} g(1)\cdot W_2^{-2i}\\ g(0)\cdot W_2^{-i}\end{bmatrix}^T \cdot \begin{bmatrix} q_0(0)+q_0(1)\,z^{-1}\\ q_1(0)+q_1(1)\,z^{-1}\end{bmatrix}\\ &= \sum_{l=0}^{1} g(l)\cdot W_2^{-i\,(l+1)} \sum_{\eta=0}^{1} q_{1-l}(\eta)\cdot z^{-\eta} \quad \text{for} \quad i\in\{\,0,1\,\}\,.\end{aligned}$$

With Eq. (4.66), the transfer function of Eq. (4.65) is now formulated by the matrix notation

$$T_\nu(z) = \underbrace{\left(\frac{1}{R}\sum_{r=0}^{R-1} W_R^{-r\,\nu}\sum_{i=0}^{M-1}\widetilde{H}_i(z\,W_R^r)\cdot\boldsymbol{v}_i^T\cdot\boldsymbol{D}^T(z)\right)}_{=\,\boldsymbol{\xi}_\nu(z)\;\in\,\mathbb{C}^{1\times L_\mathrm{q}L}}\cdot\boldsymbol{p};\quad \nu\in\{0,1,\ldots,R-1\}. \qquad (4.67)$$

For the special case of a *uniform* filter-bank where $a(m) = 0 \wedge b(m) = 0 \ \forall \ m$ and $L_\mathrm{q} = L$, the coefficients of the synthesis sub-filters are given by

$$\boldsymbol{p} = \left[\mathbf{0}_{L-1}^T, 1, \mathbf{0}_{L-2}^T, 1, \mathbf{0}_{L-2}^T, 1, \ \ldots \ , \mathbf{0}_{L-2}^T, 1, \mathbf{0}_{L-1}^T \right]^T \in \mathbb{R}^{L^2 \times 1} \tag{4.68}$$

with $\mathbf{0}_L$ denoting a column vector with L zeros.

4.3.3 Constrained NPR Design

The introduced matrix representation of the filter-bank is now exploited to develop a numerical NPR design which aims for a complete aliasing cancellation. The design is based on the results of Sec. 4.2.2 where it is shown that the magnitude responses of the synthesis filters strive towards those of the warped analysis filters, if a sufficient phase equalization is performed, cf., Eq. (4.50). However, an improved phase equalization does not achieve a (significantly) improved aliasing cancellation as demonstrated by Example 4.2. Therefore, the LS FIR phase equalizer design of Sec. 4.2.2 is now extended by the additional requirement for a complete aliasing cancellation. Thus, a *linear time-invariant* (LTI) system is demanded, which can be expressed by means of the transfer function of Eq. (4.65) as follows

$$T_\nu(z) \stackrel{!}{=} T_0(z) \ \forall \ \nu \in \{ \, 1, 2, \ldots, R-1 \, \} \, . \tag{4.69}$$

The condition of Eq. (4.69) can be cast into a matrix notation by means of Eq. (4.67)

$$\underbrace{\begin{bmatrix} \boldsymbol{\xi}_1(z) - \boldsymbol{\xi}_0(z) \\ \boldsymbol{\xi}_2(z) - \boldsymbol{\xi}_0(z) \\ \vdots \\ \boldsymbol{\xi}_{R-1}(z) - \boldsymbol{\xi}_0(z) \end{bmatrix}}_{= \boldsymbol{\Xi}_\Delta(z) \ \in \mathbb{C}^{R-1 \times L_\mathrm{q} L}} \cdot \ \boldsymbol{p} \stackrel{!}{=} \mathbf{0}_{R-1} \, . \tag{4.70}$$

If Eq. (4.69) is fulfilled, $T_\nu(z) = \overline{T}_\mathrm{lin}(z)$ where the linear transfer function of Eq. (4.34) can be expressed by means of Eq. (4.15) and Eq. (4.32) as follows

$$\begin{aligned} \overline{T}_\mathrm{lin}(z) &= \frac{1}{R} \sum_{i=0}^{M-1} \widetilde{H}_i(z) \cdot \bar{G}_i(z) && [4.34] \\ &= \frac{1}{R} \, \Lambda(z) \sum_{i=0}^{M-1} \sum_{l=0}^{L-1} \sum_{m=0}^{L-1} h(l) \cdot g(m) \cdot \Theta^l(z) \cdot Q_{L-1-m}(z) \cdot W_M^{-i \, (l+m+1)} \\ &= \frac{M}{R} \, \Lambda(z) \sum_{\lambda \in \mathbb{Z}} \sum_{l=0}^{L-1} h(l) \cdot g(\lambda \, M - 1 - l) \cdot \Theta^l(z) \cdot Q_{L-\lambda \, M+l}(z) \, . && (4.71) \end{aligned}$$

This linear transfer function of the filter-bank equals

$$\overline{T}_\mathrm{lin}(z) = z^{-D_\circ}, \tag{4.72}$$

if the prototype filters comply with Eq. (2.32) and if

$$\Lambda(z) \cdot \Theta^l(z) \cdot Q_l(z) \stackrel{!}{=} z^{-D_\circ} \;\forall\; l \in \{\,0, 1, \ldots, L-1\,\}\,. \tag{4.73}$$

This requirement can be expressed by means of the matrices introduced in Eq. (4.66):

$$\underbrace{\left(\left(\mathbf{1}_{L L_\mathrm{q}}^T \otimes \begin{bmatrix} \Lambda(z) \\ \Lambda(z)\cdot\Theta(z) \\ \vdots \\ \Lambda(z)\cdot\Theta^{L-1}(z) \end{bmatrix}\right) \odot \boldsymbol{D}^T(z)\right)}_{=\boldsymbol{U}(z)\;\in\mathbb{C}^{L\times L_\mathrm{q}\,L}} \cdot \boldsymbol{p} \stackrel{!}{=} \underbrace{z^{-D_\circ}\,\mathbf{1}_L}_{=\boldsymbol{v}(z)} \tag{4.74}$$

with $\odot$ denoting the element-wise multiplication of two matrices of the same dimensions (Hadamard product) and $\mathbf{1}_L$ representing a column vector with L ones. The conditions of Eq. (4.70) and Eq. (4.74)

$$\boldsymbol{\Xi}_\Delta(z) \cdot \boldsymbol{p} \stackrel{!}{=} \mathbf{0}_{R-1} \quad \wedge \quad \boldsymbol{U}(z) \cdot \boldsymbol{p} \stackrel{!}{=} \boldsymbol{v}(z) \tag{4.75}$$

shall be fulfilled for $\mathcal{N}$ discrete z-values on the unit circle

$$z = W_\mathcal{N}^m = e^{-j\,\frac{2\pi}{\mathcal{N}}\,m} \;\forall\; m \in \{0, 1, \ldots, \mathcal{N}-1\} \quad \text{with} \quad \mathcal{N} = L_\mathrm{q}\,L\,. \tag{4.76}$$

Other choices for $\mathcal{N}$ are possible as far as the resulting set of equations is over-determined.[12] Evaluating the matrix $\boldsymbol{U}(z)$ and vector $\boldsymbol{v}(z)$ of Eq. (4.75) at these points can be expressed by the (stacking) notation

$$\boldsymbol{U}^{[\mathcal{N}]} = \begin{bmatrix} \boldsymbol{U}(1) \\ \boldsymbol{U}\left(W_\mathcal{N}\right) \\ \vdots \\ \boldsymbol{U}\left(W_\mathcal{N}^{\mathcal{N}-1}\right) \end{bmatrix} \in \mathbb{C}^{L\mathcal{N}\times\mathcal{N}} \tag{4.77}$$

$$\boldsymbol{v}^{[\mathcal{N}]} = \begin{bmatrix} \mathbf{1}_L \\ W_\mathcal{N}^{-D_\circ}\,\mathbf{1}_L \\ \vdots \\ W_\mathcal{N}^{-D_\circ\,(\mathcal{N}-1)}\,\mathbf{1}_L \end{bmatrix} \in \mathbb{C}^{L\mathcal{N}}\,. \tag{4.78}$$

The matrix $\boldsymbol{\Xi}_\Delta^{[\mathcal{N}]}$ is derived from the matrix $\boldsymbol{\Xi}_\Delta(z)$ of Eq. (4.75) in the same manner

$$\boldsymbol{\Xi}_\Delta^{[\mathcal{N}]} = \begin{bmatrix} \boldsymbol{\Xi}_\Delta(1) \\ \boldsymbol{\Xi}_\Delta\left(W_\mathcal{N}\right) \\ \vdots \\ \boldsymbol{\Xi}_\Delta\left(W_\mathcal{N}^{\mathcal{N}-1}\right) \end{bmatrix} \in \mathbb{C}^{(R-1)\mathcal{N}\times\mathcal{N}}\,. \tag{4.79}$$

[12] A high value for $\mathcal{N}$ allows to achieve a lower approximation error at the price of an increased computational burden to solve the optimization problem and vice versa. Taking an infinite set of z-values into account would lead to a semi-infinite program which, however, is much harder to solve than a semi-definite program.

The $\mathcal{N} = L_\mathrm{q}\, L$ synthesis sub-filter coefficients $\boldsymbol{p}$ to fulfill Eq. (4.75) can now be determined by means of the following equality constrained least-squares error (CLS) minimization

$$\widehat{\boldsymbol{p}} = \arg\left\{ \underset{\boldsymbol{p}}{\text{minimize}} \left\| \boldsymbol{U}^{[\mathcal{N}]} \cdot \boldsymbol{p} - \boldsymbol{v}^{[\mathcal{N}]} \right\|_2^2 \right\} \tag{4.80a}$$

$$\text{subject to} \quad \boldsymbol{\Xi}_{\Delta}^{[\mathcal{N}]} \cdot \boldsymbol{p} = \boldsymbol{0}_{(R-1)\,\mathcal{N}} \,. \tag{4.80b}$$

Such an optimization problem is a *linearly constrained quadratic program* (LCQP) according to Eq. (D.11). It can be solved, e.g., by means of the functions `lsqlin` (used here) or `quadprog` of the MATLAB optimization toolbox.[13] With this approach, linear signal distortions are minimized with the constraints for complete aliasing cancellation and a desired signal delay D_o. The problem of Eq. (4.80) is a *convex* optimization problem as the objective function of Eq. (4.80a) is convex and the equality constraints are linear. Thus, the solution of this problem has a global optimum which is unique, if the objective function is strictly convex on the feasible region.

The synthesis filter-bank design of Eq. (4.80) is originally proposed in [LDV09] and contains some previous proposals as *special cases*: The design of [LDV08b] is obtained for an allpass transformation of first order according to Eq. (4.17) with a real allpass pole ($a = \alpha$) and a prototype filter length restricted to $L = M$. The approach of [LV07c] is given for an allpass transformation of first order and if Eq. (4.80a) is solved without the constraint of Eq. (4.80b). In this case, the synthesis sub-filters with system functions $Q_l(z)$ act purely as phase equalizers designed by an LS error criterion as discussed in Sec. 4.2.2 and Sec. 4.2.3. The coefficients of the sub-filters can then of course be determined by the closed-form expression of Eq. (3.81) instead of solving Eq. (4.80a) numerically.

Example 4.3: A warped DFT AS FB with ELT prototype filters according to Eq. (2.33) is considered. Its design by the LCQP of Eq. (4.80) is analyzed in Figure 4.17 where the magnitude of the BSF is provided by Figure 2.6-b. A comparison of the magnitude responses of the analysis and synthesis filters of Figure 4.17-a and Figure 4.17-b reveals that their curve progressions are very similar owing to the implicit phase equalization. The plot of the peak aliasing distortions in Figure 4.17-e shows that the design constraint for perfect aliasing cancellation is fulfilled with a very high numerical accuracy. This is also demonstrated by the BSF plotted in Figure 2.6-b, which exhibits no alias components on its side diagonals. The BSF as well as the analysis of the transfer function $T_0(e^{j\,\Omega})$ in Figure 4.17-c and Figure 4.17-d demonstrate the NPR property.

The design of Eq. (4.80) aims for a filter-bank with complete aliasing cancellation. However, such a behavior may not be required by some applications. Instead, it can be beneficial to tolerate some aliasing distortions in an exchange for a lower amount of linear distortions. Therefore, a *generalization* of the CLS design of Eq. (4.80) is now devised to gain a more flexible control over its signal reconstruction error.

One approach to achieve this goal is to utilize the *method of weighting* [Gv96]. The

[13] The 64bit MATLAB version 7.9.0.529 (R2009b) for the operating system Linux has been used for this work [TM09].

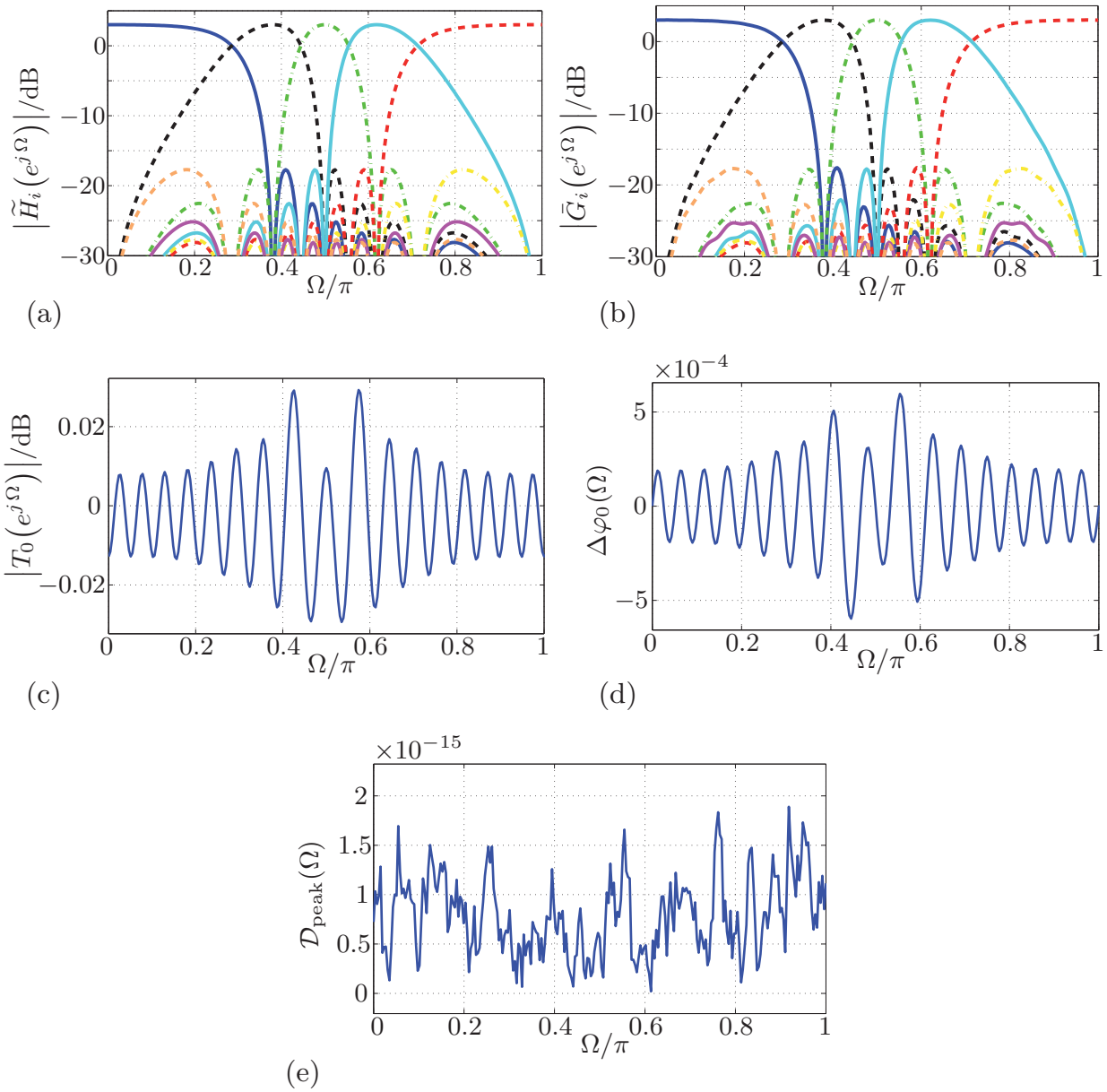

Figure 4.17: *Design of an allpass transformed DFT AS FB according to Figure 4.3 and Figure 4.7 by the LCQP of Eq.* (4.80) *with parameters* $L = 2\,M = 16$, $R = M/4 = 2$, $a(0) = -j0.5$, $a(1) = j0.5$, $L_q = 60$ *and* $D_o = 56$*:*
(a) *magnitude responses of the analysis filters*
(b) *magnitude responses of the synthesis filters*
(c) *magnitude response of the overall transfer function*
(d) *phase error of the overall transfer function according to Eq.* (2.21)
(e) *peak aliasing distortions according to Eq.* (2.12)*.*

CLS minimization of Eq. (4.80) can be rewritten as follows

$$\hat{\boldsymbol{p}} = \arg\left\{ \underset{\boldsymbol{p}}{\text{minimize}} \left\| \begin{bmatrix} \boldsymbol{U}^{[\mathcal{N}]} \\ \mu \cdot \boldsymbol{\Xi}_{\Delta}^{[\mathcal{N}]} \end{bmatrix} \cdot \boldsymbol{p} - \begin{bmatrix} \boldsymbol{v}^{[\mathcal{N}]} \\ \boldsymbol{0}_{(R-1)\,\mathcal{N}} \end{bmatrix} \right\|_2^2 \right\} \tag{4.81}$$

$$= \begin{bmatrix} \boldsymbol{U}^{[\mathcal{N}]} \\ \mu \cdot \boldsymbol{\Xi}_{\Delta}^{[\mathcal{N}]} \end{bmatrix}^{\#} \begin{bmatrix} \boldsymbol{v}^{[\mathcal{N}]} \\ \boldsymbol{0}_{(R-1)\,\mathcal{N}} \end{bmatrix} \; ; \quad \mu \in \mathbb{R}_+ \tag{4.82}$$

provided that the pseudo-inverse of the matrix (marked by a hash) exists. For $\mu \to 0$, an unconstrained optimization is performed and the synthesis sub-filters with system functions $Q_l(z)$ become LS FIR phase equalizers according to Eq. (4.45). For $\mu \to \infty$, the optimization problem of Eq. (4.81) becomes equivalent to that of Eq. (4.80).

An advantage of this design approach is its simplicity; Eq. (4.81) constitutes an unconstrained LS error optimization which can be easily solved. A drawback is that the aliasing distortions are only controlled implicitly by the choice of the weighting factor μ. In addition, some precautions are necessary for high values of μ to avoid numerical problems, cf., [Gv96].

An explicit bound on the aliasing distortions can be imposed by the following reformulation of Eq. (4.80)

$$\underset{\boldsymbol{p}}{\text{minimize}} \left\| \boldsymbol{U}^{[\mathcal{N}]} \cdot \boldsymbol{p} - \boldsymbol{v}^{[\mathcal{N}]} \right\|_2^2 \tag{4.83a}$$

$$\text{subject to} \quad \left\| \boldsymbol{\Xi}_{\Delta}^{[\mathcal{N}]} \cdot \boldsymbol{p} \right\|_2^2 \leq \epsilon_{\mathrm{a}}; \quad 0 \leq \epsilon_{\mathrm{a}} \tag{4.83b}$$

where the indication $\widehat{\boldsymbol{p}} = \arg\{\ldots\}$ is omitted to ease the notation. The equality constraint for an LTI system is now relaxed by tolerating a bounded LS error. The choice $\epsilon_{\mathrm{a}} \to \infty$ leads to an unconstrained LS error optimization and $\epsilon_{\mathrm{a}} \to 0$ to the original problem of Eq. (4.80). In contrast to the method of weighting, these extremal values for ϵ_{a} pose no specific numerical problems.

As shown in App. B.3, the *quadratically constrained quadratic program* (QCQP) of Eq. (4.83) can be expressed in an epigraph form with the epigraph variable $\rho \geq 0$, which can than be converted into the following *semi-definite program* (SDP) with *real* linear matrix inequalities (LMIs)

$$\underset{\boldsymbol{p}_{\mathrm{a}}}{\text{minimize}} \; \boldsymbol{l}^T \boldsymbol{p}_{\mathrm{a}} \tag{4.84a}$$

$$\text{subject to} \begin{bmatrix} \Re\{\boldsymbol{L}_1\} & \Im\{\boldsymbol{L}_1\} \\ -\Im\{\boldsymbol{L}_1\} & \Re\{\boldsymbol{L}_1\} \end{bmatrix} \succeq 0 \tag{4.84b}$$

$$\begin{bmatrix} \Re\{\boldsymbol{L}_2\} & \Im\{\boldsymbol{L}_2\} \\ -\Im\{\boldsymbol{L}_2\} & \Re\{\boldsymbol{L}_2\} \end{bmatrix} \succeq 0 \tag{4.84c}$$

with

$$\boldsymbol{p}_{\mathrm{a}} = \left[\rho, \boldsymbol{p}^T \right]^T \tag{4.84d}$$

$$\boldsymbol{l} = \left[1, \boldsymbol{0}_{\mathcal{N}}^T \right]^T \tag{4.84e}$$

$$\boldsymbol{L}_1 = \begin{bmatrix} \boldsymbol{I}_{L\,\mathcal{N}} & \boldsymbol{U}^{[\mathcal{N}]}\boldsymbol{p} \\ \left(\boldsymbol{U}^{[\mathcal{N}]}\boldsymbol{p}\right)^H & \rho + \left(\boldsymbol{v}^{[\mathcal{N}]}\right)^H \left(\boldsymbol{U}^{[\mathcal{N}]}\boldsymbol{p}\right) + \left(\boldsymbol{U}^{[\mathcal{N}]}\boldsymbol{p}\right)^H \boldsymbol{v}^{[\mathcal{N}]} - \left(\boldsymbol{v}^{[\mathcal{N}]}\right)^H \boldsymbol{v}^{[\mathcal{N}]} \end{bmatrix} \tag{4.84f}$$

$$\boldsymbol{L}_2 = \begin{bmatrix} \boldsymbol{I}_{(R-1)\,\mathcal{N}} & \boldsymbol{\Xi}_{\Delta}^{[\mathcal{N}]}\boldsymbol{p} \\ \left(\boldsymbol{\Xi}_{\Delta}^{[\mathcal{N}]}\boldsymbol{p}\right)^H & \epsilon_{\mathrm{a}} \end{bmatrix}. \tag{4.84g}$$

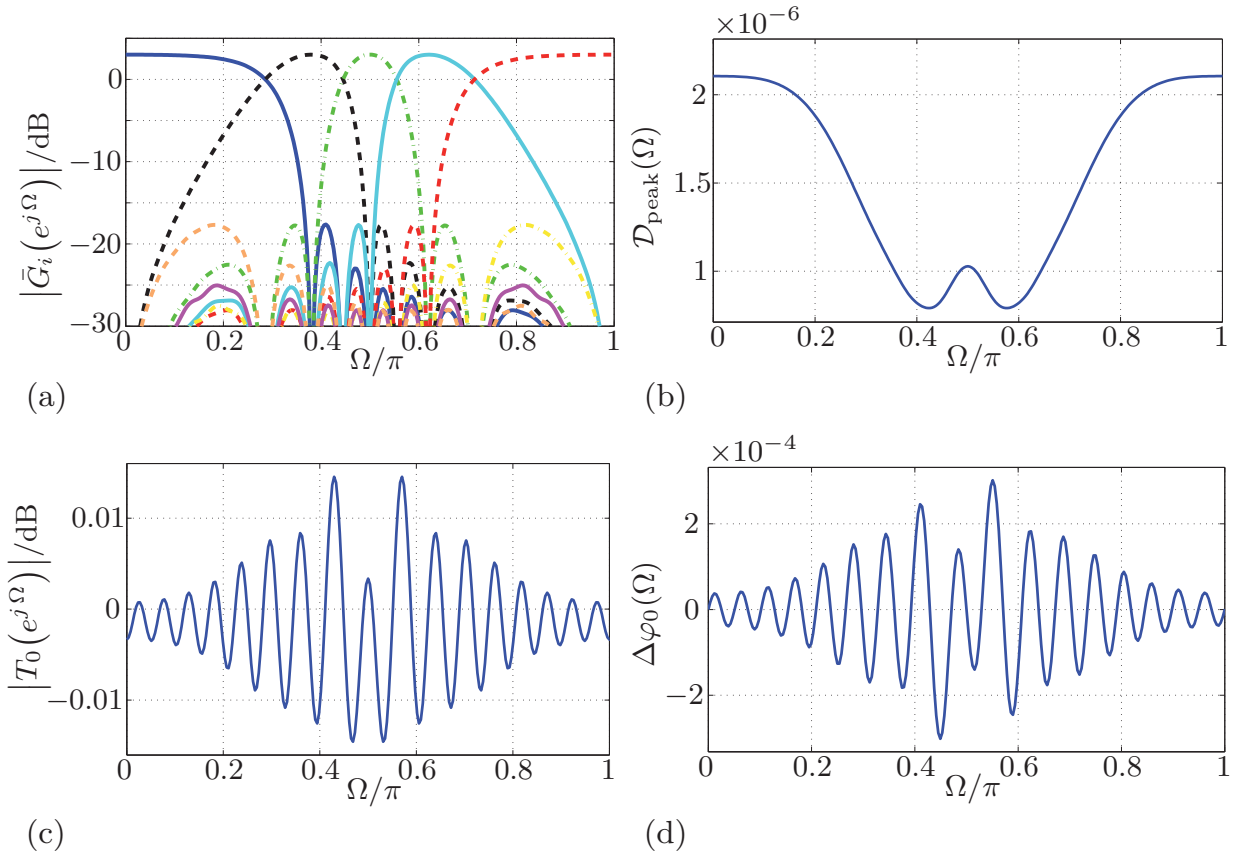

Figure 4.18: *Design of an allpass transformed DFT AS FB according to Figure 4.3 and Figure 4.7 with parameters $L = 2\,M = 16$, $R = M/4 = 2$, $a(0) = -j0.5$, $a(1) = j0.5$ by the QCQP of Eq. (4.83) with a threshold of $\epsilon_a = 10^{-8}$, sub-filter length $L_q = 60$ and signal delay $D_o = 56$:*
(a) *magnitude responses of the synthesis filters*
(b) *peak aliasing distortions*
(c) *magnitude response of the overall transfer function*
(d) *phase error of the overall transfer function.*

In contrast to the original optimization problem of Eq. (4.83), the mathematical program of Eq. (4.84) can now be solved by means of the MATLAB function `mincx` of the 'Robust Control Toolbox' where the LMIs can be specified by using the LMI Lab package [TM09]. Besides, there are different other software packages to solve SDPs such as [FKNY04, BY05, Bor06, TTT06] or the CVX toolbox [GB09] which is employed here.

Example 4.4: The effect of the QCQP design stated by Eq. (4.83) is demonstrated in Figure 4.18. The design parameters are identical to those of Example 4.3 where now a threshold of $\epsilon_\mathrm{a} = 10^{-8}$ is applied to the constraint of Eq. (4.83b). As before, the synthesis bandpass filters have magnitude responses which are very similar to those of the analysis filters plotted in Figure 4.17-a. The comparison of Figure 4.18 with Figure 4.17 shows how the relaxation of the LTI constraint provokes higher peak aliasing distortions, but achieves a lower amount of linear magnitude and phase distortions. The diminished aliasing cancellation is also demonstrated by Figure 2.6: It shows the magnitude of the BSF for this design $\left(\epsilon_\mathrm{a} = 10^{-8}\right)$ in Figure 2.6-a and the BSF for

Example 4.3 ($\epsilon_\mathrm{a} = 0$) in Figure 2.6-b. It can be seen how the permission of a threshold $\epsilon_\mathrm{a} > 0$ leads to a small non-compensated alias component.

The presented designs consider the $\mathcal{L}_2$-norm as error norm (LS error), but the use of other $\mathcal{L}_p$-norms (outlined in App. D.1) is possible as well and poses no specific problems as the resulting optimization problems are still convex and thus tractable, i.e., solvable in polynomial time.

4.3.4 Sparse Design

The synthesis filter-banks considered so far are designed with the objective to achieve a low signal reconstruction error. Another design target, which is also of great practical importance, is to obtain a synthesis filter-bank with a low algorithmic complexity. This can be accomplished by a *sparse* design, which aims for a low number of non-zero filter coefficients in order to achieve a reduced number of multiplications and summations. This can be beneficial, e.g., for an ASIC implementation to save circuit components and power consumption or it can help to reduce the quantization noise and complexity for an implementation with fixed-point arithmetic due to the diminished number of summation and multiplication operations.

The design of signal processing systems with the sparseness constraint is done for various applications, e.g., [Rao98]. One is the design of sparse FIR filters, which is treated in several publications, e.g., [WM93, WM96, SL97, MPH02]. However, a sparse synthesis filter-bank design for a warped analysis filter-bank has not been proposed so far. Using known sparse FIR filter designs for the considered synthesis filter-bank design is difficult as they are often either relying on a specific FIR filter structure (as, e.g., linear-phase filters) and/or have a high design complexity. In the following, a sparse synthesis filter-bank design for a warped analysis filter-bank is developed which can handle the large number of filter coefficients being involved in a simple manner.

4.3.4.1 Concepts

The design of a synthesis filter-bank according to Figure 4.7 with a low algorithmic complexity can be accomplished by different concepts.

A straightforward approach is to use for Eq. (4.33) synthesis sub-filters of lower filter length $L'_\mathrm{q} < L_\mathrm{q}$. However, it turns out that a sparse design with higher filter length L_q but the same number of non-zero filter coefficients clearly outperforms such a design. This is due to the fact that a sparse design with a higher filter length offers more degrees of freedom to fulfill a given optimization criterion.[14]

Another simple method is to set the $\mathcal{N}_\mathrm{z}$ coefficients of the vector $\boldsymbol{p}$ with the smallest magnitude equal to zero. This approach is referred to as *zero-forcing* in the following. A drawback of this technique is that the original optimization constraints may not be fulfilled anymore.

A *brute-force method* is to optimize the synthesis filters for all possible sparsity patterns and to select the best design according to the given design criterion. Here, the unknown vector $\boldsymbol{p}$ contains $\mathcal{N} = L_\mathrm{q}\, L$ coefficients. If $\mathcal{N}_\mathrm{z}^\mathrm{max}$ denotes the maximal

[14] Such an observation is also known from sparse FIR filter designs, e.g., [WM96, MPH02].

number of coefficients set to zero, there are

$$\sum_{m=\mathcal{N}-\mathcal{N}_\mathrm{z}^{\max}}^{\mathcal{N}} \binom{\mathcal{N}}{m} \leq 2^{\mathcal{N}}\,;\quad \mathcal{N}_\mathrm{z}^{\max} \leq \mathcal{N} \tag{4.85}$$

sparsity patterns to be evaluated where the equality holds for $\mathcal{N}_\mathrm{z}^{\max} = \mathcal{N}$. Thus, the problem is NP-complete and the algorithmic complexity increases exponentially with $\mathcal{N}$. Even the use of effective techniques for the search of the optimal solution such as the branch-and-bound algorithm [SL97] does not solve this problem, especially as there is not only a single but L sub-filters of length L_q to be determined (see Figure 4.7).

An approach to alleviate this problem is to exploit *a priori knowledge* about the specific impulse response of a filter and to place the zeros accordingly. Such an approach is proposed in [WM93, WM96] for a sparse Chebyshev design of linear-phase FIR filters. An improvement of this approach is proposed in [SL97] where a wider class of FIR filters is considered.

Another concept, which does not require any *a priori* knowledge, is to employ an $\mathcal{L}_1$-norm regularization, e.g., [BV04]. This technique is employed for the problem at hand as it can be neatly incorporated into the new design framework. The principle of this approach should be explained by a simple but instructive example.

An arbitrary, over-determined set of linear equations is considered

$$\boldsymbol{C} \cdot \boldsymbol{b} = \boldsymbol{a} \tag{4.86}$$

where the vector $\boldsymbol{b}$ is of dimension $N_b \times 1$.[15] An LS error solution for this set of equations with the constraint that the vector $\boldsymbol{b}$ is *sparse* is given by

$$\underset{\boldsymbol{b}}{\text{minimize}}\ \left\|\boldsymbol{C} \cdot \boldsymbol{b} - \boldsymbol{a}\right\|_2^2 \tag{4.87a}$$

$$\text{subject to}\quad \|\boldsymbol{b}\|_0 \leq N_b' < N_b\,;\quad N_b', N_b \in \mathbb{N}\,. \tag{4.87b}$$

The *zero-norm* $\|\boldsymbol{p}\|_0$ returns the cardinality (or size) of a vector, which is the number of its non-zero components.[16] The above optimization problem is *non-convex* and finding a global optimum requires to verify all possible sparsity patterns, which causes an immense computational burden, cf., Eq. (4.85). An approach to circumvent this problem is to solve the optimization problem of Eq. (4.87) approximately by means of an $\mathcal{L}_1$*-norm regularization* [BV04]

$$\underset{\boldsymbol{b}}{\text{minimize}}\ \left\{\left\|\boldsymbol{C} \cdot \boldsymbol{b} - \boldsymbol{a}\right\|_2^2 + \gamma_\mathrm{p} \left\|\boldsymbol{b}\right\|_1\right\}\,;\quad \gamma_\mathrm{p} \geq 0\,. \tag{4.88}$$

The *penalty factor* γ_p determines the trade-off between the residual LS error on the one hand, and the sparseness of the vector $\boldsymbol{b}$ on the other hand. The objective function of

[15] For a determined set of equations, $\boldsymbol{C}$ is an invertible square matrix and the residual vector $\boldsymbol{C}\,\boldsymbol{b} - \boldsymbol{a}$ a zero-vector.

[16] The zero-norm is not a norm in a strict sense as it is not positive homogeneous, because the statement $\|c\,\boldsymbol{b}\|_0 = c\,\|\boldsymbol{b}\|_0$ is not true for all $c > 0$ and $\boldsymbol{b} \neq \boldsymbol{0}$.

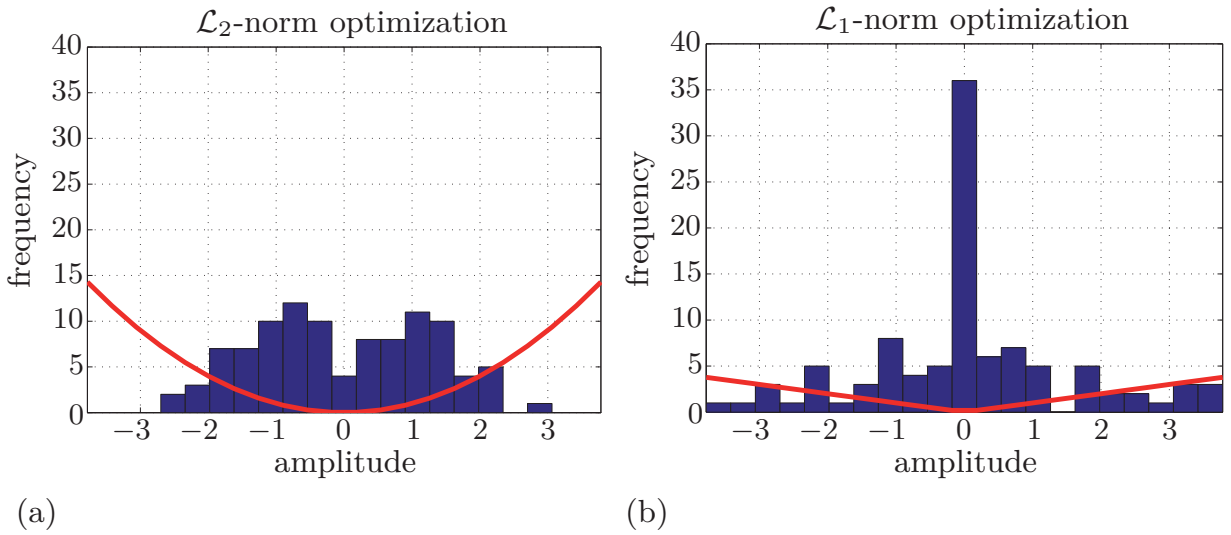

Figure 4.19: *Histograms for the coefficients of residual vector $\boldsymbol{r}_p$ determined by Eq. (4.89) for the $\mathcal{L}_2$-norm (a) and $\mathcal{L}_1$-norm (b). The matrices $\boldsymbol{C} \in \mathbb{R}^{102\times 30}$ and $\boldsymbol{a} \in \mathbb{R}^{102}$ contain uniformly distributed random numbers generated by the MATLAB function* `rand`*. The solid line marks the respective penalty function (squared magnitude and magnitude of the amplitude).*

Eq. (4.88) is the sum of two convex functions (norms) so that Eq. (4.88) constitutes a *convex* optimization problem, which is much easier to solve than the original non-convex optimization problem of Eq. (4.87).

The motivation for using the $\mathcal{L}_1$-norm as *penalty function* can be explained by a look at the residual (error) vector

$$\boldsymbol{r}_p = \boldsymbol{C} \cdot \hat{\boldsymbol{b}}_p - \boldsymbol{a} \tag{4.89a}$$

obtained by the $\mathcal{L}_p$-norm optimization

$$\widehat{\boldsymbol{b}}_p = \arg\left\{ \underset{\boldsymbol{b}}{\text{minimize}} \left\| \boldsymbol{C} \cdot \boldsymbol{b} - \boldsymbol{a} \right\|_p \right\} \quad \text{for} \quad p \in \{\,1, 2\,\}\,. \tag{4.89b}$$

The amplitude distributions of the residual vector $\boldsymbol{r}_p$ are plotted in Figure 4.19 for the two considered norms along with the respective penalty function. The $\mathcal{L}_2$-norm puts very low weight on small residuals and a strong weight on large residuals. In contrast, the $\mathcal{L}_1$-norm penalty puts more weight on small residuals and less weight on large residuals. Therefore, the $\mathcal{L}_1$-norm penalty function tends to produce a *sparse* solution for the residual vector $\boldsymbol{r}_1$ with a lot of coefficients being equal or close to zero. The use of other penalty functions, which achieve a better approximation of the zero-norm than the $\mathcal{L}_1$-norm penalty function, has the decisive drawback that they are not convex (such as the zero-norm itself) [BV04].

4.3.4.2 Sparse NPR Design by $\mathcal{L}_1$-Norm Regularization

The introduced $\mathcal{L}_1$-norm regularization is now applied to the QCQP of Eq. (4.83), which yields the following optimization problem

$$\underset{\boldsymbol{p}}{\text{minimize}} \ \left\{ \left\| \boldsymbol{U}^{[\mathcal{N}]} \cdot \boldsymbol{p} - \boldsymbol{v}^{[\mathcal{N}]} \right\|_2^2 + \gamma_\mathrm{p} \left\| \boldsymbol{p} \right\|_1 \right\} \tag{4.90a}$$

$$\text{subject to} \ \left\| \boldsymbol{\Xi}_\Delta^{[\mathcal{N}]} \cdot \boldsymbol{p} \right\|_2^2 \leq \epsilon_\mathrm{a} \,; \quad \epsilon_\mathrm{a} \geq 0 \,. \tag{4.90b}$$

This program can be easily converted to the 'standard form' of a convex program as listed in App. D.2, which is required for some solvers: For a real vector $\boldsymbol{p}$, Eq. (4.90) can be written in an epigraph form by means of the variables ρ and $\boldsymbol{t}$ as follows

$$\underset{\boldsymbol{p},\, \rho,\, \boldsymbol{t}}{\text{minimize}} \ \left\{ \rho + \gamma_\mathrm{p} \, \mathbf{1}_\mathcal{N}^T \boldsymbol{t} \right\} \tag{4.91a}$$

$$\text{subject to} \ \left\| \boldsymbol{\Xi}_\Delta^{[\mathcal{N}]} \cdot \boldsymbol{p} \right\|_2^2 \leq \epsilon_\mathrm{a} \tag{4.91b}$$

$$\left\| \boldsymbol{U}^{[\mathcal{N}]} \cdot \boldsymbol{p} - \boldsymbol{v}^{[\mathcal{N}]} \right\|_2^2 \leq \rho \tag{4.91c}$$

$$-\boldsymbol{t} \preceq \boldsymbol{p} \preceq \boldsymbol{t} \quad \text{for} \quad \boldsymbol{p} \in \mathbb{R}^\mathcal{N} ; \quad \boldsymbol{t} \in \mathbb{R}_+^\mathcal{N} ; \quad \epsilon_\mathrm{a},\, \gamma_\mathrm{p},\, \rho \geq 0 \,. \tag{4.91d}$$

This is equivalent to the formulation

$$\underset{\boldsymbol{p}_\mathrm{a}}{\text{minimize}} \ \boldsymbol{y}^T \boldsymbol{p}_\mathrm{a} \tag{4.92a}$$

$$\text{subject to} \ \left\| \left[\boldsymbol{O}_{(R-1)\mathcal{N} \times \mathcal{N}+1} \quad \boldsymbol{\Xi}_\Delta^{[\mathcal{N}]} \right] \cdot \boldsymbol{p}_\mathrm{a} \right\|_2^2 \leq \epsilon_\mathrm{a} \tag{4.92b}$$

$$\left\| \left[\boldsymbol{O}_{L\mathcal{N} \times \mathcal{N}+1} \quad \boldsymbol{U}^{[\mathcal{N}]} \right] \cdot \boldsymbol{p}_\mathrm{a} - \boldsymbol{v}^{[\mathcal{N}]} \right\|_2^2 \leq \begin{bmatrix} 1 \\ \mathbf{0}_{2\mathcal{N}} \end{bmatrix}^T \boldsymbol{p}_\mathrm{a} \tag{4.92c}$$

$$0 \leq \boldsymbol{f}_m^T \cdot \left(\boldsymbol{p}_\mathrm{a} + \boldsymbol{t}_\mathrm{a} \right) \tag{4.92d}$$

$$0 \leq \boldsymbol{f}_m^T \cdot \left(\boldsymbol{t}_\mathrm{a} - \boldsymbol{p}_\mathrm{a} \right) \tag{4.92e}$$

with

$$\boldsymbol{p}_\mathrm{a} = \begin{bmatrix} \rho \\ \boldsymbol{t} \\ \boldsymbol{p} \end{bmatrix} ; \quad \boldsymbol{y} = \begin{bmatrix} 1 \\ \gamma_\mathrm{p} \, \mathbf{1}_\mathcal{N} \\ \mathbf{0}_\mathcal{N} \end{bmatrix} ; \quad \boldsymbol{t}_\mathrm{a} = \begin{bmatrix} \mathbf{0}_{\mathcal{N}+1} \\ \boldsymbol{t} \end{bmatrix} ; \quad \boldsymbol{f}_m = \begin{bmatrix} \mathbf{0}_{\mathcal{N}+m} \\ 1 \\ \mathbf{0}_{\mathcal{N}-m} \end{bmatrix} \tag{4.92f}$$

$$\boldsymbol{p} \in \mathbb{R}^\mathcal{N} ; \quad \boldsymbol{t} \in \mathbb{R}_+^\mathcal{N} ; \quad \epsilon_\mathrm{a},\, \gamma_\mathrm{p},\, \rho \geq 0 ; \quad m \in \{\, 1, 2, \ldots, \mathcal{N} \,\} \tag{4.92g}$$

where $\boldsymbol{O}_{M \times N}$ represents a zero-matrix of dimension $M \times N$. The optained optimization problem of Eq. (4.92) is a *second order cone program* (SOCP) without equality constraints according to Eq. (D.9). Such a problem can be solved by MATLAB using solvers such as SeDuMi [Stu99] or SDPT3 [TTT06].[17]

[17] The employed CVX toolbox [GB09] uses SeDuMi and SDPT3 as core solvers.

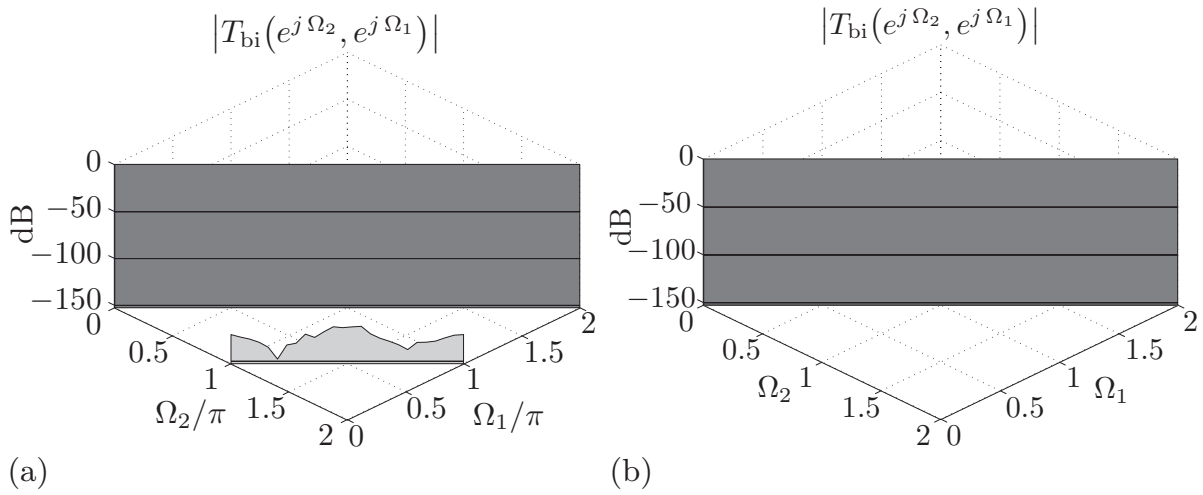

Figure 4.20: *Design of an allpass transformed DFT AS FB according to Figure 4.3 and Figure 4.7 with* $L = 2\,M = 16$, $R = M/4 = 2$, $a(0) = -j0.5$, $a(1) = j0.5$ *by the QCQP of Eq.* (4.90) *with* $L_q = 60$, $D_o = 56$, $\epsilon_a = 0$ *and two different penalty factors* γ_p. *A subsequent zero-forcing to* 50% *of the smallest coefficients of* $\widehat{\boldsymbol{p}}$ *is performed in both cases:*
(a) *magnitude of the BSF for* $\gamma_p = 0$
(b) *magnitude of the BSF for* $\gamma_p = 0.3$.

Example 4.5: The design of Example 4.3 is revisited to demonstrate the effect of the proposed sparse design. The synthesis filter-bank of Figure 4.7 is designed by the QCQP of Eq. (4.90) with the constraint for complete aliasing cancellation ($\epsilon_{\mathrm{a}} = 0$). This optimization is performed with $\mathcal{L}_1$-norm regularization ($\gamma_{\mathrm{p}} = 0.3$) and without $\mathcal{L}_1$-norm regularization ($\gamma_{\mathrm{p}} = 0$), which is here equivalent to Eq. (4.80) since $\epsilon_{\mathrm{a}} = 0$. Afterwards, the $\mathcal{N}_{\mathrm{z}} = \mathcal{N}/2$ smallest coefficients of the vector $\widehat{\boldsymbol{p}}$ are set to zero for both designs, i.e., a zero-forcing is applied to 50% of the sub-filter coefficients.

The signal reconstruction errors of both designs are analyzed in Figure 4.20 and Figure 4.21. (The magnitude responses of the synthesis filters are not plotted as they are almost identical to those of Figure 4.17-b.) Comparing Figure 4.17 with Figure 4.21 shows that the zero-forcing affects mainly the peak aliasing distortions and less the linear phase and magnitude distortions. A comparison of Figure 4.21-a with Figure 4.21-b reveals that the sparse design with $\mathcal{L}_1$-norm regularization achieves a much better aliasing compensation than the design without $\mathcal{L}_1$-norm regularization.

This effect is also demonstrated by the BSFs plotted in Figure 4.20. It can be seen that the sparse design achieves actually a complete aliasing cancellation as opposed to the non-sparse design, which exhibits a small non-compensated alias component on its side diagonal.

This difference for the aliasing cancellation can be explained by means of Figure 4.22. It shows the number of coefficients of vector $\widehat{\boldsymbol{p}}$ whose magnitudes are below a certain threshold ϵ_p. For the design according to Eq. (4.90) with $\mathcal{L}_1$-norm regularization, about 50% of the coefficients have a magnitude of less then $\epsilon_p = 10^{-12}$. In contrast, the coefficients obtained by the design without $\mathcal{L}_1$-norm regularization have all a magnitude

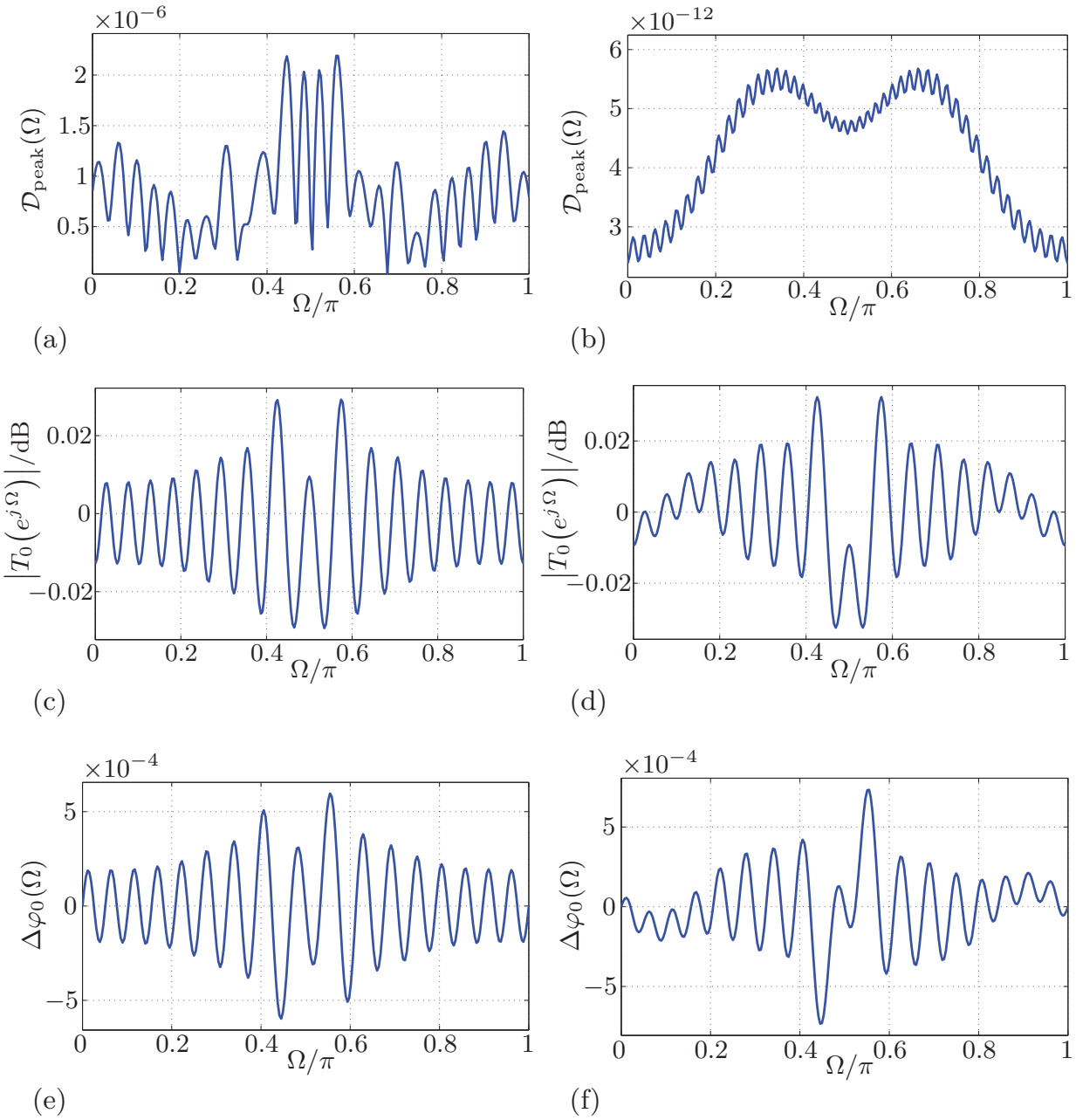

Figure 4.21: *Design of an allpass transformed DFT AS FB according to Figure 4.3 and Figure 4.7 with* $L = 2\,M = 16$, $R = M/4 = 2$, $a(0) = -j0.5$, $a(1) = j0.5$ *by the QCQP of Eq.* (4.90) *with* $L_q = 60$, $D_o = 56$, $\epsilon_a = 0$ *and two different penalty factors* γ_p. *A subsequent zero-forcing to* 50% *of the smallest coefficients of* $\widehat{\boldsymbol{p}}$ *is performed in both cases:*
(a) *peak aliasing distortions for* $\gamma_p = 0$
(b) *peak aliasing distortions for* $\gamma_p = 0.3$
(c) *magnitude response of the overall transfer function for* $\gamma_p = 0$
(d) *magnitude response of the overall transfer function for* $\gamma_p = 0.3$
(e) *phase error of the overall transfer function for* $\gamma_p = 0$
(f) *phase error of the overall transfer function for* $\gamma_p = 0.3$.

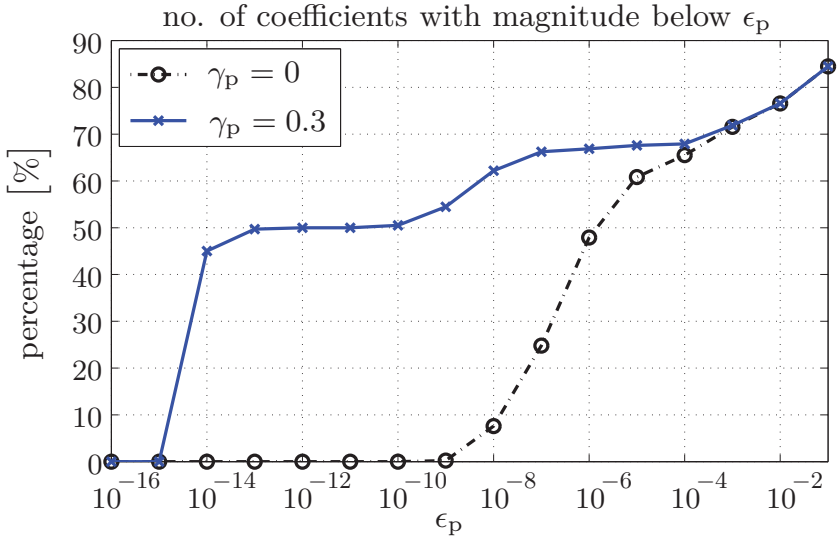

Figure 4.22: *Number of coefficients of vector $\widehat{\boldsymbol{p}}$ whose magnitudes are below the threshold ϵ_p. The vectors are determined by the design of Eq.* (4.90) *with $\epsilon_a = 0$ and two different penalty factors γ_p. The other design parameters are listed in Figure 4.21.*

which is above 10^{-11}. Accordingly, the subsequent zero-forcing has a much lower effect if an $\mathcal{L}_1$-norm regularization is applied before as only coefficients with a very small magnitude are set to zero in this case. Therefore, the sparse design fulfills the constraint for complete aliasing compensation much better than the design without $\mathcal{L}_1$-norm regularization ($\gamma_\mathrm{p} = 0$).

Finally, it should be mentioned that repeating the design of Example 4.3 with a subfilter length L_q reduced by 50% leads to a synthesis filter-bank with the same number of non-zero filter coefficients as for the sparse designs of Example 4.5, but a much higher signal reconstruction error so that this approach is not treated in more detail.

4.3.5 Unconstrained PR Design

A numerical LS error design which strives for an allpass transformed AS FB with *perfect reconstruction* is now derived based on [LV10]. The condition for perfect reconstruction with a delay of D_o sample instants can be expressed by the transfer function of Eq. (4.65) as follows

$$T_\nu(z) \stackrel{!}{=} z^{-D_\mathrm{o}} \;\forall\; \nu \in \{0, 1, \ldots, R-1\}\,. \tag{4.93}$$

This requirement can be stated by means of Eq. (4.67):

$$\underbrace{\begin{bmatrix} \boldsymbol{\xi}_0(z) \\ \boldsymbol{\xi}_1(z) \\ \vdots \\ \boldsymbol{\xi}_{R-1}(z) \end{bmatrix}}_{=\boldsymbol{\Xi}_R(z)} \cdot \boldsymbol{p} \stackrel{!}{=} z^{-D_\mathrm{o}}\,\mathbf{1}_R\,. \tag{4.94}$$

The $L_\mathrm{q}\,L$ coefficients of vector $\boldsymbol{p}$ are determined by the requirement that Eq. (4.94) shall be fulfilled for $\mathcal{N} = L_\mathrm{q}\,L$ discrete values on the unit circle according to Eq. (4.76). With the compact notation

$$\boldsymbol{A} = \begin{bmatrix} \boldsymbol{\Xi}_R(1) \\ \boldsymbol{\Xi}_R(W_\mathcal{N}) \\ \vdots \\ \boldsymbol{\Xi}_R\left(W_\mathcal{N}^{\mathcal{N}-1}\right) \end{bmatrix} \in \mathbb{C}^{\mathcal{N}R \times \mathcal{N}} \tag{4.95}$$

$$\boldsymbol{w} = \begin{bmatrix} \mathbf{1}_R \\ W_\mathcal{N}^{-D_\mathrm{o}}\,\mathbf{1}_R \\ \vdots \\ W_\mathcal{N}^{-(\mathcal{N}-1)D_\mathrm{o}}\,\mathbf{1}_R \end{bmatrix} \in \mathbb{C}^{\mathcal{N}R}, \tag{4.96}$$

Eq. (4.94) turns into an R-times over-determined set of $\mathcal{N}\,R$ linear equations

$$\boldsymbol{A} \cdot \boldsymbol{p} \stackrel{!}{=} \boldsymbol{w}\,. \tag{4.97}$$

An LS error solution is obtained by

$$\underset{\boldsymbol{p}}{\text{minimize}} \left\| \boldsymbol{A} \cdot \boldsymbol{p} - \boldsymbol{w} \right\|_2^2 . \tag{4.98}$$

If $\mathrm{rank}\,(\boldsymbol{A}) = \mathcal{N}$, the solution of Eq. (4.98) is given by[18]

$$\widehat{\boldsymbol{p}} = \left(\boldsymbol{A}^H\,\boldsymbol{A}\right)^{-1}\boldsymbol{A}^H\,\boldsymbol{w} \tag{4.99a}$$

$$= \boldsymbol{A}^\#\,\boldsymbol{w}\,. \tag{4.99b}$$

If the matrix $\boldsymbol{A}$ is rank deficient, i.e., $\mathrm{rank}\,(\boldsymbol{A}) < \mathcal{N}$, the matrix $\boldsymbol{A}^H\boldsymbol{A}$ becomes singular so that the pseudo-inverse $\boldsymbol{A}^\#$ of matrix $\boldsymbol{A}$ does not exist. In this case, there exist an LS error solution according to Eq. (4.98) as well which, however, is not unique any more.

Example 4.6: The warped analysis filter-bank of Figure 4.3 is considered whose frequency resolution is adjusted by an allpass transformation of second order as shown in Figure 4.4. The synthesis filter-bank of Figure 4.7 is determined by the unconstrained PR design of Eq. (4.98). The result is analyzed in Figure 4.23. The synthesis filters shown in Figure 4.23-a exhibit a distinctive bandpass characteristic and their magnitude responses exhibit a course similar to that of the analysis filters plotted in Figure 4.4 (which cannot be achieved by the closed-form PR designs discussed in Sec. 4.2.4). The evaluation of the peak aliasing distortions $\mathcal{D}_\mathrm{peak}(\Omega)$ according to Eq. (2.12) shows a negligible amount of aliasing distortions. The plots of magnitude response and phase error for the overall transfer function $T_0(e^{j\,\Omega})$ show insignificant magnitude and phase distortions. The BSF for this design is not plotted as it is like that of Figure 2.6-b.

[18] In practice, the LS error solution of Eq. (4.97) is calculated, e.g., by QR decomposition, but not a direct calculation of the pseudo-inverse to avoid numerical problems, cf., [Gv96].

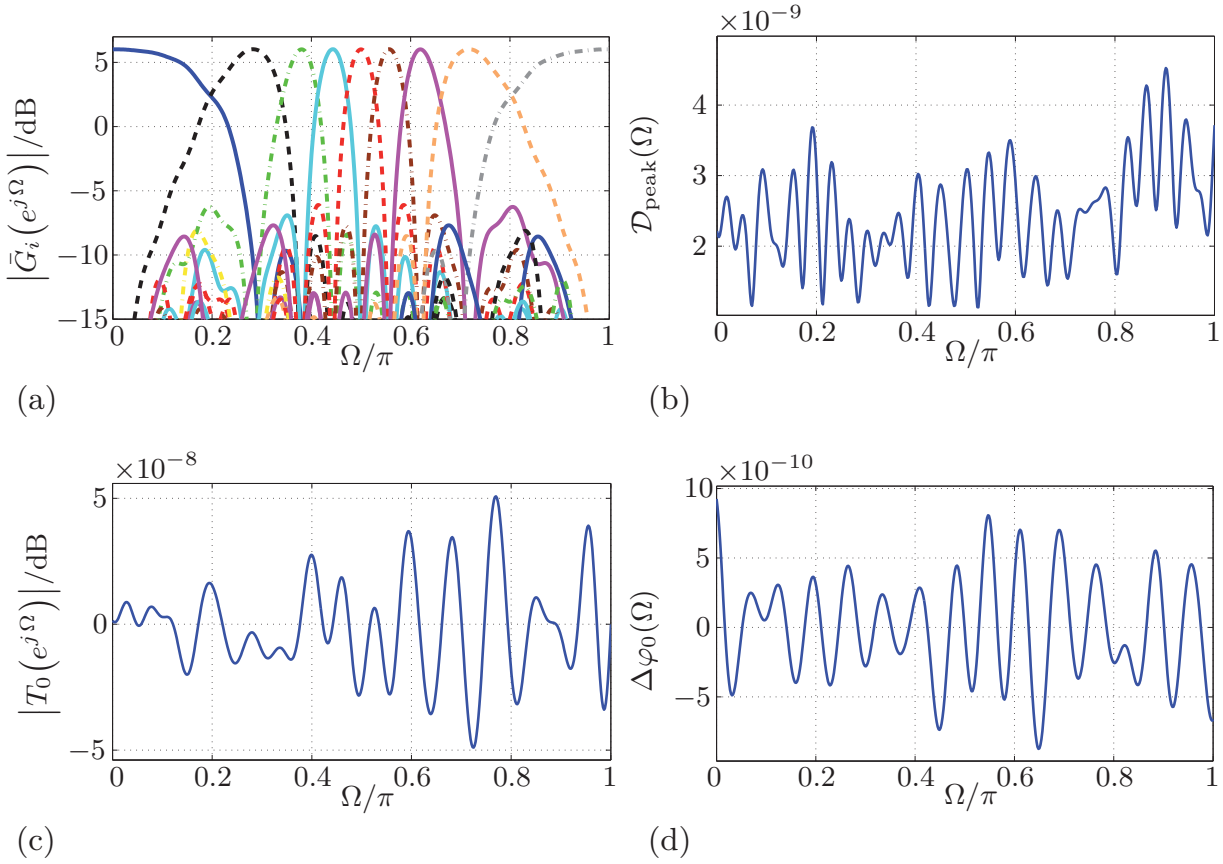

Figure 4.23: *Design of an allpass transformed DFT AS FB according to Figure 4.3 and Figure 4.7 with parameters $L = M = 16$, $R = M/4 = 4$, $a(0) = -j0.5$, $a(1) = j0.5$ by the unconstrained PR design of Eq. (4.98) with sub-filter length $L_q = 60$ and signal delay $D_o = 52$:*
(a) *magnitude responses of the synthesis filters*
(b) *peak aliasing distortions*
(c) *magnitude response of the overall transfer function*
(d) *phase error of the overall transfer function.*

It should be noted that the proposed *numerical PR design* strives towards perfect reconstruction, which can inherently only be achieved with a certain numerical accuracy. This accuracy depends on the chosen design parameters as well as the algorithm and software to solve the optimization problem.

4.3.6 Constrained PR Design

The numerical designs developed so far are based on the synthesis filter-bank of Figure 4.7. The original approach of designing the L synthesis sub-filters as phase equalizers is successively extended by incorporating additional design constraints for aliasing cancellation, sparseness etc. The demand for synthesis filters with a bandpass characteristic is incorporated implicitly so far, but not as an explicit design target. Therefore, an alternative design approach is now devised, which strives for perfect reconstruction as the previous one, but with the explicit design constraint for synthesis

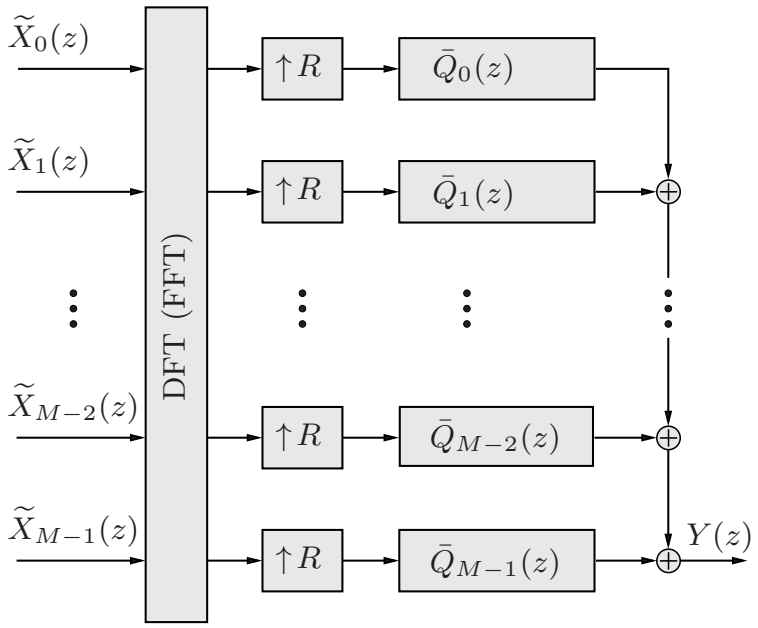

Figure 4.24: *FIR synthesis filter-bank for the constrained PR design. The corresponding analysis filter-bank is given by Figure 4.3.*

filters with a pronounced bandpass characteristic. The proposed synthesis filter-bank is shown in Figure 4.24. It is obtained form the filter-bank of Figure 4.7 for a synthesis prototype filter with

$$g(l) = 1 \quad \text{for} \quad l \in \{\, 0, 1, \ldots, L_\mathrm{s} \,\} \quad \text{and} \quad L_\mathrm{s} = M \tag{4.100}$$

where the considered allpass transformed DFT analysis filter-bank is still given by Figure 4.3. In contrast to the previous designs, there are not L but only M synthesis sub-filters with system functions

$$\bar{Q}_l(z) = \sum_{\eta=0}^{L_\mathrm{q}-1} q_l(\eta) \cdot z^{-\eta} \;\; \forall \;\; l \in \{\, 0, 1 \ldots, M-1 \,\} \,. \tag{4.101}$$

These FIR sub-filters can be implemented by means of an efficient polyphase network according to Figure 4.11 (which is not shown in Figure 4.24 for the sake of clarity).

Inserting Eq. (4.100) and Eq. (4.101) into Eq. (4.32) yields the following matrix representation for the system functions of the new synthesis filters

$$F_i(z) = \sum_{l=0}^{M-1} W_M^{-i\,(l+1)}\, \bar{Q}_{M-1-l}(z) \tag{4.102a}$$

$$= \sum_{l=0}^{M-1} W_M^{-i\,(l+1)} \sum_{\eta=0}^{L_\mathrm{q}-1} q_{M-1-l}(\eta) \cdot z^{-\eta}$$

$$= \overline{\boldsymbol{v}}_i^T \cdot \overline{\boldsymbol{D}}^T(z) \cdot \overline{\boldsymbol{p}} \quad \text{for} \quad i \in \{\, 0, 1, \ldots, M-1 \,\} \tag{4.102b}$$

with

$$\overline{\boldsymbol{v}}_i = \left[\, W_M^{-M\,i},\, W_M^{-(M-1)\,i},\, \ldots,\, W_M^{-2\,i},\, W_M^{-i} \,\right]^T \tag{4.102c}$$

$$\overline{\boldsymbol{D}}(z) = \boldsymbol{I}_M \otimes \boldsymbol{d}_{L_\mathrm{q}}(z) \tag{4.102d}$$

$$\boldsymbol{d}_{L_\mathrm{q}}(z) = \left[\, 1,\, z^{-1},\, \ldots,\, z^{-(L_\mathrm{q}-1)} \,\right]^T \tag{4.102e}$$

$$\overline{\boldsymbol{p}} = \left[\, \boldsymbol{q}_0^T,\, \boldsymbol{q}_1^T,\, \ldots,\, \boldsymbol{q}_{M-1}^T \,\right]^T \tag{4.102f}$$

$$\boldsymbol{q}_l = [\, q_l(0), q_l(1), \ldots, q_l(L_\mathrm{q}-1) \,]^T \quad \text{for} \quad l \in \{\, 0, 1, \ldots, M-1 \,\}\,. \tag{4.102g}$$

The overall transfer function of Eq. (4.67) is now given by

$$T_\nu(z) = \underbrace{\left(\frac{1}{R} \sum_{r=0}^{R-1} W_R^{-r\,\nu} \sum_{i=0}^{M-1} \widetilde{H}_i\left(z\, W_R^r\right) \cdot \overline{\boldsymbol{v}}_i^T \cdot \overline{\boldsymbol{D}}^T(z) \right)}_{= \overline{\boldsymbol{\xi}}_\nu(z)\ \in \mathbb{C}^{1\times\mathcal{M}}} \cdot \overline{\boldsymbol{p}} \tag{4.103a}$$

$$\nu \in \{\, 0, 1, \ldots, R-1 \,\} \quad \text{and} \quad \mathcal{M} = M\, L_\mathrm{q}\,. \tag{4.103b}$$

The design rule for a synthesis filter-bank to achieve perfect reconstruction is obtained directly from Eq. (4.97):

$$\bar{\boldsymbol{A}} \cdot \overline{\boldsymbol{p}} \stackrel{!}{=} \overline{\boldsymbol{w}}\,. \tag{4.104}$$

The composition of the matrices $\bar{\boldsymbol{A}} \in \mathbb{C}^{R\mathcal{M}\times\mathcal{M}}$ and $\overline{\boldsymbol{w}} \in \mathbb{C}^{R\mathcal{M}}$ follows from the derivation of Sec. 4.3.5 where the synthesis filters are now given by Eq. (4.102) such that

$$\bar{\boldsymbol{A}} = \begin{bmatrix} \overline{\boldsymbol{\Xi}}_R(1) \\ \overline{\boldsymbol{\Xi}}_R(W_\mathcal{M}) \\ \vdots \\ \overline{\boldsymbol{\Xi}}_R\left(W_\mathcal{M}^{\mathcal{M}-1}\right) \end{bmatrix} \quad \text{with} \quad \overline{\boldsymbol{\Xi}}_R(z) = \begin{bmatrix} \overline{\boldsymbol{\xi}}_0(z) \\ \overline{\boldsymbol{\xi}}_1(z) \\ \vdots \\ \overline{\boldsymbol{\xi}}_{R-1}(z) \end{bmatrix} \tag{4.105}$$

$$\bar{\boldsymbol{w}} = \begin{bmatrix} \boldsymbol{1}_R \\ W_\mathcal{M}^{-D_\circ}\, \boldsymbol{1}_R \\ \vdots \\ W_\mathcal{M}^{-(\mathcal{M}-1)D_\circ}\, \boldsymbol{1}_R \end{bmatrix}\,. \tag{4.106}$$

The demand for synthesis filters with optimized bandpass characteristic is now explicitly taken into account by the additional design constraint to minimize the stopband energy of the synthesis filters

$$E_\mathrm{S} = \sum_{i=0}^{M-1} \int\limits_{\Omega\in I_\mathrm{S}(i)} \left| F_i\left(e^{j\,\Omega}\right) \right|^2 \,\mathrm{d}\,\Omega\,. \tag{4.107}$$

The frequency intervals for the stopbands are given by

$$I_{\mathrm{S}}(i) = \begin{cases} \left[\Omega_{\mathrm{r}}^{(\mathrm{s})}(i),\, 2\,\pi - \Omega_{\mathrm{r}}^{(\mathrm{s})}(i)\right] & \text{for } i = 0 \\ \left[0,\, \Omega_{\mathrm{l}}^{(\mathrm{s})}(i)\right] \cup \left[\Omega_{\mathrm{r}}^{(\mathrm{s})}(i),\, 2\,\pi\right] & \text{for } i \in \{\,1, 2, \ldots, M-1\,\}\,. \end{cases} \tag{4.108}$$

The left and right band edges are determined as follows

$$\Omega_{\mathrm{l}}^{(\mathrm{s})}(i) = \varphi_{\Theta}^{[-1]}\left(\frac{2\,\pi}{M}\,i - \frac{\Omega_{\mathrm{s}}}{2}\right) \tag{4.109}$$

$$\Omega_{\mathrm{r}}^{(\mathrm{s})}(i) = \varphi_{\Theta}^{[-1]}\left(\frac{2\,\pi}{M}\,i + \frac{\Omega_{\mathrm{s}}}{2}\right) \tag{4.110}$$

with Ω_{s} denoting the normalized stopband frequency of the original (non-warped) prototype lowpass filter. The band edges are determined by the inverse function of the allpass phase response $\varphi_{\Theta}(\Omega)$ of Eq. (4.19b) in order to take the frequency warping of the subband filters into account. For the common case of an allpass transformation of first order, the inverse phase response reads, e.g., [Kap98]

$$\varphi_{a}^{[-1]}(\Omega) = \gamma + 2\,\arctan\left(\frac{1-\alpha}{1+\alpha}\,\tan\frac{\Omega-\gamma}{2}\right)\,. \tag{4.111}$$

It is obvious from Eq. (4.102b) that

$$\left|F_i\left(e^{j\,\Omega}\right)\right|^2 = \overline{\boldsymbol{p}}^{H} \cdot \underbrace{\overline{\boldsymbol{D}}^{*}\left(e^{j\,\Omega}\right) \cdot \overline{\boldsymbol{v}}_i^{*} \cdot \overline{\boldsymbol{v}}_i^{T} \cdot \overline{\boldsymbol{D}}^{T}\left(e^{j\,\Omega}\right)}_{= \boldsymbol{B}_i(\Omega) \,\in\, \mathbb{C}^{\mathcal{M}\times\mathcal{M}}} \cdot \overline{\boldsymbol{p}} \tag{4.112}$$

such that Eq. (4.107) can be expressed by the matrix formulation

$$E_{\mathrm{S}} = \overline{\boldsymbol{p}}^{H} \cdot \left(\sum_{i=0}^{M-1} \int\limits_{\Omega\in I_{\mathrm{S}}(i)} \boldsymbol{B}_i(\Omega)\;\mathrm{d}\,\Omega\right) \cdot \overline{\boldsymbol{p}} = \overline{\boldsymbol{p}}^{H}\,\boldsymbol{Q}_{\mathrm{S}}\,\overline{\boldsymbol{p}}\,. \tag{4.113}$$

The matrix $\boldsymbol{Q}_{\mathrm{S}}$ can be calculated by numerical integration for a finite set of frequency points. It follows from Eq. (4.112) and Eq. (4.113) that this matrix is real $\left(\boldsymbol{Q}_{\mathrm{S}} \in \mathbb{R}^{\mathcal{M}\times\mathcal{M}}\right)$ and positive definite.

An additional design target is to minimize the passband error of the synthesis filters

$$E_{\mathrm{P}} = \sum_{i=0}^{M-1} \int\limits_{\Omega\in I_{\mathrm{P}}(i)} \left|F_0(1) - F_i\left(e^{j\,\Omega}\right)\right|^2\;\mathrm{d}\,\Omega\,. \tag{4.114}$$

The frequency intervals of the passbands are given by

$$I_{\mathrm{P}}(i) = \begin{cases} \left[0,\, \Omega_{\mathrm{r}}^{(\mathrm{p})}(i)\right] \cup \left[2\,\pi - \Omega_{\mathrm{r}}^{(\mathrm{p})}(i),\, 2\,\pi\right] & \text{for } i = 0 \\ \left[\Omega_{\mathrm{l}}^{(\mathrm{p})}(i),\, \Omega_{\mathrm{r}}^{(\mathrm{p})}(i)\right] & \text{for } i \in \{\,1, 2, \ldots, M-1\,\}\,. \end{cases} \tag{4.115}$$

The left and right band edges are now given by

$$\Omega_{\mathrm{l}}^{(\mathrm{p})}(i) = \varphi_{\Theta}^{[-1]}\left(\frac{2\,\pi}{M}\,i - \frac{\Omega_{\mathrm{p}}}{2}\right) \tag{4.116}$$

$$\Omega_{\mathrm{r}}^{(\mathrm{p})}(i) = \varphi_{\Theta}^{[-1]}\left(\frac{2\,\pi}{M}\,i + \frac{\Omega_{\mathrm{p}}}{2}\right) \tag{4.117}$$

with Ω_{p} denoting the normalized passband frequency of the original prototype lowpass filter. The integrand of Eq. (4.114) can be expressed by means of Eq. (4.102) as follows

$$\begin{aligned}\left|F_0(1) - F_i\left(e^{j\,\Omega}\right)\right|^2 &= \left|\mathbf{1}_M^T \cdot \overline{\boldsymbol{D}}^T(1) \cdot \overline{\boldsymbol{p}} - \overline{\boldsymbol{v}}_i^T \cdot \overline{\boldsymbol{D}}^T\left(e^{j\,\Omega}\right) \cdot \overline{\boldsymbol{p}}\right|^2 \\ &= \left[\left(\mathbf{1}_{\mathcal{M}}^T - \overline{\boldsymbol{v}}_i^T \cdot \overline{\boldsymbol{D}}^T\left(e^{j\,\Omega}\right)\right)\overline{\boldsymbol{p}}\right]^H \left[\left(\mathbf{1}_{\mathcal{M}}^T - \overline{\boldsymbol{v}}_i^T \cdot \overline{\boldsymbol{D}}^T\left(e^{j\,\Omega}\right)\right)\overline{\boldsymbol{p}}\right] \\ &= \overline{\boldsymbol{p}}^H \underbrace{\left(\mathbf{1}_{\mathcal{M}}^T - \overline{\boldsymbol{v}}_i^T \cdot \overline{\boldsymbol{D}}^T\left(e^{j\,\Omega}\right)\right)^H \left(\mathbf{1}_{\mathcal{M}}^T - \overline{\boldsymbol{v}}_i^T \cdot \overline{\boldsymbol{D}}^T\left(e^{j\,\Omega}\right)\right)}_{= \boldsymbol{C}_i\left(e^{j\,\Omega}\right) \in \mathbb{C}^{\mathcal{M}\times\mathcal{M}}} \overline{\boldsymbol{p}}\,.\end{aligned} \tag{4.118}$$

Similar to Eq. (4.113), the passband error is formulated by the matrix representation

$$E_{\mathrm{P}} = \overline{\boldsymbol{p}}^H \cdot \left(\sum_{i=0}^{M-1} \int\limits_{\Omega\in I_{\mathrm{P}}(i)} \boldsymbol{C}_i(\Omega)\;\mathrm{d}\,\Omega\right) \cdot \overline{\boldsymbol{p}} = \overline{\boldsymbol{p}}^H\,\boldsymbol{Q}_{\mathrm{P}}\,\overline{\boldsymbol{p}}\,. \tag{4.119}$$

As the matrix $\boldsymbol{Q}_{\mathrm{S}}$, the matrix $\boldsymbol{Q}_{\mathrm{P}}$ is real and positive definite. It should be noted that the M contributions for the passband error of Eq. (4.119) as well as the stopband energy of Eq. (4.113) can be multiplied with individual weighting factors, cf., Eq. (D.1). Such a weighted LS error minimization can be useful, if the bandpass or stopband characteristic of individual synthesis filters is of different importance.

The aim to minimize stopband energy and passband error of Eq. (4.107) and Eq. (4.114) while fulfilling the PR constraint of Eq. (4.104) can now be expressed by an equality constrained quadratic minimization

$$\underset{\overline{\boldsymbol{p}}\,\in\,\mathbb{R}^{\mathcal{M}}}{\text{minimize}}\;\; \overline{\boldsymbol{p}}^H\,\boldsymbol{R}_\eta\,\overline{\boldsymbol{p}} \tag{4.120a}$$

$$\text{subject to}\;\; \bar{\boldsymbol{A}}\,\overline{\boldsymbol{p}} = \overline{\boldsymbol{w}} \tag{4.120b}$$

with

$$\boldsymbol{R}_\eta = \eta\,\boldsymbol{Q}_{\mathrm{S}} + (1-\eta)\,\boldsymbol{Q}_{\mathrm{P}} \quad \text{for} \quad 0 \le \eta \le 1\,. \tag{4.120c}$$

This convex optimization problem is a *linearly constrained quadratic program* (LCQP) according to Eq. (D.11) since the matrix $\boldsymbol{R}_\eta$ is the sum of positive definite matrices and thus positive definite. The real factor η adjusts the trade-off between a low passband

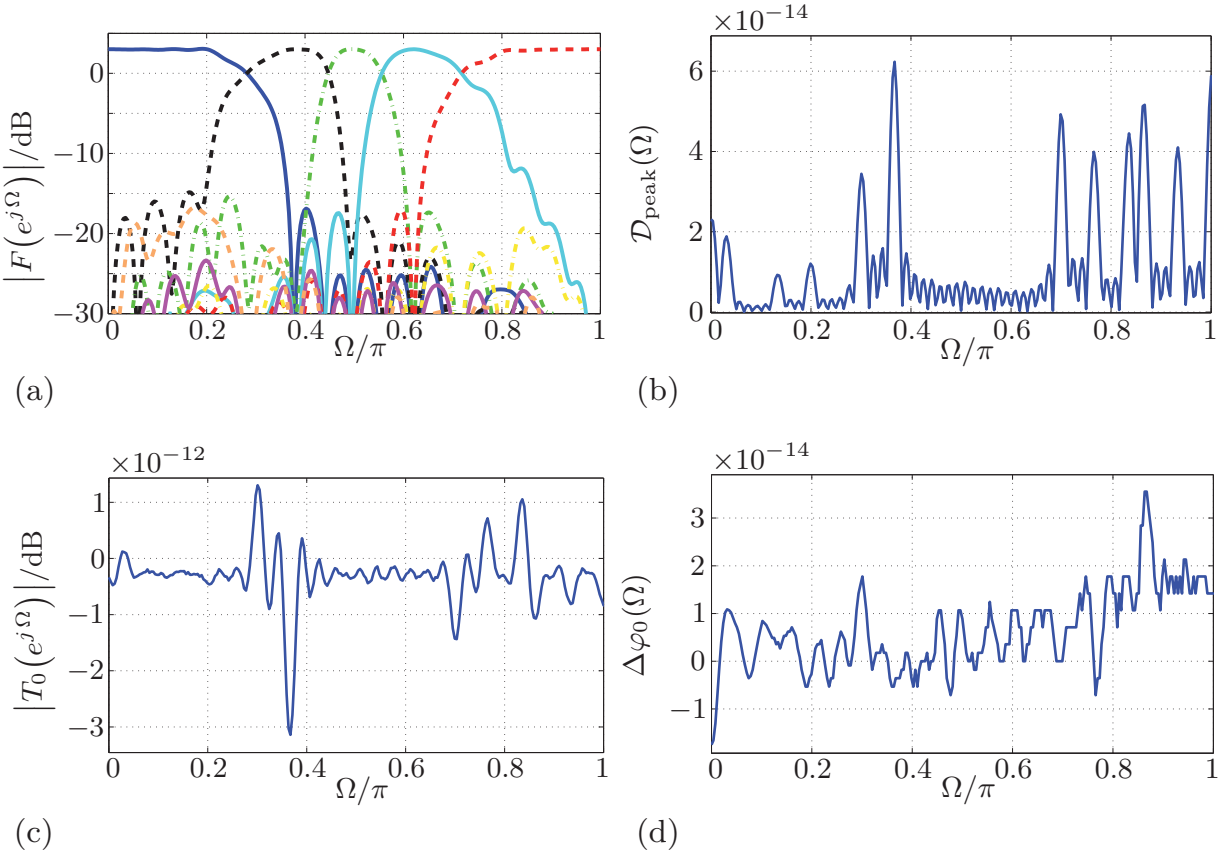

Figure 4.25: *Design of an allpass transformed DFT AS FB according to Figure 4.3 and Figure 4.24 with parameters* $L_a = 2\,M = 16$, $R = M/4 = 2$, $a(0) = -j0.5$, $a(1) = j0.5$ *by the LCQP of Eq.* (4.120) *with* $\eta = 0.85$, $\Omega_s = 1.1\,\frac{2\,\pi}{M}$, $\Omega_p = 0.9\,\frac{2\,\pi}{M}$, $L_q = 60$ *and signal delay* $D_o = 52$*:*
(a) *magnitude responses of the synthesis filters*
(b) *peak aliasing distortions*
(c) *magnitude response of the overall transfer function*
(d) *phase error of the overall transfer function.*

error and a low stopband energy. The mathematical program of Eq. (4.120) can be solved, e.g., by using either the function `quadprog` or `lsqlin` of the MATLAB optimization toolbox [TM09] where the later mentioned function is employed here. As for all the previous numerical filter-bank designs, the choice

$$D_\mathrm{o} = L_\mathrm{q} - 2\,R \tag{4.121}$$

for the signal delay turns out to be favorable.

Example 4.7: The warped analysis filter-bank of Example 4.3 is considered again. The synthesis filter-bank of Figure 4.24 is employed designed by the LCQP of Eq. (4.120) with a trade-off factor of $\eta = 0.85$. The stopband and passband edge are given by $\Omega_\mathrm{s} = 1.1\,\frac{2\,\pi}{M}$ and $\Omega_\mathrm{p} = 0.9\,\frac{2\,\pi}{M}$. The obtained DFT AS FB is analyzed in Figure 4.25. The curves for the peak aliasing distortions as well as magnitude response and phase error of the overall transfer function reveal that this filter-bank design achieves actually a perfect signal reconstruction. The magnitude responses of the synthesis filters in Figure 4.25-a

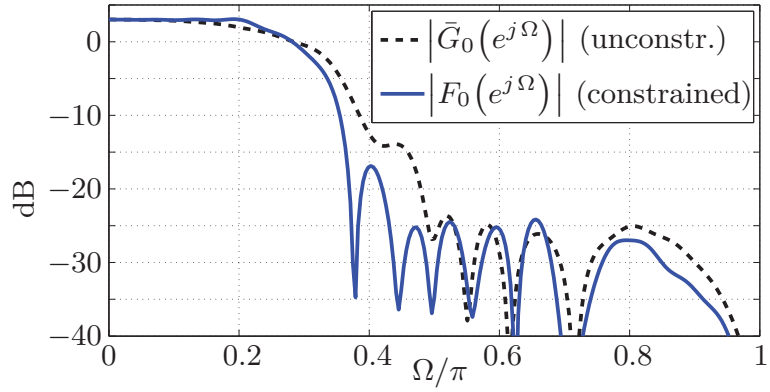

Figure 4.26: *Magnitude responses* $\left|\bar{G}_0\left(e^{j\,\Omega}\right)\right|$ *and* $\left|F_0\left(e^{j\,\Omega}\right)\right|$ *of the synthesis lowpass filters obtained by the unconstrained PR design of Eq.* (4.98) *and the constrained PR design of Eq.* (4.120)*. The design parameters for both filter-banks are listed in Figure 4.25.*

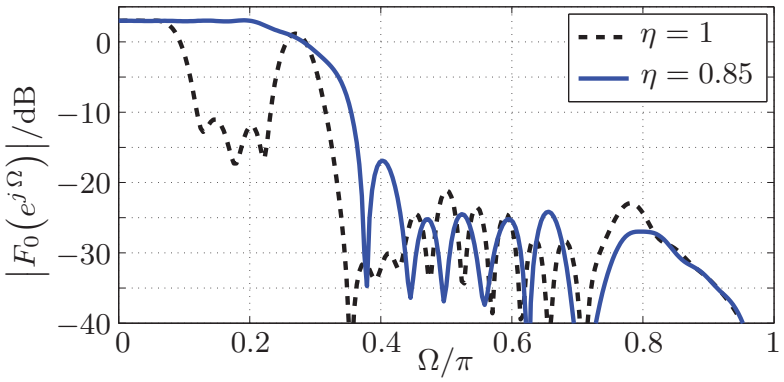

Figure 4.27: *Magnitude responses of the synthesis lowpass filters designed by the LCQP design of Eq.* (4.120) *with different trade-off factors* η*. The other design parameters are listed in Figure 4.25.*

exhibit a pronounced bandpass characteristic. The course of the magnitude responses is not identical to that of the analysis filters shown in Figure 4.17-a as the bandpass characteristic of the synthesis filters is now enforced by formulating this requirement as an explicit design target. In contrast, the previous designs achieve implicitly a bandpass characteristic where the magnitude responses of analysis and synthesis filters are similar (see, e.g., Figure 4.17-a and Figure 4.17-b).

Figure 4.26 exemplifies how the constrained PR design achieves an improved stopband attenuation for the synthesis filters in comparison to the unconstrained PR design of the previous section. (The results for the other synthesis filters are similar.)

The choice for the trade-off factor η plays a crucial role as demonstrated by the two magnitude responses plotted in Figure 4.27. The value of $\eta = 0.85$ chosen for this example results in a stopband energy of $E_{\mathrm{S}} = 1.13$ and a passband error of $E_{\mathrm{P}} = 6.7119$. Hence, this rather high value for η avoids that the passband error is predominantly minimized, which would result in a low stopband attenuation. However, taking a value of $\eta = 1$ yields an insufficient passband characteristic as illustrated by Figure 4.27.

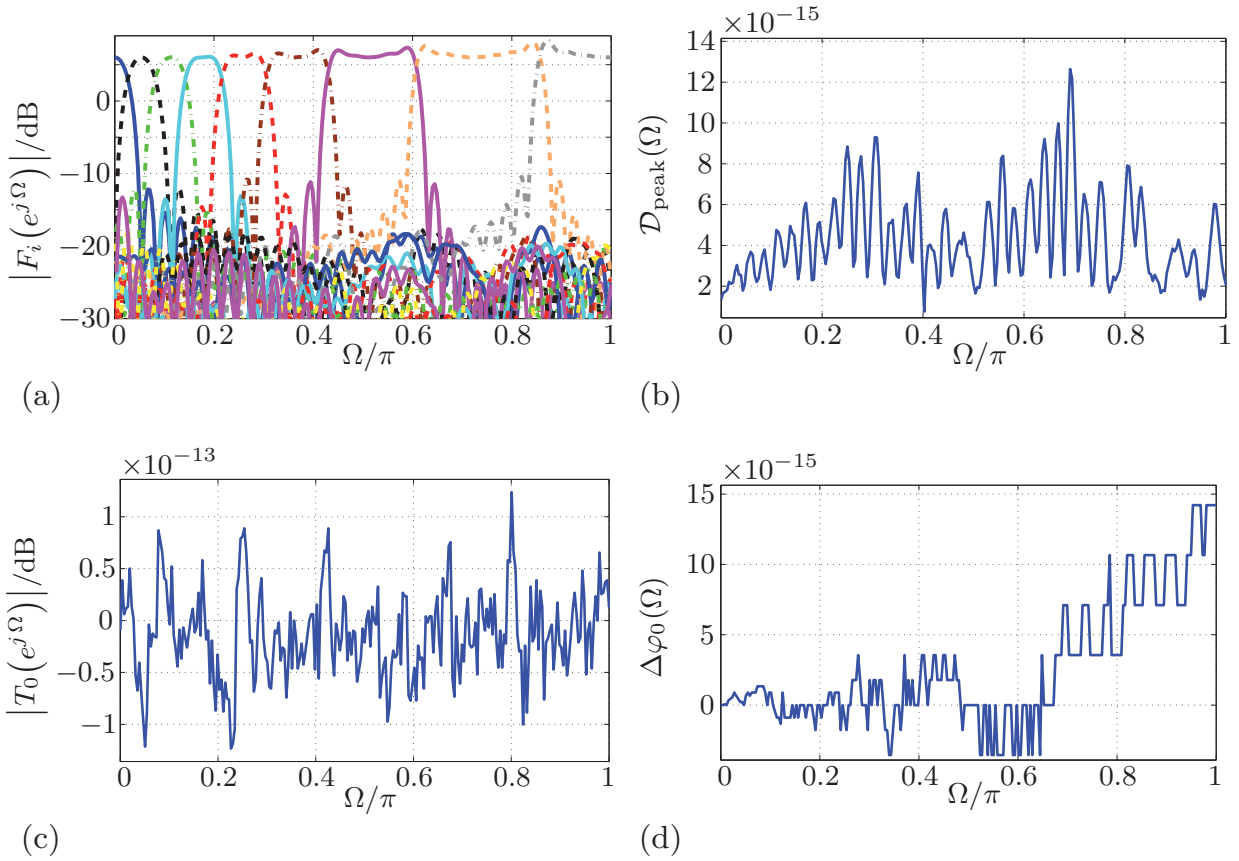

Figure 4.28: *Design of an allpass transformed DFT AS FB with analysis filter-bank given by Figure 4.6 and synthesis filter-bank given by Figure 4.24 with parameters* $L_a = 2\,M = 32$, $R = M/4 = 4$, $a = 0.4$ *by the LCQP of Eq.* (4.120) *with* $\eta = 1$, $\Omega_s = 1.1\,\frac{2\,\pi}{M}$, $L_q = 72$ *and signal delay* $D_o = 64$*:*
(a) *magnitude responses of the synthesis filters*
(b) *peak aliasing distortions*
(c) *magnitude response of the overall transfer function*
(d) *phase error of the overall transfer function.*

The design of a synthesis filter-bank to achieve (almost) perfect reconstruction with synthesis filters having a pronounced bandpass characteristic is especially difficult in case of an allpass transformation of higher order and analysis prototype filters of length $L_{\text{a}} > M$. Therefore, the analysis filter-bank of Example 4.3 is considered for the design examples in this and the previous sections to demonstrate the performance of the proposed designs. This challenging design problem has also motivated the approach of Eq. (4.120) with its joint minimization of stopband energy and passband error (see also Figure 4.27). If the more common allpass transformation of first order is used, it is also possible to obtain a good bandpass characteristic by minimizing the stopband energy only as demonstrated by the following example.

Example 4.8: A design example for an allpass transformation of first order is provided by Figure 4.28. The allpass transformed analysis filter-bank of Figure 4.6 is now considered where the magnitude responses of the analysis filters are plotted in Figure 4.13. The synthesis filter-bank of Figure 4.24 is designed by the LCQP design

of Eq. (4.120) with a trade-off factor of $\eta = 1$. Figure 4.28 demonstrates that synthesis filters with a good passband and pronounced bandpass characteristic are obtained in this case, even if the passband error is not minimized. The evaluation shows that a perfect signal reconstruction is actually achieved given the limited numerical accuracy to implement (and analyze) a filter-bank in practice. The signal distortions caused by the limited arithmetic precision of a practical implementation, e.g., on a (fixed-point) DSP, are usually much more dominant.

The constrained PR design presented in this section can be further extended by performing an $\mathcal{L}_1$-norm regularization to seek for a sparse design or by permitting a bounded LS error for the PR constraint to improve the bandpass characteristic. These design objectives can be incorporated in a similar manner as for the previous designs. However, it has to be taken into account that the LCQP of Eq. (4.120) strives towards the trivial solution (zero-vector), if the PR constraint of Eq. (4.120b) ceases to apply. In contrast, solving Eq. (4.83) without the constraint of Eq. (4.83b) states a phase equalizer design and yields a feasible solution, but not a zero-vector.

Finally, it should be noted that the devised designs cannot only be applied to the considered allpass transformed DFT filter-banks, but also to filter-banks with other transformation kernels such as the DCT.

4.4 Conclusions

The allpass transformation is a simple and flexible method to convert a uniform filter-bank into a non-uniform one. This transformation causes a frequency warping where a frequency interval of 2π is mapped bijectively onto a frequency interval of 2π on the warped frequency scale. Such a unique mapping is essential for a filter-bank design to avoid an undesirable comb-filter effect and more difficult to achieve by non-recursive frequency warping techniques such as [OMM76, CR76, AR79]. Another alternative to the allpass transformation is to replace the DFT transformation kernel of a filter-bank by that of a WDFT [MM01]. However, this yields a shift of the center frequencies where the bandwidths of the subband filters remain the same, which causes 'spectral gaps'. Such spectral gaps are avoided by allpass transformed filter-banks, which possess a non-uniform time *and* frequency resolution in contrast to a WDFT filter-bank.

Different concepts to design the synthesis filter-bank for an allpass transformed analysis filter-bank are elaborated in this chapter. They have individual pros and cons such that they do not exclude but complement each other.

One option is to design the synthesis filter-bank by means of analytical *closed-form* expressions. The linear phase distortions due to the allpass transformed analysis filter-bank can be made arbitrarily small by a *phase equalization* at the synthesis side. A closed-form FIR phase equalizer design for this purpose is presented in [GK02, Gal02], which yields an allpass-transformed AS FB with near-perfect reconstruction. A drawback of this design is that it results in a filter-bank with a high signal delay. Therefore, an alternative synthesis filter-bank with LS FIR phase equalizers is proposed, which can achieve a similar reconstruction error as the approach of [Gal02], but with a significantly lower signal delay and lower complexity. It is proven that the magnitude responses of the synthesis filters become equal to those of the analysis filters in case of

a perfect phase equalization. Hence, a good phase equalization ensures inherently synthesis filters with a pronounced bandpass characteristic. In addition, it is shown that all the proposed FIR synthesis filter-banks can be efficiently implemented by means of a polyphase network (PPN).

The closed-form designs by means of phase equalization have different benefits in common: The coefficients of the synthesis filter-bank are determined by simple analytical expressions whose evaluation poses no numerical difficulties even for a high number of subbands. In addition, the trade-off between reconstruction error and signal delay can be controlled in a simple and flexible manner. A drawback of these closed-form designs for the synthesis filter-bank is that the incorporation of further design objectives as, for example, a complete aliasing cancellation is very difficult. This problem is tackled by a new *numerical* design framework. It is based on a novel matrix representation for allpass transformed AS FBs from which different designs are deduced.

A generalization of the closed-form synthesis filter-bank design with LS FIR phase equalizers is devised. The filter coefficients are also determined by the requirement for minimized phase distortions, but with the additional constraint for complete aliasing cancellation. The evaluation of this design reveals that this constraint can be fulfilled with a very high numerical accuracy such that a perfect aliasing cancellation can be actually achieved. A distinctive advantage of this numerical design method is that additional design constraints can be easily incorporated. One generalization is to allow a limited (least-squares) error for the aliasing distortions in exchange for a lower amount of linear distortions. Another extension is to aim for a *sparse* solution. This approach strives for a low number of non-zero coefficients in order to reduce the computational complexity of the synthesis filter-bank. However, the constraint for a sparse design leads to a non-convex optimization problem, which is cumbersome to solve. This problem is circumvented by means of an $\mathcal{L}_1$-norm regularization. In contrast to a simple zero-forcing of the smallest filter coefficients, the devised sparse design can fulfill the additional constraint for complete aliasing cancellation with a much higher accuracy. Besides, the trade-off between sparseness and reconstruction error can be simply controlled by a single penalty factor.

An unconstrained LS error design which strives for *perfect reconstruction* is introduced. This design has several advantages in comparison to the closed-form PR designs of [Kap98, SM02a, FK03]: Firstly, the synthesis filter-bank is inherently causal and stable, even in case of an allpass transformation of higher order. Secondly, the numerical design provides also a solution for a PPN filter-bank where the prototype filter degree exceeds the number of subbands. Finally, the new design provides synthesis filters with a bandpass characteristic in contrast to the closed-form PR designs.

An advantage of the new unconstrained PR design is its simplicity as the filter coefficients are merely determined by a set of linear equations. However, this design does not incorporate explicitly the demand for synthesis filters with a high frequency selectivity. Therefore, an alternative, constrained PR design is developed. Passband error and stopband energy of the synthesis filters are minimized with the requirement for perfect signal reconstruction. It turns out that the PR constraint can be fulfilled with a very high numerical accuracy. Hence, a perfect signal reconstruction can be achieved effectively with synthesis filters having a pronounced bandpass characteristic.

A common property of all the proposed numerical designs is that they are stated as a *semi-definite program* (SDP) or special cases thereof. Such convex optimization problems provide a global optimum and can be solved rather efficiently, e.g., [BV04].

The proposed designs differ substantially from the numerical designs presented in [dHGCN02, VN03, WdDC03]. These designs aim for a reduction of the signal reconstruction error by a prototype filter design for an allpass transformed AS FB according to Figure 4.6 (without phase equalization). In contrast, the proposed designs consider the synthesis filter-bank of Figure 4.7 and Figure 4.24, respectively. As a result, the devised numerical designs can achieve a significantly lower signal reconstruction error than approaches based on a prototype filter design at the expense of a moderately increased computational complexity and signal delay. Thus, these two different numerical design approaches for allpass transformed filter-banks do not preclude but supplement each other.

The devised numerical design approaches for allpass-transformed filter-banks pave the way for further extensions and applications: One possibility is to strive for a robust design which considers a possible quantization of its filter coefficients, cf., [BV04, BTN98, GL97]. The incorporation of this design constraint leads here to a tractable problem as the proposed designs are all based on a convex optimization [ALM10].

Another interesting aspect for further investigations is to account explicitly for the effects of (time-varying) spectral gain factors within the design process as done, e.g., in [AGK09] for uniform filter-banks.

Chapter 5

The Filter-Bank Equalizer

The signal delay is an important property of a filter-bank and plays a crucial role for various applications. One example are filter-banks used for subband coding or noise reduction in cell phones where a low signal delay is needed for a pleasant communication. Another prominent example are filter-banks employed for signal enhancement in digital hearing aids. A low overall processing delay is required to avoid a disturbing comb filter effect, cf., [AT00, SM02b].[1] To prevent this, the algorithmic signal delay of the employed filter-bank must be considerably lower than the tolerable overall processing delay, which lies within a range of 5–15 ms.

The difficulty in the design of low delay filter-banks is to balance the trade-off between the conflicting goals of a high spectral resolution on the one hand, and a low signal delay on the other hand. Various approaches have been proposed to tackle this problem.

A low delay analysis-synthesis system for noise reduction is proposed, for example, in [MM07]. The analysis window can be changed during operation without violating the PR constraint. The length of the analysis window is thereby adapted to the 'span of stationarity' of the (noisy) speech signal. This approach has a low complexity, but is only applicable to the uniform DFT filter-bank where the length of the analysis window equals the number of subbands.

The design of filter-banks with low signal delay becomes even more demanding with regard to *non-uniform* filter-banks, cf., [HV89, AV99]. A common approach to design such a filter-bank is to employ a tree-structured filter-bank which, however, results in a high signal delay (as explained in App. C.2.2). One approach to reduce the delay of such a filter-bank is to impose a delay constraint for the design of the underlying two-channel filter-bank, e.g., [NBS94].

Another approach is to exploit the *lifting scheme*. This idea is originally proposed for the construction of 'second generation wavelets' [Swe96, DS98] and enables the design of wavelet as well as QMF-banks with a low delay (as exemplified in Figure 3.5). The application of the lifting scheme to design (uniform) cosine modulated AS FBs with low delay is proposed in [KM97, KMS01]. In [GK02, Gal02], the lifting scheme is applied to *allpass transformed* AS FBs. The higher aliasing distortions due to the frequency warping are reduced by improving the stopband attenuation of the subband filters.

[1] A comb filter effect can occur if the user of a hearing aid is talking such that the processed speech signal can interfere with the original speech signal, which reaches the cochlea with minimal delay via bone conduction or through the hearing aid vent. This is especially problematic for hearing aids with a so-called open-fitting.

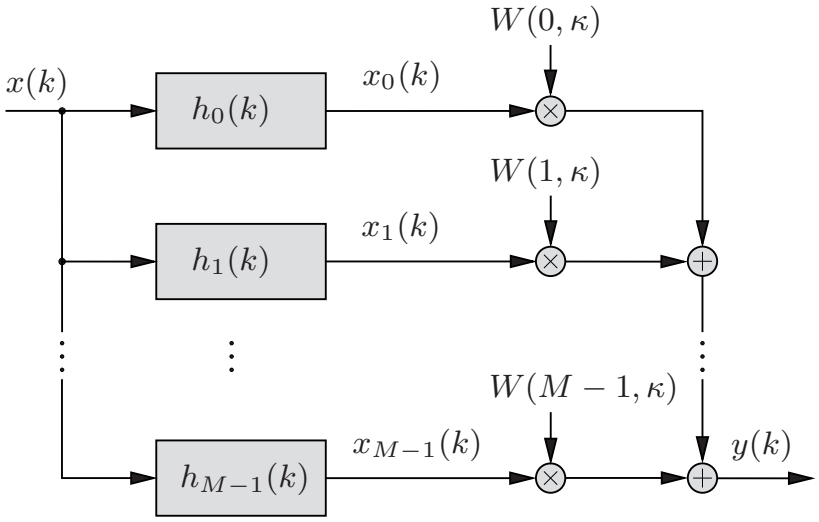

Figure 5.1: *Filter-bank summation method (FBSM) with time-varying spectral gain factors adapted at decimated sample instants κ.*

The lifting scheme is used to increase the prototype filter degree while constraining the signal delay of the filter-bank. However, the adding of further (zero-delay) lifting steps shows no improvement after some stages. Therefore, only a limited enhancement of the stopband attenuation and the associated aliasing cancellation can be achieved with constrained delay.

There are other ways to derive a non-uniform low delay filter-bank from a uniform filter-bank. One approach, for example, is to combine an appropriate number of cosine modulated subband filters termed as 'feasible partitioning' [LNT97, DMFB07]. Another method is to use two different uniform filter-banks for the upper and lower frequency bands which are linked by a 'transition filter', e.g., [CJ03, DBSN06]. In contrast to warped filter-banks, a good approximation of the Bark scale is more difficult to achieve by this approach. The subband filters of these filter-banks need to have a relatively high filter degree to achieve a sufficient stopband attenuation in order to avoid noticeable aliasing distortions.

Many designs for uniform and non-uniform AS FBs allow to impose a constraint on the signal delay, e.g., [NBS94, KM98, SK00, DBSN06, DMFB07]. However, it is inherently problematic to achieve simultaneously a high stopband attenuation for the subband filters as well as a low signal delay. As a consequence, there is always a trade-off between a low signal delay on the one hand and low aliasing distortions on the other hand, cf., [NBS94, DMFB07]. This motivates to consider a *non-subsampled* AS FB for low delay processing as the aliasing compensation by means of a synthesis filter-bank ceases to apply.

If a (uniform) DFT AS FB performs no subsampling ($R = 1$), the signal reconstruction can be simply performed by summing up the subband signals $x_i(k)$ such that no dedicated synthesis filters are needed, i.e., $G_i(z) \equiv 1$. This special case of an AS FB is referred to as *filter-bank summation method* (FBSM) and depicted in Figure 5.1.

The FBSM can also be derived from the filter-bank interpretation of the short-time DFT, e.g., [CR83]. Obviously, the FBSM ensures an alias-free signal reconstruction and

has a much lower signal delay than a corresponding AS FB with subsampling. However, a severe drawback is its very high computational complexity as no subsampling is performed. Therefore, the AS FB is considered to be more suitable than the FBSM for practical applications such as speech enhancement in [Eng98, Chap. 4].[2] Moreover, the computational complexity of the FBSM is significantly increased, if an allpass transformation is applied to achieve a non-uniform frequency resolution. A straightforward approach to reduce the computational complexity is to implement the FBSM by a PPN according to Sec. 2.3. However, this does not solve the problem satisfactorily as all operations (including the FFT) have still to be executed at each sample instant.

In the following, the FBSM is considered to derive a uniform and non-uniform low delay filter-bank with a much lower algorithmic complexity. The devised system is denoted as *filter-bank equalizer* (FBE) and originally presented in [LV05a, Var06]. This concept is further improved and generalized in [LV07b, LV08a], which form the basis for the following treatment.

5.1 The Uniform Filter-Bank Equalizer

The FBSM of Figure 5.1 is considered. The real input signal $x(k)$ is split into subband signals $x_i(k)$ by means of M subband filters. In contrast to the AS FB of Figure 2.1, these subband signals are not downsampled. Therefore, such a filter-bank is more suitable for adaptive subband filtering than for subband coding where critically subsampled AS FBs are preferred. The adaptation of the time-varying spectral gain factors $W(i,\kappa)$ can be done by the same algorithms as for the AS FB, e.g., to perform speech enhancement. This adaptation is usually based on the subband signals $x_i(k)$ and executed at intervals of R sample instants. The discrete time index κ is given by[3]

$$\kappa = \lfloor k/R \rfloor \cdot R; \quad R \in \mathbb{N}\,. \tag{5.1}$$

The impulse response $h_i(k)$ of the i-th analysis filter is obtained by modulation of a prototype lowpass filter with impulse response $h(k)$ of length L according to

$$h_i(k) = \begin{cases} h(k) \cdot \Phi(i,k) & \text{for } i \in \{\,0,1,\ldots,M-1\,\};\quad k \in \{\,0,1,\ldots,L-1\,\} \\ 0 & \text{otherwise}\,. \end{cases} \tag{5.2}$$

For the following treatment, it is beneficial to consider a broader class of modulated filter-banks besides the DFT filter-bank. The general modulation sequence or *transformation kernel* of the filter-bank is denoted by $\Phi(i,k)$ and exhibits the periodicity

$$\Phi(i, k + m\,M) = \Phi(i,k) \cdot \varrho(m); \quad m \in \mathbb{Z}\,. \tag{5.3}$$

The sequence $\varrho(m)$ depends on the chosen transform as shown later in Sec. 5.1.1. For many transforms including the DFT, it is given by $\varrho(m) = 1\,\forall\, m \in \mathbb{Z}$.

[2] For the sake of clarity and simplicity, the term AS FB refers henceforth exclusively to a filter-bank with subsampling excluding the special case of the FBSM.

[3] This definition is more suitable for the following treatment than the (more common) convention $k' = k\,R$ according to Eq. (2.2).

The input-output relation for the FBSM of Figure 5.1 can now be written as follows

$$y(k) = \sum_{i=0}^{M-1} W(i,\kappa) \cdot x_i(k) \tag{5.4}$$

$$= \sum_{i=0}^{M-1} W(i,\kappa) \sum_{l=0}^{L-1} x(k-l) \cdot h_i(l)$$

$$= \sum_{l=0}^{L-1} x(k-l) \cdot h(l) \sum_{i=0}^{M-1} W(i,\kappa) \cdot \Phi(i,l) \tag{5.5}$$

for the modulated bandpass filters of Eq. (5.2). The second summation is the spectral transform of the time-varying gain factors $W(i,\kappa)$, which yields the coefficients

$$w(l,\kappa) = \sum_{i=0}^{M-1} W(i,\kappa) \cdot \Phi(i,l); \quad l \in \{\,0,1,\ldots,L-1\,\} \tag{5.6}$$

$$= \mathcal{S}_{\mathrm{T}}\{\,W(i,\kappa)\,\}\,. \tag{5.7}$$

These L *time-domain weighting factors* have the periodicity

$$w(l + m\,M,\kappa) = w(l,\kappa) \cdot \varrho(m) \tag{5.8}$$

due to Eq. (5.3) and Eq. (5.6). The input-output relation finally reads

$$y(k) = \sum_{l=0}^{L-1} x(k-l) \cdot h(l) \cdot w(l,\kappa) \tag{5.9}$$

$$= \sum_{l=0}^{L-1} x(k-l) \cdot h_{\mathrm{s}}(l,\kappa)\,. \tag{5.10}$$

The obtained filter-bank structure is a *single* time-domain filter whose coefficients

$$h_{\mathrm{s}}(l,\kappa) = h(l) \cdot w(l,\kappa); \quad l \in \{\,0,1,\ldots,L-1\,\} \tag{5.11}$$

are the product of the finite impulse response of the prototype lowpass filter $h(l)$ and the time-varying weighting factors $w(l,\kappa)$ adapted in the short-term spectral-domain.[4] The derived efficient implementation of the FBSM (which resembles a filter-bank used as equalizer) is termed as *filter-bank equalizer* (FBE) [Var06, LV05a]. A sketch of this filter-bank structure is given in Figure 5.2. This scheme has a significantly lower algorithmic complexity than the equivalent FBSM of Figure 5.1 as mainly only a single time-domain filter has to be operated at a non-decimated sampling rate. Moreover, a non-uniform (warped) frequency resolution can be achieved by means of the allpass transformation

[4] For the sake of clarity, the index l instead of the discrete time index k is used to indicate that L filter coefficients are considered.

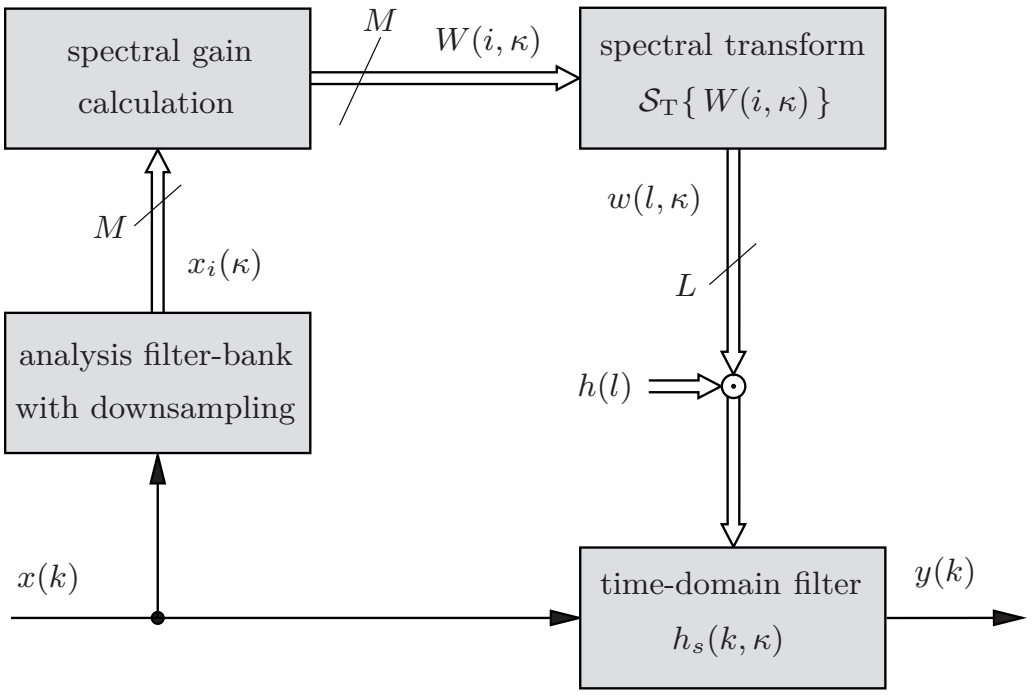

Figure 5.2: *Filter-bank equalizer (FBE) for adaptive subband filtering.*

with lower efforts as for an AS FB (with subsampling) as shown later in Sec. 5.2. A similar approach to that of the warped FBE has been proposed independently in [KA05] for dynamic-range compression in hearing aids. The concept of expressing a spectral weighting as time-domain filtering is of course not novel, e.g., [CR83]. For acoustic echo cancellation and active noise control applications, it can be beneficial to perform the filtering in the time-domain while the coefficients are adapted in the (uniform) frequency-domain, e.g., [MT95]. However, the following treatment will show that the concept of the FBE is a much more comprehensive and versatile approach to perform adaptive filtering by means of a uniform *and* non-uniform low delay filter-bank.

5.1.1 Prototype Filter Design

The objective of the prototype lowpass filter design is to achieve perfect reconstruction according to Eq. (2.13a). The FBE meets this condition if the following two requirements are fulfilled [LV05a]: Firstly, the general modulation sequence of Eq. (5.2) must have the property

$$\sum_{i=0}^{M-1} \Phi(i,k) = \begin{cases} \varrho(m) \cdot C \neq 0 & \text{for } k = k_0 + m\,M \\ 0 & \text{for } k \neq k_0 + m\,M \end{cases} \quad \text{with} \quad k, k_0, m \in \mathbb{Z}\,. \tag{5.12}$$

Secondly, a generalized *M th band filter* with impulse response

$$h(k) = \begin{cases} \dfrac{1}{\varrho(m_c) \cdot C} & \text{for } k = k_0 + m_c\,M\,; \quad m_c, k_0 \in \mathbb{Z} \\ 0 & \text{for } k = k_0 + m\,M\,; \quad m \in \mathbb{Z}\backslash\{m_c\} \\ \text{arbitrary} & \text{for } k \neq k_0 + m\,M\,; \quad m \in \mathbb{Z} \end{cases} \tag{5.13}$$

is needed as prototype lowpass filter. Such a filter has equidistant zeros at intervals of M samples and a summation of its modulated versions leads to (cf., [Vai93])

$$\sum_{i=0}^{M-1} H\left(z\, W_M^i\right) \cdot W_M^{i k_0} = \frac{M}{C\, \varrho(m_c)}\, z^{-(k_0 + m_c\, M)}\,. \tag{5.14}$$

The requirements of Eq. (5.12) and Eq. (5.13) can be easily met to achieve perfect reconstruction according to Eq. (2.13) with a scaling of $c_\mathrm{s} = 1$ and a delay of

$$D_\mathrm{o} = k_0 + m_c\, M \tag{5.15}$$

sample instants. A suitable Mth band filter according to Eq. (5.13) is given by

$$h(k) = \frac{1}{C\, \varrho(m_c)}\, \frac{\sin\left(\frac{\pi}{M}\,(k - D_\mathrm{o})\right)}{\frac{\pi}{M}\,(k - D_\mathrm{o})}\, \mathrm{win}_L(k) \tag{5.16}$$

with the general window sequence defined by

$$\mathrm{win}_L(k) = \begin{cases} \text{arbitrary} & \text{for } 0 \le k \le L-1 \\ 0 & \text{otherwise}\,. \end{cases} \tag{5.17}$$

A rectangular window achieves an LS error approximation, but other window sequences are often preferred to influence properties of the filter such as transition bandwidth or sidelobe attenuation, e.g., [OSB99]. Commonly used window sequences are the Kaiser window or the parametric window sequence

$$\mathrm{win}_{L,\upsilon}(k) = \begin{cases} \upsilon + (\upsilon - 1)\, \cos\left(\frac{2\,\pi}{L-1}\, k\right) & \text{for } 0 \le k \le L-1;\ \ 0.5 \le \upsilon \le 1 \\ 0 & \text{otherwise}\,. \end{cases} \tag{5.18}$$

The rectangular window ($\upsilon = 1$), the Hann window ($\upsilon = 0.5$) and the Hamming window ($\upsilon = 0.54$) are included as special cases [PM96].

The condition of Eq. (5.12) is met by various transformations such as the Walsh and Hadamard transform (cf., [Bea75]) as well as the *generalized discrete Fourier transform* (GDFT). The Walsh and Hadamard transform are employed, among others, for image processing, cf., [GW77]. The GDFT FBE is of interest for speech and audio processing, which is treated in Sec. 6.2. Thus, the GDFT is considered primarily in the following without loss of generality. The transformation kernel of the GDFT reads

$$\begin{aligned} &\Phi_\mathrm{GDFT}(i,k) = \exp\left\{-j\,\frac{2\,\pi}{M}\,(i + i_0)\,(k - k_0)\right\} \\ &k,\, k_0 \in \mathbb{Z};\ \ i \in \{\,0, 1, \ldots, M-1\,\};\ \ i_0 \in \{\,0,\, 1/2\,\} \end{aligned} \tag{5.19}$$

such that Eq. (5.3) applies with $\varrho(m) = (-1)^{2\,i_0\,m}$. The DFT is included as special case for $k_0 = i_0 = 0$. For $i_0 = 1/2$, a GDFT filter-bank with *oddly-stacked* frequency bands is obtained, cf., [CR83]. A value of $i_0 = 0$ leads to the *evenly-stacked* GDFT where the

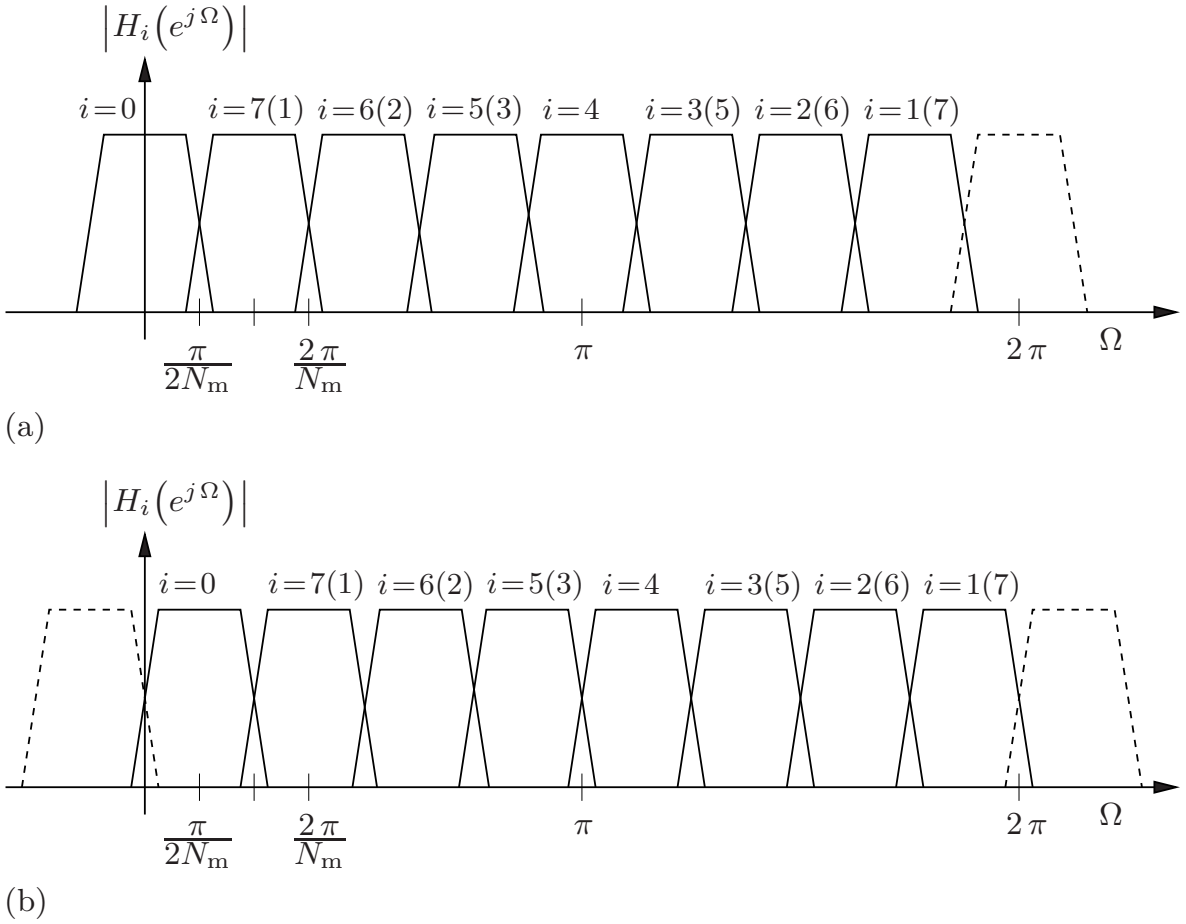

Figure 5.3: *Schematic sketch of the analysis filters for the GDFT FBE with an even number of $M = 2\,N_m = 8$ subbands:*
(a) *evenly-stacked GDFT* ($i_0 = 0$)
(b) *oddly-stacked GDFT* ($i_0 = 1/2$).
The subband numbers in case of an IGDFT are enclosed in brackets.

above equations apply with $\varrho(m) \equiv 1$ and $C = M$. The analysis filters of these two GDFT filter-banks are sketched in Figure 5.3. It can be seen that the analysis filters of the oddly-stacked filter-bank expose a frequency shift of π/M. The use of the inverse generalized discrete Fourier transform (IGDFT) instead of the GDFT yields merely a different mapping as indicated by the subband numbers enclosed in brackets. In the following, the evenly-stacked GDFT is considered as transformation kernel and it is assumed that Eq. (5.13) applies with $m_c = 0$ if not mentioned otherwise.

5.1.2 Relation between GDFT FBE and GDCT FBE

For applications such as speech enhancement, the time-varying spectral gain factors $W(i,\kappa)$ are often calculated by means of a spectral speech estimator, e.g., [EM84, MCA99, LV05d]. For a DFT-based adaptation, the gain factors have the property

$$\epsilon \leq W(i,\kappa) \leq 1 \quad \text{for} \quad W(i,\kappa) \in \mathbb{R} \quad \text{and} \quad 0 \leq \epsilon < 1 \tag{5.20}$$

and possess the symmetry

$$W(i,\kappa) = W(M-i,\kappa);\;\; i \in \{\,0,1,\ldots,M-1\,\};\;\; M \text{ even} \tag{5.21}$$

as the input sequence $x(k)$ is real (see also Figure 5.3-a). The limitation of the gain factors by a lower, possibly time-varying threshold ϵ is favorable to avoid unnatural sounding artifacts such as musical noise, cf., [VM06, Chap. 11]. The (I)DFT of the real gain factors of Eq. (5.20) yields time-domain weighting factors $w(l,\kappa)$ corresponding to a (non-causal) zero-phase filter. A causal filter with linear phase response is obtained for the considered evenly-stacked GDFT of Eq. (5.19) if $k_0 = (L-1)/2 \in \mathbb{N}$ so that the coefficients exhibit the symmetry

$$w(l,\kappa) = w(L-1-l,\kappa) \;\forall\; l \in \{\,0,1,\ldots,L-1\,\}\,. \tag{5.22}$$

If the used prototype filter has the same symmetry

$$h(l) = h(L-1-l)\,, \tag{5.23}$$

the time-varying FIR filter of Eq. (5.11) exhibits the property

$$h_{\mathrm{s}}(l,\kappa) = h_{\mathrm{s}}(L-1-l,\kappa) \;\forall\; l \in \{\,0,1,\ldots,L-1\,\} \tag{5.24}$$

which implies a *linear phase response*. The GDFT of the gain factors $W(i,\kappa)$ can be computed by the FFT with a subsequent cyclic shift of the obtained time-domain weighting factors by k_0 samples. For noise reduction, a DFT analysis filter-bank instead of a GDFT analysis filter-bank can be used for the FBE of Figure 5.2, because the magnitude of the complex subband signals is usually only needed for the spectral gain calculation in this case.

For the evenly-stacked GDFT, the weighting factors of Eq. (5.6) are given by

$$w(l,\kappa) = \sum_{i=0}^{M-1} W(i,\kappa)\cdot e^{-j\,\frac{2\pi}{M}\,i\,(l-k_0)};\;\; l \in \{\,0,1,\ldots,L-1\,\}\,. \tag{5.25}$$

The substitution $M = 2\,N_m$ and exploiting the symmetry of Eq. (5.21) allows the following conversion

$$\begin{aligned} w(l,\kappa) &= \sum_{i=0}^{2N_m-1} W(i,\kappa)\cdot e^{-j\,\frac{2\pi}{2N_m}\,i\,(l-k_0)} \\ &= W(0,\kappa) + \sum_{i=1}^{N_m-1} W(i,\kappa)\cdot e^{-j\,\frac{\pi}{N_m}\,i\,(l-k_0)} + W(N_m,\kappa)\cdot(-1)^{l-k_0} \\ &\qquad + \sum_{i=1}^{N_m-1} W(2N_m-i,\kappa)\cdot e^{-j\,\frac{\pi}{N_m}\,(2N_m-i)\,(l-k_0)} \\ &= \sum_{i=0}^{N_m} W(i,\kappa)\cdot\phi(i)\cdot\cos\left(\frac{\pi}{N_m}\,i\,(l-k_0)\right) \end{aligned} \tag{5.26a}$$

with

$$\phi(i) = \begin{cases} 1 & \text{for } i \in \{0, N_m\} \\ 2 & \text{for } i \in \{1, 2, \ldots, N_m - 1\}\,. \end{cases} \tag{5.26b}$$

Eq. (5.26) represents an FBE with $N_m + 1$ channels and the evenly-stacked *generalized discrete cosine transform* (GDCT) as modulation sequence

$$\Phi^{(I)}_{\mathrm{GDCT}}(i,k) = \phi(i) \cdot \cos\!\left(\frac{\pi}{N_m}\, i\,(k - k_0)\right);\quad i \in \{\,0, 1, \ldots, N_m\,\};\quad k, k_0 \in \mathbb{Z}\,. \tag{5.27}$$

For this transformation kernel, the condition of Eq. (5.12) is fulfilled with $M = N_m + 1$ and $C = 2\,N_m$. Except for a normalization factor, the so-called DCT-I is obtained from Eq. (5.27) for $k_0 = 0$, cf., [RY90]. For the oddly-stacked GDFT FBE ($i_0 = 1/2$), a similar derivation leads to the oddly-stacked GDCT as shown in App. B.4.

The relation between GDCT FBE and GDFT FBE is derived so far without considering the specific process of the spectral gain calculation. For noise reduction, the spectral gain factors are usually calculated as (linear or non-linear) functions of the squared magnitude of the subband signals (spectral coefficients), cf., [BMC05]. This can be expressed by the notation

$$W(i,\kappa) = f\!\left(\,\overline{|x_i(\kappa)|^2}\,\right);\quad i \in \{\,0, 1, \ldots, N_m\,\}\,. \tag{5.28}$$

Only $N_m + 1$ gain factors need to be calculated due to the symmetry of Eq. (5.21). The bar indicates that an averaged value (short-term expectation) is mostly taken inherently. Examples are the calculation of the *a priori* signal-to-noise ratio (SNR) by the decision-directed approach [EM84] or the estimation of the noise power spectral density (PSD) by recursively smoothed periodograms [Mar01]. For the (G)DFT, the subband signals are complex such that

$$W(i,\kappa) = f\!\left(\,\overline{\Re\{x_i(\kappa)\}^2} + \overline{\Im\{x_i(\kappa)\}^2}\,\right)\,. \tag{5.29}$$

It can be assumed that the real and imaginary part are uncorrelated and that both have equal variances and equal probability density functions, e.g., [Lot04, BMC05]. Therefore, almost the same gain factors are obtained by considering the real part of the subband signals only

$$W(i,\kappa) \approx f\!\left(\,2\,\overline{\Re\{x_i(\kappa)\}^2}\,\right) \tag{5.30}$$

if a sufficient averaging is performed. In this case, the gain factors calculated by complex DFT values are very similar to those computed by real DCT values and the replacement of the GDFT of Eq. (5.19) by the GDCT of Eq. (5.27) causes no noticeable differences for the speech enhanced by the FBE.[5]

[5] In [Eng98], a different comparison between DFT AS FB and DCT-II AS FB reveals a slightly lower noise suppression for the DCT filter-bank.

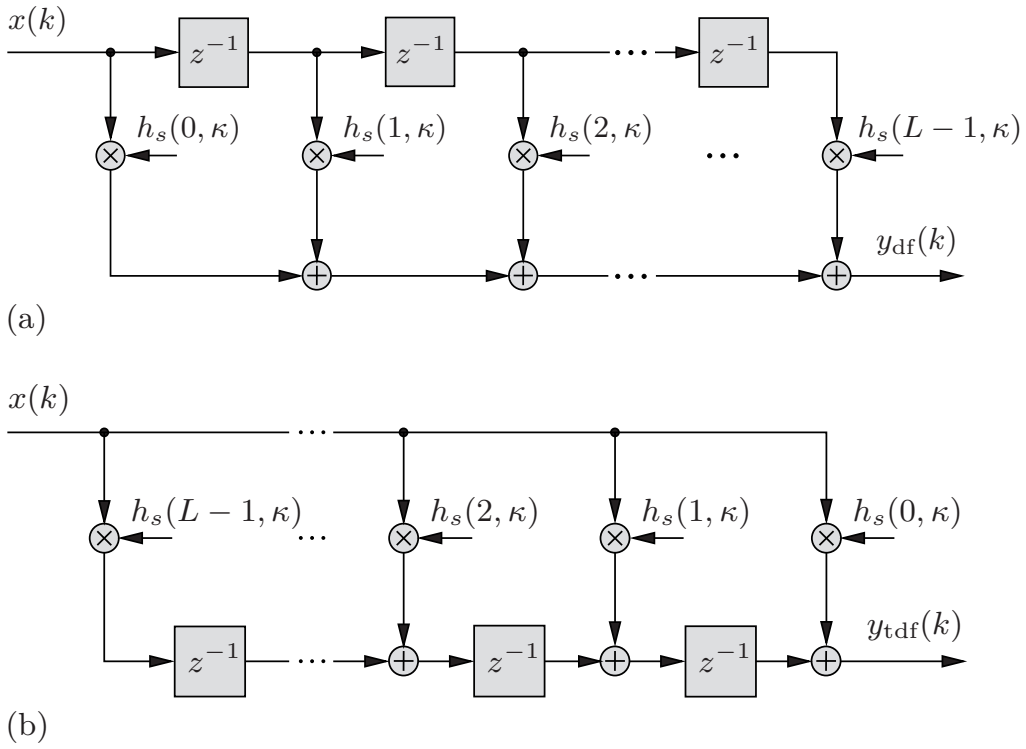

Figure 5.4: *Implementations of a time-varying FIR filter with filter length L:*
(a) *direct form*
(b) *transposed direct form.*

5.1.3 Realization for Different Filter Structures

The choice of the filter structure plays an important role for digital filter implementations with finite precision arithmetic as well as for *time-varying* filters. Here, only the direct forms of a filter are considered as they do not require an involved conversion of the time-varying filter coefficients $h_\mathrm{s}(l, \kappa)$ such as the parallel form or the cascade form, cf., [OSB99].

The realization of an FIR filter by means of the direct form and transposed direct form is shown in Figure 5.4. The input-output relations for these two filter forms can be stated as follows

$$y_\mathrm{df}(k) = \sum_{l=0}^{L-1} x(k-l) \cdot h_\mathrm{s}(l, \kappa) \tag{5.31}$$

$$y_\mathrm{tdf}(k) = \sum_{l=0}^{L-1} x(k-l) \cdot h_\mathrm{s}(l, \kappa - l)\,. \tag{5.32}$$

Obviously, the derived FBE according to Eq. (5.10) uses a time-domain filter in the *direct form* as given by Eq. (5.31).

The input-output relation for the transposed direct form is obtained by inserting

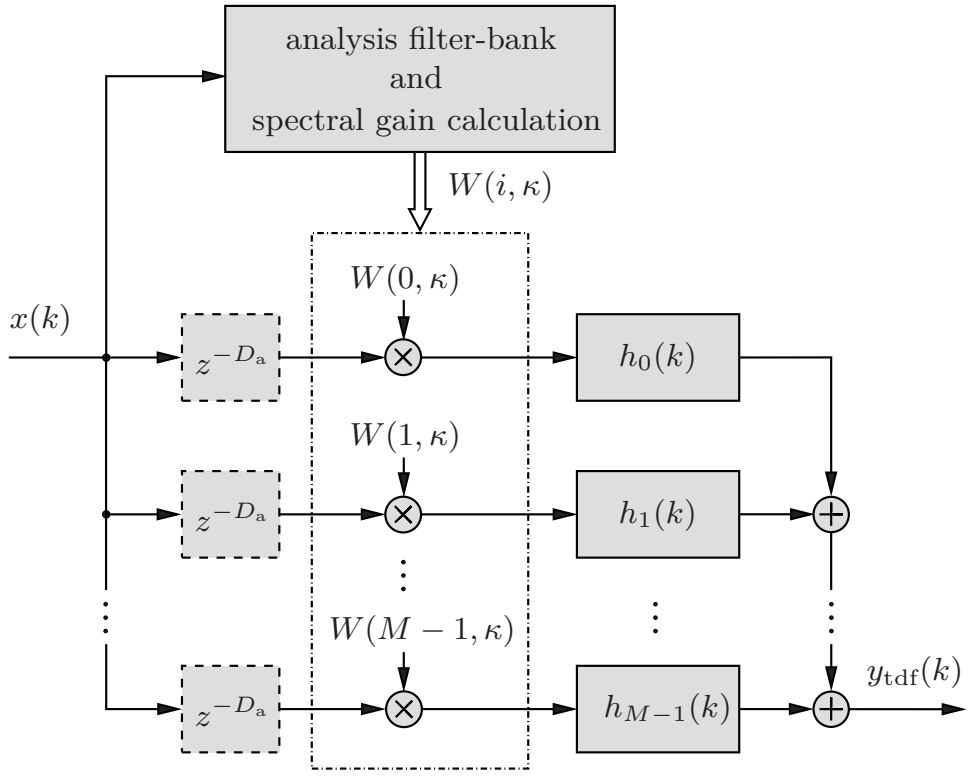

Figure 5.5: *Filter-bank summation method (FBSM) corresponding to the filter-bank equalizer (FBE) with time-domain filter in transposed direct form.*

Eq. (5.11) into Eq. (5.32) so that

$$\begin{aligned} y_{\mathrm{tdf}}(k) &= \sum_{l=0}^{L-1} x(k-l)\cdot h(l)\cdot w(l,\kappa-l) \\ &= \sum_{l=0}^{L-1} x(k-l)\cdot h(l) \sum_{i=0}^{M-1} W(i,\kappa-l)\cdot \Phi(i,l) \\ &= \sum_{i=0}^{M-1}\sum_{l=0}^{L-1} x(k-l)\cdot W(i,\kappa-l)\cdot h_i(l) \end{aligned} \tag{5.33}$$

due to Eq. (5.6) and Eq. (5.2). The derived relation for the *transposed direct form* corresponds to the FBSM shown in Figure 5.5. An important difference to the FBSM of Figure 5.1 is that the spectral gain factors are now applied *before* the subband filters. Therefore, additional delay elements are now needed to account for the signal delay D_a of analysis filter-bank and gain calculation. These delay elements might be omitted for moderately time-varying (smoothed) gain factors to avoid an additional signal delay.

Switching the coefficients of a digital filter during operation leads to transients, which can cause 'filter-ringing' effects.[6] These effects might be perceived by perceptually annoying artifacts. The application to noise reduction revealed that the FBE

[6]The term 'filter-ringing' is sometimes used with a slightly different meaning in the context of speech coding.

with time-domain filter in transposed direct form reduces these artifacts. This can be explained by comparing the equivalent FBSMs of Figure 5.1 and Figure 5.5: For the transposed direct form, the transients caused by the switching gain factors are smoothed by the following subband filters, which is not the case for the direct form implementation.

An alternative method to smooth the FIR filter coefficients independently of the filter form is to perform a kind of 'cross-fading' according to

$$\bar{h}_{\mathrm{s}}(l,k) = \big(1 - c_f(k)\big) \cdot h_{\mathrm{s}}(l, \kappa - R) + c_f(k) \cdot h_{\mathrm{s}}(l,\kappa) \tag{5.34a}$$

$$c_f(k) = \frac{k-\kappa}{R} \tag{5.34b}$$

with $l \in \{\,0, 1, \ldots, L-1\,\}$ and κ defined by Eq. (5.1). An existing linear-phase property is maintained. The proposed cross-fading method is very effective to avoid audible filter-ringing artifacts and especially useful if the filter in direct form is used.

5.1.4 Polyphase Network Implementation

An efficient polyphase network (PPN) implementation of the FBE is now developed, which eases the utilization of prototype filters with a long or even infinite impulse response. This can be exploited, e.g., to improve the spectral selectivity of the subband filters and to reduce the so-called cross-talk between adjacent frequency bands.

The FBE is a *time-varying* system. It can be described by the z-transform of the frozen-time impulse response, which yields the so-called *frozen-time system function* [LA84]. The direct form time-domain filter of Eq. (5.11) at sample instant κ has the frozen-time system function

$$H_{\mathrm{s}}(z,\kappa) = \sum_{l=0}^{L-1} w(l,\kappa) \cdot h(l) \cdot z^{-l}\,. \tag{5.35}$$

This system function[7] can be expressed by means of the type 1 polyphase components of Eq. (2.35b) as follows

$$\begin{aligned} H_{\mathrm{s}}(z,\kappa) &= \sum_{\lambda=0}^{M-1} w(\lambda,\kappa) \sum_{m=0}^{l_M-1} h(\lambda + m\,M) \cdot z^{-(\lambda+mM)} \cdot \varrho(m) \\ &= \sum_{\lambda=0}^{M-1} w(\lambda,\kappa) \cdot H_{0,\lambda}^{(M)}\big(z^M\big) \cdot z^{-\lambda} \quad \text{if} \quad \varrho(m) \equiv 1 \end{aligned} \tag{5.36}$$

with l_M defined by Eq. (2.36). The subband signals $x_i(k)$ of Eq. (5.4) read

$$x_i(k) = \sum_{l=0}^{L-1} x(k-l) \cdot h(l) \cdot \Phi(i,l); \quad i \in \{\,0, 1, \ldots, M-1\,\}\,. \tag{5.37}$$

[7] For the sake of brevity, the term *system function* refers either to the frozen-time system function or the conventional system function dependent on the context.

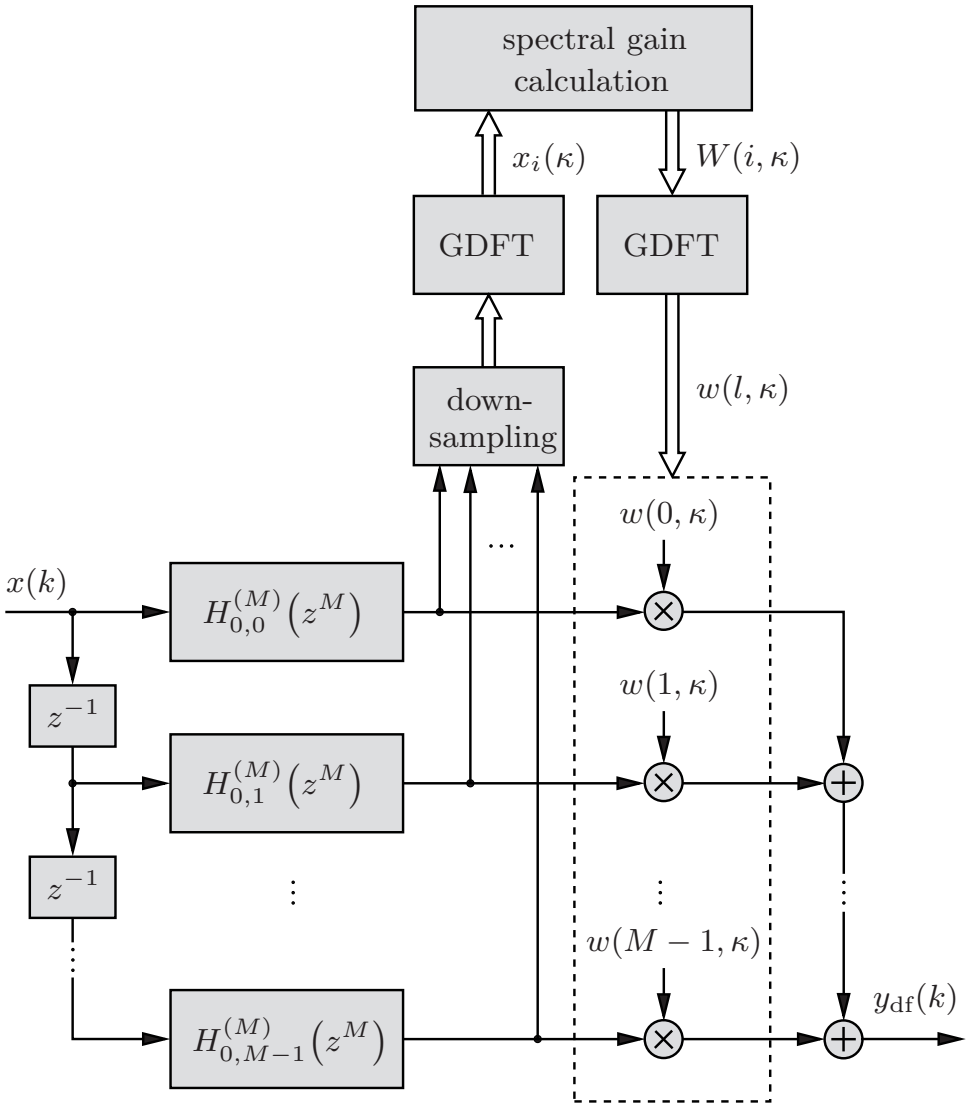

Figure 5.6: *Polyphase network (PPN) implementation of the GDFT FBE in direct form.*

The z-transform leads to

$$X_i(z) = X(z) \sum_{l=0}^{L-1} h(l) \cdot z^{-l} \cdot \Phi(i,l)\,. \tag{5.38}$$

Applying Eq. (2.35b) and Eq. (5.3) with $\varrho(m) \equiv 1$ results in

$$\begin{aligned} X_i(z) &= X(z) \sum_{\lambda=0}^{M-1} \sum_{m=0}^{l_M-1} h(\lambda + m\,M) \cdot z^{-(\lambda+m\,M)} \cdot \Phi(i,\lambda) \\ &= X(z) \sum_{\lambda=0}^{M-1} z^{-\lambda} \cdot H_{0,\lambda}^{(M)}\left(z^M\right) \cdot \Phi(i,\lambda)\,. \end{aligned} \tag{5.39}$$

The derived PPN implementation of the FBE in *direct form* according to Eq. (5.36) and Eq. (5.39) is illustrated in Figure 5.6. In contrast to the FBE realization of Figure 5.2,

time-domain filtering and calculation of the subband signals is partly done by the same network. The PPN realization for the oddly-stacked GDFT FBE can be derived in a similar manner, cf., [LV05a]. The same applies for an implementation with type 2 polyphase components.

The transposed direct form of a filter is derived from the direct form representation by transposition of its signal flow graph [OSB99]: Branch nodes and summations are interchanged as well as system input and output. All signal directions are reversed. The obtained PPN implementation of the FBE for the *transposed direct form* is shown in Figure 5.7. Delay elements z^{-D_a} might be inserted in each branch of the time-domain filter to account for the execution time to calculate the time-domain weighting factors. These weighting factors are calculated by a separate network similar to that of Figure 5.6, but with the difference that the downsampling is performed directly after the delay elements. A comparison of Figure 5.6 and Figure 5.7 shows that the PPN realization for the transposed direct form requires a slightly higher algorithmic complexity than the direct form realization, which is discussed in Sec. 5.3 in more detail.

As mentioned before, a PPN decomposition can be performed for FIR filters [BBC76] as well as for IIR filters [Var79]. One option to design an IIR Mth band filter is to employ allpass polyphase filters as described in Sec. 3.2.1. Hence, the developed PPN realization of the FBE enables also a realization of Eq. (5.9) for L being infinite, i.e., a *recursive* prototype filter.

5.2 The Allpass Transformed Filter-Bank Equalizer

The application of an allpass transformation of first order to the subband filters of Eq. (5.2) yields the warped frequency responses

$$H_i\left(e^{j\,\varphi_a(\Omega)}\right) = \sum_{l=0}^{L-1} h(l)\cdot\Phi(i,l)\cdot e^{-j\,l\,\varphi_a(\Omega)} \tag{5.40}$$

$$= \widetilde{H}_i\left(e^{j\,\Omega}\right);\quad i\in\{\,0,1,\ldots,M-1\,\}\,. \tag{5.41}$$

The effect of this frequency warping on the frequency characteristic of the subband filters is discussed in Sec. 4.1.1. Figure 5.8 provides a block diagram of the obtained allpass transformed FBE. This warped FBE can be implemented efficiently by the PPN structures derived in Sec. 5.1.4 with all delay elements being substituted by allpass filters.

The uniform FBE with perfect reconstruction fulfills Eq. (2.13a) with $c_\mathrm{s}=1$, which can be expressed in the frequency-domain by the relation

$$\widehat{X}\left(e^{j\,\Omega}\right) = X\left(e^{j\,\Omega}\right)\cdot e^{-j\,D_\mathrm{o}\,\Omega}\,. \tag{5.42}$$

For the allpass transformed FBE, this relation turns into

$$\widehat{\widetilde{X}}\left(e^{j\,\Omega}\right) = X\left(e^{j\,\Omega}\right)\cdot e^{-j\,D_\mathrm{o}\,\varphi_a(\Omega)}\,. \tag{5.43}$$

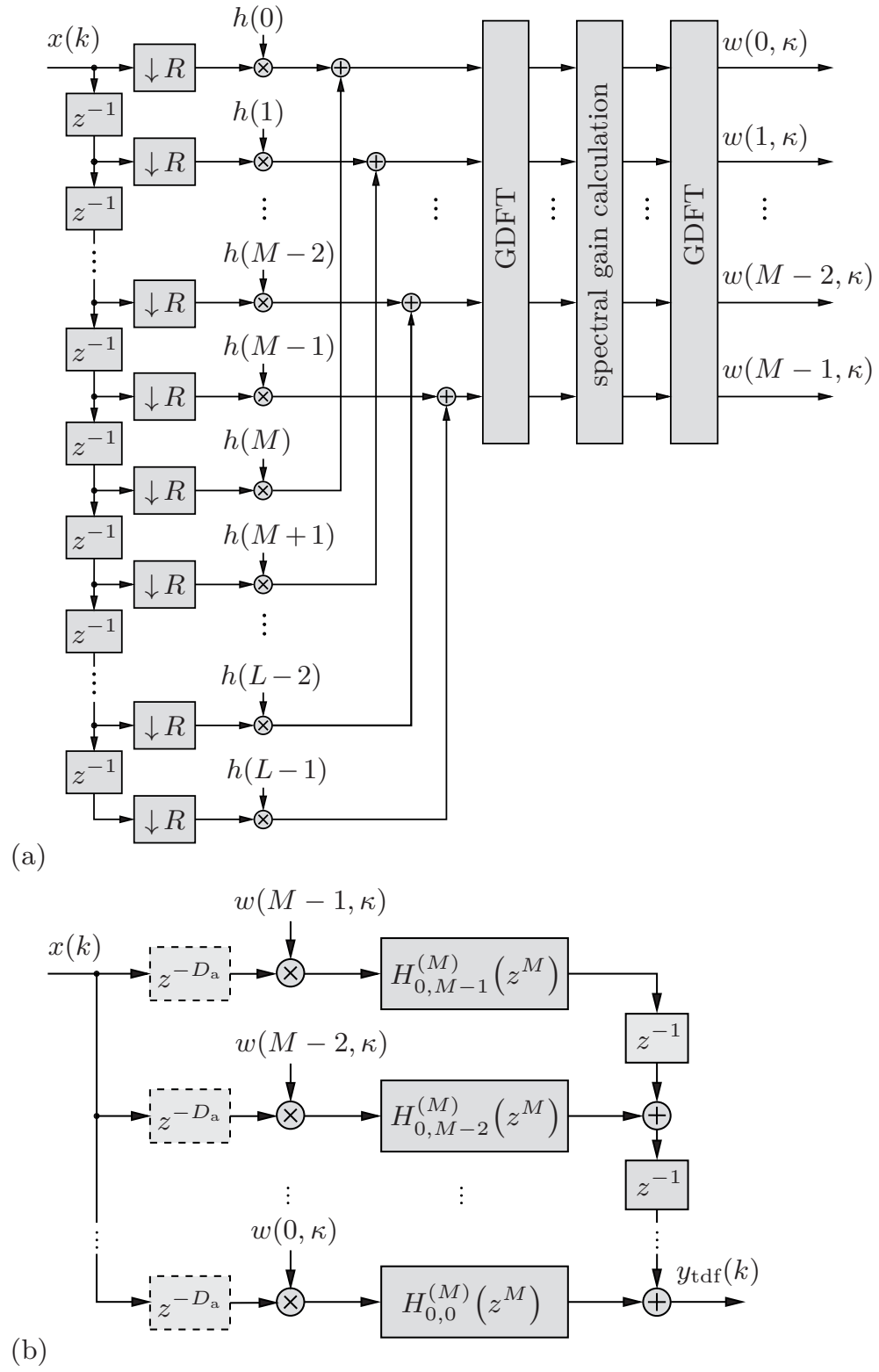

Figure 5.7: *PPN implementation of the GDFT FBE in transposed direct form:*
(a) *calculation of time-domain weighting factors*
(b) *time-domain filter.*

Hence, the linear phase distortions due to the allpass transformation can be made arbitrarily small by a phase equalizer of sufficient degree. This equalizer must be designed

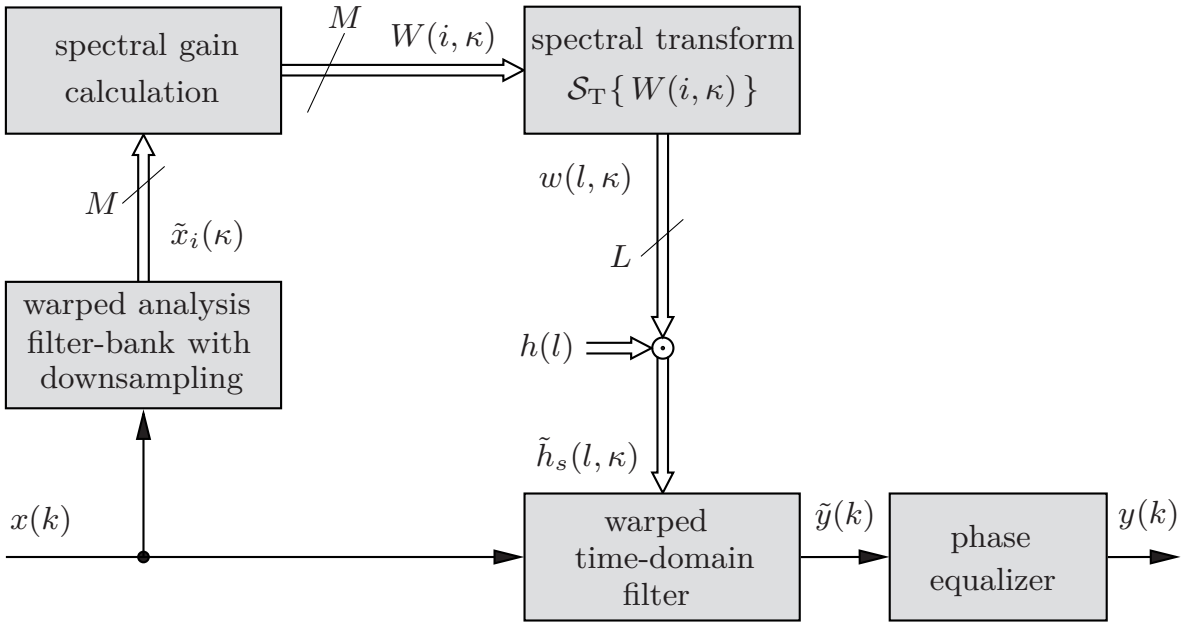

Figure 5.8: *Allpass transformed FBE with phase equalizer.*

for an allpass chain of length $L_{\mathrm{ac}} = D_{\mathrm{o}}$ as discussed in Sec. 3.3. The filtering of the output signal $\tilde{y}(k)$ by a phase equalizer as depicted Figure 5.8 is similar to the approach of Figure 4.6 for a warped AS FB. However, a phase equalizer with a lower filter degree N can be used for the FBE due to its lower signal delay D_{o} in comparison to a corresponding warped AS FB with subsampling. Besides, the described phase compensation is not affected by *time-varying* filter coefficients, if the symmetry of Eq. (5.24) holds: For the warped FBE with direct form filter, the (frozen-time) frequency response reads

$$\widetilde{H}_{\mathrm{s}}\left(e^{j\,\Omega}, \kappa\right) = \sum_{l=0}^{L-1} h_{\mathrm{s}}(l, \kappa) \cdot e^{-j\,l\,\varphi_a(\Omega)} \,. \tag{5.44}$$

If the real filter coefficients exhibit the symmetry of Eq. (5.24), it can be shown that the system function of Eq. (5.44) can be expressed by

$$\widetilde{H}_{\mathrm{s}}\left(e^{j\,\Omega}, \kappa\right) = e^{-j\,\frac{L-1}{2}\,\varphi_a(\Omega)} \begin{cases} \sum\limits_{l=0}^{\frac{L-1}{2}} 2\,\mathcal{A}_{l,\kappa}(\Omega) - h_{\mathrm{s}}\left(\frac{L-1}{2}, \kappa\right) & \text{if } L \text{ is odd} \\ \sum\limits_{l=0}^{\frac{L}{2}} 2\,\mathcal{A}_{l,\kappa}(\Omega) & \text{if } L \text{ is even} \end{cases} \tag{5.45a}$$

with

$$\mathcal{A}_{l,\kappa}(\Omega) = h_{\mathrm{s}}(l, \kappa) \cdot \cos\left(\left[\frac{L-1}{2} - l \right] \varphi_a(\Omega) \right) \,. \tag{5.45b}$$

A similar result can be obtained for a filter with symmetry $h(l) = -h(L-1-l)$, but such a prototype filter cannot realize a lowpass filter. The effect of the non-linear phase

term $\varphi_a(\Omega)\,(L-1)/2$ can be compensated by a phase equalizer designed for an allpass chain of length $L_{\mathrm{ac}} = (L-1)/2$. The expressions to the right of the curly brace are real and cause only phase shifts of $\pm\pi$. Thus, the warped FBE can achieve a time-invariant, *generalized* linear phase response despite the time-varying coefficients, if a sufficient phase compensation is performed.[8] A system with a generalized linear phase response features a constant group delay, if the discontinuities that result from the addition of phase shifts by $\pm\pi$ due to the real function are neglected [OSB99]. For the filter in transposed direct form, Eq. (5.45) is approximately fulfilled in case of moderately time-varying coefficients.

5.3 Comparison between FBE and AS FB

The AS FBs (with subsampling) discussed in the previous chapter and the FBE are very different methods to realize a uniform and warped filter-bank. Therefore, both filter-bank types have specific pros and cons and it depends on the intended application which filter-bank is preferable. A comparison with the uniform and warped AS FB according to Figure 2.4 and Figure 4.6 shows that the concept of the FBE exhibits the following benefits:

- The FBE is not affected by aliasing distortions for the reconstructed signal. Hence, the difficult problem of achieving a sufficient aliasing cancellation, especially for time-varying spectral gain factors, does not occur. One consequence is that the FBE does not require a prototype filter with high degree and/or a low subsampling rate R in order to reduce aliasing distortions. Moreover, the prototype filter design for the FBE is easier than for the AS FB.

- For the allpass transformed FBE, only the phase modifications due to the frequency warping need to be compensated, but not additional aliasing distortions. Hence, near-perfect reconstruction can be achieved with lower efforts than for the warped AS FB.

- The algorithmic signal delay D_{o} of the FBE is significantly lower than for the corresponding AS FB. The uniform AS FB with linear-phase prototype filters has a signal delay of $D_{\mathrm{o}} = L - 1$ samples. In contrast, the uniform FBE with linear-phase prototype filter has a signal delay of $D_{\mathrm{o}} = (L-1)/2$, which can be further reduced by a prototype filter with non-linear phase response. As a consequence, the warped AS FB requires a phase equalizer with a higher filter degree than the corresponding warped FBE to achieve a similar phase error.

- The warped FBE can achieve an almost linear overall phase characteristic even for time-varying coefficients, which can be beneficial for multi-channel processing.

However, the time-varying coefficients of the FBE can create filter-ringing artifacts. These artifacts can be avoided by an appropriate smoothing, but at the price of a

[8] This can also be shown for complex coefficients with symmetry $h(l) = h^*(L-1-l)$, cf., [LV05a].

Table 5.1: *Algorithmic complexity for different realizations of a PPN DFT filter-bank with real-valued prototype filter of length $L = l_M\, M$.*

	2 real FFTs	remaining operations	additional operations due to warping
DFT AS FB			
multiplications	$2\,\frac{M}{R}\,\log_2 M$	$\frac{1}{R}(2\,L + M)$	$4\,L + N - 3$
summations	$3\,\frac{M}{R}\,\log_2 M$	$\frac{1}{R}(L - M) + L - 1$	$4\,L + N - 4$
delay elements	$2\,M$	$2\,L - 2$	N
FBE in direct form			
multiplications	$2\,\frac{M}{R}\,\log_2 M$	$L + M$	$2\,L + N - 1$
summations	$3\,\frac{M}{R}\,\log_2 M$	$L - 1$	$2\,L + N - 2$
delay elements	$2\,M$	$L - 1$	N
FBE in transposed direct form			
multiplications	$2\,\frac{M}{R}\,\log_2 M$	$L + M + \frac{L-1}{R}$	$4\,L + N - 3$
summations	$3\,\frac{M}{R}\,\log_2 M$	$L - 1 + \frac{1}{R}(L - M)$	$4\,L + N - 4$
delay elements	$2\,M$	$2\,L - 2$	N

higher computational complexity as shown before. In contrast, artifacts due to time-varying coefficients are less a concern for AS FBs because of the inherent smoothing effect of the synthesis filter-bank with upsampling.

An allpass transformed AS FB can achieve a perfect signal reconstruction where the allpass transformed FBE achieves only near-perfect reconstruction (if no phase equalizer of high degree can be used).[9] Another limitation of the FBE is that it is not suitable for subband coding applications where AS FBs with (critical) subsampling are needed.

The FBE has a higher algorithmic complexity for some configurations in comparison to a corresponding AS FB, which is exposed by Table 5.1. It contrasts the algorithmic complexity of the developed uniform and warped FBE according to Figure 5.2 and Figure 5.8 to that of a corresponding uniform and warped AS FB according to Figure 2.4 and Figure 4.6. The same values for the prototype filter length L, the DFT size M, the downsampling rate R and the phase equalizer degree N are considered. The DFT can be computed in-place by a radix-2 FFT, e.g., [PM96]. The FFT of a real sequence of size M can be calculated by a complex FFT of size $M/2$, which requires approximately half the algorithmic complexity of that of a complex M-point FFT, e.g., [PTVF92]. The GDFT can be computed by the FFT with similar complexity as for the DFT.

[9] A perfect reconstruction or linear overall phase response can be achieved for the underlying allpass transformed FBSM by the PR designs developed in Chap. 4, which comprise the warped FBSM as special case for $R = 1$. However, this approach would preclude the efficient realization of the FBSM by the FBE.

The last column contains the additional operations and delay elements due to the allpass transformation. The implementation of an allpass filter according to Figure 2.8 is considered, which requires two real multiplications, two real summations and one delay element for a real allpass coefficient $a = \alpha$. An LS FIR phase equalizer with filter degree N according to Sec. 3.3.4.1 is considered for the phase compensation at the output. However, it should be noted that allpass transformed filter-banks are usually operated with a lower number of channels than uniform filter-banks.

As reasoned before, a higher subsampling rate R and a lower phase equalizer degree N can be taken for the warped FBE in comparison to the warped AS FB. Therefore, the warped FBE possesses a lower algorithmic complexity than the corresponding warped AS FB for most parameter configurations. Contrariwise, the uniform AS FB exhibits a lower complexity than the uniform FBE. A concrete example for the design and algorithmic complexity of these filter-banks is given later in Sec. 6.2.

5.4 Further Measures for Signal Delay Reduction

Even though the FBE causes only about half the algorithmic signal delay of that of the corresponding AS FB, a further reduced delay might be required for applications with very demanding system delay constraints. For such cases, a modification of the FBE concept is now discussed, which allows a further lowering of the signal delay in a simple and flexible manner.

5.4.1 Concept

One approach to reduce the signal delay of a filter-bank is to reduce the transform size M to allow for a lower prototype filter degree and to adjust the gain calculation to the altered time-frequency resolution (smoothing factors etc.), e.g., [GNC01].

For the FBE, a further reduction of the signal delay can also be accomplished by approximating the original time-domain filter by a filter of lower degree as depicted in Figure 5.9. In contrast to the FBE of Figure 5.2, an additional module for the filter approximation is now inserted, which determines $L_{\mathrm{ld}} < L$ filter coefficients $v_l(\kappa)$ from the L original filter coefficients $h_{\mathrm{s}}(l, \kappa)$. This approach offers a greater flexibility for the choice of the time-domain filter and requires no adjustment of the spectral gain calculation in comparison to a lowering of the transform size M.

In the following, an FIR and IIR filter approximation for the uniform FBE are investigated and the results are extended to the more general case of allpass transformed filters afterwards.

5.4.2 Approximation by a Moving-Average Filter

The time-domain filter of the FBE can be approximated by an FIR filter of length $L_{\mathrm{ld}} < L$ following a technique very similar to FIR filter design by windowing, e.g., [PM96]. The impulse response $h_{\mathrm{s}}(l, \kappa)$ of Eq. (5.11) is truncated by a window sequence of length L_{ld}. This yields the FIR filter coefficients

$$v_l(\kappa) = \hat{h}_{\mathrm{s}}(l, \kappa) = h_{\mathrm{s}}(l + l_c, \kappa) \cdot \mathrm{win}_{L_{\mathrm{ld}}}(l); \quad l \in \{\, 0, 1, \ldots, L_{\mathrm{ld}} - 1 \,\} \tag{5.46}$$

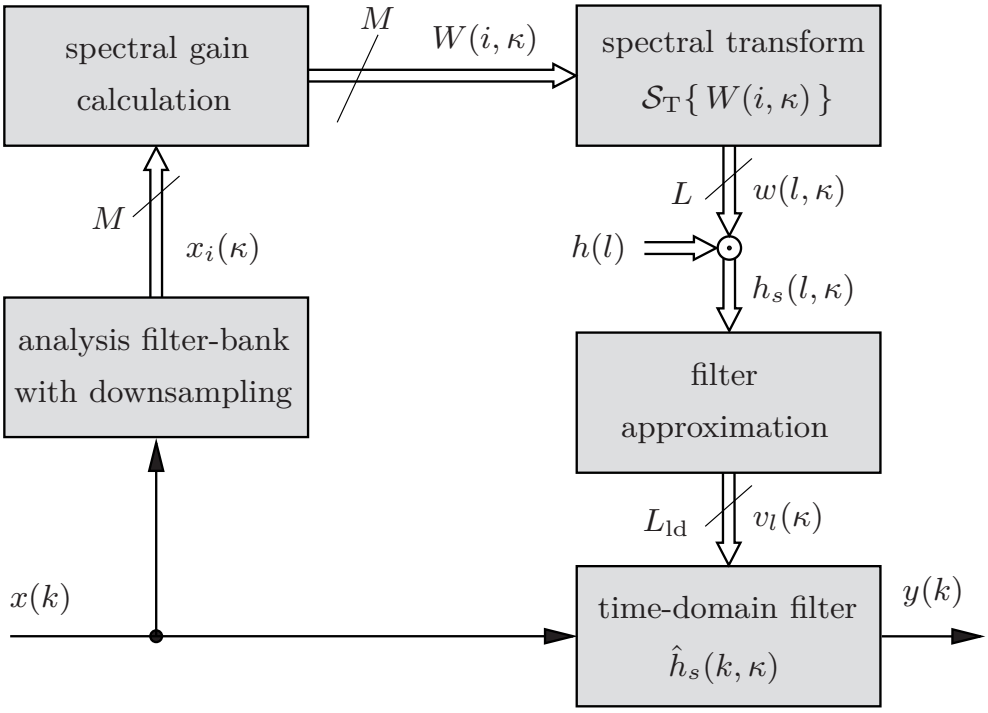

Figure 5.9: *Modification of the FBE to achieve a further reduced signal delay.*

where the general window sequence is defined by Eq. (5.17). The value for l_c determines the part of the impulse response to be truncated, e.g., to maintain the symmetry of Eq. (5.24) for linear-phase filters. The truncation by a window results in a smoothed frequency response which is influenced by the choice of the window sequence, cf., [OSB99].

This modified FBE based on an FIR filter approximation is named as moving-average low delay filter (MA LDF) [LV05c, LV06b]. The term *low delay filter* (LDF) refers to the overall system according to Figure 5.9, while the term *moving-average (MA) filter* is used to denote the actual time-domain filter. The parameter

$$N_{\mathrm{ld}} = L_{\mathrm{ld}} - 1 \tag{5.47}$$

marks the degree of this filter.

5.4.3 Approximation by an Auto-Regressive Filter

Instead of a (linear-phase) FIR filter, a *minimum-phase* IIR filter is now considered for the filter approximation. A filter can always be decomposed into a cascade of an allpass filter and a minimum-phase filter, e.g., [OSB99]. The group delay of the minimum-phase filter is lower than or equal to the group delay of the original filter for all frequencies. The approximation of a mixed-phase filter by a minimum-phase filter yields a filter with the same magnitude response, but a different phase response. An altered phase, however, is mostly tolerable for speech and audio processing as the human ear is relatively insensitive towards phase modifications, cf., [Var85, ZF99].

However, the approximation of a time-varying FIR filter by a general minimum-phase IIR filter demands a rather high computational complexity for the calculation

of its filter coefficients. Therefore, an *auto-regressive* (AR) filter is considered for the filter approximation due to the lower computational complexity for the calculation of its coefficients. An AR filter is an allpole filter and, thus, of minimum-phase, but has no zeros outside the origin. Therefore, an AR filter cannot provide a magnitude response with zeros. However, this is usually less problematic for speech enhancement applications where the thresholding of Eq. (5.20) comes mostly into effect.

The (frozen-time) system function of the considered AR filter of degree N_{ld} reads

$$\hat{H}_{\mathrm{s}}(z,\kappa) = H_{\mathrm{AR}}(z,\kappa) = \frac{v_0(\kappa)}{1 - \sum_{l=1}^{N_{\mathrm{ld}}} v_l(\kappa) \cdot z^{-l}} \,. \tag{5.48}$$

The dependence on κ is skipped in the following to ease the notation. The AR filter coefficients can be determined by the Yule-Walker equations, e.g., [PM96]

$$\begin{bmatrix} \varphi_{\bar{h}\bar{h}}(1) \\ \vdots \\ \varphi_{\bar{h}\bar{h}}(N_{\mathrm{ld}}) \end{bmatrix} = \begin{bmatrix} \varphi_{\bar{h}\bar{h}}(0) & \dots & \varphi_{\bar{h}\bar{h}}(1-N_{\mathrm{ld}}) \\ \vdots & \ddots & \vdots \\ \varphi_{\bar{h}\bar{h}}(N_{\mathrm{ld}}-1) & \dots & \varphi_{\bar{h}\bar{h}}(0) \end{bmatrix} \cdot \begin{bmatrix} v_1 \\ \vdots \\ v_{N_{\mathrm{ld}}} \end{bmatrix} . \tag{5.49}$$

The $N_{\mathrm{ld}} + 1$ auto-correlation coefficients $\varphi_{\bar{h}\bar{h}}(\lambda)$ are computed by the rule[10]

$$\varphi_{\bar{h}\bar{h}}(\lambda) = \sum_{l=0}^{L-1-|\lambda|} \bar{h}(l) \cdot \bar{h}(l+\lambda); \quad 0 \le |\lambda| \le N_{\mathrm{ld}}; \quad \lambda \in \mathbb{Z} \tag{5.50a}$$

$$\bar{h}(l) = h_{\mathrm{s}}(l) \cdot \mathrm{win}_L(l); \quad l \in \{\, 0, 1, \dots, L-1 \,\} \,. \tag{5.50b}$$

The scaling factor v_0 in Eq. (5.48) is given by

$$v_0 = \sqrt{\varphi_{\bar{h}\bar{h}}(0) - \sum_{l=1}^{N_{\mathrm{ld}}} v_l \cdot \varphi_{\bar{h}\bar{h}}(l)} \tag{5.51}$$

and ensures that the AR filter causes the same amplification as the original filter. The calculation of the auto-correlation coefficients according to Eq. (5.50) guarantees a symmetric Toeplitz structure for the auto-correlation matrix of Eq. (5.49). This allows to solve the Yule-Walker equations efficiently by means of the Levinson-Durbin recursion. The auto-correlation matrix is positive definite so that the obtained AR filter is of minimum-phase and thus stable, cf., [PM96].

The devised modification of the FBE is named as *auto-regressive low delay filter* (AR LDF) in analogy to the terminology of the previous section [LV05c, LV06b].

5.4.4 Algorithmic Complexity

The algorithmic complexity for the low delay filter concept in terms of arithmetic operations and memory consumption is listed in Table 5.2. The complexity for the calculation

[10] An alternative to this *auto-correlation method* is the use of the *covariance method* which, however, results in a more complex procedure to calculate the AR filter coefficients, cf., [VM06, Chap. 6].

Table 5.2: *Algorithmic complexity for the MA and AR low delay filter with filter degree N_{ld}.*

calculation of $h_\mathrm{s}(l,\kappa)$ and MA/AR filtering	
multiplications	$\frac{1}{R}(2M\log_2 M + 2\,L) + N_\mathrm{ld} + 1$
summations	$\frac{1}{R}(3M\log_2 M + L - M) + N_\mathrm{ld}$
delay elements	$L - 1 + 2\,M + N_\mathrm{ld}$
calculation of MA filter coefficients $v_l(\kappa)$	
multiplications	$\frac{1}{R}(N_\mathrm{ld} + 1)$
summations	0
registers	0
calculation of AR filter coefficients $v_l(\kappa)$	
multiplications	$\frac{1}{R}\left((N_\mathrm{ld}+1)\,(L+3) + N_\mathrm{ld}\,(\mathcal{M}_\mathrm{div} + \mathcal{M}_\mathrm{sqrt})\right)$
summations	$\frac{1}{R}\left((N_\mathrm{ld}+1)\,(L+1) + N_\mathrm{ld}\,(\mathcal{A}_\mathrm{div} + \mathcal{A}_\mathrm{sqrt})\right)$
registers	$3\,N_\mathrm{ld}$

of the original filter coefficients $h_\mathrm{s}(l,\kappa)$ is discussed in Sec. 5.3 and a rectangular window is considered for Eq. (5.50b). The variable $\mathcal{M}_\mathrm{div}$ marks the number of multiplications needed for a division operation and $\mathcal{M}_\mathrm{sqrt}$ represents the number of multiplications needed for a square-root operation. Accordingly, the variables $\mathcal{A}_\mathrm{div}$ and $\mathcal{A}_\mathrm{sqrt}$ denote the additions needed for a division and square-root operation, respectively. Their values depend on the numeric procedure and accuracy to execute these arithmetic operations. In this work, an equivalent of 15 operations is assigned to each of these variables for the calculation of the algorithmic complexity (see Sec. 6.2.1).

Most of the computational complexity for the AR filter conversion is required to compute the $N_\mathrm{ld} + 1$ auto-correlation coefficients according to Eq. (5.50). A lower computational complexity can be achieved by calculating Eq. (5.50) by means of the fast convolution or the Rader algorithm [Rad70] with savings dependent on N_ld and L.

The MA filter conversion needs no multiplications, if a rectangular window is used for Eq. (5.46). However, the AR filter degree is usually significantly lower than the MA filter degree so that both approaches have a similar overall algorithmic complexity in practice as exemplified later in Sec. 6.2.1.

5.4.5 Warped Filter Approximation

The discussed filter approximations can also be applied to the allpass transformed FBE [LV06c]. In the process, the delay elements of the analysis filter-bank and the time-domain filter are replaced by allpass filters. For the obtained warped MA LDF, a phase equalizer can be applied as for the warped FBE to obtain an approximately linear phase response.

The direct realization of the warped AR filter is not possible since the allpass transformation leads to delay-less feedback loops. Different approaches have been proposed to solve this problem for an allpass transformation of first order with real allpass coefficient ($a = \alpha$) [Ste80, Här98, Här00]. Here, the algorithm of Steiglitz [Ste80] is preferred due to its low computational efforts for time-varying filters. The modified system function of the allpass transformed AR filter without delay-less feedback loops is given by

$$\widetilde{H}_{\mathrm{AR}}(z) = \frac{v_0\,\tilde{v}_0}{1 - \tilde{v}_0\,\dfrac{\left(1-\alpha^2\right)\,z^{-1}}{1-\alpha\,z^{-1}}\,\displaystyle\sum_{l=1}^{N_{\mathrm{ld}}} \tilde{v}_l \cdot \Big(A(z)\Big)^{l-1}} \tag{5.52}$$

with coefficients $\tilde{v}_l$ calculated by the recursion

$$\tilde{v}_{N_{\mathrm{ld}}} = v_{N_{\mathrm{ld}}} \tag{5.53a}$$

$$\tilde{v}_l = v_l - \alpha\,\tilde{v}_{l+1}\,;\quad l = N_{\mathrm{ld}}-1,\ldots,2,1 \tag{5.53b}$$

$$\tilde{v}_0 = \frac{1}{1+\tilde{v}_1\,\alpha}\,. \tag{5.53c}$$

The derivation of this scheme from Steiglitz is provided by App. B.5. The computation of the new filter coefficients $\tilde{v}_l(\kappa)$ needs only N_{ld} multiplications, N_{ld} summations and one division at intervals of R sample instants. The warped AR filter according to Eq. (5.52) requires $3N_{\mathrm{ld}}+2$ real multiplications and $3N_{\mathrm{ld}}$ real summations per sample instant as well as $N_{\mathrm{ld}}+1$ delay elements.

It is shown in App. B.6 that the minimum-phase property of an AR filter is maintained despite an allpass transformation of first order. This is an important property as it guarantees stability for the warped AR filter. The use of a fixed phase equalizer as for the warped MA LDF is neither feasible nor required.

The cross-fading approach of Eq. (5.34) cannot be applied to the coefficients of an IIR filter in its direct form.[11] Instead, a second filter with the previous coefficients is used to achieve a smooth transition by a cross-fading of both output signals. This approach can be applied to an arbitrary FIR or IIR filter with frozen-time system function $H_{\mathrm{g}}(z,k)$ as follows

$$\bar{H}_{\mathrm{g}}(z,k) = \Big(1-c_f(k)\Big)\cdot H_{\mathrm{g}}(z,\kappa-R) + c_f(k)\cdot H_{\mathrm{g}}(z,\kappa) \tag{5.54a}$$

$$c_f(k) = \frac{k-\kappa}{R} \tag{5.54b}$$

with k and κ related by Eq. (5.1). This smoothing technique does not cause an additional signal delay and preserves a time-invariant phase response.

It is important to notice that the application of the allpass transformation of *higher order* is straightforward for the FBE as well as the MA LDF, but not the AR LDF

[11] A cross-fading might be applied to the reflection coefficients of a Lattice implementation for an IIR filter where filter stability can be ensured by reflection coefficients with a magnitude of less than one.

since the delay-less feedback loops cannot be eliminated in the same manner as for an allpass transformation of first order.

Another option for an LDF is to approximate the time-domain filter of the *uniform* FBE by a warped AR filter. This approach is investigated in [LV07a] in great detail and should not be discussed here.

5.5 Conclusions

The concept of the *filter-bank equalizer* (FBE) is presented in this chapter. The FBE is derived as an efficient implementation of the filter-bank summation method (FBSM) and performs time-domain filtering with coefficients adapted in the frequency-domain. Perfect signal reconstruction is achieved for a broad class of transformation kernels with significantly lower efforts than for a common AS FB with subsampling. It is shown how the FBE can be efficiently implemented by a polyphase network (PPN) structure. The explicit consideration of the time-varying coefficients in the derivation reveals the influence of the filter structure on system delay, computational complexity and signal quality. It is shown, amongst others, how the transposed direct form implementation achieves a stronger smoothing effect for time-varying coefficients in comparison to the direct form implementation of the FBE, which is beneficial to avoid artifacts for the processed signal (filter-ringing). An advantage of the direct form implementation of the FBE is that a time-mismatch between the adaptation of the spectral gain factors and the actual time-domain filtering has not to be compensated as for the transposed direct form implementation. Possible artifacts due to the switching of the time-domain filter coefficients can be avoided by an appropriate smoothing (cross-fading).

The presented allpass transformed FBE achieves near-perfect reconstruction with significantly lower efforts than a corresponding allpass transformed AS FB with subsampling. The uniform FBE has a higher algorithmic complexity than the corresponding uniform AS FB for most parameter configurations, while the opposite applies for the allpass transformed FBE in comparison to the allpass transformed AS FB. The uniform and warped FBE achieve a significantly lower algorithmic signal delay than the corresponding AS FBs. A nearly linear phase response can be maintained even for time-varying coefficients, which can be exploited, e.g., for multi-channel processing.

The concept of the *low delay filter* (LDF) is an extension of the FBE to achieve a further reduction of the signal delay and algorithmic complexity in a simple and flexible manner. In the process, the time-domain filter of the FBE is approximated by either a moving-average (MA) filter or auto-regressive (AR) filter of lower degree. The use of the uniform and warped MA filter allows to maintain a time-invariant or even linear phase response, which can be beneficial, e.g., for binaural speech processing in hearing aids. The uniform and warped AR filter are minimum-phase systems and can achieve an algorithmic signal delay of only a few sample instants.

A primary application of the FBE (including the LDF concept) are systems for low delay speech enhancement, which is discussed in the following chapter.

Chapter 6

Applications

DIFFERENT DESIGNS of allpass-based filter-banks are presented in the previous chapters. They have rather diverse properties which make them attractive for different applications. The allpass-based (Pseudo) QMF-banks of Chap. 3 are uniform filter-banks with critical subsampling and low algorithmic complexity, which is of interest for subband coding systems. The allpass transformed filter-banks treated in Chap. 4 and Chap. 5 can achieve an auditory frequency resolution, which is beneficial for speech enhancement systems. This chapter elaborates such applications in more detail to exemplify the properties and benefits of the devised allpass-based IIR filter-banks.

In Sec. 6.1, the use of the IIR/IIR QMF-bank of Sec. 3.1.2 for subband coding is investigated. Important design and implementation aspects are discussed and the performance of the devised IIR filter-bank is contrasted to that of a comparable FIR QMF-bank.

In Sec. 6.2, the use of the filter-bank equalizer (FBE) for adaptive subband filtering with low signal delay is investigated. It is shown how this filter-bank concept can be exploited to perform different kinds of speech enhancement such as noise reduction, speech dereverberation, or speech intelligibility improvement.

6.1 QMF-Bank Design for Speech and Audio Coding

Analysis-synthesis filter-banks with critical subsampling are commonly employed for speech and audio subband coding, cf., [SPA07, VK95, VHH98]. QMF-banks are of special interest for such purposes and are proposed already in early publications about speech subband coding [CWF76, EG77, RF80, Rot83]. A uniform two-channel FIR QMF-bank is used for the first standardized 7 kHz wideband (WB) audio codec, ITU-T Rec. G.722 [ITU88].[1] In [Pau96], an improvement of this codec is proposed where a non-uniform two-channel FIR/FIR QMF-bank (with critical subsampling) is used. Tree-structured QMF-banks including wavelet packets can be used to achieve either an octave-band or critical-band analysis (as described in App. C.2.2). Such filter-banks are commonly exploited for perceptual audio coding, e.g., [ST93, PdL99].

More recently, QMF-banks are also used for *hierarchical* speech and audio coding as, for example, ITU-T Rec. G.729.1 [ITU06, RKT+07], shortly termed as G.729.1 codec. This codec generates a layered bit-stream format where each additional layer succes-

[1] ITU-T is the telecommunication standardization sector of the International Telecommunication Union (ITU).

sively improves the audio fidelity of the decoded signal. Bit rate scalability can thus be achieved by truncating the hierarchical bit-stream so that bit rate synchronization of encoder and decoder as well as any transcoding become dispensable. The G.729.1 codec is built 'on top' of an embedded so-called legacy codec, the narrowband codec G.729 CS-ACELP [ITU96], which generates the core layer of the bit-stream. Thus, interoperability with existing codecs is simply achieved by discarding the bit-streams added to the core bit-stream layer. Such features are of particular interest for heterogeneous, packet-switched networks (e.g., Voice-over-IP) having connections with different bit rates and/or different terminal equipments. The bandwidths of the decoded speech and audio signals depend on the bit rate such that this hierarchical codec provides bit rate as well as bandwidth scalability. To achieve this, a wideband input signal sampled at 16 kHz is split into subband signals by the encoder using a (uniform) two-channel analysis QMF-bank. If no bit-stream layers are discarded, the wideband signal is reconstructed at the decoder by means of a corresponding synthesis QMF-bank.

At present, *non-recursive* QMF-banks are used predominately for such purposes (e.g., [ITU88, ITU06]) and only a comparatively low number of publications (or an ITU-T recommendation) deals with recursive filter-banks for subband coding such as [RF80, CM96]. Hence, the design and application of IIR filter-banks for subband coding is a subject that is considered to be "largely unexplored" [SPA07, Chap. 8].

In 2008, a new speech and audio codec has been developed by a consortium of Huawei (China) and ETRI (South Korea) in collaboration with the Institute of Communication Systems and Data Processing of RWTH Aachen University. It has been submitted to ITU-T as *candidate proposal* for the super-wideband (SWB) and stereo extensions of ITU-T Rec. G.729.1 and Rec. G.718 [GKL+09]. This hierarchical speech and audio codec employs the allpass-based IIR QMF-bank design of Sec. 3.1.2.3 instead of a more common FIR QMF-bank as used, for example, in ITU-T Rec. G.729.1 [ITU06] and Rec. G.722 [ITU88]. The new filter-bank has helped to achieve a high signal quality with a low signal delay. In the following, the design and implementation of the proposed IIR QMF-bank for this application is elaborated in more detail based on [GKL+09, LV09b].

6.1.1 Codec Overview

A signal flow chart of the proposed codec is provided by Figure 6.1 adopted from [GKL+09] where further details can be found.[2] The sampling rate for the input signal can be 8, 16 and 32 kHz. For a sampling rate of 32 kHz, the input signal is split by an *allpass-based* analysis QMF-bank into two critically subsampled signals $s_{\mathrm{wb}}(k)$ and $s'_{\mathrm{swb}}(k)$ having a bandwidth of 0–16 kHz and 16–32 kHz, respectively. For the sake of clarity, this IIR filter-bank, marked by the red shaded boxes in Figure 6.1, is termed as *outer* QMF-bank, where the QMF-bank of the core codec, marked by the blue shaded boxes, is denoted as *inner* QMF-bank.

The lower subband signal $s_{\mathrm{wb}}(k)$ of the outer QMF-bank is encoded by the *core codec*, marked by the green shaded box, which is almost identical to ITU-T Rec. G.729.1 [ITU06, RKT+07]. This hierarchical speech and audio codec has a scalable bit rate of 8–32 kbit/s and provides a bit-stream with 12 embedded layers where the core layer

[2] The stereo extension is not considered here.

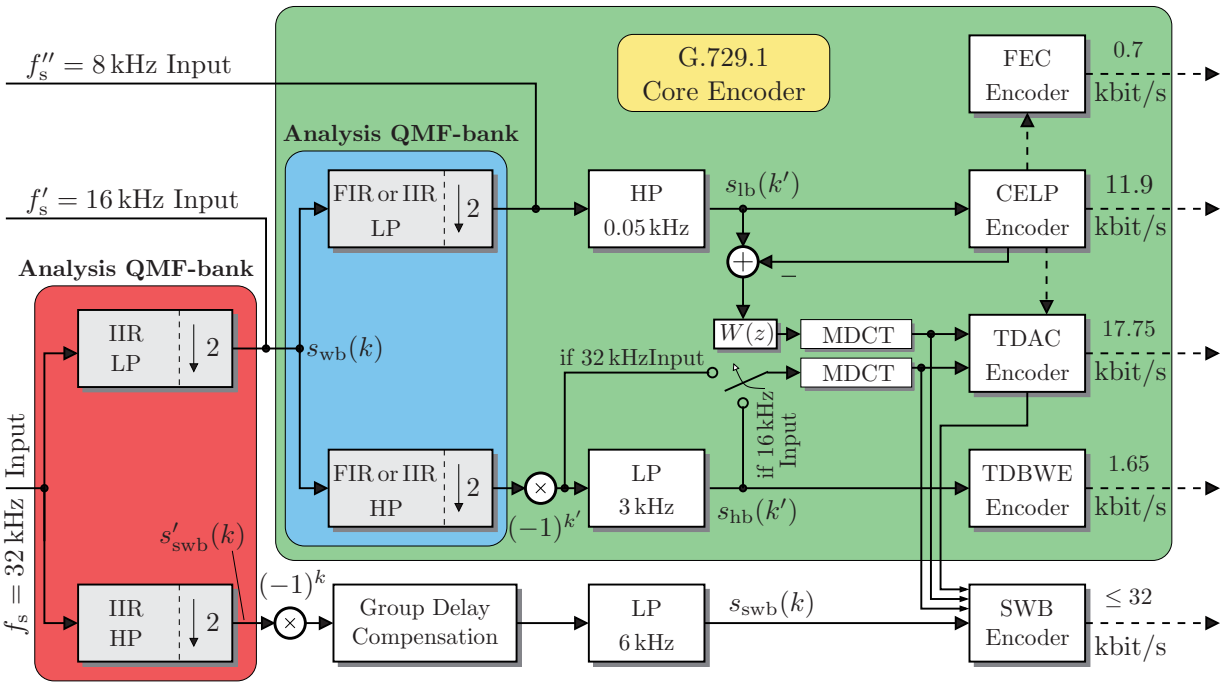

(a) *encoder*

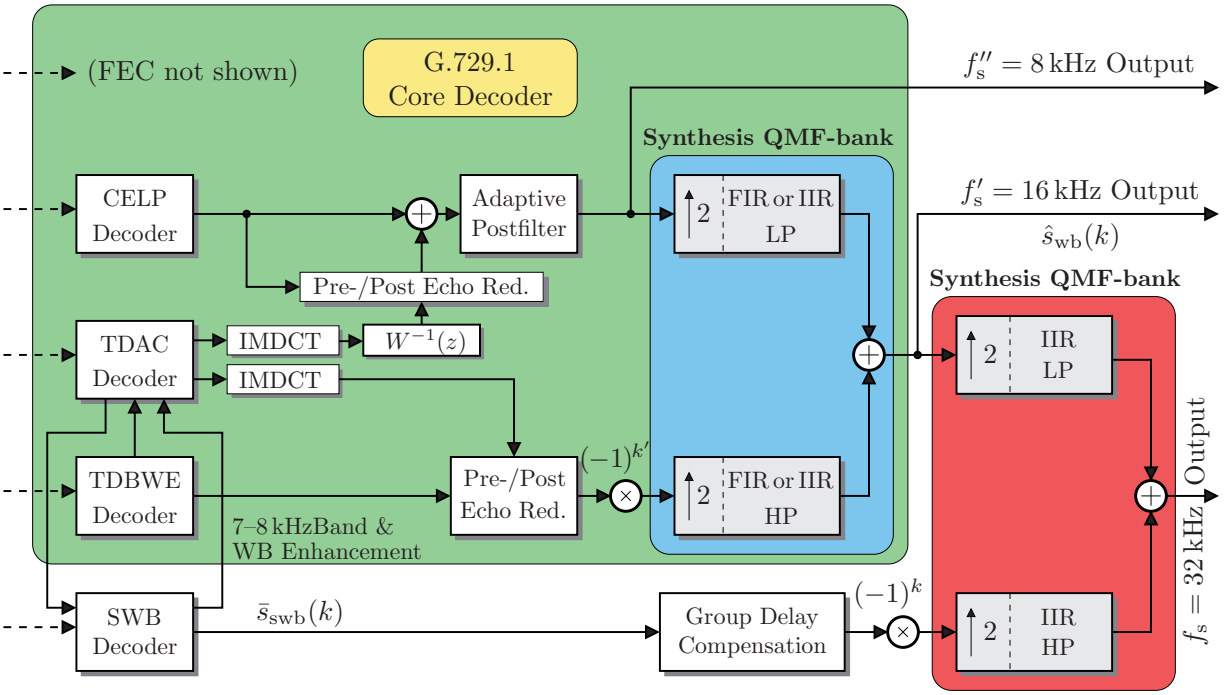

(b) *decoder*

Figure 6.1: *High level block diagram of the codec proposed in [GKL+09]. Solid lines mark time-domain signals and dashed lines parameters. For the sake of clarity, the QMF-banks are depicted in a direct implementation and not their actual PPN implementation.*

is interoperable with the G.729 codec [ITU96]. In a first stage, the wideband signal $s_{wb}(k)$ is spilt into two critically downsampled subband signals with a bandwidth of

4 kHz by means of an analysis QMF-bank.[3] The inner QMF-bank can be optionally either the FIR/FIR QMF-bank of Rec. G.729.1 or the proposed IIR/IIR QMF-bank as described later in Sec. 6.1.2. The lower subband of the inner analysis QMF-bank is pre-processed by an elliptic IIR highpass (HP) filter with a cutoff frequency of 50 Hz whose output signal $s_{\mathrm{lb}}(k')$ is then encoded by a two-stage code excited linear prediction (CELP) coder, which is compatible to the embedded G.729 codec. The higher subband signal is multiplied by $(-1)^{k'}$ to reverse the 'spectral mirroring' (cf., [VHH98, Chap. 4]) and filtered by an elliptic lowpass (LP) filter with cutoff frequency of 3 kHz. The obtained signal $s_{\mathrm{hb}}(k')$ is encoded by means of a time-domain bandwidth extension (TDBWE) [GJV+07]. The decoded signal of the embedded CELP codec is subtracted form the suitably aligned lowpass signal $s_{\mathrm{lb}}(k')$. The obtained difference signal and the highpass signal $s_{\mathrm{hb}}(k')$ are jointly encoded by a so-called time-domain aliasing cancellation (TDAC) encoder, which uses a modified discrete cosine transform (MDCT). Some parameters for frame erasure concealment (FEC) are also transmitted.

The operations of the core decoder are dependent on the received bit rate due to the hierarchical coding concept (see Figure 6.1-b). For bit rates of 8 and 12 kbit/s, only the CELP decoder is active. After post-processing and filtering by the synthesis QMF-bank, a narrowband output signal is obtained sampled at 16 kHz. For bit rates of 14 kbit/s and more, the TDBWE decoder is activated [GJV+07]. The produced highband signal is multiplied with $(-1)^{k'}$ to reverse the spectral mirroring at the encoder. The output signal $\hat{s}_{\mathrm{wb}}(k)$ of the inner synthesis QMF-bank is now a wideband signal sampled at 16 kHz. For a bit rate of 16 kbit/s and more, the TDAC further improves the audio quality. For this, its lowband output signal is added to the decoded CELP signal. The high frequency bands of the TDBWE signal are replaced by the subband signals of the TDAC decoder. Alternatively, if no TDAC subbands are received, the synthesis signal of the TDBWE is scaled according to the spectral envelope of the TDAC. The TDAC is a transform coder which employs an MDCT with a relatively long window of 40 ms. Dependent on the signal and the used quantizer, this can cause pre-echo and post-echo artifacts, which are reduced by dedicated processing units.

The higher subband signal $s'_{\mathrm{swb}}(k)$ of the outer analysis QMF-bank with a bandwidth of 16–32 kHz band is encoded by a *super-wideband* (SWB) encoder. First, the subband signal is multiplied by $(-1)^k$ to reverse the spectral mirroring. A *group delay compensation* is performed to account for the signal delay of the inner analysis QMF-bank. The output signal is then filtered by a lowpass filter with a cutoff frequency of 6 kHz and encoded by a new SWB encoder, which uses the MDCT coefficients of the core codec.

For bit rates of 36 kbit/s and more, the SWB decoder provides the additional signal $\bar{s}_{\mathrm{swb}}(k)$ with a bandwidth of 8–14 kHz (due to the lowpass filtering at the encoder). The time-aligned output signals of SWB decoder and core decoder are processed by a synthesis QMF-bank to obtain the decoded SWB signal sampled at 32 kHz.

The design of the inner and outer QMF-bank has a noticeable effect on the overall performance of the coder regarding its latency, signal quality and computational load.

[3] As indicated in Figure 6.1, ITU-T Rec. G.729.1 also defines a mode for a narrowband input signal sampled at 8 kHz. In this case, the bit rate is 8 kbit/s and the processing by a QMF-bank is omitted, but this case is not considered here.

This motivates to elaborate an IIR QMF-bank design as alternative to commonly used FIR QMF-banks. Special emphasis is given to the inner filter-bank design as it allows to compare the devised IIR QMF-bank with the FIR QMF-bank of a *standardized* codec for which a floating-point and fixed-point reference implementation in C exist.[4]

6.1.2 Inner QMF-Bank

Primary goals of the QMF-bank design are to achieve a low (inaudible) signal reconstruction error as well as analysis filters with a high stopband attenuation and low transition bandwidth. The latter goal is important to achieve a good separation between the subband signals to avoid a significant cross-talk on the one hand, and to prevent noticeable aliasing distortions despite subband processing (quantization) on the other hand. The filter-bank design is thereby subject to the constraint for a (coding) system with low signal delay.

6.1.2.1 Filter-Bank Design

In ITU-T Rec. G.729.1 [ITU06], an FIR/FIR QMF-bank is used to address the above mentioned trade-off. It is designed by the approach of Johnston [Joh80], which is briefly described in App. C.1. This FIR QMF-bank achieves near-perfect reconstruction with perfect aliasing cancellation and can be efficiently implemented due to the use of linear-phase subband filters. The prototype lowpass filter has a filter length of $L = 64$ and is designed for a stopband frequency of $\Omega_\mathrm{s} = 0.586\,\pi$.[5]

A drawback of this FIR filter-bank is that a rather high filter degree is needed to achieve the desired stopband attenuation. In contrast, IIR subband filters can achieve a comparable frequency selectivity with a much lower filter degree. Their non-linear phase response is less problematic here as the human auditory system is rather insensitive towards (moderate) phase distortions. Therefore, the IIR/IIR QMF-bank design II of Sec. 3.1.2 is considered as an alternative.

In a first step, the allpass sub-filters of the *analysis filters* according to Eq. (3.16) have to be determined in order to achieve a frequency selectivity similar to that of the original FIR analysis filters. A direct approach to calculate the allpass coefficients of these filters is to minimize the stopband energy of Eq. (3.21). This non-linear optimization problem can be solved, e.g., by means of the MATLAB function `fmincon` [TM09]. However, this approach turns out to be less suitable as the final result depends strongly on the initial solution if $K_0, K_1 > 1$. For allpass degrees $K_0, K_1 \geq 3$, no further improvements of the frequency selectivity have been obtained. In contrast, the use of the equiripple IIR lowpass filter design of [ZY99] shows a superior performance as it converges to a unique solution even for higher allpass filter degrees. This algorithm has been executed for different stopband frequencies Ω_s to find the most favorable design.

[4] In principle, the FIR QMF-bank of ITU-T Rec. G.729.1 can also be used for the outer filter-bank. However, a comparison with the proposed IIR QMF-bank is questionable in this case as this FIR QMF-bank is not designed for a sampling rate of 32 kHz.

[5] The design method for the QMF-bank is not specified in [ITU06], but the coefficients of the prototype lowpass filter used in the C source code are given by the 64D design listed in [CR83, Chap. 7].

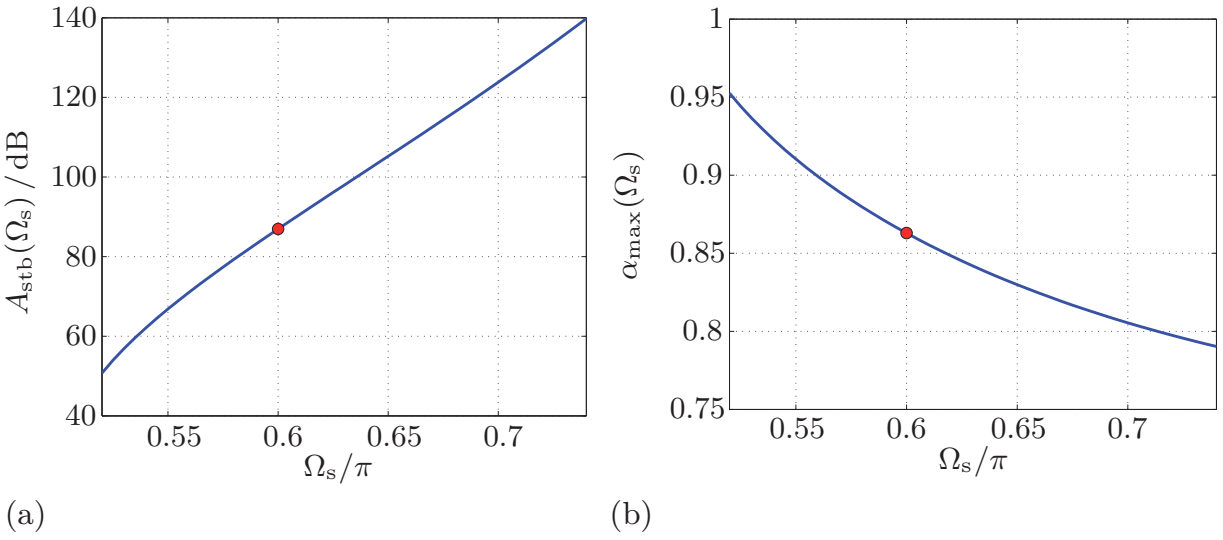

Figure 6.2: *Evaluation of the equiripple IIR lowpass filter design of [ZY99] with real allpass coefficients and degrees $K_0 = 3$, $K_1 = 2$ for different stopband frequencies Ω_s. The dots mark the chosen design at $\Omega_s = 0.6\,\pi$:*
(a) *stopband attenuation*
(b) *magnitude of the largest allpass pole.*

Figure 6.2 shows the obtained results. Figure 6.2-a illustrates the well-known trade-off between the conflicting goals for a low transition bandwidth and a high stopband attenuation. Furthermore, the absolute values for the allpass poles are also important here. For the proposed IIR QMF-bank design, a pole close to one requires synthesis polyphase filters of high degrees to achieve a sufficient phase equalization according to Sec. 3.1.2. Besides, poles near the unit circle are also problematic w.r.t. a fixed-point implementation. Figure 6.2-b reveals that a higher stopband frequency Ω_{s} yields a lower magnitude for the largest allpass pole

$$\alpha_{\max} = \max_{m,i} \{|\alpha_i(m)|\}\,; \quad m \in \{\,1, 2, \ldots, K_i\,\}; \quad i \in \{\,0, 1\,\}\,. \tag{6.1}$$

The design marked by the dots has been found most suitable for the intended application. The allpass filters of Eq. (3.18) have degrees $K_0 = 3$ and $K_1 = 2$. Their poles according to Eq. (2.48b) are real ($a_i(m) = \alpha_i(m)$) and given by

$$\begin{aligned}
&\alpha_0(1) = -0.054237173613906; \quad \alpha_1(1) = -0.621126121753022\\
&\alpha_0(2) = -0.398827412661577; \quad \alpha_1(2) = -0.199719749994964\\
&\alpha_0(3) = -0.862931529517508\,.
\end{aligned} \tag{6.2}$$

Figure 6.3 shows that these equiripple IIR analysis filters achieve a higher stopband attenuation as well as a lower transition bandwidth in comparison to the FIR analysis filters of the Johnston design being used for the original G.729.1 codec.

For the *synthesis* QMF-bank, the design II of Sec. 3.1.2.3 is chosen as non-cancelled alias components can have a noticeable impact for the considered subband coding system. In contrast, the design I of Sec. 3.1.2.2 turned out to be less suitable, despite its

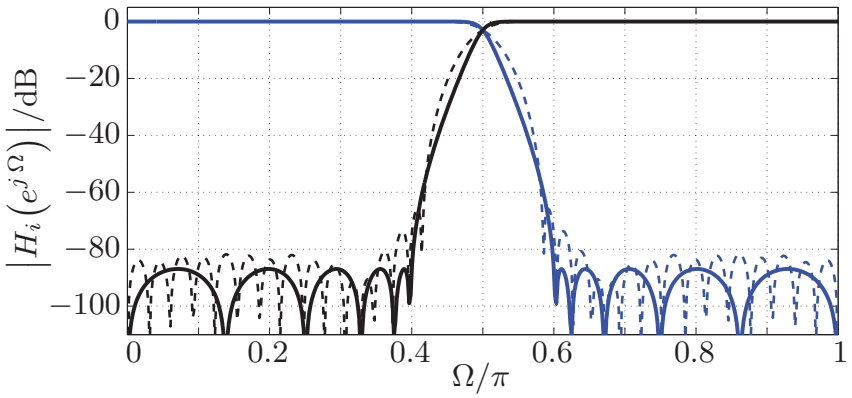

Figure 6.3: *Magnitude responses of different analysis filters: The dashed lines correspond to the FIR analysis filters of ITU-T Rec. G.729.1 and the solid lines mark the alternative equiripple IIR analysis filters.*

lower signal delay in comparison to design II, as phase equalizers with a rather high filter degree are needed to achieve a sufficient aliasing cancellation.

For the phase equalizer of Eq. (3.34), the parameters

$$J_i(m) = \begin{cases} 4 & \text{for } i = 0 \quad \wedge \quad m = 3 \\ 0 & \text{otherwise} \end{cases} \tag{6.3}$$

are taken. Hence, only the allpass pole $\alpha_0(3)$, which is closest to the unit circle, is considered by the phase equalization, which turned out to be sufficient to avoid audible phase distortions. It follows from Eq. (3.46), Eq. (3.36) and Eq. (6.3) that the overall transfer function of the inner QMF-bank is equal to the linear transfer function

$$T_{\text{lin}}^{(\text{inner})}(z) = z^{-1} \frac{1 - \left(\alpha_0(3) \cdot z^2\right)^{16}}{z^{32} - \left(\alpha_0(3)\right)^{16}} \prod_{i=0}^{1} \prod_{m=1}^{2} \frac{1 - \alpha_i(m) \cdot z^2}{z^2 - \alpha_i(m)} \,. \tag{6.4}$$

with $\alpha_i(m)$ given by Eq. (6.2). The frequency response of the overall transfer function for the FIR QMF-bank is obtained by Eq. (C.3). Overall magnitude response and group delay of the two considered QMF-banks are contrasted in Figure 6.4. The overall transfer function of the IIR QMF-bank is an allpass filter, which results in a constant magnitude response and a non-linear phase response. In contrast, the overall transfer function of the FIR QMF-bank has a linear phase response, but a non-constant magnitude response. Figure 6.4-b shows that the frequency dependent group delay of the IIR QMF-bank is significantly lower than the constant group delay of its FIR counterpart. Informal listening tests with different audio samples have revealed that the frequency dependent group delay of the IIR filter-bank design causes no audible signal distortions.

6.1.2.2 Fixed-Point Implementation

In practice, digital systems are implemented by arithmetic operations with finite precision as used, for example, on a (fixed-point) DSP. This leads to round-off effects, which

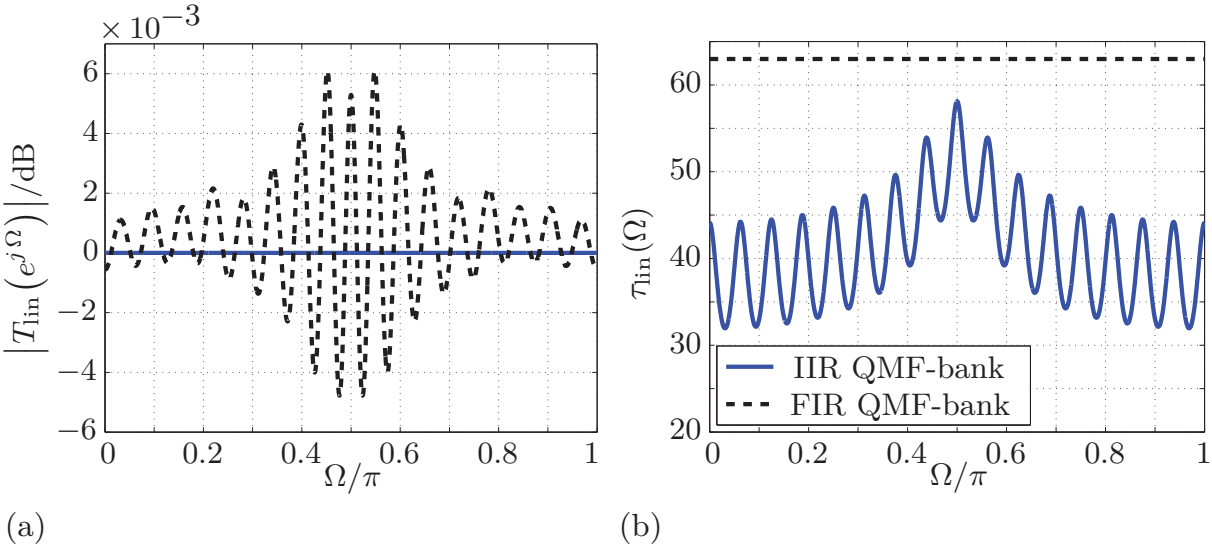

Figure 6.4: *Analysis of the overall transfer functions of the FIR QMF-bank of Rec. G.729.1 (dashed lines) and the proposed IIR QMF-bank (solid lines):*
(a) *magnitude response of the linear transfer function*
(b) *group delay of the linear transfer function.*

can have a significant impact on the performance of a system. Therefore, the investigation of such effects for the devised IIR QMF-bank is an important issue regarding its applicability.

The proposed IIR QMF-banks consists solely of different allpass polyphase filters. It is beneficial to implement these allpass filters in a cascade form according to Eq. (2.48). The single allpass filters of first order in turn can also be implemented differently. In [LV07a], the effects of fixed-point arithmetic are analyzed for five different allpass filter implementations using a linear quantization noise model, e.g., [Vai93, Jac96, OSB99]. It models rounding errors as quantization noise added at summation nodes. This noise is assumed to be wide-sense stationary, uniformly distributed and uncorrelated with the input signal of the quantizer. The theoretical analysis reveals that the implementation of Figure 2.8 is of special interest.[6] The calculation of its *noise gain*, which describes the amplification of the quantization noise by a system [Vai93], yields

$$\mathcal{G}_{\text{noise}} = \frac{\sigma_{\text{out}}^2}{\sigma_q^2} = \frac{1}{1-\alpha^2} \tag{6.5}$$

where σ_q^2 represents the variance of the input (quantization) noise and σ_{out}^2 marks the variance of the output noise. Due to Eq. (6.2), the noise gain for the used allpass filters of first order lies only between $1 < \mathcal{G}_{\text{noise}} < 4$. Besides, the input signal of the implementation of Figure 2.8 needs not to be scaled in order to reduce overflows by means of the $\mathcal{L}_2$-norm scaling rule [Vai93, LV07a].

[6] In [LV07a], the fixed-point effects for different allpass filter forms are investigated w.r.t. allpass transformed systems, but the obtained results apply also to the considered allpass-based QMF-bank.

Table 6.1: *SQNR for different QMF-banks and audio signals taken from the EBU-SQAM database.*

audio sequence	FIR QMF-bank	IIR QMF-bank
sinus sweep	84.52 dB	83.10 dB
guitar (Sarasate)	68.09 dB	62.01 dB
female speech	73.90 dB	68.25 dB

In order to investigate effects due to fixed-point arithmetic, the discussed IIR QMF-bank has been implemented in C using the 16 bit fixed-point operations of ITU-T [ITU05], which emulate a generic fixed-point DSP.[7] The effects of rounding errors are measured here by the *signal-to-quantization-noise ratio* (SQNR). It is determined by the difference between the output signals of the floating-point and fixed-point implementation, $y_{\mathrm{flo}}(k)$ and $y_{\mathrm{fix}}(k)$, according to

$$\mathrm{SQNR} = \frac{\sum\limits_{k} y_{\mathrm{flo}}^2(k)}{\sum\limits_{k} \big(y_{\mathrm{flo}}(k) - y_{\mathrm{fix}}(k)\big)^2} \,. \tag{6.6}$$

The results for the considered FIR QMF-bank and IIR QMF-bank are compiled in Table 6.1. The fixed-point implementation of the FIR QMF-bank achieves a slightly higher SQNR in comparison to the IIR QMF-bank. The SQNR of the IIR QMF-bank can of course be improved at the price of an increased computational complexity. However, informal listening tests with different speech and audio signals have revealed no audible differences between the input and output signals obtained by the fixed-point implementations of the FIR QMF-bank and IIR QMF-bank (without subband coding). Besides, the signal distortions due to the non-perfect reconstruction of the QMF-bank as well as its fixed-point implementation are lower than the distortions due to coding operations, especially at lower bit rates.

6.1.2.3 Signal Delay & Algorithmic Complexity

Algorithmic signal delay and computational complexity of the FIR QMF-bank and IIR QMF-bank are contrasted in Table 6.2. The computational complexity of the two filterbanks is counted in *weighted million operations per second* (WMOPS) and determined by the C floating-point implementation submitted to ITU-T.[8] It can be observed that the computational complexity of the IIR QMF-bank is about 28% lower than for the FIR QMF-bank.

[7] The submission of a codec implementation in fixed-point was not part of the candidate proposal for ITU-T [GKL+09].

[8] The number of WMOPS is used for the evaluation of different speech codecs by ITU-T and provides a rough measure for the computational complexity of a system if implemented on a DSP.

Table 6.2: *Computational complexity measured in weighted million operations per second (WMOPS) and signal delay for the inner FIR QMF-bank and IIR QMF-bank ($f_s = 16$ kHz).*

	FIR QMF-bank	IIR QMF-bank
analysis filter-bank	0.6549 WMOPS	0.2846 WMOPS
synthesis filter-bank	0.7035 WMOPS	0.6929 WMOPS
sum	1.3584 WMOPS	0.9775 WMOPS
signal delay D'_{o}	3.9375 ms	2.4375 ms

The algorithmic *signal delay* of the filter-banks is measured by the cross-correlation between input signal $x(k)$ and reconstructed input signal $\hat{x}(k)$ for a unit sample sequence as input signal

$$D_{\mathrm{o}} = \arg\left\{\max_{\kappa}\left\{\mathrm{corr}\left\{x(k-\kappa), \hat{x}(k)\right\}\right\}\right\} . \tag{6.7}$$

This delay calculation accounts for the frequency dependent group delay of the IIR QMF-bank. The actual signal delay (in seconds) is then given by

$$D'_{\mathrm{o}} = \frac{D_{\mathrm{o}}}{f_{\mathrm{s}}} . \tag{6.8}$$

Table 6.2 reveals that the replacement of the FIR QMF-bank by the IIR QMF-bank results in a signal delay reduction of about 38%.

6.1.3 Outer QMF-Bank

The design of the outer QMF-bank for the SWB extension is done in a similar manner as the inner QMF-bank taking into account the higher sampling frequency of 32 kHz (see also Figure 6.1). The IIR lowpass prototype filter is designed by the algorithm of [ZY99] for allpass filter decrees $K_0 = K_1 = 3$ and a stopband frequency $\Omega_{\mathrm{s}} = 0.57\,\pi$. This yields the real allpass poles

$$\begin{aligned}
&\alpha_0(1) = -0.358332481220107; \quad \alpha_1(1) = -0.905525274279610\\
&\alpha_0(2) = -0.049358046260363; \quad \alpha_1(2) = -0.181159826230283\\
&\alpha_0(3) = -0.727333561657933; \quad \alpha_1(3) = -0.546113666698959 .
\end{aligned} \tag{6.9}$$

The magnitude responses of the obtained analysis filters are plotted in Figure 6.5. These IIR filters achieve a stopband attenuation of 90 dB, which is about 3 dB higher as for the analysis filters of the inner IIR QMF-bank shown in Figure 6.3. For the phase equalizer of Eq. (3.34), the number of stages are now given by

$$J_i(m) = \begin{cases} 4 & \text{for } i = 1 \quad \wedge \quad m = 1 \\ 0 & \text{otherwise.} \end{cases} \tag{6.10}$$

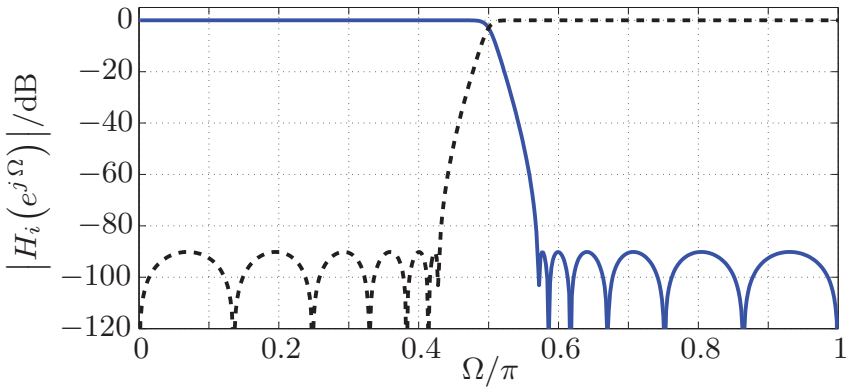

Figure 6.5: *Magnitude responses of the analysis filters of the outer QMF-bank.*

Again, only the largest allpass pole $\alpha_1(1)$ is considered by the phase equalizer, which turned out to be sufficient to avoid audible phase or group delay distortions, respectively.

As indicated in Figure 6.1, a group delay compensation is needed to account for the signal delay of the inner QMF-bank. The frequency response of the FIR QMF-bank has a linear phase response according to Eq. (C.3). Therefore, a frequency independent group delay of 3.9375 ms needs to be compensated according to Figure 6.4-b, which can be accomplished by simple delay elements (shift registers) at encoder and decoder.

For the IIR QMF-bank, a frequency dependent group delay compensation is needed (see also Figure 6.4). This group delay compensation is derived by splitting the transfer function of the inner QMF-bank according to Eq. (6.4) into two parts

$$T_{\text{lin}}^{(\text{inner})}(z) = \underbrace{\prod_{i=0}^{1}\prod_{m=1}^{2}\frac{1-\alpha_i(m)\cdot z^2}{z^2-\alpha_i(m)}}_{=C_{\text{I}}(z)} \cdot \underbrace{z^{-1}\,\frac{1-\left(\alpha_0(3)\cdot z^2\right)^{16}}{z^{32}-\left(\alpha_0(3)\right)^{16}}}_{=C_{\text{II}}(z)} . \tag{6.11}$$

A filter with system function $C_{\text{I}}(z)$ is taken for the group delay compensation at the encoder to account approximately for the group delay of the inner IIR analysis filter-bank. Accordingly, a filter with system function $C_{\text{II}}(z)$ is employed for the group delay compensation at the decoder.

The overall transfer function of the three-channel QMF-bank with group delay compensation (and without any coding operations) is analyzed in Figure 6.6. The magnitude response of the transfer function is a constant, if the IIR QMF-bank is used as inner filter-bank. If the FIR QMF-bank is used for the core codec, magnitude distortions occur within the region $\Omega \in [0, \pi/2]$ in compliance with Figure 6.4-a.

Figure 6.6-b shows that a significantly lower group delay is achieved by using the IIR QMF-bank instead of the FIR QMF-bank as inner filter-bank. Informal listening tests have revealed that the frequency dependency of the group delay causes no noticeable distortions in both cases.

The computational complexity of the outer QMF-bank and the group delay compensation are listed in Table 6.3. The WMOPS are again determined by means of the C floating-point code submitted to ITU-T. A comparison with Table 6.2 shows that the complexity of the inner IIR QMF-bank is 0.381 WMOPS lower than for the inner

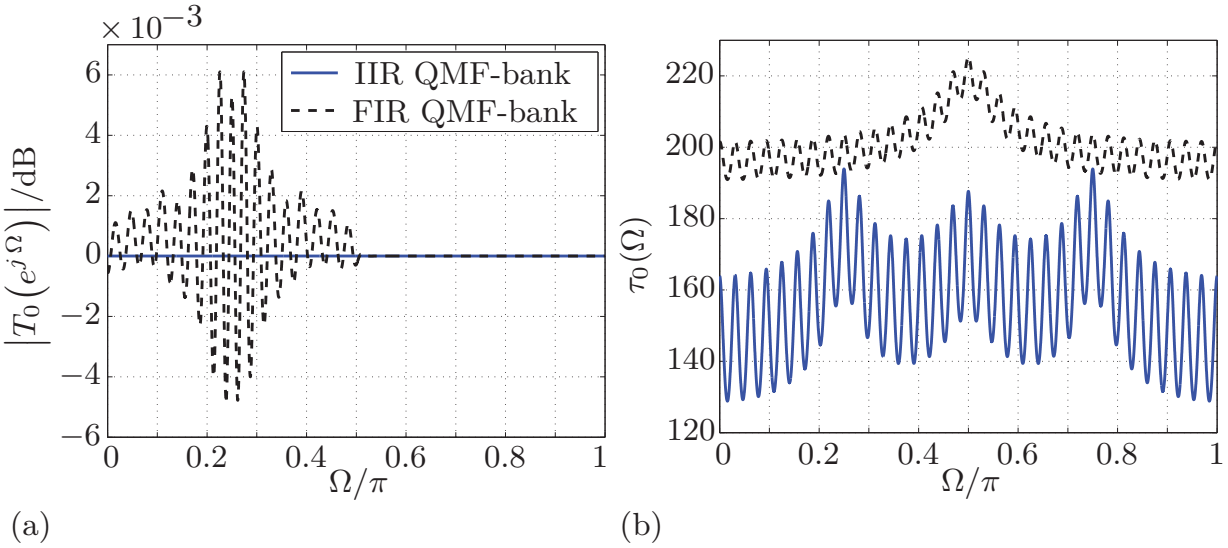

Figure 6.6: *Analysis of three-channel filter-bank where the inner QMF-bank is either the FIR QMF-bank of Rec. G.729.1 (dashed lines) or the proposed IIR QMF-bank (solid lines):*
(a) *magnitude response of the overall transfer function*
(b) *group delay of the overall transfer function.*

Table 6.3: *Computational complexity of outer IIR QMF-bank and group delay (GD) compensation ($f_s = 32$ kHz).*

	encoder	decoder	sum
IIR QMF-bank	0.2846 WMOPS	0.6929 WMOPS	0.9775 WMOPS
GD compensation	0.6085 WMOPS	0.1606 WMOPS	0.7691 WMOPS

FIR QMF-bank. The group delay compensation for the inner IIR QMF-bank causes an additional complexity of 0.388 WMOPS. For comparison, the complete SWB extension has a complexity of about 15 WMOPS. The calculation of the signal delay of the outer QMF-bank by Eq. (6.7) and Eq. (6.8) results a value of only 2.21875 ms.

The overall ITU-T test results for the complete (mono) codec are documented in [GKL+09]. The proposed codec was the only candidate who passed *all* requirements for mono coding as defined in the 'Terms of Reference' [ITU08].

6.2 Low Delay Speech Enhancement

The concept of the *filter-bank equalizer* (FBE) developed in Chap. 5 allows to perform adaptive subband filtering with a low signal delay. In addition, the allpass transformed FBE can achieve an approximately Bark-scaled frequency division with a much lower algorithmic complexity than allpass transformed or tree-structured AS FBs. These benefits bring about that the FBE is of special interest for *speech enhancement algorithms* as employed in cell phones, hands-free devices, or digital hearing aids where the overall signal delay and computational complexity of the filter-bank is of special importance

[SBS+06, LV07b, LV09a, SLV08]. In the following, the use of the FBE and its LDF extension for noise reduction, speech dereverberation and near-end listening enhancement is investigated in more detail.

6.2.1 Noise Reduction

A frequent problem of many communication devices is that the received signal

$$x(k) = s(k) + u(k) \tag{6.12}$$

contains the desired speech signal $s(k)$ as well as unwanted noise $u(k)$. The aim of a noise reduction system is to recover an estimate $\hat{s}(k)$ of the original speech signal $s(k)$. Numerous algorithms for noise reduction have been proposed, which are reviewed, e.g., in [BMC05, VM06, Loi07]. The well-known overlap-add method, which is a PPN DFT AS FB as described in Sec. 2.3, is mostly employed for this purpose. However, several authors have pointed out the benefits of using a non-uniform (Bark-scaled) AS FB for speech enhancement, e.g., [EG97, GEH98, GLH03, dHCG03, Coh01, PPB04, DMFB07]. One common rationale for these approaches is that a filter-bank with a non-uniform, approximately Bark-scaled frequency resolution incorporates a perceptual model for the non-uniform frequency resolution of the human auditory system. Another reason is that on average most of the energy and harmonics of speech signals are located at the lower frequencies. However, most proposals are based on AS FBs with subsampling, which exhibit a rather high signal delay. The following analysis will show that the FBE is an attractive alternative.

6.2.1.1 System Overview

The use of different filter-banks for noise reduction is now investigated based on [LV08a]. The enhancement of the noisy speech is performed by the DFT AS FB, the GDFT FBE, the MA LDF and AR LDF. The uniform and allpass transformed version of these filter-banks are used each.[9] A real allpass coefficient of $a = 0.4$ is taken, which yields a good approximation of the Bark scale for the considered sampling frequency of 8 kHz according to Eq. (4.7). In all cases, a transform size of $M = 64$ channels and a linear-phase FIR prototype filter of length $L = 65$ are used.[10]

A square-root Hann window derived from Eq. (5.18) is employed as common prototype filter for the DFT AS FB. The uniform DFT AS FB according to Figure 2.4 with a subsampling rate of $R = 32$ is used as well as the allpass transformed AS FB of Figure 4.6 with a subsampling rate of $R = 8$. The use of a higher subsampling rate R is possible, but increases the signal delay significantly since subband filters with a higher stopband attenuation are needed to achieve a sufficient aliasing cancellation. The LS

[9] The low delay filter of Sec. 5.4 can be seen as a filter-bank system as it is derived from the filter-bank equalizer or filter-bank summation method, respectively.

[10] A lower number of frequency channels can be used for warped filter-banks where a value of $M = 256$ is often preferred for speech enhancement using the uniform DFT filter-bank (at 8 kHz sampling frequency). However, such different configurations are not considered to ease the comparison of the filter-banks.

FIR phase equalizer of Sec. 3.3.4.1 with a filter degree of $N = 141$ is applied to the filter-bank output (see Figure 4.6).

The GDFT FBE is implemented in the transposed direct form according to Figure 5.7. The MA LDF possesses a filter degree of $N_{\mathrm{ld}} = 48$. The LS FIR phase equalizer with filter degree $N = 80$ and $N = 56$ is applied to the warped FBE and the warped MA LDF, respectively. The considered AR LDF has a filter degree of $N_{\mathrm{ld}} = 16$. The cross-fading technique according to Eq. (5.54) is applied to the filter output signals in order to avoid filter-ringing artifacts. A subsampling rate of $R = 64$ is taken for the analysis filter-banks of FBE and LDF.

The spectral gain factors are computed by the super-Gaussian joint maximum a posteriori (MAP) estimator of [LV05d]. This joint spectral amplitude and phase estimator is derived by the more accurate assumption that the real and imaginary parts of speech DFT coefficients are rather Laplace distributed (considered here) or Gamma distributed than Gaussian distributed. The needed *a priori* SNR is determined by the decision-directed approach [EM84] with a fixed smoothing parameter of 0.9. The short-term noise power spectral density (PSD) is estimated by minimum statistics [Mar01]. Speech presence uncertainty is taken into account by applying soft-gains [MCA99]. Independent of the subsampling rate R of the filter-bank, the spectral gain factors are always adapted at intervals of 64 sample instants and no individual parameter tuning is performed to ease the comparison.

The used audio signals of 8 kHz sampling frequency are taken from the noisy speech corpus NOIZEUS presented in [HL06]. A total of 20 sentences spoken by male and female speakers is used, each disturbed by five different, non-stationary noise sequences (airport, babble, car, station and street noise) with SNRs between 0 dB and 15 dB.

The quality of the enhanced speech is evaluated by informal listening tests and instrumental quality measures described in App. E. As time-domain measures, the *segmental signal-to-noise ratio* $\mathrm{SNR}_{\mathrm{seg}}$ and the *segmental noise attenuation* $\mathrm{NA}_{\mathrm{seg}}$ are used. The *cepstral distance* CD is used as frequency-domain measure. For all instrumental measures, a frame size of $M_{\mathrm{m}} = 256$ is used and 40 cepstral coefficients are considered for the cepstral distance (CD) measure. The signal delay of the systems is determined by Eq. (E.2) and the complexity by means of Table 5.1 and Table 5.2.

6.2.1.2 Simulation Results for Uniform Filter-Banks

The instrumental speech quality obtained with the uniform filter-banks is plotted in Figure 6.7. The FBE achieves the same (or even better) objective speech quality as the AS FB. Table 6.4 reveals that the FBE possesses a higher complexity, but achieves a significantly lower delay than the AS FB. The MA and AR LDF achieve a further reduction of the signal delay and algorithmic complexity. Contrary to the MA LDF, the enhancement by the AR LDF leads to a significantly decreased *objective* speech quality according to Figure 6.7.[11] The AR filter approximation causes phase modifications, which can have a very detrimental effect on the instrumental measures.[12] However,

[11] Here, the terms *instrumental quality* and *objective quality* are used interchangeably.

[12] Such an effect can also be observed for warped filter-banks with an imperfect phase compensation.

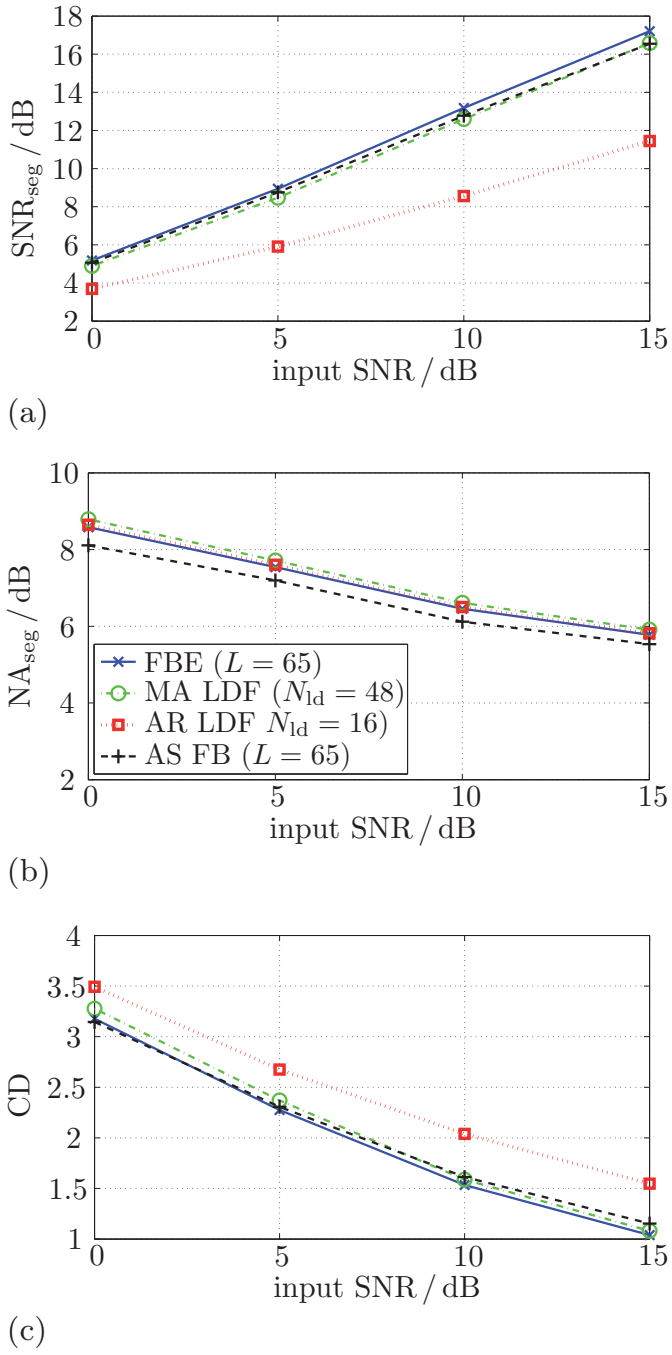

Figure 6.7: *Objective speech quality obtained by the uniform FBE (Figure 5.2), the uniform MA and AR LDF (Figure 5.9) and the uniform DFT AS FB (Figure 2.4) with $M = L - 1 = 64$ channels:*
(a) *segmental SNR*
(b) *segmental noise attenuation*
(c) *cepstral distance.*

informal listening tests have revealed barely audible differences for the perceived *subjective* speech quality. Therefore, a perceptual evaluation of the speech quality (PESQ) according to [ITU01] has been conducted in addition. This PESQ measure ranges from -0.5 (bad quality) to 4.5 (excellent quality). The PESQ measure is mainly used for

Table 6.4: *Measured signal delay and average algorithmic complexity per sample for the uniform filter-banks* ($M = L - 1 = 64$).

uniform filter-bank	signal delay [samples]	summations (real)	multiplications (real)	delay elements
AS FB	64	101	31	256
FBE	32	83	142	256
MA LDF	24	67	64	240
AR LDF	0-2	75	74	272

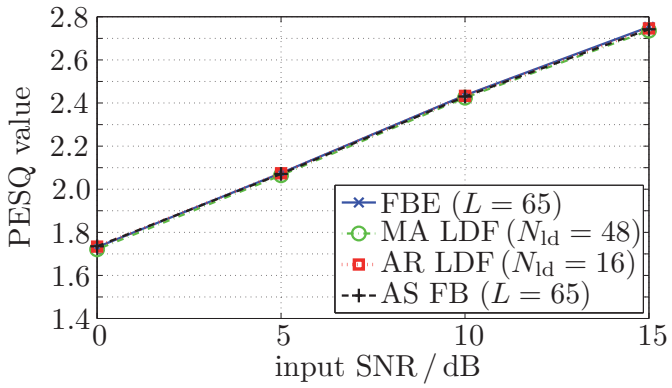

Figure 6.8: *Perceptual evaluation of the speech quality for the enhanced speech* $\hat{s}(k)$ *achieved with the uniform filter-banks.*

the assessment of speech codecs, but also employed as perceptual quality measure for speech enhancement systems, e.g., [BMC05]. The measured PESQ values in Figure 6.8 show that the four uniform filter-banks achieve all an almost identical perceptual speech quality. The PESQ measure is no all-embracing quantity for the subjective speech quality, but it complies well with the results of our informal listening tests. Thus, the low delay filter concept is suitable to achieve a further reduced signal delay in a flexible and simple manner with negligible loss for the perceived subjective speech quality.

6.2.1.3 Simulation Results for Warped Filter-Banks

The curves for the objective speech quality obtained by means of the different allpass transformed filter-banks are shown in Figure 6.9. The measured PESQ values are not plotted again since they are as close together as in Figure 6.8 but all about 0.25 PESQ units higher. Thus, the warped filter-banks achieve an improved instrumental speech quality in comparison to the corresponding uniform filter-banks. These results comply with our informal listening tests where the speech enhanced by the warped filter-banks was rated to be superior.

The measured signal delay and algorithmic complexity of the used allpass transformed filter-banks are listed in Table 6.5. A comparison with Table 6.4 shows the increase of signal delay and algorithmic complexity due to the allpass transformation, if the *same* values for M and L are taken (which is usually not the case). The warped

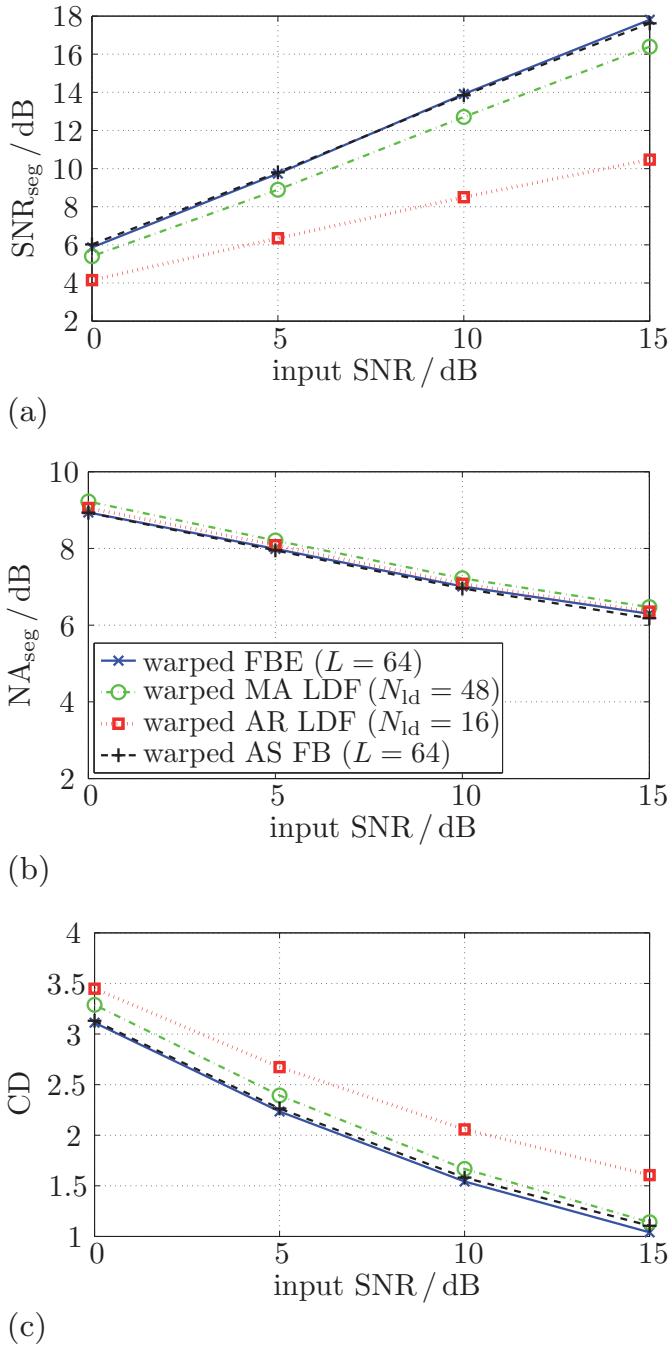

Figure 6.9: *Objective speech quality obtained by the warped FBE (Figure 5.8), the warped MA and AR LDF (Sec. 5.4.5) and the warped DFT AS FB (Figure 4.6) with $M = L - 1 = 64$ channels and warping coefficient $a = 0.4$:*
(a) *segmental SNR*
(b) *segmental noise attenuation*
(c) *cepstral distance.*

FBE causes a significantly lower delay and possesses a lower complexity than the corresponding warped AS FB, but achieves the same objective and subjective speech quality.

As for the uniform filter-banks, a further reduction of the signal delay and algorithmic complexity can be achieved by the low delay filter approximation with no noticeable

Table 6.5: *Measured signal delay and average algorithmic complexity per sample for the allpass transformed filter-banks* ($M = L - 1 = 64$).

warped filter-bank	signal delay [samples]	summations (real)	multiplications (real)	delay elements
AS FB	141	605	518	397
FBE	80	418	478	336
MA LDF	56	347	335	296
AR LDF	0-2	268	268	274

loss for the *subjective* speech quality. The AR LDF is a minimum-phase system and causes a very low signal delay of only a few sample instants.

6.2.2 Speech Dereverberation

The FBE can also be used for joint noise reduction and speech dereverberation with low delay, which is proposed originally in [LV08e, LV09d]. In the following, the general concept of this approach is only outlined where a more detailed description can be found in [LV09a] and the references cited within.

In practice, the speech recorded by a device is often a superposition of reverberant speech $z_\mathrm{r}(k)$ and additive (background) noise $u(k)$ according to

$$\begin{aligned} x(k) &= z_\mathrm{r}(k) + u(k) \\ &= \sum_{l=0}^{L_\mathrm{r}-1} s(k-l) \cdot h_\mathrm{r}(l,k) + u(k) \end{aligned} \tag{6.13}$$

with $h_\mathrm{r}(l,k)$ representing the time-varying room impulse response of (possibly infinite) length L_r between source and receiver. The reverberant speech $z_\mathrm{r}(k)$, in turn, can be decomposed into its early and late reverberant part

$$z_\mathrm{r}(k) = \underbrace{\sum_{l=0}^{L_\mathrm{e}-1} s(k-l) \cdot h_\mathrm{r}(l,k)}_{= z_\mathrm{e}(k)} + \underbrace{\sum_{l=L_\mathrm{e}}^{L_\mathrm{r}-1} s(k-l) \cdot h_\mathrm{r}(l,k)}_{= z_\mathrm{l}(k)} \; . \tag{6.14}$$

The early reverberant speech $z_\mathrm{e}(k)$ – and not the speech signal $s(k)$ – is here taken as target signal. This allows to suppress the late reverberant speech $z_\mathrm{l}(k)$ and additive noise $u(k)$ by modelling them as uncorrelated noise processes and to apply well-known speech enhancement techniques such as Wiener filtering or spectral subtraction. This concept has been introduced by Lebart et al. [LBD01] and further improved by Habets [Hab07]. The spectral gain factors can be calculated by means of the *a posteriori signal-to-interference ratio* (SIR)

$$\zeta_\mathrm{post}(i,\kappa) = \frac{|Z_\mathrm{r}(i,\kappa)|^2}{\sigma_{z_\mathrm{l}}^2(i,\kappa) + \sigma_u^2(i,\kappa)} \;\; \forall \;\; i \in \{\,0, 1, \ldots, M-1\,\} \tag{6.15}$$

or the *a priori* SIR

$$\zeta_{\text{prio}}(i,\kappa) = \frac{|Z_{\text{e}}(i,\kappa)|^2}{\sigma_{z_1}^2(i,\kappa) + \sigma_u^2(i,\kappa)} \tag{6.16}$$

with $Z_{\text{r}}(i,\kappa)$ marking the spectral coefficients of the reverberant speech at sample instant κ. The spectral coefficients of the early reverberant speech $Z_{\text{e}}(i,\kappa)$ are unknown, but the *a priori* SIR can be estimated by the decision-directed approach of [EM85]. The spectral variance of the noise $\sigma_u^2(i,\kappa)$ can be estimated, e.g., by minimum statistics [Mar01]. The spectral variance of the late reverberant speech $\sigma_{z_1}^2(i,\kappa)$ can be determined by a model-based approach, which is derived by a statistical model of the room impulse response [LBD01, Hab07]. This model-based approach requires a blind estimation of the reverberation time, which can be performed by the algorithm developed in [LV08d, LYJV10].

The *a posteriori* SIR of Eq. (6.15) and *a priori* SIR of Eq. (6.16) reduce to the *a posteriori* SNR and *a priori* SNR, if the spectral variance of the late reverberant speech is (assumed to be) zero, i.e., $\sigma_{z_1}^2(i,\kappa) \equiv 0$. Thus, the algorithm can be seen as a kind of 'generalized' noise reduction. Accordingly, the benefits of using the FBE instead of a common DFT AS FB for the adaptive filtering are essentially the same as for the noise reduction system treated before. Therefore, the application of the FBE for this purpose should not be treated in more detail at this point.

Finally, it should be noted that speech enhancement algorithms for cell phones or digital hearing aids are often implemented on a DSP with *fixed-point* arithmetic. As for the previously treated IIR QMF-bank designs for speech and audio coding, the investigation of rounding errors due to fixed-point arithmetic is an important issue regarding the applicability of the (recursive) FBE. A comprehensive investigation of these aspects is conducted in [LV04b, LV07a] where it is shown that these rounding effects can be handled by an appropriate design and implementation of the system.

6.2.3 Near-End Listening Enhancement

The use of a cell phone often takes place in noisy environments, which can significantly impair the conversation. One common problem is that a noisy speech signal is often recorded by the microphone and transmitted to the *far-end* speaker. A way to enhance the noisy signal before speech coding and transmission is to employ a noise reduction system as treated before. Another problem is that the *near-end* speaker might perceive a mixture of the far-end speech signal and acoustical background noise. This can lead to a reduced *speech intelligibility* and increased listening efforts, respectively. This problem can be tackled by means of *near-end listening enhancement* as proposed in [SV06]. In the following, it is shown that the use of the *filter-bank equalizer* is especially suitable for this purpose based on [SLV08] where this idea is originally presented.

6.2.3.1 Concept

This principle of near-end listening enhancement is illustrated in Figure 6.10 where the involved A/D and D/A conversion is not considered for the sake of simplicity. The near-end speaker listens to a superposition of a processed far-end speech signal $\bar{s}(k)$

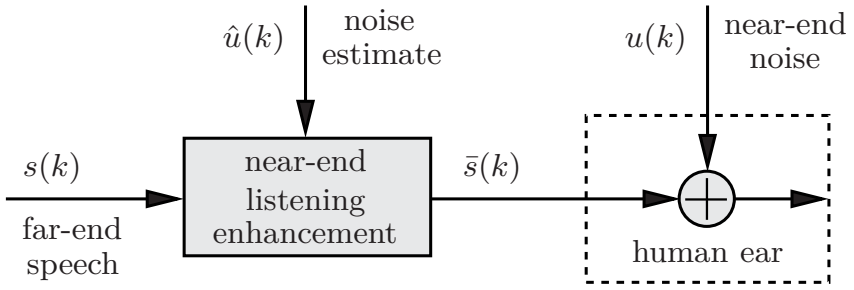

Figure 6.10: *Principle of near-end listening enhancement.*

emitted by the loudspeaker and near-end background noise $u(k)$. The aim of near-end listening enhancement is thereby to modify the original speech signal $s(k)$ of the far-end speaker in such a manner that the near-end speaker experiences an improved speech intelligibility. This is accomplished by adaptive subband filtering based on an estimation of the background noise $\hat{u}(k)$.

The original proposal for near-end listening enhancement employs the overlap-add method [SV06]. The replacement by the *warped FBE*, as proposed in [SLV08], is motivated by several reasons: The aim of near-end listening enhancement is to improve the speech intelligibility, which can be measured by the *speech intelligibility index* (SII) [ANS97]. The calculation of the SII is done within critical frequency bands, which correspond to those of the Bark scale. This motivates the use of an allpass transformed filter-bank due to is ability to mimic the Bark scale with high accuracy, cf., Sec. 4.1.1. An advantage of the allpass transformed FBE in comparison to an allpass transformed AS FB with subsampling is thereby its lower signal delay and computational complexity as shown in Sec. 5.2. The warped AR LDF of Sec. 5.4.5 can further reduce the algorithmic signal delay to only a few samples. This ability to achieve a low signal delay is a further motivation for using the FBE or its LDF extension. A promising application of near-end listening enhancement by means of the FBE are cell phones where a low signal delay is essential, cf., [SBS+06].

The use of the warped FBE for near-end listening enhancement is sketched in Figure 6.11. In contrast to the FBE shown in Figure 5.8, a second analysis filter-bank is now needed for the noise estimation as indicated by Figure 6.10. The DFT instead of the GDFT is used for the analysis filter-bank as only magnitude spectra are needed for the spectral gain calculation described in the following.

6.2.3.2 Spectral Gain Calculation

According to [SV06], the time-varying gain factors $W(i,\kappa)$ are chosen in a way that the ratio of the short-term PSD of the amplified speech $\Phi_{\bar{s}\bar{s}}(i,\kappa)$ and the short-term PSD of the noise signal $\Phi_{uu}(i,\kappa)$ should be greater than or equal to a target SNR ζ_o:

$$\frac{\Phi_{\bar{s}\bar{s}}(i,\kappa)}{\Phi_{uu}(i,\kappa)} \geq \zeta_\mathrm{o} \tag{6.17}$$

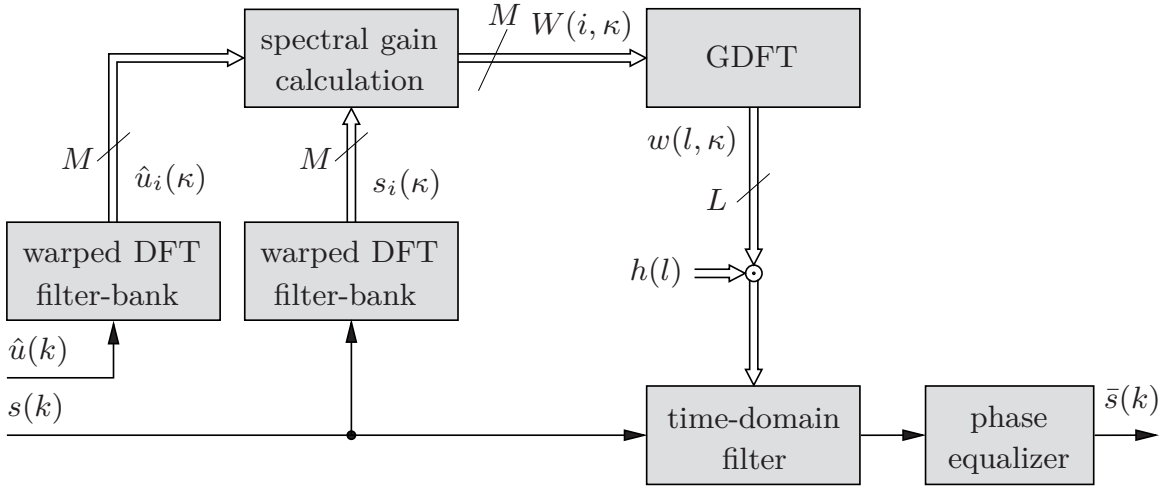

Figure 6.11: *Near-end listening enhancement by means of the warped FBE.*

with, e.g., $\zeta_o \mathrel{\widehat{=}} 15\,\text{dB}$. In order to assure that the speech signal is not attenuated in a noise-free environment, the gain factors should not be lower than one

$$W'(i,\kappa) = \max\left\{\sqrt{\zeta_o \frac{\Phi_{uu}(i,\kappa)}{\Phi_{ss}(i,\kappa)}}, 1\right\} . \tag{6.18}$$

The spectral coefficients of the speech are weighted according to the spectral characteristics (PSD) of the noise signal. This approach, however, 'over-amplifies' spectral speech components with low energy since it tries to raise anything over the noise level by the same amount ζ_o independent of the original signal strength. This effect can be reduced by limiting the gain factors $W'(i,\kappa)$ to a maximum gain factor $W_{\max}$ with, e.g., $W_{\max} \mathrel{\widehat{=}} 30\,\text{dB}$. Hence, the spectral gain factors are finally given by

$$W(i,\kappa) = \min\left\{\max\left\{\sqrt{\zeta_o \frac{\Phi_{uu}(i,\kappa)}{\Phi_{ss}(i,\kappa)}}, 1\right\}, W_{\max}\right\} . \tag{6.19}$$

The short-term PSDs $\Phi_{ss}(i,\kappa)$ and $\Phi_{uu}(i,\kappa)$ are estimated by recursive averaging[13]

$$\widehat{\Phi}_{ss}(i,\kappa) = \beta_s \cdot \widehat{\Phi}_{ss}(i,\kappa - R) + (1-\beta_s) \cdot |S(i,\kappa)|^2 ; \quad 0 < \beta_s < 1 \tag{6.20a}$$

$$\widehat{\Phi}_{uu}(i,\kappa) = \beta_u \cdot \widehat{\Phi}_{uu}(i,\kappa - R) + (1-\beta_u) \cdot |U(i,\kappa)|^2 ; \quad 0 < \beta_u < 1 . \tag{6.20b}$$

The choice of the time constants β_s and β_u is crucial for the performance of the algorithm. If they are too small, the amplified speech follows the noise too quickly and tends to lose its amplitude structure. If they are close to one, the system does not react to changing speech and noise signals. As discussed in [SV06], the values $\beta_s = 0.996$ and $\beta_u = 0.96$ turn out to be a good choice for a downsampling rate of $R = 80$ and a prototype lowpass filter with 160 non-zero coefficients and 96 zeros for zero-padding.

[13] In a double-talk situation, the noise PSD can usually not be calculated by Eq. (6.20b) and needs to be estimated, e.g., by minimum statistics [Mar01], but this case is not considered in the later simulations where Eq. (6.20) is used.

However, the used warped filter-bank with Bark-scaled bandwidths features a non-uniform time *and* frequency resolution. For a positive allpass coefficient a, the subband filters at higher frequencies have higher bandwidths (lower frequency resolution) and a shorter impulse response (higher time resolution), and vice versa for lower frequencies. This effect should be considered for the determination of the time constants β_s and β_u introduced in Eq. (6.20). For a shorter impulse response, the time constants β_s and β_u should become greater in order to average over approximately the same number of samples. Therefore, the time constants are interpolated between the reference case and a maximum value of one depending on the warped bandwidth $\Delta\widetilde{\Omega}_i$ of each subband

$$\beta_s'(i) = 1 - (1 - \beta_s)\,\frac{\Delta\Omega_{\mathrm{ref}}}{\Delta\widetilde{\Omega}_i} \tag{6.21}$$

and the same applies for β_u. The overlap-add method considered in [SV06] uses 160 samples per DFT frame. Therefore, a 'reference bandwidth' of $\Delta\Omega_{\mathrm{ref}} = \frac{2\pi}{160}$ is taken for Eq. (6.21).[14] The individual bandwidth of each Bark-scaled subband can be approximated by the distance of the center frequencies of the warped subbands as follows

$$\Delta\widetilde{\Omega}_i = \varphi_a(\Omega_i) - \varphi_a(\Omega_{i-1}) \quad \text{with} \quad \Omega_i = 2\tfrac{\pi}{M}i; \quad i \in \{\,0, 1, \ldots, M-1\,\} \tag{6.22}$$

where the phase response of the allpass filter is given by Eq. (2.54). The devised method is of course a heuristic approach which, however, provides good results in practice.

6.2.3.3 Simulation Results

The performance of the proposed algorithms has been evaluated in terms of the SII [ANS97]. The SII is supposed to be correlated with the intelligibility of speech under a variety of adverse listening conditions. It is basically computed by adding the speech-to-noise ratio in each contributing frequency band weighted according to its contribution to speech intelligibility. According to [ANS97], good communication systems have an SII of 0.75 or above, while poor communication systems have an SII below 0.45. The SII has been calculated with the so-called critical band procedure. In order to calculate the speech and noise spectrum level of each sound file, the spectrum level is averaged for half-overlapping Hann-windowed frames of 20 ms length. An average speech spectrum level of the whole speech database has been achieved by this, which is comparable to the standard speech spectrum level for normal vocal effort as specified in [ANS97]. For this evaluation, the SII has been calculated for every speech file of the TIMIT database, in total 5.4 hours, disturbed by 'factory 1' noise from the NOISEX-92 database for a sampling rate of 8 kHz.

The mean values of the SIIs without processing and after processing with the proposed enhancement system, i.e., a warped FBE and warped AR LDF with $M = 64$ subbands and allpass coefficient $a = 0.4$, are depicted in Figure 6.12 for different SNRs. For comparison, the mean SII after processing with a uniform DFT AS FB with $M = 256$ subbands as proposed in [SV06] is also plotted. As a second reference, each half-overlapping speech frame of 160 samples length is amplified with one

[14] The DFT filter-bank considered in [SV06] has a uniform bandwidth of $\Delta\Omega = \frac{2\pi}{256}$.

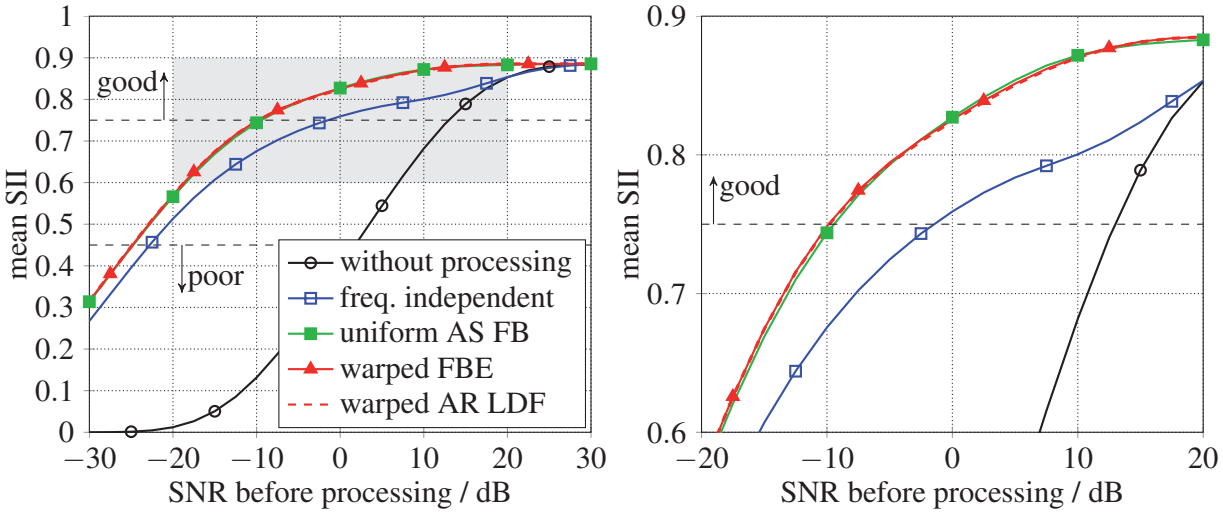

Figure 6.12: *Mean SII after frequency independent and frequency dependent subband processing using a uniform DFT AS FB (Figure 2.4) with $M = 256$ subbands ($L = M$), a warped FBE (Figure 5.8) with $M = 64$ subbands ($N = 159$) and a warped AR LDF (Sec. 5.4.5) with filter degree $N_{ld} = 11$. The right plot magnifies the highlighted area of the left plot.*

frequency independent factor such that the output power of each speech frame is the same as after processing with the uniform DFT AS FB (overlap-add method).

It can be seen that the warped FBE with $M = 64$ subbands achieves a similar performance in terms of the SII as the uniform AS FB with $M = 256$ subbands. Informal listening tests, however, have shown a preference for the warped FBE in comparison to the uniform AS FB. The frequency dependent amplification, in turn, results in a better speech intelligibility than the frequency independent amplification, which is also confirmed by informal listening tests.

The mean SII after processing with the warped AR filter approximation and $M = 64$ subbands (dashed line) is compared to the above mentioned algorithms. It can be observed that the AR LDF achieves almost the same performance as the warped FBE with 64 subbands and slightly outperforms the uniform AS FB with 256 subbands.

The processing with the overlap-add method has an algorithmic signal delay of 159 samples. Using the warped FBE reduces the algorithmic delay to 95 samples. The algorithmic signal delay of the AR LDF is determined by Eq. (6.7), which resulted values between 0 and 2 samples. Thus, the use of the warped FBE and AR LDF, respectively, allows to achieve a low signal delay without a noticeable impact on the achieved instrumental speech intelligibility.

6.3 Conclusions

The application of the proposed allpass-based filter-banks is discussed for some selected examples and the achieved performance is compared with that of commonly used FIR filter-banks.

The closed-form IIR/IIR QMF-bank design presented in Sec. 3.1.2.3 can achieve a signal reconstruction without aliasing and amplitude distortions while the remaining phase distortions can be traded against signal delay in a simple and flexible fashion. Due to these benefits, this QMF-bank design has been adopted in a candidate proposal for the super-wideband and stereo extension of ITU-T Rec. G.729.1 and Rec. G.718 [GKL+09, LV09b]. This hierarchical speech and audio codec is developed especially for heterogeneous communication networks. The encoder generates a layered bit-stream to provide a coding scheme with bit rate as well as bandwidth scalability. To achieve this scalability, critically subsampled QMF-banks are employed. They split a wideband or super-wideband input signal into downsampled subband signals, which are encoded separately to obtain a layered bit-stream.

The new codec is built on top of a core codec given by ITU-T Rec. G.729.1 [ITU06]. One proposal is to replace the FIR/FIR QMF-bank of this core codec optionally by the new allpass-based IIR/IIR QMF-bank. The investigation of the fixed-point implementations for these two filter-banks reveals that the devised IIR QMF-bank reaches almost the same signal-to-quantization-noise ratio (SQNR) as the FIR QMF-bank of ITU-T Rec. G.729.1. However, the proposed allpass-based QMF-bank achieves a significantly lower algorithmic complexity and signal delay than its FIR counterpart without causing audible signal distortions. Therefore, the new IIR QMF-bank is also used for the first stage of the codec where a super-wideband signal ($f_\mathrm{s} = 32\,\mathrm{kHz}$) is split into two subbands. Owing to this filter-bank, the super-wideband extension of the new codec increases the signal delay of the G.729.1 core codec of 48.9375 ms only by 2.21875 ms.

The concept of the filter-bank equalizer (FBE) presented in Chap. 5 allows to perform uniform or non-uniform subband processing with low delay. This effects that this filter-bank is of special interest for low delay speech enhancement to be used, e.g., in cell phones, hands-free devices, or (not at least) digital hearing aids. The application of the FBE for noise reduction and near-end listening enhancement is discussed. The aim of a noise reduction system is to improve the speech quality by reducing the effects of additive background noise, while a system for near-end listening enhancement improves the speech quality in terms of the speech intelligibility index (SII).

The comparison of the FBE with subsampled AS FBs, which are commonly employed for adaptive subband filtering, reveals the following properties: The uniform or warped FBE can achieve a similar (or even better) objective and subjective speech quality, but with a significantly lower signal delay than a corresponding uniform or warped AS FB with subsampling. The uniform FBE has a higher algorithmic complexity than the corresponding uniform AS FB (e.g., overlap-add method), while the opposite applies for the allpass transformed FBE in comparison to the allpass transformed AS FB. The use of a warped filter-bank allows either to achieve an improved speech quality in comparison to a uniform filter-bank with the same number of subbands or it can achieve a similar speech quality with a lower number of subbands.

The low delay filter (LDF) extension of the FBE allows to further decrease its signal delay in a simple and flexible manner, but without a noticeable effect on the *subjective* speech quality. The AR LDF is of special interest for applications with very demanding signal delay constraints as it can achieve a latency of only a few sample instants.

Chapter 7

Summary

THIS THESIS addresses the theory and design of allpass-based analysis-synthesis filter-banks (AS FBs) and their application to speech and audio processing. The considered allpass-based QMF-banks and Pseudo QMF-banks are uniform filter-banks with critical subsampling. Their analysis filter-banks consist of allpass polyphase filters, which enables a high frequency selectivity with a low filter degree. The second class of allpass-based filter-banks that is taken into account are allpass-transformed AS FBs. These filter-banks can achieve a non-uniform frequency resolution which resembles that of the human auditory system. A common design issue of all treated allpass-based filter-banks is that the non-linear phase responses of the IIR analysis filters need to be compensated by an appropriate phase equalization within the synthesis filter-bank. Based on a careful analysis of existing design methods, various novel design approaches for allpass-based filter-banks are developed.

Design of IIR QMF-Banks and Pseudo QMF-Banks

Different designs for a critically subsampled two-channel QMF-bank are proposed in this thesis where analysis *and* synthesis filter-bank consist of allpass polyphase components. The allpass polyphase filters of the synthesis filter-bank act as *phase equalizers,* which are designed by simple analytical closed-form expressions. A first QMF-bank design achieves a minimization of amplitude, phase and aliasing distortions with a low signal delay and low algorithmic complexity. A second design causes no amplitude distortions and achieves a complete aliasing cancellation at the expense of a higher algorithmic complexity and signal delay in comparison to the first design. These QMF-bank designs are extended to a critically subsampled Pseudo QMF-bank, which results in a recursive M-channel DFT AS FB whose analysis and synthesis filters consist of allpass polyphase filters.

A benefit of the proposed closed-from designs is that the trade-off between reconstruction error and signal delay can be adjusted in a simple and flexible manner. In comparison to the related IIR/FIR QMF-bank designs of [GK00, KD02], the proposed IIR/IIR QMF-bank designs achieve a lower algorithmic complexity and cause no or negligible amplitude distortions at the expense of higher phase distortions. Therefore, the presented designs are especially attractive for speech and audio processing where phase distortions are less critical.

The proposed allpass-based IIR/IIR QMF-bank design with complete aliasing cancellation was part of a candidate proposal of an ITU-T contest for a new super-wideband

and stereo extension of ITU-T Rec. G.729.1 and G.718 [GKL+09, LV09b]. This hierarchical speech and audio codec employs the new IIR/IIR QMF-bank to split a super-wideband signal ($f_s = 32\,\text{kHz}$) into two subband signals, which are encoded separately in order to generate a layered bit-stream. The design of the new IIR/IIR QMF-bank attains that the super-wideband extension increases the signal delay of the G.729.1 core codec of 48.9375 ms only by 2.21875 ms. One option of the new codec proposal is to replace the original FIR/FIR QMF-bank of the embedded G.729.1 core codec by the new IIR/IIR QMF-bank, which reduces its signal delay by about 38% and its computational complexity (measured in terms of weighted million operations per second) by about 28%.

Phase Equalizer Design for Allpass-Based Filter-Banks

An essential design issue for allpass-based filter-banks is to equalize the non-linear phase response of allpass filters. Therefore, different phase equalizer designs for this purpose are elaborated in more detail.

One approach to perform the phase equalization for allpass-based filter-banks is by means of *non-causal filtering*, e.g., [MCB92, CM96]. The approach of [MCB92] can achieve a perfect phase equalization, but requires the transmission of initial filter states from the analysis filter-bank to the synthesis filter-bank. The investigation of this method shows that it is very susceptible towards modifications of the subband signals, which makes this approach less suitable for practical applications. The transmission of filter states can be avoided at the expense of an increased signal delay and complexity by the technique of [CM96], which achieves a nearly perfect phase equalization. The analysis of this approach reveals that this phase equalizer is a linear periodically time-varying (LPTV) system. Hence, the use of this technique for filter-banks leads to additional aliasing distortions, even if no subsampling is performed.

These problems are avoided by FIR or IIR phase equalizers which are linear time-invariant (LTI) systems. For allpass-based filter-banks, the needed phase equalizers can be designed by simple *closed-form expressions* [Gal02, LV06d] instead of a general and more complex numerical phase equalizer design, e.g., [Lan93, Lan98]. The closed-form FIR phase equalizer design of [Gal02] is constructed for an allpass filter of first order where the phase equalization of allpass filters of higher order is achieved by a cascade of phase equalizers. For the phase equalization of an allpass filter of first order or an allpass chain, it is proven that this cascaded FIR phase equalizer achieves an equiripple approximation error for the desired phase response, group delay and magnitude response. The closed-form allpass phase equalizer design of [LV06d] is a cascaded phase equalizer as well. The phase and group delay approximation error exhibits an equiripple behavior with extrema being (exactly) twice as high as for the FIR phase equalizer of [Gal02], but this allpass phase equalizer causes no amplitude distortions and has a lower algorithmic complexity.

For the phase equalization of allpass filters of higher order or long allpass chains, respectively, it turns out that the use of a cascaded (FIR or allpass) phase equalizer leads to a high signal delay. Therefore, it is proposed to use an alternative phase equalizer which is obtained by truncating and shifting the anti-causal impulse response

of an 'ideal' phase equalizer (i.e., an inverse allpass filter). The resulting phase equalizer is a least-squares (LS) error approximation for the ideal phase equalizer. It is shown that this LS FIR phase equalizer is particularly suited for the construction of allpass transformed filter-banks.

Allpass Transformed Analysis-Synthesis Filter-Banks

Allpass transformed filter-banks are obtained by replacing the delay elements of the analysis filter-bank by allpass filters of first or higher order [OJS71, BO74, Var78, Kap98]. This leads, in contrast to the related warped DFT [MM01], to analysis filters with non-uniform bandwidths. The non-uniform time-frequency resolution of such a *frequency warped* filter-bank is simply adjusted by the common pole of the employed allpass filters. Allpass transformed AS FBs can achieve a frequency resolution which is very similar to that of the human auditory system (represented by the Bark frequency scale). Another benefit of allpass transformed filter-banks is that their signal delay and complexity is usually lower than for comparable tree-structured filter-banks.

A synthesis filter-bank to achieve *near-perfect reconstruction* (NPR) can be constructed by means of *phase equalizers* to compensate the non-linear phase responses of the allpass transformed analysis filters. The design of [GK00, Gal02], which employs *cascaded* FIR phase equalizers, is considerably improved by the use of the LS FIR phase equalizer. The proposed synthesis filter-bank achieves a significantly lower signal reconstruction error with a lower signal delay than the design of [GK00, Gal02]. The magnitude responses of the synthesis filters are almost equal to those of the analysis filters if a good phase equalization is performed. For the same signal delay, the improved design with LS FIR phase equalizers achieves therefore a better bandpass characteristic for the synthesis filters in comparison to the original design with cascaded FIR phase equalizers.

An advantage of the presented closed-form NPR designs by means of phase equalization is that the coefficients of the synthesis filter-bank are determined by simple analytical expressions. Furthermore, these design approaches allow to adjust the trade-off between reconstruction error and signal delay in an easy manner. However, a general drawback of such closed-form designs is their inability to incorporate (explicitly) further design objectives. This problem is tackled by a novel *numerical* design framework. It is based on a new matrix representation for the transfer function of an allpass transformed AS FB from which different FIR synthesis filter-bank designs are derived.

A first design approach is a generalization of the closed-form NPR filter-bank design with LS FIR phase equalizers. The FIR synthesis filters are determined by a linearly constrained quadratic program (LCQP) where the phase distortions are minimized with the additional constraint for an LTI system. The obtained synthesis filter-bank is capable to achieve a complete aliasing cancellation.

This design is extended in a second step to involve further design objectives. One generalization is to permit a constrained (LS) error for the aliasing distortions in an exchange for a lower amount of linear signal distortions.

Another extension is a *sparse* design where the number of non-zero filter coefficients is minimized in order to achieve a reduced number of multiplications and summations.

A sparse design can be beneficial, e.g., for an ASIC implementation to save circuit components and power consumption or it can help to reduce the quantization noise and complexity for an implementation with fixed-point arithmetic due to the reduced number of multipliers and adders. The constraint for sparseness leads to a rather involved non-convex optimization problem. This difficulty is circumvented by means of an $\mathcal{L}_1$-norm regularization, which results in a fairly simple second order cone program (SOCP) to determine the synthesis filter coefficients. In contrast to a mere zero-forcing of the lowest synthesis filter coefficients, the devised sparse design can fulfill the additional design constraint for complete aliasing cancellation with a much higher numerical accuracy.

A second numerical design approach strives for *perfect reconstruction* (PR). This is accomplished by an unconstrained LS error design. An advantage of the developed unconstrained PR design is that the coefficients of the FIR synthesis filters are merely determined by a set of linear equations (linear program). However, this design does not incorporate explicitly the demand for synthesis filters with a high stopband attenuation. This is addressed by a constrained PR design. Passband error and stopband energy of the synthesis filters are minimized with the constraint for perfect reconstruction, which results in a linearly constrained quadratic program (LCQP). This new design can achieve a prefect signal reconstruction with a high numerical accuracy and provides at the same time synthesis filters with a pronounced bandpass characteristic.

The introduced numerical PR designs have some distinctive advantages over the closed-form PR designs of [Kap98, SM02a, FK03]: Firstly, the presented designs provide (inherently) a stable synthesis filter-bank even in case of an allpass transformation of *higher order*. Secondly, these designs apply also for a polyphase network (PPN) implementation of an AS FB where the length of the prototype filter exceeds the number of channels. This allows to use prototype filters with a higher frequency selectivity. Finally, the presented designs provide synthesis filters with a distinctive bandpass characteristic.

The introduced numerical designs are all stated as a *semi-definite program* (SDP) or special cases thereof. Such convex optimization problems can be efficiently solved and provide a global optimum, e.g., [VB96, BV04]. In contrast to previous numerical designs for allpass transformed AS FBs filter-banks [dHGCN02, VN03, WdDC03], the devised design framework is the first one that can achieve a complete aliasing cancellation or even a prefect signal reconstruction. In addition, the developed filter-bank designs consider explicitly the more general case of an allpass transformation of higher order, which offers more degrees of freedom to adjust the time-frequency resolution of the filter-bank.

A brief overview of the new designs for allpass transformed DFT AS FBs is provided by Table 7.1. The designs follow different objectives and it depends on the intended application which filter-bank design is preferable. All the presented synthesis filter-banks are based on FIR filters and can be implemented efficiently by a polyphase network. The new designs are elaborated for allpass transformed DFT filter-banks, but they can also be applied to other modulated filter-banks such as DCT filter-banks in a straightforward fashion.

Table 7.1: *Overview of the novel design approaches for allpass transformed DFT AS FBs developed in Chap. 4.*

design	section	optimization method	special property
NPR design by phase equalization	4.2.2	closed-form solution	minimized phase distortions
constrained NPR design	4.3.3	LCQP	perfect aliasing cancellation
generalized constrained NPR design	4.3.3	SDP	controllable aliasing error
sparse NPR design	4.3.4	SOCP	filter-bank with low complexity
unconstrained PR design	4.3.5	linear program	simple optimization
constrained PR design	4.3.6	LCQP	minimized stopband and bandpass error

Low Delay Filter-Banks

Many applications require filter-banks with a low signal delay. Examples are speech enhancement systems in cell phones or digital hearing aids where a low latency is an essential design constraint. For such applications, the concept of the *filter-bank equalizer* (FBE) is developed. This system allows for adaptive filtering with a uniform and non-uniform frequency resolution as well as a low signal delay. The FBE is derived as an efficient implementation of the filter-bank summation method (FBSM), which can be regarded as a special case of an AS FB without subsampling. The FBE can achieve a perfect signal reconstruction for a broad class of transformation kernels with lower efforts than for comparable AS FBs with subsampling.

It is shown how the choice of the filter structure influences signal delay, computational complexity and signal quality of the FBE if used for adaptive subband filtering. The transposed direct form implementation achieves a stronger smoothing effect for time-varying coefficients in comparison to the direct form implementation of the FBE, which is beneficial to avoid artifacts for the processed signal. An advantage of the direct form implementation of the FBE is that a time-mismatch between the adaptation of the spectral gain factors and the actual time-domain filtering has not to be compensated by additional delay elements as for the transposed direct form. Possible artifacts due to the switching of the time-domain filter coefficients can be avoided by smoothing (cross-fading).

The devised allpass transformed FBE achieves near-perfect reconstruction with lower efforts than a comparable allpass transformed AS FBs with subsampling. The (uniform and warped) FBE can be efficiently implemented by means of a polyphase

network. In general, the uniform FBE has a higher algorithmic complexity than the corresponding uniform AS FB, while the opposite applies for the allpass transformed FBE in comparison to the allpass transformed AS FB. The uniform and warped FBE achieve a significantly lower algorithmic signal delay than a corresponding uniform and warped AS FB with subsampling. Furthermore, a nearly linear phase response can be maintained even for time-varying coefficients, which is advantageous, e.g., for multi-channel processing.

The concept of the *low delay filter* (LDF) is an extension of the (uniform and warped) FBE where the time-domain filter of the FBE is approximated by a filter of lower degree. This allows to reduce the signal delay and algorithmic complexity of the FBE in a simple and flexible manner: An adjustment of the spectral gain calculation is not required and this approach provides an increased flexibility for the choice of the time-domain filter. The approximation by a *moving-average* (MA) filter and an *auto-regressive* (AR) filter is elaborated. The use of the uniform or warped MA filter allows to maintain a time-invariant phase response where a nearly linear phase can be achieved by a phase equalization. Such a property can be beneficial, e.g., for binaural speech processing in hearing aids. The uniform or warped AR filter is a minimum-phase system and can achieve an algorithmic signal delay of only a few sample instants. This property is of special interest for systems with very demanding signal delay constraints.

The application of the FBE for speech enhancement by noise reduction, speech dereverberation and speech intelligibility improvement in noisy environments is investigated. It is shown that the uniform or warped FBE can achieve a similar (or even better) objective and subjective speech quality than a comparable AS FB, but with a significantly lower signal delay. The use of a warped filter-bank allows either to achieve an improved speech quality in comparison to a uniform filter-bank or to achieve a similar speech quality, but with a lower number of subbands. The use of the LDF achieves a further reduction of signal delay and complexity in a simple fashion with a negligible effect on the perceived speech quality.

Besides the speech enhancement systems considered in this work, the use of the FBE and LDF is also attractive for other applications such as acoustic echo cancellation [SSBF08, YIEB10] or pre-echo control [GRV10]. Likewise, allpass-transformed AS FBs are not only proposed for noise reduction [GEH98], but also for subband beamforming [dHGCN02], multiple description coding [SM02a], or speech and audio coding [FKK05]. The use of the presented, improved filter-bank designs for such applications is an interesting and promising topic for further works.

Appendix A

Abbreviations & Notation

A.1 List of Abbreviations

AR	auto-regressive
AS	analysis-synthesis
ASIC	application-specific integrated circuit
BSF	bifrequency system function
CD	cepstral distance
CELP	code excited linear prediction
CLS	constrained least-squares error
DCT	discrete cosine transform
DFT	discrete Fourier transform
DSP	digital signal processor
ELT	extended lapped transform
ERB	equivalent rectangular bandwidth
FB	filter-bank
FBE	filter-bank equalizer
FBSM	filter-bank summation method
FEC	frame erasure concealment
FFT	fast Fourier transform
FIR	finite impulse response
GDCT	generalized discrete cosine transform
GDFT	generalized discrete Fourier transform
HP	highpass (filter)
IDFT	inverse discrete Fourier transform
IFFT	inverse fast Fourier transform
IGDFT	inverse generalized discrete Fourier transform
IIR	infinite impulse response
ITU	International Telecommunication Union
LCQP	linearly constrained quadratic program
LDF	low delay filter
LMIs	linear matrix inequalities
LP	lowpass (filter)
LPTV	linear periodically time-varying
LS	least-squares

LTI	linear time-invariant
MA	moving-average
MAP	maximum a posteriori
MDCT	modified discrete cosine transform
NPR	near-perfect reconstruction
PE	phase equalizer
PESQ	perceptual evaluation of the speech quality
PPN	polyphase network
PR	perfect reconstruction
PSD	power spectral density
QCQP	quadratically constrained quadratic program
QMF	quadrature-mirror filter
SDP	semi-definite program
SII	speech intelligibility index
SIR	signal-to-interference ratio
SNR	signal-to-noise ratio
SOCP	second order cone program
SQNR	signal-to-quantization-noise ratio
SWB	super-wideband
TDAC	time-domain aliasing cancellation
TDBWE	time-domain bandwidth extension
WB	wideband
WDFT	warped discrete Fourier transform
WMOPS	weighted million operations per second

A.2 Nomenclature for Filters

An arbitrary filter or system with impulse response $f(k)$ and sample index $k \in \mathbb{Z}$ is considered. In general, input and output signal of a filter (as well as a filter-bank) are denoted by $x(k)$ and $y(k)$, respectively. It is assumed that the filter is *stable* and $f(k_0) \neq 0$ for some $k_0 \in \mathbb{Z}$ such that

$$0 < \sum_{k=-\infty}^{\infty} |f(k)| < \infty \,. \tag{A.1}$$

The filter is *causal*, if its impulse response features the property

$$f(k) = 0 \quad \text{for} \quad k < 0 \,. \tag{A.2}$$

Otherwise, the filter is *non-causal*. A non-causal filter is *anti-causal*, if

$$f(k) = 0 \quad \text{for} \quad k > 0 \,. \tag{A.3}$$

The rational *system function* of a filter is given by[1]

$$f(k) \;\circ\!\!-\!\!\bullet\; F(z) = \frac{\sum_{n=0}^{N_1} c_n \cdot z^{-n}}{1 + \sum_{m=1}^{N_2} d_m \cdot z^{-m}}; \quad c_{N_1} \neq 0; \quad d_{N_2} \neq 0\,. \tag{A.4}$$

The *degree* or order of a filter refers to the maximum of N_1 and N_2. For an FIR filter, $d_m = 0 \,\forall\, m$ and the value $L_1 = N_1 + 1$ is referred to as *filter length*. The *para-conjugate* of the system function $F(z)$ is marked by a breve

$$\breve{F}(z) = \frac{\sum_{n=0}^{N_1} c_n^* \cdot z^{n}}{1 + \sum_{m=1}^{N_2} d_m^* \cdot z^{m}}\,. \tag{A.5}$$

The *allpass transformation* of a filter with system function $F(z)$ is marked by a tilde

$$\widetilde{F}(z) = F\left(z = A^{-1}(z)\right) \tag{A.6}$$

with $A(z)$ marking the system function of an allpass filter. The tilde notation is also used to mark the output signal of an allpass transformed system without phase equalization

$$\widetilde{Y}(z) = X(z) \cdot \widetilde{F}(z)\,. \tag{A.7}$$

The *frequency response* of a filter is given by

$$F\left(e^{j\,\Omega}\right) = \left|F\left(e^{j\,\Omega}\right)\right| \cdot e^{-j\,\varphi(\Omega)}\,. \tag{A.8}$$

The *magnitude response* of a filter is expressed mostly in decibel where

$$\left|F\left(e^{j\,\Omega}\right)\right| / \text{dB} = 20\,\log_{10}\left|F\left(e^{j\,\Omega}\right)\right|\,. \tag{A.9}$$

For the *phase response* $\varphi(\Omega)$, the negative sign in the exponent is excluded, which is beneficial for our treatment, but differs to some definitions in literature.

A.3 Mathematical Notation & Principal Symbols

The following conventions are used to denote quantities. Bold upper-case letters refer to matrices, e.g., $\boldsymbol{A}$, bold lower-case letters refer to vectors, e.g., $\boldsymbol{a}$ and scalars are not bold, e.g., a. Furthermore, reconstructed, approximated or estimated sequences and quantities are labeled with a hat. For example, the reconstructed input signal of a filter-bank is denoted by $\hat{x}(k)$, the vector obtained by solving an optimization problem is marked, e.g., by $\widehat{\boldsymbol{p}}$ and the estimated speech signal provided by a noise reduction

[1] The *system function* is here different to the *system response* introduced in Sec. 2.4.

system is written as $\hat{s}(k)$. Time-domain sequence are denoted by lower-case letters and their respective z-transform or Fourier transform is marked by capital letters, e.g., $\mathcal{Z}\{f(k)\} = F(z)$ and $\mathcal{F}\{f(k)\} = F\left(e^{j\,\Omega}\right)$.

In the following, the used mathematical symbols, operators and principal variables are listed excluding auxiliary variables.

Mathematical Symbols and Operators

a	scalar
a^*	complex conjugate value
$\boldsymbol{a}$	vector
$\boldsymbol{A}$	matrix
$\boldsymbol{A}^T$	transpose of a matrix
$\boldsymbol{A}^H$	conjugate transpose of a matrix
$\boldsymbol{A}^{-1}$	inverse of a square matrix
$\boldsymbol{A}^{\#}$	pseudo-inverse of a matrix
$\approx$	approximately equal to
$\stackrel{!}{=}$	shall be equal to
$\equiv$	equal for all arguments
$\widehat{=}$	equivalent to
$\wedge$	logical AND
$\vee$	logical OR
$a > b$	a greater than b
$a \geq b$	a greater than or equal to b
$a \gg b$	a much greater than b
$a < b$	a smaller than b
$a \leq b$	a smaller than or equal to b
$a \ll b$	a much smaller than b
$\boldsymbol{a} \succeq \boldsymbol{b}$	components of $\boldsymbol{a}$ are greater than or equal to components of $\boldsymbol{b}$
$\boldsymbol{A} \succeq 0$	matrix is positive semi-definite
$\boldsymbol{A} \succ 0$	matrix is positive definite
$\mathrm{rank}\,(\boldsymbol{A})$	rank of a matrix
$\boldsymbol{A} \odot \boldsymbol{B}$	Hadamard product of two matrices
$\boldsymbol{A} \otimes \boldsymbol{B}$	Kronecker product of two matrices
$\mathbf{1}_L$	column vector with L ones
$\boldsymbol{I}_L$	identity matrix of dimension $L \times L$
$\mathbf{0}_L$	column vector with L zeros
$\boldsymbol{O}_{N \times L}$	zero-matrix of dimension $N \times L$
$\|\boldsymbol{a}\|_0$	zero-norm (cardinality) of a vector
$\|\boldsymbol{a}\|_2$	least-squares norm ($\mathcal{L}_2$-norm)
$\|\boldsymbol{a}\|_\infty$	Chebyshev norm ($\mathcal{L}_\infty$-norm)

$\|\boldsymbol{a}\|_p$	general $\mathcal{L}_p$-norm with $p \in \{1, 2, \ldots, \infty\}$
$\|x\|$	absolute value of x
$\lfloor x \rfloor$	greatest integer which is lower than or equal to x
$\lceil x \rceil$	lowest integer which is greater than or equal to x
$\mathrm{sign}(x)$	sign of x
$\Re\{x\}$	real part of x
$\Im\{x\}$	imaginary part of x
$\tan(x)$	tangent function
$\arctan(x)$	inverse tangent function (unwrapped)
$\cos(x)$	cosine function
$\arccos(x)$	inverse cosine function (unwrapped)
$\sin(x)$	sine function
$\log_{10}(x)$	logarithm with base 10
$\log_2(x)$	logarithm with base 2 (binary logarithm)
$\max_x \{f(x)\}$	maximum of $f(x)$ over x
$\min_x \{f(x)\}$	minimum of $f(x)$ over x
$\arg\{f(x)\}$	argument x of $f(x)$
$\mathrm{corr}\{x(k), y(k)\}$	cross-correlation of two sequences
$\mathrm{gdl}\{f(\Omega)\}$	group delay of $f(\Omega)$
$\mathcal{F}\{x(k)\}$	Fourier transform of $x(k)$
$\mathcal{Z}\{x(k)\}$	z-transform of $x(k)$
$\mathcal{C}(\mathbb{F})$	no. of elements of set $\mathbb{F}$
$n!$	factorial of a positive integer
$\binom{k}{n} = \frac{k!}{n!\,(k-n)}$	binomial coefficient for integer values $0 \leq n \leq k$
$j = \sqrt{-1}$	imaginary unit
e	2.718281828459045...
π	3.141592653589793...
$\in$	element of
$\notin$	not element of
$\forall$	for all (elements)
$\cup$	union of sets
$\mathbb{N}_0$	set of all positive integers including zero
$\mathbb{N}$	set of all positive integers excluding zero
$\mathbb{Z}$	set of all integers
$\mathbb{R}$	set of all real numbers
$\mathbb{R}_+$	set of all positive real numbers excluding zero
$\mathbb{C}$	set of all complex numbers
$\circ\!\!-\!\!\bullet$	transformation from time-domain to z-domain

Latin Symbols

a	complex allpass pole ($K = 1$)	Eq. (2.52)
$a(m)$	complex allpass pole ($K \geq 1$)	Eq. (2.48)
a_i	complex pole of allpass polyphase filter ($K_i = 1$)	Eq. (3.31)
$a_i(m)$	complex pole of allpass polyphase filter ($K_i \geq 1$)	Eq. (3.15)
a_{bark}	allpass pole for Bark scale approximation	Eq. (4.7)
a_{erb}	allpass pole for ERB scale approximation	Eq. (4.9)
$A(z)$	allpass of first order	Eq. (2.52)
$A^{[K]}(z)$	allpass of higher order	Eq. (2.47)
$\breve{A}^{[K]}(z)$	para-conjugate allpass system function	Eq. (3.79)
$A_I^{[K_I]}(z)$	allpass sub-filter I	Eq. (3.11)
$A_{II}^{[K_{II}]}(z)$	allpass sub-filter II	Eq. (3.11)
$A_i^{[K_i]}(z)$	allpass polyphase filter ($K_i \geq 1$)	Eq. (3.14)
$A_{\mathrm{stb}}(\Omega_{\mathrm{s}})$	stopband attenuation at Ω_{s}	Figure 6.2
$\mathcal{A}_0(z)$	component of lifting scheme	Eq. (3.22)
$\boldsymbol{A}$	matrix for unconstrained PR design	Eq. (4.95)
$\bar{\boldsymbol{A}}$	matrix for constrained PR design	Eq. (4.104)
$\boldsymbol{A}_{\mathrm{alias}}(z)$	alias component matrix	Eq. (4.57b)
$b(m)$	complex allpass pole ($K \geq 1$)	Eq. (4.12)
$B^{[K]}(z)$	allpass for allpass transformation ($K \geq 1$)	Eq. (4.12)
$\mathcal{B}_1(z)$	component of lifting scheme	Eq. (3.22)
$B_i(z)$	synthesis polyphase component	Eq. (3.24)
c_{s}	scaling factor for signal reconstruction	Eq. (2.13a)
$\bar{c}$	nominal magnitude for PE design	Eq. (3.74a)
$c(m)$	allpass coefficient for direct form	Eq. (2.47)
$c_f(k)$	sequence for cross-fading	Eq. (5.34)
C	constant for FBE design	Eq. (5.12)
CD	(mean) cepstral distance	Eq. (E.6)
d_i	degree of transfer function $\Psi_i^{\mathrm{ap}}(z)$	Eq. (3.37)
$d_{\max}$	maximal value for d_λ	Eq. (3.62)
$\boldsymbol{d}_{L_{\mathrm{q}}}$	vector for numerical FB design	Eq. (4.66)
D	degree of transfer function $\Psi(z)$	Sec. 3.3.1
D_{s}	degree of transfer function $\Psi_{\mathrm{s}}(z)$	Eq. (3.86b)
D_{f}	degree of IIR analysis filter	Eq. (3.12)
D_{o}	signal delay of AS FB	Eq. (2.13a)
D'_{o}	signal delay of AS FB in seconds	Eq. (6.8)
D_{a}	signal delay of analysis FB (and gain calculation)	Figure 5.5
$D_{\mathrm{o}}^{\mathrm{tree}}$	signal delay of tree-structured AS FB	Eq. (C.10)
$D_{\mathrm{o}}^{\mathrm{qmfb}}$	signal delay of two-channel QMF-bank	Eq. (C.11)

$\mathcal{D}_{\text{alias}}(z)$	aliasing distortions	Eq. (2.9)
$\widetilde{\mathcal{D}}_{\text{alias}}(z)$	warped aliasing distortions	Eq. (4.29)
$\mathcal{D}_{\text{peak}}(\Omega)$	peak aliasing distortions	Eq. (2.12)
$\boldsymbol{D}(z)$	matrix for numerical FB design	Eq. (4.66)
$\overline{\boldsymbol{D}}(z)$	matrix for constrained PR design	Eq. (4.102)
E_{P}	passband error energy	Eq. (4.114)
E_{S}	stopband energy	Eq. (3.21)
E_{η}	objective function of Johnston design	Eq. (C.5)
f	frequency (in Hz)	Eq. (2.5)
$f_{\text{s}} = 1/T_{\text{s}}$	sampling frequency	Eq. (2.5)
$F_i(z)$	synthesis filter for constrained PR design	Eq. (4.102)
$\mathbb{F}$	set with all frame indices	Eq. (E.4)
$\mathbb{F}_{\text{s}}$	set with frame indices for speech activity	Eq. (E.3)
$g(k)$	impulse response of synthesis prototype filter	Eq. (2.27)
$g_i(k)$	impulse response of synthesis filter	Sec. 2.1
$G(z)$	synthesis prototype filter	Eq. (2.26)
$G_i(z)$	uniform synthesis filter	Eq. (2.26)
$G'_i(z)$	IIR synthesis QMF with linearized phase	Eq. (3.52)
$\bar{G}^{(M)}_{0,\lambda}(z)$	synthesis polyphase filter (type 2)	Eq. (2.37)
$\widetilde{G}_i(z)$	warped synthesis filter without PE	Eq. (4.30)
$\widetilde{\widetilde{G}}_i(z)$	warped synthesis filter with PE	Eq. (4.42)
$\bar{G}_i(z)$	FIR synthesis filter for warped analysis FB	Eq. (4.32)
$\bar{G}^{(\text{ideal})}_i(z)$	synthesis filter for 'ideal' PE	Eq. (4.49)
$\mathcal{G}_{\text{noise}}$	noise gain	Eq. (6.5)
$h(k)$	impulse response of analysis prototype filter	Eq. (2.23)
$h_i(k)$	impulse response of analysis filter	Sec. 2.1
$h^{[L_{\text{ac}}]}_{\text{apc}}(k)$	impulse response of allpass chain	Figure 4.9
$h_c(\nu)$	coefficients for non-recursive warping	Eq. (4.28)
$h_{\text{lin}}(l)$	coefficients of linear-phase filter	Eq. (4.27)
$h_{\text{s}}(k,\kappa)$	time-domain filter of FBE	Eq. (5.11)
$\bar{h}_{\text{s}}(l,k)$	FIR filter coefficients after cross-fading	Eq. (5.34)
$\hat{h}_{\text{s}}(l,\kappa)$	filter coefficients of MA low delay filter	Eq. (5.46)
$h_{\text{r}}(l,k)$	room impulse response	Eq. (6.13)
$H(z)$	analysis prototype filter	Eq. (2.22)
$H_i(z)$	uniform analysis filter	Eq. (2.22)
$H'_i(z)$	IIR analysis QMF with linearized phase	Eq. (3.51)
$H^{(\text{wdft})}_i(z)$	analysis filter of WDFT FB	Eq. (4.26)
$H^{(\text{gam})}_i(z)$	gammatone analysis filter	Figure C.3

$H_i^{(\mathrm{tree})}(z)$	analysis filter of tree-structured FB	Figure C.5
$\widetilde{H}_i(z)$	warped analysis filter	Eq. (4.2)
$H_{0,\lambda}^{(M)}(z)$	analysis polyphase filter (type 1)	Eq. (2.35)
$H_{\mathrm{lin}}(z)$	linear-phase filter	Eq. (4.27)
$H_{\mathrm{AR}}(z,\kappa)$	AR low delay filter	Eq. (5.48)
$\widetilde{H}_{\mathrm{AR}}(z,\kappa)$	warped AR low delay filter	Eq. (5.52)
$H_{\mathrm{s}}(z,\kappa)$	time-domain filter of FBE	Eq. (5.35)
$\widetilde{H}_{\mathrm{s}}(z,\kappa)$	time-domain filter of warped FBE	Eq. (5.44)
$\hat{H}_{\mathrm{s}}(z,\kappa)$	approximated time-domain filter of FBE	Eq. (5.48)
$H_{\mathrm{g}}(z,k)$	general time-varying filter	Eq. (5.54)
$\bar{H}_{\mathrm{g}}(z,k)$	general time-varying filter after cross-fading	Eq. (5.54)
i	index for FB subband	Sec. 2.1
i_0	frequency shift for GDFT or GDCT	Eq. (5.19)
i_1, i_2	frequency indices for discrete BSF	Eq. (2.40)
$I_{\mathrm{S}}(i)$	stopband interval for subband i	Eq. (4.108)
$I_{\mathrm{P}}(i)$	passband interval for subband i	Eq. (4.115)
J	no. of cascaded phase equalizers ($K = 1$)	Eq. (3.101)
J_i	no. of cascaded phase equalizers in branch i ($K = 1$)	Eq. (3.30)
$J_i(m)$	no. of cascaded phase equalizers in branch i ($K \geq 1$)	Eq. (3.34)
J_{s}	no. of stages of tree-structured FB	Eq. (C.10)
k	discrete time index (sample index)	Sec. 2.1
k_0	discrete time shift	Eq. (5.12)
k_1, k_2	discrete time indices of system response $t_{\mathrm{bi}}(k_2, k_1)$	Sec. 2.4
k_i	sample index after downsampling by R_i	Sec. 2.1
k'	sample index after downsampling by R	Eq. (2.2)
K	degree of allpass filter	Eq. (2.47)
K_i	degree of i-th allpass polyphase filter	Eq. (3.15)
K_c	order of non-recursive frequency warping	Eq. (4.28)
l	index of FIR filter coefficient	Eq. (2.23)
l_M	integer multiple of transformation size M	Eq. (2.36)
L	length of FIR prototype filter if $L_{\mathrm{s}} = L_{\mathrm{a}}$	Eq. (2.28)
L_{a}	length of FIR analysis prototype filter	Eq. (2.23)
L_{s}	length of FIR synthesis prototype filter	Eq. (2.27)
L_{ld}	length of MA low delay filter	Eq. (5.46)
L_{ac}	length of allpass chain	Eq. (2.60)
L_{q}	length of FIR synthesis sub-filter	Eq. (4.33)
L_{e}	length of 'early' room impulse response	Eq. (6.14)
L_{r}	length of room impulse response	Eq. (6.13)
m	index for allpass coefficients	Eq. (2.47)

m_c	parameter of Mth band filter	Eq. (5.13)
M	no. of (FB) subbands (frequency bands)	Sec. 2.1
M_{m}	frame length for segmental measures	(E.3)
M_{CD}	no. of CD values	Eq. (E.7)
$\mathcal{M}$	no. of sub-filter coefficients for constrained PR design	Eq. (4.103)
N	degree of PE in general	Sec. 3.3.1
N_l	degree of PE for allpass chain of length l	Eq. (4.51)
N_i^{ap}	degree of allpass PE in branch i	Eq. (3.35)
N_{s}	degree of PE for single allpass	Eq. (3.85)
N_{lin}	delay of linear phase filter	Eq. (4.27)
N_{ld}	degree of low delay filter	Eq. (5.47)
N_{bi}	no. of discrete frequency points for BSF calculation	Eq. (2.40)
N_m	no. of 'unique' frequency bands	Eq. (5.26)
$\mathrm{NA}_{\mathrm{seg}}$	segmental noise attenuation	Eq. (E.4)
$\mathcal{N}$	no. of sub-filter coefficients if $L_{\mathrm{s}} = L_{\mathrm{a}}$	Eq. (4.76)
$\mathcal{N}_{\mathrm{z}}$	no. of sub-filter coefficients set to zero	Sec. 4.3.4
$\mathcal{N}_{\mathrm{z}}^{\max}$	maximal no. of sub-filter coefficients set to zero	Eq. (4.85)
$p_K^{\mathrm{ideal}}(k)$	anti-causal impulse response of 'ideal' PE	Eq. (3.80)
$p_K^{\mathrm{ls}}(k)$	impulse response of LS FIR PE	Eq. (3.81)
$\boldsymbol{p}$	sub-filter coefficients for numerical design	Eq. (4.66)
$\overline{\boldsymbol{p}}$	sub-filter coefficients for constrained PR design	Eq. (4.104)
$\widehat{\boldsymbol{p}}$	optimal sub-filter coefficients	Eq. (4.80)
$\boldsymbol{p}_{\mathrm{a}}$	augmented vector of $\boldsymbol{p}$	Eq. (4.84)
$P_K(z)$	PE for allpass of order K	Eq. (3.69)
$P^{\mathrm{ap}}(z)$	allpass PE in general	Eq. (3.48)
$P_K^{\mathrm{ideal}}(z)$	'ideal' PE for allpass of order K	Eq. (3.79)
$P_K^{\mathrm{ls}}(z)$	LS FIR PE for allpass of order K	Eq. (3.83)
$\mathcal{P}(z) = P_1(z)$	PE for allpass of first order	Eq. (3.76)
$\mathcal{P}_m(z)$	PE for m-th allpass of first order	Eq. (3.77)
$\mathcal{P}^{\mathrm{ap}}(z)$	allpass PE for allpass of first order	Eq. (3.101)
$\mathcal{P}_{i,1}^{\mathrm{ap}}(z)$	cascaded allpass PE for allpass of first order in branch i	Eq. (3.30)
$\mathcal{P}_{i,K_i}^{\mathrm{ap}}(z)$	cascaded allpass PE for allpass of order K_i in branch i	Eq. (3.34)
$\mathcal{P}^{\mathrm{fir}}(z)$	FIR PE for allpass of first order	Eq. (3.85)
$q_l(\eta)$	coefficients of FIR synthesis sub-filter	Eq. (4.33)
$Q_l(z)$	synthesis sub-filter for $l \in \{0, 1, \ldots, L-1\}$	Eq. (4.33)
$\bar{Q}_i(z)$	synthesis sub-filter for $i \in \{0, 1, \ldots, M-1\}$	Eq. (4.101)
$Q_i^{\mathrm{cf}}(z)$	synthesis sub-filter for closed-form PR design	Eq. (4.55)
$Q_{l,\,r}^{(R)}(z)$	polyphase component of synthesis sub-filter	Eq. (4.54)
$\boldsymbol{Q}_{\mathrm{P}}$	matrix for passband error of constrained PR design	Eq. (4.119)

$\boldsymbol{Q}_{\mathrm{S}}$	matrix for stopband energy of constrained PR design	Eq. (4.113)
r	index for alias components	Eq. (2.8)
$\boldsymbol{r}_p$	residual (error) vector for $\mathcal{L}_p$-norm	Eq. (4.89)
R	common subsampling rate	Sec. 2.1
R_i	individual subsampling rate	Eq. (2.1)
$\mathcal{R}_{\mathrm{c}}$	region of convergence	Eq. (2.48c)
$\boldsymbol{R}_\eta$	'sum matrix' for constrained PR design	Eq. (4.120)
$s(k)$	speech signal	Eq. (6.12)
$\hat{s}(k)$	estimated speech signal	Sec. 6.2.1
$\breve{s}(k)$	filtered speech signal	Eq. (E.1)
$s_{\mathrm{lb}}(k')$	low band signal of G.729.1 core codec ($f_{\mathrm{s}} = 8\,\mathrm{kHz}$)	Figure 6.1
$s_{\mathrm{hb}}(k')$	high band signal of G.729.1 core codec ($f_{\mathrm{s}} = 8\,\mathrm{kHz}$)	Figure 6.1
$s_{\mathrm{wb}}(k)$	wideband signal ($f_{\mathrm{s}} = 16\,\mathrm{kHz}$)	Figure 6.1
$\hat{s}_{\mathrm{wb}}(k)$	decoded wideband signal ($f_{\mathrm{s}} = 16\,\mathrm{kHz}$)	Figure 6.1
$s'_{\mathrm{swb}}(k)$	signal for SWB extension ($f_{\mathrm{s}} = 16\,\mathrm{kHz}$)	Figure 6.1
$s_{\mathrm{swb}}(k)$	signal for SWB extension after lowpass filter ($f_{\mathrm{s}} = 16\,\mathrm{kHz}$)	Figure 6.1
$\bar{s}_{\mathrm{swb}}(k)$	decoded signal of SWB extension ($f_{\mathrm{s}} = 16\,\mathrm{kHz}$)	Figure 6.1
$\bar{s}(k)$	amplified speech for near-end listening enhancement	Figure 6.10
$S(i, \kappa)$	spectral speech coefficients	Eq. (6.20)
$\mathcal{S}_r(z)$	alias components of closed-form PR design	Eq. (4.55)
$\mathcal{S}_{\mathrm{T}}\{\, W(i,\kappa)\,\}$	spectral transform of gain factors	Eq. (5.7)
$\mathrm{SNR}_{\mathrm{seg}}$	segmental signal-to-noise ratio	Eq. (E.3)
SQNR	signal-to-quantization-noise ratio	Eq. (6.6)
$t_{\mathrm{bi}}(k_2, k_1)$	system response of (multi-rate) system	Sec. 2.4
$\boldsymbol{t}$	vector for epigraph form	Eq. (4.91)
$T_{\mathrm{bi}}\left(e^{j\,\Omega_2}, e^{j\,\Omega_1}\right)$	bifrequency system function	Eq. (2.39)
T_{s}	sampling instant	Sec. 2.1
T'_{s}	sampling instant after downsampling by R	Sec. 2.1
$T_{\mathrm{s}i}$	sampling instant after downsampling by R_i	Sec. 2.1
$T_{\mathrm{lin}}(z)$	linear transfer function of uniform AS FB	Eq. (2.9)
$\widetilde{T}_{\mathrm{lin}}(z)$	linear transfer function of warped AS FB without PE	Eq. (4.29)
$\overline{T}_{\mathrm{lin}}(z)$	linear transfer function of warped AS FB with PE	Eq. (4.34)
$T_{\mathrm{alias}}(z)$	aliasing transfer function	Eq. (3.3)
$T_{\mathrm{lin}}^{(\mathrm{inner})}(z)$	linear transfer function of inner QMF-bank	Eq. (6.4)
$T_{\mathrm{pc}}(z)$	zero-phase half-band filter	Eq. (C.9)
$T_\nu(z)$	overall transfer function of AS FB	Eq. (2.17)
$\mathcal{T}_{\mathrm{des}}(z)$	desired total response for prototype filter design	Eq. (4.62)
$u(k)$	noise signal	Eq. (6.12)
$\hat{u}(k)$	estimated noise signal	Figure 6.10

$\breve{u}(k)$	filtered noise signal	Eq. (E.1)
$U(i,\kappa)$	spectral noise coefficients	Eq. (6.20)
$U_r(z)$	alias component of Pseudo QMF-bank	Eq. (3.57)
$\boldsymbol{U}^{[\mathcal{N}]}$	matrix for CLS design	Eq. (4.77)
$v_l(\kappa)$	coefficients of low delay filter	Eq. (5.46)
$\tilde{v}_l(\kappa)$	coefficients of warped low delay filter	Eq. (5.52)
$\boldsymbol{v}^{[\mathcal{N}]}$	vector for CLS design	Eq. (4.78)
$\mathrm{win}_L(k)$	general window sequence of length L	Eq. (5.17)
$\mathrm{win}_{L,\upsilon}(k)$	parametric window sequence of length L	Eq. (5.18)
$w(l,\kappa)$	time-domain weighting factors	Eq. (5.6)
$\boldsymbol{w}$	vector for numerical FB design	Eq. (4.96)
$\overline{\boldsymbol{w}}$	vector for constrained PR design	Eq. (4.104)
$W(i,\kappa)$	time-varying spectral gain factors	Eq. (5.4)
$W_{\max}$	maximal gain for near-end listening enhancement	Eq. (6.19)
W_R	R-th root of unity $e^{-j\frac{2\pi}{R}}$	Eq. (2.4)
$x(k)$	input signal of filter or FB	Figure 2.1
$\hat{x}(k)$	reconstructed input signal of AS FB	Eq. (2.13a)
$x_i(k)$	subband signal without downsampling	Eq. (5.4)
$x_i(k')$	subband signal with downsampling by R	Sec. 2.1
$x_i(k_i)$	subband signal with downsampling by R_i	Figure 2.1
$\widehat{X}(z)$	reconstructed input signal of AS FB	Eq. (2.8)
$\widehat{X}_\nu(z)$	reconstructed input signal of AS FB for $X(z)=z^{-\nu}$	Eq. (2.17)
$\widehat{\widetilde{X}}(z)$	reconstructed input signal of warped AS FB without PE	Eq. (4.29)
$X_i^{(\mathrm{wdft})}(k)$	WDFT coefficients for $x(k)$	Eq. (4.25)
$y(k)$	output signal of filter or AS FB	Figure 2.1
$y_i(k)$	upsampled subband signal	Figure 2.1
$y_{\mathrm{df}}(k)$	output signal of filter in direct form	Eq. (5.31)
$y_{\mathrm{tdf}}(k)$	output signal of filter in transposed direct form	Eq. (5.32)
$y_{\mathrm{fix}}(k)$	output signal of fixed-point system	Eq. (6.6)
$y_{\mathrm{flo}}(k)$	output signal of floating-point system	Eq. (6.6)
$z_{\mathrm{e}}(k)$	early reverberant speech	Eq. (6.14)
$z_{\mathrm{l}}(k)$	late reverberant speech	Eq. (6.14)
$z_{\mathrm{r}}(k)$	reverberant speech	Eq. (6.14)
$Z_{\mathrm{e}}(i,\kappa)$	spectral coefficients of early reverberant speech	Eq. (6.16)

Greek Symbols

α	real allpass pole ($K=1$)	Eq. (2.52)
$\alpha(m)$	real allpass pole ($K\geq 1$)	Eq. (2.49)
$\alpha_{\max}$	real allpass pole closest to unity ($K\geq 1$)	Eq. (6.1)

β_s	smoothing factor for speech PSD	Eq. (6.20)
β_u	smoothing factor for noise PSD	Eq. (6.20)
$\beta'_s(i)$	modified smoothing factor for (warped) subband i	Eq. (6.21)
γ	phase of complex allpass pole a	Eq. (2.52)
$\gamma(m)$	phase of complex allpass pole $a(m)$	Eq. (2.49)
γ_p	penalty factor for numerical design	Eq. (4.88)
ϵ	threshold for spectral gain factors	Eq. (5.20)
ϵ_bi	threshold for BSF calculation	Eq. (2.45)
ϵ_ls	threshold for LS FIR PE design	Eq. (3.84)
ϵ_a	upper bound for LS aliasing error	Eq. (4.83b)
ϵ_p	threshold for coefficients of $\widehat{\boldsymbol{p}}$	Figure 4.22
ζ_o	target SNR	Eq. (6.17)
$\zeta_\mathrm{prio}(i,\kappa)$	*a priori* SIR	Eq. (6.16)
$\zeta_\mathrm{post}(i,\kappa)$	*a posteriori* SIR	Eq. (6.15)
η	trade-off factor for constrained PR design	Eq. (4.120)
κ	sample index after downsampling	Eq. (5.1)
λ	index for polyphase components	Eq. (2.35)
μ	weighting factor for numerical FB design	Eq. (4.81)
ν	index for overall transfer function $T_\nu(z)$	Eq. (2.17)
$\xi_\mathrm{bark}(f)$	relation between frequency and Bark	Eq. (4.6)
$\xi_\mathrm{erb}(f)$	relation between frequency and ERB	Eq. (4.8)
$\boldsymbol{\xi}_\nu(z)$	vector of transfer function $T_\nu(z)$	Eq. (4.67)
$\overline{\boldsymbol{\xi}}_\nu(z)$	vector of transfer function for constrained PR design	Eq. (4.103)
ρ	epigraph variable	Eq. (4.84d)
$\varrho(m)$	periodicity of transformation kernel	Eq. (5.3)
σ_q^2	variance of input quantization noise	Eq. (6.5)
σ_out^2	variance of output quantization noise	Eq. (6.5)
$\sigma_{z_\mathrm{l}}^2(i,\kappa)$	short-term PSD of late reverberant speech	Eq. (6.16)
$\sigma_u^2(i,\kappa)$	short-term PSD of noise	Eq. (6.16)
$\tau(\Omega)$	group delay in general	Figure 3.11
$\tau_\mathrm{lin}(\Omega)$	group delay of linear transfer function $T_\mathrm{lin}\left(e^{j\,\Omega}\right)$	Eq. (2.11)
$\tau_\nu(\Omega)$	group delay of overall transfer function $T_\nu\left(e^{j\,\Omega}\right)$	Eq. (2.19)
$\tau_a(\Omega)$	group delay of allpass $A(z)$	Eq. (2.55)
$\tau_{\boldsymbol{a}}^{[K]}(\Omega)$	group delay of allpass $A^{[K]}(z)$	Eq. (2.59)
$\bar{\tau}$	nominal group delay in general	Eq. (3.73)
$\bar{\tau}^\mathrm{ap}$	nominal group delay for allpass PE	Eq. (3.111)
$\bar{\tau}^\mathrm{fir}$	nominal group delay for FIR PE	Eq. (3.98)
$\tau_\Psi(\Omega)$	group delay of transfer function $\Psi\left(e^{j\,\Omega}\right)$	Eq. (3.73)
$\tau_\Psi^\mathrm{ap}(\Omega)$	group delay of transfer function $\Psi^\mathrm{ap}\left(e^{j\,\Omega}\right)$	Eq. (3.107)

$\tau_{\Psi_\mathrm{s}}^{\mathrm{ap}}(\Omega)$	group delay of transfer function $\Psi_\mathrm{s}^{\mathrm{ap}}\left(e^{j\,\Omega}\right)$	Eq. (B.39)
$\tau_{\Psi}^{\mathrm{fir}}(\Omega)$	group delay of transfer function $\Psi^{\mathrm{fir}}\left(e^{j\,\Omega}\right)$	Eq. (3.97)
$\tau_{\Psi_\mathrm{s}}^{\mathrm{fir}}(\Omega)$	group delay of transfer function $\Psi_\mathrm{s}^{\mathrm{fir}}\left(e^{j\,\Omega}\right)$	Eq. (B.20)
υ	parameter for window function	Eq. (5.18)
$\phi(i)$	factor of GDCT	Eq. (5.26b)
$\varphi_{\bar{h}\bar{h}}(\lambda)$	auto-correlation coefficients	Eq. (5.50)
$\varphi(\Omega)$	phase response in general	Figure 3.3
$\varphi_{\mathrm{lin}}(\Omega)$	phase response of linear transfer function $T_{\mathrm{lin}}\left(e^{j\,\Omega}\right)$	Eq. (2.10)
$\varphi_{\nu}(\Omega)$	phase response of overall transfer function $T_{\nu}\left(e^{j\,\Omega}\right)$	Eq. (2.18)
$\varphi_{0}(\Omega)$	phase response of overall transfer function for $\nu = 0$	Eq. (2.21)
$\varphi_{a}(\Omega)$	phase response of allpass $A(z)$	Eq. (2.54)
$\varphi_{\alpha}^{[-1]}(\Omega)$	inverse phase response of allpass $A(z)$ with real pole	Eq. (4.111)
$\varphi_{\boldsymbol{a}}^{[K]}(\Omega)$	phase response of allpass $A^{[K]}(z)$	Eq. (2.58)
$\varphi_{\boldsymbol{b}}^{[K]}(\Omega)$	phase response of allpass $B^{[K]}(z)$	Eq. (4.13)
$\varphi_{\Psi}(\Omega)$	phase response of transfer function $\Psi\left(e^{j\,\Omega}\right)$	Eq. (3.71)
$\varphi_{\Psi}^{\mathrm{ap}}(\Omega)$	phase response of transfer function $\Psi^{\mathrm{ap}}\left(e^{j\,\Omega}\right)$	Eq. (3.106)
$\varphi_{\Psi_\mathrm{s}}^{\mathrm{ap}}(\Omega)$	phase response of transfer function $\Psi_\mathrm{s}^{\mathrm{ap}}\left(e^{j\,\Omega}\right)$	Eq. (B.38)
$\varphi_{\Psi}^{\mathrm{fir}}(\Omega)$	phase response of transfer function $\Psi^{\mathrm{fir}}\left(e^{j\,\Omega}\right)$	Eq. (3.92)
$\varphi_{\Psi_\mathrm{s}}^{\mathrm{fir}}(\Omega)$	phase response of transfer function $\Psi_\mathrm{s}^{\mathrm{fir}}\left(e^{j\,\Omega}\right)$	Eq. (B.17)
$\varphi_{\Theta}(\Omega)$	phase response of allpass $\Theta(z)$	Eq. (4.19b)
$\varphi_{\Theta}^{[-1]}(\Omega)$	inverse phase response of allpass $\Theta(z)$	Eq. (4.109)
$\chi(\Omega)$	integer to ensure unwrapped phase response	Eq. (2.54a)
$\bar{\psi}$	nominal phase factor in general	Eq. (3.28)
$\bar{\psi}^{\mathrm{ap}}$	nominal phase factor for allpass PE	Eq. (3.108)
$\bar{\psi}^{\mathrm{fir}}$	nominal phase factor for FIR PE	Eq. (3.93)
$\bar{\psi}_\mathrm{s}$	nominal phase factor for PE of single allpass	Eq. (3.76)
$\bar{\psi}_\mathrm{s}(m)$	nominal phase factor for PE of m-th single allpass	Eq. (3.77)
$\Theta(z)$	allpass for allpass transformation ($K \geq 1$)	Eq. (4.16)
$\Lambda(z)$	allpass for allpass transformation ($K \geq 1$)	Eq. (4.16)
$\boldsymbol{\Xi}_{\Delta}^{[\mathcal{N}]}$	matrix for CLS design	Eq. (4.79)
$\Phi_{ss}(i,\kappa)$	speech PSD	Eq. (6.18)
$\widehat{\Phi}_{ss}(i,\kappa)$	estimated speech PSD	Eq. (6.20a)
$\Phi_{\bar{s}\bar{s}}(i,\kappa)$	PSD of amplified speech	Eq. (6.17)
$\Phi_{uu}(i,\kappa)$	noise PSD	Eq. (6.17)
$\widehat{\Phi}_{uu}(i,\kappa)$	estimated noise PSD	Eq. (6.20b)
$\Phi(i,k)$	transformation kernel in general	Eq. (5.2)
$\Phi_{\mathrm{GDCT}}^{(I)}(i,k)$	transformation kernel for evenly-stacked GDCT	Eq. (5.27)
$\Phi_{\mathrm{GDCT}}^{(II)}(i,k)$	transformation kernel for oddly-stacked GDCT	Eq. (B.73)

$\Phi_{\mathrm{GDFT}}(i,k)$	transformation kernel for GDFT	Eq. (5.19)
$\Psi(z)$	transfer function of allpass and PE	Eq. (3.69)
$\Psi_{\mathrm{d}}(z)$	desired transfer function of allpass and PE	Eq. (3.70)
$\Psi_{\mathrm{s}}(z)$	transfer function of allpass and PE ($K=1$)	Eq. (3.76)
$\Psi^{\mathrm{fir}}(z)$	transfer function of allpass and FIR PE ($K \geq 1$)	Eq. (3.86)
$\Psi_{\mathrm{s}}^{\mathrm{fir}}(z)$	transfer function of allpass and FIR PE ($K=1$)	Eq. (3.85)
$\Psi^{\mathrm{ap}}(z)$	transfer function of allpass and allpass PE ($K \geq 1$)	Eq. (3.104)
$\Psi_{\mathrm{s}}^{\mathrm{ap}}(z)$	transfer function of allpass and allpass PE ($K=1$)	Eq. (3.101)
$\Psi_{i}^{\mathrm{ap}}(z)$	transfer function of allpass and allpass PE in branch i	Eq. (3.36)
Ω	normalized frequency (shortly termed as frequency)	Eq. (2.5)
Ω_1, Ω_2	frequencies of BSF	Eq. (2.39)
Ω_{s}	stopband frequency of prototype filter	Eq. (3.21)
Ω_{μ}	extremal frequencies	Eq. (3.89b)
$\Omega_{\mathrm{l}}^{(\mathrm{s})}(i)$	left stopband frequency of subband i	Eq. (4.109)
$\Omega_{\mathrm{r}}^{(\mathrm{s})}(i)$	right stopband frequency of subband i	Eq. (4.110)
$\Omega_{\mathrm{l}}^{(\mathrm{p})}(i)$	left passband frequency of subband i	Eq. (4.116)
$\Omega_{\mathrm{r}}^{(\mathrm{p})}(i)$	right passband frequency of subband i	Eq. (4.117)
$\Delta\Omega$	passband width of uniform analysis filter	Sec. 2.1
$\Delta\Omega_i$	passband widths of i-th analysis filter	Sec. 2.1
$\Delta\widetilde{\Omega}_i$	passband widths of i-th warped analysis filter	Eq. (6.22)
$\Delta\tau_{\Psi}(\Omega)$	group delay error of phase equalization in general	Eq. (3.74c)
$\Delta\tau_{\Psi}^{\mathrm{ap}}(\Omega)$	group delay error for allpass PE	Eq. (3.111)
$\Delta\tau_{\Psi}^{\mathrm{fir}}(\Omega)$	group delay error for FIR PE	Eq. (3.98)
$\Delta\varphi_{\Psi}(\Omega)$	phase error of phase equalization in general	Eq. (3.74b)
$\Delta\varphi_{\Psi}^{\mathrm{ap}}(\Omega)$	phase error for allpass PE	Eq. (3.108)
$\Delta\varphi_{\Psi}^{\mathrm{fir}}(\Omega)$	phase error for FIR PE	Eq. (3.93)
$\Delta\varphi_0(\Omega)$	phase error of overall transfer function for $\nu=0$	Eq. (2.21)
$\Delta\varphi_{\mathrm{lin}}(\Omega)$	phase error of linear transfer function	Eq. (2.16)
$\Delta\left\lvert\Psi\left(e^{j\,\Omega}\right)\right\rvert$	magnitude error of phase equalization in general	Eq. (3.74a)
$\Delta\left\lvert\Psi^{\mathrm{fir}}\left(e^{j\,\Omega}\right)\right\rvert$	magnitude error for FIR PE	Eq. (3.88)

Units

dB	decibel
Hz	Hertz
kHz	kiloHertz
kbit/s	kilobit per second
ms	milliseconds
s	seconds

Appendix B

Proofs & Derivations

B.1 Evaluation of the Discrete BSF

The frequency sampled version for the bifrequency system function (BSF) according to Eq. (2.41) is considered

$$T_{\mathrm{bi}}\left(e^{j\,\frac{2\,\pi}{N_{\mathrm{bi}}}\,i_2}, e^{j\,\frac{2\,\pi}{N_{\mathrm{bi}}}\,i_1}\right) = \frac{1}{N_{\mathrm{bi}}^2}\sum_{k_1=0}^{N_{\mathrm{bi}}-1}\sum_{k_2=0}^{N_{\mathrm{bi}}-1} t_{\mathrm{bi}}(k_2,k_1)\cdot e^{j\,\frac{2\,\pi}{N_{\mathrm{bi}}}\,(k_1\,i_1-k_2\,i_2)}\,. \qquad [2.41]$$

It follows from Eq. (2.38) that

$$t_{\mathrm{bi}}(k_2,k_1) = \frac{1}{N_{\mathrm{bi}}}\sum_{m=0}^{N_{\mathrm{bi}}-1} t_{\mathrm{bi}}(k_2+m\,R,k_1+m\,R)\,. \qquad \text{(B.1)}$$

This relation and the substitution

$$k_2 = k_1 + k;\quad k_1 \in \{0,1,\ldots,R-1\};\quad k \in \{0,1,\ldots,N_{\mathrm{bi}}-1\} \qquad \text{(B.2)}$$

allow the following conversion of Eq. (2.41)

$$\begin{aligned} T_{\mathrm{bi}}\left(e^{j\,\frac{2\pi}{N_{\mathrm{bi}}}\,i_2}, e^{j\,\frac{2\pi}{N_{\mathrm{bi}}}\,i_1}\right) &= \frac{1}{R\,N_{\mathrm{bi}}^2}\sum_{k_1=0}^{R-1}\sum_{k=0}^{N_{\mathrm{bi}}-1}\sum_{m=0}^{N_{\mathrm{bi}}-1} t_{\mathrm{bi}}(k_1+k+m\,R,k_1+m\,R) \\ &\qquad\qquad \cdot e^{j\,\frac{2\,\pi}{N_{\mathrm{bi}}}\left(i_1\,(k_1+m\,R)-i_2\,(k_1+k+m\,R)\right)} \\ &= \frac{1}{R\,N_{\mathrm{bi}}^2}\sum_{k_1=0}^{R-1}\sum_{k=0}^{N_{\mathrm{bi}}-1} t_{\mathrm{bi}}(k_1+k,k_1)\cdot e^{j\,\frac{2\,\pi}{N_{\mathrm{bi}}}\,k_1\,(i_1-i_2)} \\ &\qquad\qquad \cdot e^{-j\,\frac{2\,\pi}{N_{\mathrm{bi}}}\,k\,i_2}\sum_{m=0}^{N_{\mathrm{bi}}-1} e^{j\,\frac{2\,\pi}{N_{\mathrm{bi}}}\,mR(i_1-i_2)}\,. \end{aligned} \qquad \text{(B.3)}$$

Since

$$\sum_{m=0}^{N_{\mathrm{bi}}-1} e^{j\,\frac{2\,\pi}{N_{\mathrm{bi}}}\,mR(i_1-i_2)} = \begin{cases} N_{\mathrm{bi}} & \text{if } i_1 = i_2 + \frac{N_{\mathrm{bi}}}{R}\,l\ \forall\ l \in \mathbb{Z} \\ 0 & \text{otherwise,} \end{cases} \qquad \text{(B.4)}$$

the discrete BSF is finally given by

$$T_{\mathrm{bi}}\left(e^{j\frac{2\pi}{N_{\mathrm{bi}}}i_2}, e^{j\frac{2\pi}{N_{\mathrm{bi}}}\left(i_2+l\frac{N_{\mathrm{bi}}}{R}\right)}\right) = \begin{cases} \dfrac{1}{R\,N_{\mathrm{bi}}}\displaystyle\sum_{k_1=0}^{R-1}\sum_{k=0}^{N_{\mathrm{bi}}-1} t_{\mathrm{bi}}(k_1+k,k_1)\cdot e^{j\frac{2\pi}{R}k_1 l}\cdot e^{-j\frac{2\pi}{N_{\mathrm{bi}}}k\,i_2} & \text{if } l\in\mathbb{Z} \\ 0 & \text{if } l\notin\mathbb{Z}\,. \end{cases} \quad [2.42]$$

It is sufficient to evaluate Eq. (2.42) only for $l \in \{0, \pm1, \pm2, \ldots \pm(R-1)\}$ due to the periodicity

$$e^{j\frac{2\pi}{R}k_1 l} = e^{j\frac{2\pi}{R}k_1(l+mR)} \;\forall\; m,l\in\mathbb{Z}\,. \tag{B.5}$$

The calculation of the discrete BSF by Eq. (2.42) is much more efficient than by means of Eq. (2.41) as $N_{\mathrm{bi}} \gg R$.

B.2 Equiripple Property of Parametric Phase Equalizers

This section provides details of the derivations in Sec. 3.3.4.2 and Sec. 3.3.4.3. To ease the treatment, only a cascade of an allpass filter of first order and a phase equalizer

$$\Psi_{\mathrm{s}}\left(e^{j\,\Omega}\right) = A\left(e^{j\,\Omega}\right)\cdot\mathcal{P}\left(e^{j\,\Omega}\right) \tag{B.6}$$

is considered as the frequency response in case of an allpass chain of length L_{ac} is simply given by

$$\Psi\left(e^{j\,\Omega}\right) = \left(\Psi_{\mathrm{s}}\left(e^{j\,\Omega}\right)\right)^{L_{\mathrm{ac}}} \tag{B.7}$$

according to Eq. (3.78).

B.2.1 FIR Phase Equalizer

The transfer function of an allpass filter of first order and FIR phase equalizer is considered according to Eq. (3.85)

$$\begin{aligned}\Psi_{\mathrm{s}}^{\mathrm{fir}}(z) &= A(z)\cdot\mathcal{P}^{\mathrm{fir}}(z)\\ &= z^{-D_{\mathrm{s}}} - (a^*)^{D_{\mathrm{s}}}\,.\end{aligned} \tag{B.8}$$

The frequency response for a complex allpass pole $a = \alpha\,e^{j\,\gamma}$ reads

$$\begin{aligned}\Psi_{\mathrm{s}}^{\mathrm{fir}}\left(e^{j\,\Omega}\right) &= e^{-j\,D_{\mathrm{s}}\,\Omega} - \alpha^{D_{\mathrm{s}}}e^{-j\,\gamma\,D_{\mathrm{s}}}\\ &= \cos(D_{\mathrm{s}}\,\Omega) - \alpha^{D_{\mathrm{s}}}\cos(D_{\mathrm{s}}\,\gamma) - j\left(\sin(D_{\mathrm{s}}\,\Omega) - \alpha^{D_{\mathrm{s}}}\sin(D_{\mathrm{s}}\,\gamma)\right)\,.\end{aligned} \tag{B.9}$$

The *magnitude response* can be written

$$\begin{aligned}\left|\Psi_{\mathrm{s}}^{\mathrm{fir}}\left(e^{j\,\Omega}\right)\right|^2 &= \cos^2(D_{\mathrm{s}}\,\Omega) - 2\,\alpha^{D_{\mathrm{s}}}\cos(D_{\mathrm{s}}\,\Omega)\,\cos(D_{\mathrm{s}}\,\gamma) + \alpha^{2D_{\mathrm{s}}}\cos^2(D_{\mathrm{s}}\,\gamma)\\ &\quad + \sin^2(D_{\mathrm{s}}\,\Omega) - 2\,\alpha^{D_{\mathrm{s}}}\sin(D_{\mathrm{s}}\,\Omega)\,\sin(D_{\mathrm{s}}\,\gamma) + \alpha^{2D_{\mathrm{s}}}\sin^2(D_{\mathrm{s}}\gamma)\\ &= 1 - 2\,\alpha^{D_{\mathrm{s}}}\Big(\cos(D_{\mathrm{s}}\Omega)\,\cos(D_{\mathrm{s}}\,\gamma) + \sin(D_{\mathrm{s}}\,\Omega)\,\sin(D_{\mathrm{s}}\,\gamma)\Big) + \alpha^{2D_{\mathrm{s}}}\\ &= 1 - 2\,\alpha^{D_{\mathrm{s}}}\cos\Big(D_{\mathrm{s}}\,(\Omega-\gamma)\Big) + \alpha^{2D_{\mathrm{s}}}\,. \end{aligned} \tag{B.10}$$

This leads to Eq. (3.87) by applying Eq. (B.7). It follows from Eq. (B.10) that the extrema

$$c_{\max}^{\mathrm{fir}} = \max_{\Omega}\left\{\left|\Psi_{\mathrm{s}}^{\mathrm{fir}}\left(e^{j\,\Omega}\right)\right|\right\} = \sqrt{1+2\,|\alpha|^{D_{\mathrm{s}}}+\alpha^{2D_{\mathrm{s}}}} = 1+|\alpha|^{D_{\mathrm{s}}} \tag{B.11}$$

$$c_{\min}^{\mathrm{fir}} = \min_{\Omega}\left\{\left|\Psi_{\mathrm{s}}^{\mathrm{fir}}\left(e^{j\,\Omega}\right)\right|\right\} = \sqrt{1-2\,|\alpha|^{D_{\mathrm{s}}}+\alpha^{2D_{\mathrm{s}}}} = 1-|\alpha|^{D_{\mathrm{s}}} \tag{B.12}$$

are obtained at the extremal frequencies

$$\Omega_\mu = \frac{\mu\,\pi}{D_{\mathrm{s}}} + \gamma \quad \text{for} \quad \mu \in \mathbb{Z}\,. \tag{B.13}$$

The magnitude error

$$\Delta\left|\Psi_{\mathrm{s}}^{\mathrm{fir}}\left(e^{j\,\Omega}\right)\right| = \left|\Psi_{\mathrm{s}}^{\mathrm{fir}}\left(e^{j\,\Omega}\right)\right| - \underbrace{\frac{1}{2}\left(c_{\min}^{\mathrm{fir}} + c_{\max}^{\mathrm{fir}}\right)}_{=\,\overline{c}^{\mathrm{fir}}} \tag{B.14}$$

has the alternating extrema

$$\max_{\Omega}\left\{\Delta\left|\Psi_{\mathrm{s}}^{\mathrm{fir}}\left(e^{j\,\Omega}\right)\right|\right\} = c_{\max}^{\mathrm{fir}} - \overline{c}^{\mathrm{fir}} = \frac{1}{2}\left(c_{\max}^{\mathrm{fir}} - c_{\min}^{\mathrm{fir}}\right) \tag{B.15}$$

$$\min_{\Omega}\left\{\Delta\left|\Psi_{\mathrm{s}}^{\mathrm{fir}}\left(e^{j\,\Omega}\right)\right|\right\} = c_{\min}^{\mathrm{fir}} - \overline{c}^{\mathrm{fir}} = -\frac{1}{2}\left(c_{\max}^{\mathrm{fir}} - c_{\min}^{\mathrm{fir}}\right)\,. \tag{B.16}$$

With these relations, it is straightforward to obtain Eq. (3.88) and Eq. (3.89). The (unwrapped) *phase response* of Eq. (B.9) is given by

$$\varphi_{\Psi_{\mathrm{s}}}^{\mathrm{fir}}(\Omega) = \arctan\left(\frac{\sin(D_{\mathrm{s}}\,\Omega) - \alpha^{D_{\mathrm{s}}}\sin(D_{\mathrm{s}}\,\gamma)}{\cos(D_{\mathrm{s}}\,\Omega) - \alpha^{D_{\mathrm{s}}}\cos(D_{\mathrm{s}}\,\gamma)}\right) + 2\,\pi\,\chi(D_{\mathrm{s}}\,\Omega)\,. \tag{B.17}$$

The phase representations of Eq. (2.54) can be exploited to rewrite Eq. (B.17) as follows

$$\varphi_{\Psi_{\mathrm{s}}}^{\mathrm{fir}}(\Omega) = \frac{1}{2}\left(\varphi_{a^{D_{\mathrm{s}}}}\left(D_{\mathrm{s}}\,\Omega\right) + D_{\mathrm{s}}\,\Omega\right) \tag{B.18}$$

$$= \arctan\left(\frac{\alpha^{D_{\mathrm{s}}}\sin\left(D_{\mathrm{s}}\,(\Omega-\gamma)\right)}{1-\alpha^{D_{\mathrm{s}}}\cos\left(D_{\mathrm{s}}\,(\Omega-\gamma)\right)}\right) + D_{\mathrm{s}}\,\Omega + \pi\,\chi(D_{\mathrm{s}}\,\Omega)\,. \tag{B.19}$$

The representation of Eq. (B.18) allows to determine the *group delay* by means of Eq. (2.55) according to

$$\tau_{\Psi_\mathrm{s}}^{\mathrm{fir}}(\Omega) = \frac{D_\mathrm{s}}{2}\left(\tau_{a^{D_\mathrm{s}}}\left(D_\mathrm{s}\,\Omega\right)+1\right) \tag{B.20}$$

$$= \frac{D_\mathrm{s}}{2}\,\frac{1-\alpha^{2D_\mathrm{s}}}{1-2\,\alpha^{D_\mathrm{s}}\cos\left(D_\mathrm{s}\,(\Omega-\gamma)\right)+\alpha^{2D_\mathrm{s}}}+\frac{D_\mathrm{s}}{2}$$

$$= D_\mathrm{s}\,\frac{1-\alpha^{D_\mathrm{s}}\cos\left(D_\mathrm{s}\,(\Omega-\gamma)\right)}{1-2\,\alpha^{D_\mathrm{s}}\cos\left(D_\mathrm{s}\,(\Omega-\gamma)\right)+\alpha^{2D_\mathrm{s}}}\,. \tag{B.21}$$

Eq. (B.19) leads to the phase error

$$\Delta\varphi_{\Psi_\mathrm{s}}^{\mathrm{fir}}(\Omega) = \varphi_{\Psi_\mathrm{s}}^{\mathrm{fir}}(\Omega) - D_\mathrm{s}\,\Omega \tag{B.22}$$

$$= \arctan\left(\frac{\alpha^{D_\mathrm{s}}\sin\left(D_\mathrm{s}\,(\Omega-\gamma)\right)}{1-\alpha^{D_\mathrm{s}}\cos\left(D_\mathrm{s}\,(\Omega-\gamma)\right)}\right)+\pi\,\chi(D_\mathrm{s}\,\Omega)\,. \tag{B.23}$$

The extremal frequencies Ω_μ are determined by

$$\frac{\partial}{\partial\,\Omega_\mu}\left(\varphi_{\Psi_\mathrm{s}}^{\mathrm{fir}}(\Omega)-D_\mathrm{s}\,\Omega\right) = \tau_{\Psi_\mathrm{s}}^{\mathrm{fir}}(\Omega_\mu)-D_\mathrm{s}\overset{!}{=}0\,. \tag{B.24}$$

Inserting Eq. (B.21) results

$$\begin{aligned}
& D_\mathrm{s}\,\frac{1-\alpha^{D_\mathrm{s}}\cos\left(D_\mathrm{s}\,(\Omega_\mu-\gamma)\right)}{1-2\,\alpha^{D_\mathrm{s}}\cos\left(D_\mathrm{s}\,(\Omega_\mu-\gamma)\right)+\alpha^{2D_\mathrm{s}}}-D_\mathrm{s}=0\\
\Leftrightarrow\quad & 1-\alpha^{D_\mathrm{s}}\cos\left(D_\mathrm{s}\,(\Omega_\mu-\gamma)\right)=1-2\,\alpha^{D_\mathrm{s}}\cos\left(D_\mathrm{s}\,(\Omega_\mu-\gamma)\right)+\alpha^{2D_\mathrm{s}}\\
\Leftrightarrow\quad & \cos\left(D_\mathrm{s}\,(\Omega_\mu-\gamma)\right)=\alpha^{D_\mathrm{s}}\quad\text{for}\quad\alpha\neq0\\
\Rightarrow\quad & \Omega_\mu=\frac{1}{D_\mathrm{s}}\left(2\,\pi\,\mu\pm\arccos\left(\alpha^{D_\mathrm{s}}\right)\right)+\gamma\quad\text{for}\quad\mu\in\mathbb{Z}\,.
\end{aligned} \tag{B.25}$$

A sufficient condition for an extrema is that the second derivative is unequal to zero at the extremal frequencies. This proof is straightforward and omitted here and the following treatments. Inserting the extremal frequencies of Eq. (B.25) into Eq. (B.23) yields the extrema

$$\Delta\varphi_{\Psi_\mathrm{s}}^{\mathrm{fir}}(\Omega_\mu) = \pm\arctan\left(\frac{\alpha^{D_\mathrm{s}}\sin\left(\arccos\left(\alpha^{D_\mathrm{s}}\right)\right)}{1-\alpha^{2D_\mathrm{s}}}\right)\,. \tag{B.26}$$

Finally, the rewriting of Eq. (B.25) and Eq. (B.26) according to Eq. (3.95b) ensures the order $\Omega_\mu < \Omega_{\mu+1} < \Omega_{\mu+2}\ldots$ for the extremal frequencies.

The extrema for the group delay

$$\Delta\tau_{\Psi_\mathrm{s}}^{\mathrm{fir}}(\Omega) = \tau_{\Psi_\mathrm{s}}^{\mathrm{fir}}(\Omega)-\overline{\tau}^{\mathrm{fir}} \tag{B.27}$$

are obtained by the partial derivative of Eq. (B.21)

$$\frac{\partial\,\tau_{\Psi_\mathrm{s}}^{\mathrm{fir}}(\Omega)}{\partial\,\Omega} = \frac{{D_\mathrm{s}}^2\,\alpha^{D_\mathrm{s}}\sin\left(D_\mathrm{s}\,(\Omega-\gamma)\right)}{f_\mathrm{D}^2(\Omega)}\left(f_\mathrm{D}(\Omega) - 2\left(1-\alpha^{D_\mathrm{s}}\cos\left(D_\mathrm{s}\,(\Omega-\gamma)\right)\right)\right) \tag{B.28}$$

with

$$f_\mathrm{D}(\Omega) = 1 - 2\,\alpha^{D_\mathrm{s}}\cos\left(D_\mathrm{s}\,(\Omega-\gamma)\right) + \alpha^{2D_\mathrm{s}}\,. \tag{B.29}$$

It follows directly that

$$\frac{\partial\,\tau_{\Psi_\mathrm{s}}^{\mathrm{fir}}(\Omega)}{\partial\,\Omega_\mu} = 0 \quad \text{if} \quad \sin\left(D_\mathrm{s}\,(\Omega_\mu-\gamma)\right) = 0\,. \tag{B.30}$$

This is fulfilled for the extremal frequencies

$$\Omega_\mu = \frac{\mu\,\pi}{D_\mathrm{s}} + \gamma \quad \text{for} \quad \mu \in \mathbb{Z} \tag{B.31}$$

while the denominator fulfills the requirement $f_\mathrm{D}(\Omega_\mu) \neq 0$. Accordingly, the group delay of Eq. (B.21) has the extremal values

$$\tau_{\max}^{\mathrm{fir}} = \max_{\Omega}\left\{\tau_{\Psi_\mathrm{s}}^{\mathrm{fir}}(\Omega)\right\} = D_\mathrm{s}\,\frac{1-|\alpha|^{D_\mathrm{s}}}{1-2\,|\alpha|^{D_\mathrm{s}}+\alpha^{2D_\mathrm{s}}} = \frac{D_\mathrm{s}}{1-|\alpha|^{D_\mathrm{s}}} \tag{B.32}$$

$$\tau_{\min}^{\mathrm{fir}} = \min_{\Omega}\left\{\tau_{\Psi_\mathrm{s}}^{\mathrm{fir}}(\Omega)\right\} = D_\mathrm{s}\,\frac{1+|\alpha|^{D_\mathrm{s}}}{1+2\,|\alpha|^{D_\mathrm{s}}+\alpha^{2D_\mathrm{s}}} = \frac{D_\mathrm{s}}{1+|\alpha|^{D_\mathrm{s}}}\,. \tag{B.33}$$

The relation

$$\begin{aligned}\overline{\tau}^{\mathrm{fir}} &= \frac{D_\mathrm{s}}{2}\,\left(\tau_{\max}^{\mathrm{fir}} + \tau_{\min}^{\mathrm{fir}}\right)\\ &= \frac{D_\mathrm{s}}{2}\,\left(\frac{1}{1-\alpha^{D_\mathrm{s}}} + \frac{1}{1+\alpha^{D_\mathrm{s}}}\right) = \frac{D_\mathrm{s}}{1-\alpha^{2D_\mathrm{s}}}\end{aligned} \tag{B.34}$$

yields the following extremal values for $\Delta\tau_{\Psi_\mathrm{s}}^{\mathrm{fir}}(\Omega_\mu)$

$$\begin{aligned}\max_{\Omega}\left\{\Delta\tau_{\Psi_\mathrm{s}}^{\mathrm{fir}}(\Omega)\right\} &= \tau_{\max}^{\mathrm{fir}} - \overline{\tau}^{\mathrm{fir}}\\ &= \frac{D_\mathrm{s}}{1-|\alpha|^{D_\mathrm{s}}} - \frac{D_\mathrm{s}}{1-\alpha^{2D_\mathrm{s}}} = \frac{|\alpha|^{D_\mathrm{s}}D_\mathrm{s}}{1-\alpha^{2D_\mathrm{s}}}\end{aligned} \tag{B.35a}$$

$$\begin{aligned}\min_{\Omega}\left\{\Delta\tau_{\Psi_\mathrm{s}}^{\mathrm{fir}}(\Omega)\right\} &= \tau_{\min}^{\mathrm{fir}} - \overline{\tau}^{\mathrm{fir}}\\ &= \frac{D_\mathrm{s}}{1+|\alpha|^{D_\mathrm{s}}} - \frac{D_\mathrm{s}}{1-\alpha^{2D_\mathrm{s}}} = \frac{-|\alpha|^{D_\mathrm{s}}D_\mathrm{s}}{1-\alpha^{2D_\mathrm{s}}}\,.\end{aligned} \tag{B.35b}$$

Therefore,

$$\Delta\tau_{\Psi_\mathrm{s}}^{\mathrm{fir}}(\Omega_\mu) = (-1)^\mu\,\frac{\alpha^{D_\mathrm{s}}D_\mathrm{s}}{1-\alpha^{2D_\mathrm{s}}} \tag{B.36}$$

which finally leads to Eq. (3.100).

B.2.2 IIR Phase Equalizer

The transfer function of an allpass filter of first order and an allpass phase equalizer is considered according to Eq. (3.101)

$$\begin{aligned}\Psi_{\mathrm{s}}^{\mathrm{ap}}(z) &= A(z)\cdot\mathcal{P}^{\mathrm{ap}}(z)\\ &= \frac{1-(a^{*}z)^{D_{\mathrm{s}}}}{z^{D_{\mathrm{s}}}-a^{D_{\mathrm{s}}}}\,.\end{aligned} \tag{B.37}$$

The transfer function of Eq. (B.37) is an allpass filter of order D_{s} with a complex pole at $\alpha^{D_{\mathrm{s}}}\,e^{j\,D_{\mathrm{s}}\,\gamma}$. Therefore, *phase response* and *group delay* are readily obtained from Eq. (2.54b) and Eq. (2.55)

$$\varphi_{\Psi_{\mathrm{s}}}^{\mathrm{ap}}(\Omega) = 2\,\arctan\left(\frac{\sin(D_{\mathrm{s}}\,\Omega)-\alpha^{D_{\mathrm{s}}}\sin(D_{\mathrm{s}}\,\gamma)}{\cos(D_{\mathrm{s}}\,\Omega)-\alpha^{D_{\mathrm{s}}}\cos(D_{\mathrm{s}}\,\gamma)}\right) - D_{\mathrm{s}}\,\Omega + 2\,\pi\,\chi(D_{\mathrm{s}}\,\Omega) \tag{B.38}$$

$$\tau_{\Psi_{\mathrm{s}}}^{\mathrm{ap}}(\Omega) = D_{\mathrm{s}}\,\frac{1-\alpha^{2D_{\mathrm{s}}}}{1-2\,\alpha^{D_{\mathrm{s}}}\cos\big(D_{\mathrm{s}}\,(\Omega-\gamma)\big)+\alpha^{2D_{\mathrm{s}}}}\,. \tag{B.39}$$

The relation of the phase response of Eq. (B.38) to that of Eq. (B.17) is given by

$$\varphi_{\Psi_{\mathrm{s}}}^{\mathrm{ap}}(\Omega) = 2\,\varphi_{\Psi_{\mathrm{s}}}^{\mathrm{fir}}(\Omega) - D_{\mathrm{s}}\,\Omega \tag{B.40}$$

such that the *phase error* can be written

$$\begin{aligned}\Delta\varphi_{\Psi_{\mathrm{s}}}^{\mathrm{ap}}(\Omega) &= \varphi_{\Psi_{\mathrm{s}}}^{\mathrm{ap}}(\Omega) - D_{\mathrm{s}}\,\Omega &\text{(B.41)}\\ &= 2\left(\varphi_{\Psi_{\mathrm{s}}}^{\mathrm{fir}}(\Omega) - D_{\mathrm{s}}\,\Omega\right)\\ &= 2\,\Delta\varphi_{\Psi_{\mathrm{s}}}^{\mathrm{fir}}(\Omega)\,. &\text{(B.42)}\end{aligned}$$

Thus, the allpass phase equalizer yields an equiripple phase error which is twice as high as for the FIR phase equalizer and has the same extremal frequencies as given by Eq. (B.25).

The group delay of Eq. (B.39) is related to the group delay of Eq. (B.20) as follows

$$\tau_{\Psi_{\mathrm{s}}}^{\mathrm{ap}}(\Omega) = 2\;\tau_{\Psi_{\mathrm{s}}}^{\mathrm{fir}}(\Omega) - D_{\mathrm{s}}\,. \tag{B.43}$$

Thus, the group delay error

$$\Delta\tau_{\Psi_{\mathrm{s}}}^{\mathrm{ap}}(\Omega) = \tau_{\Psi_{\mathrm{s}}}^{\mathrm{ap}}(\Omega) - \overline{\tau}^{\mathrm{ap}} \tag{B.44}$$

has the extremal frequencies Ω_{μ} of Eq. (B.31) as the group delay error $\Delta\tau_{\Psi_{\mathrm{s}}}^{\mathrm{fir}}(\Omega)$. The extremal values of the group delay $\tau_{\Psi_{\mathrm{s}}}^{\mathrm{ap}}(\Omega_{\mu})$ are given by

$$\tau_{\max}^{\mathrm{ap}} = D_{\mathrm{s}}\,\frac{1-\alpha^{2D_{\mathrm{s}}}}{1-2\,|\alpha|^{D_{\mathrm{s}}}+\alpha^{2D_{\mathrm{s}}}} = D_{\mathrm{s}}\,\frac{1+|\alpha|^{D_{\mathrm{s}}}}{1-|\alpha|^{D_{\mathrm{s}}}} \tag{B.45}$$

$$\tau_{\min}^{\mathrm{ap}} = D_{\mathrm{s}}\,\frac{1-\alpha^{2D_{\mathrm{s}}}}{1+2\,|\alpha|^{D_{\mathrm{s}}}+\alpha^{2D_{\mathrm{s}}}} = D_{\mathrm{s}}\,\frac{1-|\alpha|^{D_{\mathrm{s}}}}{1+|\alpha|^{D_{\mathrm{s}}}} \tag{B.46}$$

such that

$$\overline{\tau}^{\mathrm{ap}} = \frac{1}{2}\left(\tau_{\min}^{\mathrm{ap}} + \tau_{\max}^{\mathrm{ap}}\right) \tag{B.47}$$

$$= \frac{D_{\mathrm{s}}}{2}\frac{\left(1+\alpha^{D_{\mathrm{s}}}\right)\left(1+\alpha^{D_{\mathrm{s}}}\right)+\left(1-\alpha^{D_{\mathrm{s}}}\right)\left(1-\alpha^{D_{\mathrm{s}}}\right)}{\left(1+\alpha^{D_{\mathrm{s}}}\right)\left(1-\alpha^{D_{\mathrm{s}}}\right)}$$

$$= D_{\mathrm{s}}\,\frac{1+\alpha^{2D_{\mathrm{s}}}}{1-\alpha^{2D_{\mathrm{s}}}}\,. \tag{B.48}$$

The yields the following extrema for the group delay error of Eq. (B.44)

$$\max_{\Omega}\left\{\Delta\tau_{\Psi_{\mathrm{s}}}^{\mathrm{ap}}(\Omega)\right\} = \tau_{\max}^{\mathrm{ap}} - \overline{\tau}^{\mathrm{ap}} \tag{B.49}$$

$$= D_{\mathrm{s}}\left(\frac{1+|\alpha|^{D_{\mathrm{s}}}}{1-|\alpha|^{D_{\mathrm{s}}}} - \frac{1+\alpha^{2D_{\mathrm{s}}}}{\left(1+\alpha^{D_{\mathrm{s}}}\right)\left(1-\alpha^{D_{\mathrm{s}}}\right)}\right)$$

$$= D_{\mathrm{s}}\,\frac{\left(1+|\alpha|^{D_{\mathrm{s}}}\right)^2 - \left(1+\alpha^{2D_{\mathrm{s}}}\right)}{\left(1-\alpha^{D_{\mathrm{s}}}\right)\left(1+\alpha^{D_{\mathrm{s}}}\right)}$$

$$= \frac{2\,|\alpha|^{D_{\mathrm{s}}} D_{\mathrm{s}}}{1-\alpha^{2D_{\mathrm{s}}}} \tag{B.50}$$

and

$$\min_{\Omega}\left\{\Delta\tau_{\Psi_{\mathrm{s}}}^{\mathrm{ap}}(\Omega)\right\} = \tau_{\min}^{\mathrm{ap}} - \overline{\tau}^{\mathrm{ap}} \tag{B.51}$$

$$= D_{\mathrm{s}}\left(\frac{1-|\alpha|^{D_{\mathrm{s}}}}{1+|\alpha|^{D_{\mathrm{s}}}} - \frac{1+\alpha^{2D_{\mathrm{s}}}}{\left(1+\alpha^{D_{\mathrm{s}}}\right)\left(1-\alpha^{D_{\mathrm{s}}}\right)}\right)$$

$$= D_{\mathrm{s}}\,\frac{\left(1-|\alpha|^{D_{\mathrm{s}}}\right)^2 - \left(1+\alpha^{2D_{\mathrm{s}}}\right)}{\left(1-\alpha^{D_{\mathrm{s}}}\right)\left(1+\alpha^{D_{\mathrm{s}}}\right)}$$

$$= \frac{-2\,|\alpha|^{D_{\mathrm{s}}} D_{\mathrm{s}}}{1-\alpha^{2D_{\mathrm{s}}}}\,. \tag{B.52}$$

Thus, the *group delay error* of Eq. (B.44) has the alternating extrema

$$\Delta\tau_{\Psi_{\mathrm{s}}}^{\mathrm{ap}}(\Omega_\mu) = (-1)^\mu\,\frac{2\,\alpha^{D_{\mathrm{s}}} D_{\mathrm{s}}}{1-\alpha^{2D_{\mathrm{s}}}} \tag{B.53}$$

such that

$$\Delta\tau_{\Psi_{\mathrm{s}}}^{\mathrm{ap}}(\Omega_\mu) = 2\,\Delta\tau_{\Psi_{\mathrm{s}}}^{\mathrm{fir}}(\Omega_\mu) \quad \text{for} \quad \Omega_\mu = \frac{\mu\,\pi}{D_{\mathrm{s}}} + \gamma; \quad \mu \in \mathbb{Z} \tag{B.54}$$

due to Eq. (B.36).

B.3 Conversion from QCQP to SDP Design

It is shown how the quadratically constrained quadratic program (QCQP) according to Eq. (4.83)

$$\underset{\boldsymbol{p}}{\text{minimize}} \left\| \boldsymbol{U}^{[\mathcal{N}]} \cdot \boldsymbol{p} - \boldsymbol{v}^{[\mathcal{N}]} \right\|_2^2 \tag{4.83a}$$

$$\text{subject to} \left\| \boldsymbol{\Xi}_{\Delta}^{[\mathcal{N}]} \cdot \boldsymbol{p} \right\|_2^2 \leq \epsilon_{\mathrm{a}}; \quad \epsilon_{\mathrm{a}} \in \mathbb{R}_+ \tag{4.83b}$$

is converted to an equivalent semi-definite program (SDP) according to Eq. (4.84). In a first step, Eq. (4.83) is formulated in an epigraph form[1]

$$\underset{\boldsymbol{p},\, \rho \geq 0}{\text{minimize}} \; \rho \tag{B.56a}$$

$$\text{subject to} \left\| \boldsymbol{U}^{[\mathcal{N}]} \cdot \boldsymbol{p} - \boldsymbol{v}^{[\mathcal{N}]} \right\|_2^2 \leq \rho \tag{B.56b}$$

$$\left\| \boldsymbol{\Xi}_{\Delta}^{[\mathcal{N}]} \cdot \boldsymbol{p} \right\|_2^2 \leq \epsilon_{\mathrm{a}} \,. \tag{B.56c}$$

The inequality of Eq. (B.56b) can be written as

$$\left(\boldsymbol{U}^{[\mathcal{N}]}\boldsymbol{p}\right)^H \left(\boldsymbol{U}^{[\mathcal{N}]}\boldsymbol{p}\right) - c(\boldsymbol{p}) - \rho \leq 0 \tag{B.57}$$

with

$$c(\boldsymbol{p}) = \left(\boldsymbol{v}^{[\mathcal{N}]}\right)^H \left(\boldsymbol{U}^{[\mathcal{N}]}\boldsymbol{p}\right) + \left(\boldsymbol{U}^{[\mathcal{N}]}\boldsymbol{p}\right)^H \boldsymbol{v}^{[\mathcal{N}]} - \left(\boldsymbol{v}^{[\mathcal{N}]}\right)^H \boldsymbol{v}^{[\mathcal{N}]} \,. \tag{B.58}$$

The Schur complement of a positive semi-definite matrix[2]

$$\begin{bmatrix} \boldsymbol{A}_{11} & \boldsymbol{A}_{12} \\ \boldsymbol{A}_{21} & \boldsymbol{A}_{22} \end{bmatrix} \succeq 0 \tag{B.59a}$$

with respect to its submatrix $\boldsymbol{A}_{11}$ is given by (e.g., [BV04])

$$\boldsymbol{S}_c\left(\boldsymbol{A}_{11}\right) = \boldsymbol{A}_{22} - \boldsymbol{A}_{21}\,\boldsymbol{A}_{11}^{-1}\,\boldsymbol{A}_{12} \succeq 0 \,. \tag{B.59b}$$

Hence, Eq. (B.57) can now be rewritten as follows

$$\rho + c(\boldsymbol{p}) - \left(\boldsymbol{U}^{[\mathcal{N}]}\boldsymbol{p}\right)^H \boldsymbol{I}_{L\,\mathcal{N}} \left(\boldsymbol{U}^{[\mathcal{N}]}\boldsymbol{p}\right) \geq 0 \tag{B.60a}$$

$$\Leftrightarrow \quad \boldsymbol{L}_1 = \begin{bmatrix} \boldsymbol{I}_{L\,\mathcal{N}} & \boldsymbol{U}^{[\mathcal{N}]}\boldsymbol{p} \\ \left(\boldsymbol{U}^{[\mathcal{N}]}\boldsymbol{p}\right)^H & \rho + c(\boldsymbol{p}) \end{bmatrix} \succeq 0 \,. \tag{B.60b}$$

[1] The epigraph form is briefly explained at the end of Sec. D.2.

[2] A matrix $\boldsymbol{A}$ is positive semi-definite if $\boldsymbol{x}^T \boldsymbol{A}\, \boldsymbol{x} \geq 0$ for an arbitrary vector $\boldsymbol{x}$.

Accordingly, the inequality of Eq. (B.56c) can be written as

$$\epsilon_\mathrm{a} - \left(\boldsymbol{\Xi}_\Delta^{[\mathcal{N}]} \cdot \boldsymbol{p}\right)^H \left(\boldsymbol{\Xi}_\Delta^{[\mathcal{N}]} \cdot \boldsymbol{p}\right) \geq 0 \tag{B.61a}$$

$$\Leftrightarrow \quad \boldsymbol{L}_2 = \begin{bmatrix} \boldsymbol{I}_{(R-1)\,\mathcal{N}} & \boldsymbol{\Xi}_\Delta^{[\mathcal{N}]} \cdot \boldsymbol{p} \\ \left(\boldsymbol{\Xi}_\Delta^{[\mathcal{N}]} \cdot \boldsymbol{p}\right)^H & \epsilon_\mathrm{a} \end{bmatrix} \succeq 0\,. \tag{B.61b}$$

With

$$\boldsymbol{U}^{[\mathcal{N}]} = [\,\boldsymbol{u}_1, \boldsymbol{u}_2, \ldots, \boldsymbol{u}_\mathcal{N}\,] \tag{B.62}$$

$$\boldsymbol{\Xi}_\Delta^{[\mathcal{N}]} = [\,\boldsymbol{\xi}_1, \boldsymbol{\xi}_2, \ldots, \boldsymbol{\xi}_\mathcal{N}\,] \tag{B.63}$$

$$\boldsymbol{p} = [\,p(1), p(2), \ldots, p(\mathcal{N})\,]^T \tag{B.64}$$

the matrices $\boldsymbol{L}_1$ and $\boldsymbol{L}_2$ can be written as follows

$$\boldsymbol{L}_1 = \begin{bmatrix} \boldsymbol{I}_{L\,\mathcal{N}} & \boldsymbol{0}_{L\,\mathcal{N}} \\ \boldsymbol{0}_{L\,\mathcal{N}}^T & \rho + c(\boldsymbol{p}) \end{bmatrix} + \sum_{n=1}^{\mathcal{N}} p(n) \begin{bmatrix} \boldsymbol{O}_{L\,\mathcal{N}\times L\,\mathcal{N}} & \boldsymbol{u}_n \\ \boldsymbol{u}_n^H & 0 \end{bmatrix} \tag{B.65}$$

$$\boldsymbol{L}_2 = \begin{bmatrix} \boldsymbol{I}_{(R-1)\,\mathcal{N}} & \boldsymbol{0}_{(R-1)\,\mathcal{N}} \\ \boldsymbol{0}_{(R-1)\,\mathcal{N}}^T & \epsilon_\mathrm{a} \end{bmatrix} + \sum_{n=1}^{\mathcal{N}} p(n) \begin{bmatrix} \boldsymbol{O}_{(R-1)\,\mathcal{N}\times(R-1)\,\mathcal{N}} & \boldsymbol{\xi}_n \\ \boldsymbol{\xi}_n^H & 0 \end{bmatrix} \tag{B.66}$$

with $\boldsymbol{O}_{M\times N}$ marking a $M \times N$ zero matrix. The expressions for $\boldsymbol{L}_1$ and $\boldsymbol{L}_2$ are each an affine project of hermitian matrices with respect to $\boldsymbol{p}$ as required by Eq. (D.8b).

The complex linear matrix inequalities (LMIs) of Eq. (B.60b) and Eq. (B.60b) can be converted to real LMIs by exploiting the fact that the field of complex numbers

$$z = a + j\,b \;\in\; \mathbb{C} \;\forall\; a, b \in \mathbb{R} \tag{B.67}$$

is isomorphic to the field of real 2×2 matrices

$$\begin{bmatrix} a & b \\ -b & a \end{bmatrix} \in \mathbb{R}^{2\times 2}\,. \tag{B.68}$$

With Eq. (B.60b) and Eq. (B.61b), the epigraph form of Eq. (B.56) can be rewritten as follows

$$\underset{\boldsymbol{p}_\mathrm{a}}{\text{minimize}}\; \boldsymbol{l}^T \boldsymbol{p}_\mathrm{a} \tag{B.69a}$$

$$\text{subject to} \quad \begin{bmatrix} \Re\{\boldsymbol{L}_1\} & \Im\{\boldsymbol{L}_1\} \\ -\Im\{\boldsymbol{L}_1\} & \Re\{\boldsymbol{L}_1\} \end{bmatrix} \succeq 0 \tag{B.69b}$$

$$\begin{bmatrix} \Re\{\boldsymbol{L}_2\} & \Im\{\boldsymbol{L}_2\} \\ -\Im\{\boldsymbol{L}_2\} & \Re\{\boldsymbol{L}_2\} \end{bmatrix} \succeq 0 \tag{B.69c}$$

with

$$\boldsymbol{p}_{\mathrm{a}} = \left[\, \rho, \boldsymbol{p}^T \,\right]^T \tag{B.69d}$$

$$\boldsymbol{l}^T = \left[\, 1, \boldsymbol{0}_{\mathcal{N}}^T \,\right]. \tag{B.69e}$$

This is an SDP according to Eq. (D.8) with $K_{\mathrm{u}} = 2$ and without the constraints of Eq. (D.8c) and Eq. (D.8d). □

B.4 Relation between GDCT and Oddly-Stacked GDFT

In Sec. 5.1.2, a relation between the evenly-stacked GDFT FBE and the GDCT FBE is established. In the following, it is shown that a similar result is also obtained for the *oddly-stacked* GDFT as transformation kernel where Eq. (5.19) applies with $i_0 = 1/2$ (see also Figure 5.3-b). In this case, the spectral gain factors have the symmetry

$$W(i,\kappa) = W(M-1-i,\kappa);\quad i \in \{\,0,1,\ldots,M-1\,\};\quad M \text{ even}\,. \tag{B.70}$$

The calculation of the time-varying time-domain of Eq. (5.6) is now performed by the oddly-stacked GDFT according to

$$w(l,\kappa) = \sum_{i=0}^{M-1} W(i,\kappa)\cdot e^{-j\,\frac{2\,\pi}{M}\,(i+1/2)\,(l-k_0)};\quad l \in \{\,0,1,\ldots,L-1\,\} \tag{B.71}$$

The substitution $M = 2\,N_m$ and exploiting the symmetry of Eq. (B.70) allows the following conversion of Eq. (B.71)

$$\begin{aligned} w(l,\kappa) &= \sum_{i=0}^{N_m-1} W(i,\kappa)\cdot e^{-j\,\frac{2\,\pi}{2\,N_m}\,(i+1/2)\,(l-k_0)} \\ &\quad + \sum_{i=0}^{N_m-1} W(2\,N_m-1-i,\kappa)\cdot e^{-j\,\frac{2\,\pi}{2\,N_m}\,(2\,N_m-1-i+1/2)\,(l-k_0)} \\ &= \sum_{i=0}^{N_m-1} W(i,\kappa)\cdot\left(e^{-j\,\frac{\pi}{N_m}\,(i+1/2)\,(l-k_0)} + e^{j\,\frac{\pi}{N_m}\,(i+1/2)\,(l-k_0)}\right) \\ &= 2\sum_{i=0}^{N_m-1} W(i,\kappa)\cdot\cos\left(\frac{\pi}{N_m}(i+1/2)\,(l-k_0)\right)\,. \end{aligned} \tag{B.72}$$

Eq. (B.72) corresponds to a FBE with N_m channels and the oddly-stacked *generalized discrete cosine transform* (GDCT) as modulation sequence

$$\Phi_{\mathrm{GDCT}}^{(II)}(i,k) = 2\,\cos\left(\frac{\pi}{N_m}\,(i+1/2)\,(k-k_0)\right);\quad i \in \{\,0,1,\ldots,N_m-1\,\}\,. \tag{B.73}$$

The condition of Eq. (5.12) is now fulfilled with $M = N_m$ and $C = 2\,N_m$.

B.5 Calculation of Warped AR Filter Coefficients

This section derives the realization of a warped AR filter without delay-less feedback loops according to Eq. (5.52) and Eq. (5.53). The system function

$$B(z) = A(z) + \alpha = \frac{z^{-1} - \alpha}{1 - \alpha\, z^{-1}} + \alpha = \frac{z^{-1} - \alpha + \alpha - \alpha^2\, z^{-1}}{1 - \alpha\, z^{-1}} \tag{B.74}$$

contains no feedback loops can be used to obtain the denominator of Eq. (5.52). This is accomplished by the equation

$$\underbrace{1 - \sum_{l=1}^{N_{\mathrm{ld}}} v_l \cdot A^l(z)}_{\text{warped denominator}} \stackrel{!}{=} \frac{1}{\tilde{v}_0} - \underbrace{\big(A(z) + \alpha\big)}_{= B(z)} \sum_{l=1}^{N_{\mathrm{ld}}} \tilde{v}_l \cdot A^{l-1}(z) \tag{B.75}$$

$$= \frac{1}{\tilde{v}_0} - \sum_{l=1}^{N_{\mathrm{ld}}} \tilde{v}_l \cdot \big(A^l(z) + \alpha \cdot A^{l-1}(z)\big)$$

$$= \frac{1}{\tilde{v}_0} - \left(\alpha\, \tilde{v}_1 + \sum_{l=1}^{N_{\mathrm{ld}}-1} (\tilde{v}_l + \alpha\, \tilde{v}_{l+1}) \cdot A^l(z) + \tilde{v}_{N_{\mathrm{ld}}} \cdot A^{N_{\mathrm{ld}}}(z)\right). \tag{B.76}$$

Comparing the terms with $A^l(z)$ on the left hand side with those of the right hand side yields the following relations

$$\tilde{v}_{N_{\mathrm{ld}}} = v_{N_{\mathrm{ld}}} \tag{B.77a}$$

$$v_l = \tilde{v}_l + \tilde{v}_{l+1} \cdot \alpha; \quad l = N_{\mathrm{ld}} - 1, \ldots, 1$$

$$\Leftrightarrow \quad \tilde{v}_l = v_l - \tilde{v}_{l+1} \cdot \alpha \tag{B.77b}$$

$$1 = \frac{1}{\tilde{v}_0} - \alpha \cdot \tilde{v}_1$$

$$\Leftrightarrow \quad \tilde{v}_0 = \frac{1}{1 + \alpha \cdot \tilde{v}_1} \tag{B.77c}$$

as given in Eq. (5.53).

B.6 Preservation of Minimum-Phase Property for Warped Filters

It is proven that the allpass transformation of a minimum-phase filter results always a filter with minimum-phase. A rational system function $F(z)$ can be expressed in a cascade form

$$F(z) = s_0\, \frac{\prod_{i=1}^{M_1} \left(1 - s_i\, z^{-1}\right) \prod_{i=1}^{M_2} \left(1 - t_i\, z^{-1}\right) \left(1 - t_i^*\, z^{-1}\right)}{\prod_{i=1}^{N_1} \left(1 - u_i\, z^{-1}\right) \prod_{i=1}^{N_2} \left(1 - v_i\, z^{-1}\right) \left(1 - v_i^*\, z^{-1}\right)}\,. \tag{B.78}$$

If $F(z)$ is of minimum-phase, all poles and zeros are inside the unit circle. Hence, it is sufficient to consider the term

$$D(z) = \frac{1}{1 - d\,z^{-1}}\,; \quad |d| < 1; \quad d \in \mathbb{C}\,. \tag{B.79}$$

Applying an allpass transformation of first order according to Eq. (4.1) results

$$\begin{aligned}\widetilde{D}(z) &= \frac{1}{1 - d\,\dfrac{z^{-1} - a^*}{1 - a\,z^{-1}}}\,; \quad |a| < 1 \qquad\qquad (B.80)\\ &= \frac{1 - a\,z^{-1}}{1 + a^* d - (a + d)\,z^{-1}}\\ &= \frac{1}{1 + a^*\,d} \cdot \frac{1 - \rho_0\,z^{-1}}{1 - \rho_\infty\,z^{-1}} \qquad\qquad (B.81)\end{aligned}$$

with zero and pole given by

$$\rho_0 = a \tag{B.82a}$$

$$\rho_\infty = \frac{a + d}{1 + a^* d}\,. \tag{B.82b}$$

The zero is always inside the unit circle as $|a| < 1$. The pole is inside the unit circle if

$$\begin{aligned}&\left|1 + a^* d\right| > |a + d|\\ \Leftrightarrow\quad &\left|1 + a^* d\right|^2 > |a + d|^2\,.\end{aligned} \tag{B.83}$$

The simplified notation

$$a_\mathrm{R} = \Re\{a\}\,; \quad a_\mathrm{I} = \Im\{a\}\,; \quad d_\mathrm{R} = \Re\{d\}\,; \quad d_\mathrm{I} = \Im\{d\} \tag{B.84}$$

leads to

$$\begin{aligned}\left|1 + a^* d\right|^2 &= \left|1 + (a_\mathrm{R} - j\,a_\mathrm{I})\;(d_\mathrm{R} + j\,d_\mathrm{I})\,\right|^2\\ &= (1 + a_\mathrm{R}\,d_\mathrm{R} + a_\mathrm{I}\,d_\mathrm{I})^2 + (a_\mathrm{R}\,d_\mathrm{I} - a_\mathrm{I}\,d_\mathrm{R})^2\\ &= 1 + 2\;(a_\mathrm{R}\,d_\mathrm{R} + a_\mathrm{I}\,d_\mathrm{I}) + (a_\mathrm{R}\,d_\mathrm{I})^2 + (a_\mathrm{I}\,d_\mathrm{I})^2 + (a_\mathrm{R}\,d_\mathrm{R})^2 + (a_\mathrm{I}\,d_\mathrm{R})^2\\ &= 1 + 2\;(a_\mathrm{R}\,d_\mathrm{R} + a_\mathrm{I}\,d_\mathrm{I}) + |a|^2\,|d|^2\,.\end{aligned} \tag{B.85}$$

The right part of Eq. (B.83) can be written as follows

$$\begin{aligned}|a + d|^2 &= (a_\mathrm{R} + d_\mathrm{R})^2 + (a_\mathrm{I} + d_\mathrm{I})^2\\ &= |a|^2 + |d|^2 + 2\,(a_\mathrm{R}\,d_\mathrm{R} + a_\mathrm{I}\,d_\mathrm{I})\,.\end{aligned} \tag{B.86}$$

Inserting of Eq. (B.85) and Eq. (B.86) into the inequality of Eq. (B.83) leads to

$$\begin{aligned}1 + |a|^2\,|d|^2 &> |a|^2 + |d|^2\\ 1 - |a|^2 - |d|^2 + |a|^2\,|d|^2 &> 0\\ \left(1 - |a|^2\right)\left(1 - |d|^2\right) &> 0\end{aligned} \tag{B.87}$$

which is true since $|a| < 1$ and $|d| < 1$. $\square$

Appendix C

Related Filter-Banks

Some related filter-banks are discussed in the following to point out characteristic differences to the treated allpass-based filter-banks. In App. C.1, FIR/FIR QMF-bank designs are briefly described which play a role in the evaluation of the new IIR/IIR QMF-bank designs in Sec. 3.1.2.5 and Sec. 6.1.2. In App. C.2, allpass-transformed filter-banks are compared with gammatone filter-banks and tree-structured filter-banks, which are the most common alternatives to realize an auditory filter-bank with an ERB or Bark-scaled frequency resolution.

C.1 FIR/FIR QMF-Banks

An FIR/FIR QMF-bank with complete aliasing cancellation and no phase distortions can be achieved by using an FIR prototype lowpass filter given by

$$H_0(z) = \sum_{l=0}^{L-1} h_0(l) \cdot z^{-l} \tag{C.1}$$

with real coefficients and linear phase response so that $h_0(l) = h_0(L-1-l)$ for $l \in \{0, 1, \ldots, L-1\}$. The corresponding frequency response reads

$$H_0\left(e^{j\,\Omega}\right) = e^{-j\,\Omega\,\frac{L-1}{2}}\,\mathcal{A}\left(e^{j\,\Omega}\right) \quad \text{with} \quad \mathcal{A}\left(e^{j\,\Omega}\right) \in \mathbb{R} \;\forall\; \Omega\,. \tag{C.2}$$

Inserting this equation into Eq. (3.6) yields

$$\begin{aligned} T_{\text{lin}}\left(e^{j\,\Omega}\right) &= \frac{1}{2}\,e^{-j\,(L-1)\,\Omega}\,\left(\left|H_0\left(e^{j\,\Omega}\right)\right|^2 - (-1)^{L-1}\,\left|H_0\left(e^{j\,(\pi-\Omega)}\right)\right|^2\right) \\ &= \frac{1}{2}\,e^{-j\,(L-1)\,\Omega}\,\left(\left|H_0\left(e^{j\,\Omega}\right)\right|^2 + \left|H_0\left(e^{j\,(\pi-\Omega)}\right)\right|^2\right) \end{aligned} \tag{C.3}$$

for an even filter length L.[1] The linear transfer function is then given by $T_{\text{lin}}\left(e^{j\,\Omega}\right) = \frac{1}{2}\,e^{-j\,(L-1)\,\Omega}$, if the analysis filters are *power complementary*

$$\left|H_0\left(e^{j\,\Omega}\right)\right|^2 + \left|H_1\left(e^{j\,\Omega}\right)\right|^2 = \left|H_0\left(e^{j\,\Omega}\right)\right|^2 + \left|H_0\left(e^{j\,(\pi-\Omega)}\right)\right|^2 = 1 \;\forall\; \Omega\,. \tag{C.4}$$

[1] An odd filter length L is not considered since $T_{\text{lin}}(e^{j\,\pi}) = 0$ in this case.

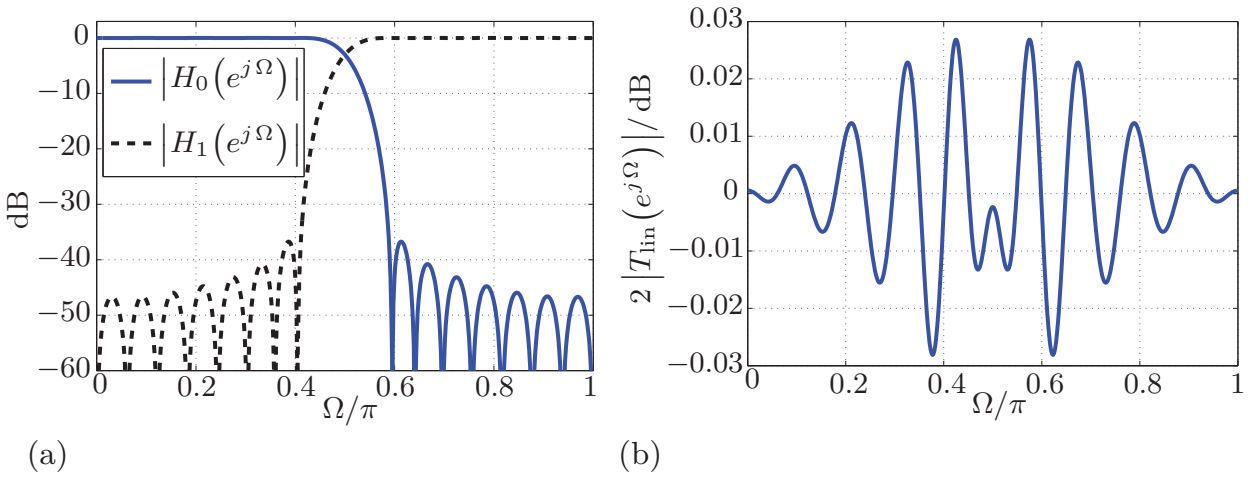

Figure C.1: *FIR QMF-bank design by LS error minimization of Eq.* (C.5) *with* $L = 32$, $\Omega_s = 0.586\,\pi$ *and* $\eta = 2$*:*
(a) *magnitude responses of the analysis filters*
(b) *magnitude response of the linear transfer function.*

A frequently applied approach to design approximately power complementary analysis filters with a good stopband attenuation and minimal amplitude distortions has been proposed by Johnston [Joh80]. The filter coefficients are determined by minimizing the objective function

$$E_\eta = 2 \int_0^\pi \left|H_0\left(e^{j\,\Omega}\right)\right|^2 + \left|H_0\left(e^{j\,(\pi-\Omega)}\right)\right|^2 - 1 \;\mathrm{d}\,\Omega + \eta \int_{\Omega_\mathrm{s}}^\pi \left|H_0\left(e^{j\,\Omega}\right)\right|^2 \;\mathrm{d}\,\Omega \quad \text{(C.5)}$$

with $0 < \eta$. A design example is provided by Figure C.1. The filter coefficients of this 32D Johnston design are listed in [CR83, Chap. 7]. This design achieves near-perfect reconstruction with linear-phase subband filters so that the obtained FIR/FIR QMF-bank requires only $L/2$ multiplications and $L/2$ summations for the analysis filter-bank as well as the synthesis filter-bank, cf., [Vai93].

A design approach to achieve *perfect reconstruction* is proposed in [SB84, Min85]. The requirement of Eq. (3.4) is replaced by the equation

$$H_1(z) = -z^{-(L-1)}\,\breve{H}_0(-z) \quad \text{(C.6)}$$

with L being even. The breve denotes the *para-conjugate* of a function, i.e., the z variable is replaced by z^{-1} and the filter coefficients are replaced by their complex conjugate counterparts, cf., [Vai93]. With the requirement of Eq. (3.5) for a complete aliasing cancellation, the linear transfer function of Eq. (3.2) is given by

$$T_{\mathrm{lin}}(z) = \frac{1}{2}\,z^{-(L-1)} \left(H_0(z) \cdot H_0\left(z^{-1}\right) + H_0(-z) \cdot H_0\left(-z^{-1}\right) \right) \quad \text{(C.7)}$$

if the coefficients of $H_0(z)$ are real. The condition

$$H_0(z) \cdot H_0\left(z^{-1}\right) + H_0(-z) \cdot H_0\left(-z^{-1}\right) \stackrel{!}{=} 1 \quad \text{(C.8)}$$

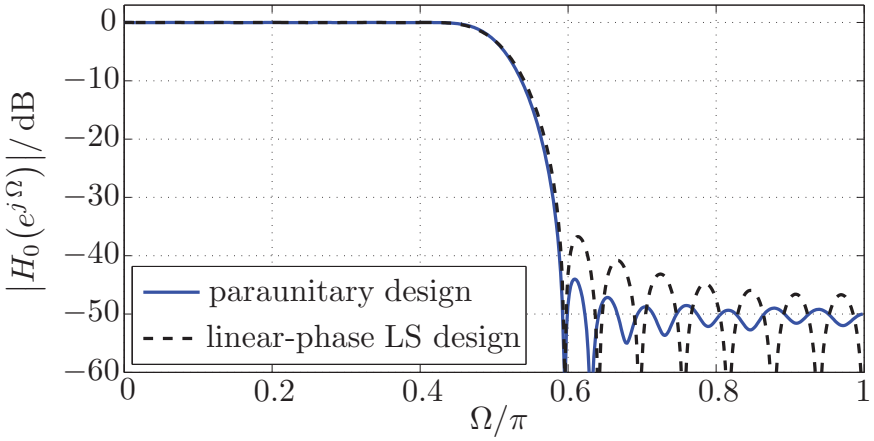

Figure C.2: *FIR lowpass filters designed by the LS error design of [Joh80] and the para-unitary Lattice design of [VH88] with prototype filter length $L = 32$ and stopband frequency $\Omega_s = 0.586\,\pi$.*

implies that the transfer function

$$T_{\mathrm{pc}}(z) = H_0(z) \cdot H_0\left(z^{-1}\right) \tag{C.9}$$

has to be a zero-phase half-band filter with the frequency response $T_{\mathrm{pc}}\left(e^{j\,\Omega}\right)$ being real and positive for all Ω. As a consequence, the lowpass filter is *power complementary* according to Eq. (C.4).

Techniques to design a prototype lowpass filter which fulfills these requirements are proposed in [SB84, Min85]. It has been shown later that the obtained QMF-bank belongs to the important class of *para-unitary* filter-banks, e.g., [Vai93].[2] A possible realization of such filter-banks is given by the QMF *Lattice structure* [VH88, Vai93]. One advantage of this structure is that it remains para-unitary despite quantization of its coefficients. A comparison of the lowpass filters obtained by the LS error design of Johnston [Joh80] according to Figure C.1 and the para-unitary Lattice design of Vaidyanathan and Hoang [VH88] is provided by Figure C.2. The lowpass filter of the para-unitary Lattice QMF-bank design exhibits a significantly better stopband attenuation than the lowpass filter obtained by the LS error design of Johnston. On the other hand, the linear-phase property of the analysis filter is lost and the para-unitary QMF-bank possesses a higher algorithmic complexity than the NPR design of Johnston (see also Sec. 3.1.2.5).

It should be noted that para-unitary filter-banks are orthogonal filter-banks and closely related to the *discrete wavelet transform*, e.g., [VK95, Fli93, Vai93]. A drawback of orthogonal filter-banks is that their FIR filters cannot be of linear-phase (with the exception of two unimportant special cases). This can be solved by a biorthogonal QMF-bank design, e.g., [Fli93, TN95, VK95, BGG98], but such filter-banks are not considered in this work.

[2] The property of being a para-unitary filter-bank is sufficient but not necessary for perfect reconstruction.

C.2 Auditory Filter-Banks

Besides frequency warped filter-banks, the use of gammatone filter-banks and tree-structured filter-banks are the most common alternatives to realize an *auditory* filter-bank with an ERB or Bark-scaled frequency resolution. The characteristic differences of these filter-banks in comparison to *allpass transformed* filter-banks are discussed in the following.

C.2.1 Gammatone Filter-Banks

Gammatone filters are widely used for computational auditory models to mimic the peripheral filtering in the cochlea [PRH+92]. It is also possible to construct an AS FB by means of such filters, e.g., [Sla93, Hoh02, FKK05]. One possibility is to use FIR analysis and synthesis filters which, however, causes a very high computational complexity and signal delay, cf., [FKK05].

A more efficient alternative is to use a *recursive* gammatone filter-bank [Sla93, Hoh02]. The bandwidths of a gammatone analysis filter-bank can be well adapted to the *equivalent rectangular bandwidth* (ERB), cf., [PRH+92, Sla93, Hoh02]. Figure C.3 compares the magnitude responses of the gammatone analysis filter-bank of [Hoh02] with those of a corresponding allpass transformed DFT analysis filter-bank.[3] The gammatone filter-bank is designed for a sampling frequency of $f_s = 16.276\,\text{kHz}$. The corresponding warped DFT filter-bank employs the ELT prototype filter of Eq. (2.33) and is adapted to the ERB scale by means of Eq. (4.9).

Figure C.3 reveals the very different curve progressions for the magnitude responses of the gammatone filter-bank and the allpass transformed DFT filter-bank: The gammatone filters exhibit a 'triangular shape' for their (logarithmic) magnitude responses where the warped analysis filters tend to a 'parabola shaped' course and they show no 'spectral gaps' at $\Omega = 0$ and $\Omega = \pi$. Another difference is that the gammatone AS FB performs no subsampling and achieves near-perfect reconstruction [Hoh02]. In contrast, allpass transformed AS FBs are modulated filter-banks, which can perform a subsampling and can provide either a perfect or nearly perfect signal reconstruction as shown in Chap. 4 and Chap. 5.

Hence, even though gammatone and allpass transformed filter-banks can both realize an ERB or Bark-scaled frequency resolution with high accuracy, they have very different properties and it is governed by the intended application (auditory modeling, subband filtering etc.) which filter-bank is preferable.

C.2.2 Tree-Structured Filter-Banks

The realization of a non-uniform filter-bank by means of a tree-structure is another important alternative to that of an allpass transformed filter-bank. The principle of such a filter-bank is exemplified in Figure C.4. The basic element forms a two-channel QMF-bank as treated before. In contrast to the filter-bank of Figure 3.1, the subband

[3] The IIR gammatone filter-bank of [Hoh02] provides complex-valued subband signals as a DFT filter-bank. A brief comparison of an FIR gammatone filter-bank with real-valued subband filters and a warped DCT filter-bank can be found in [FKK05].

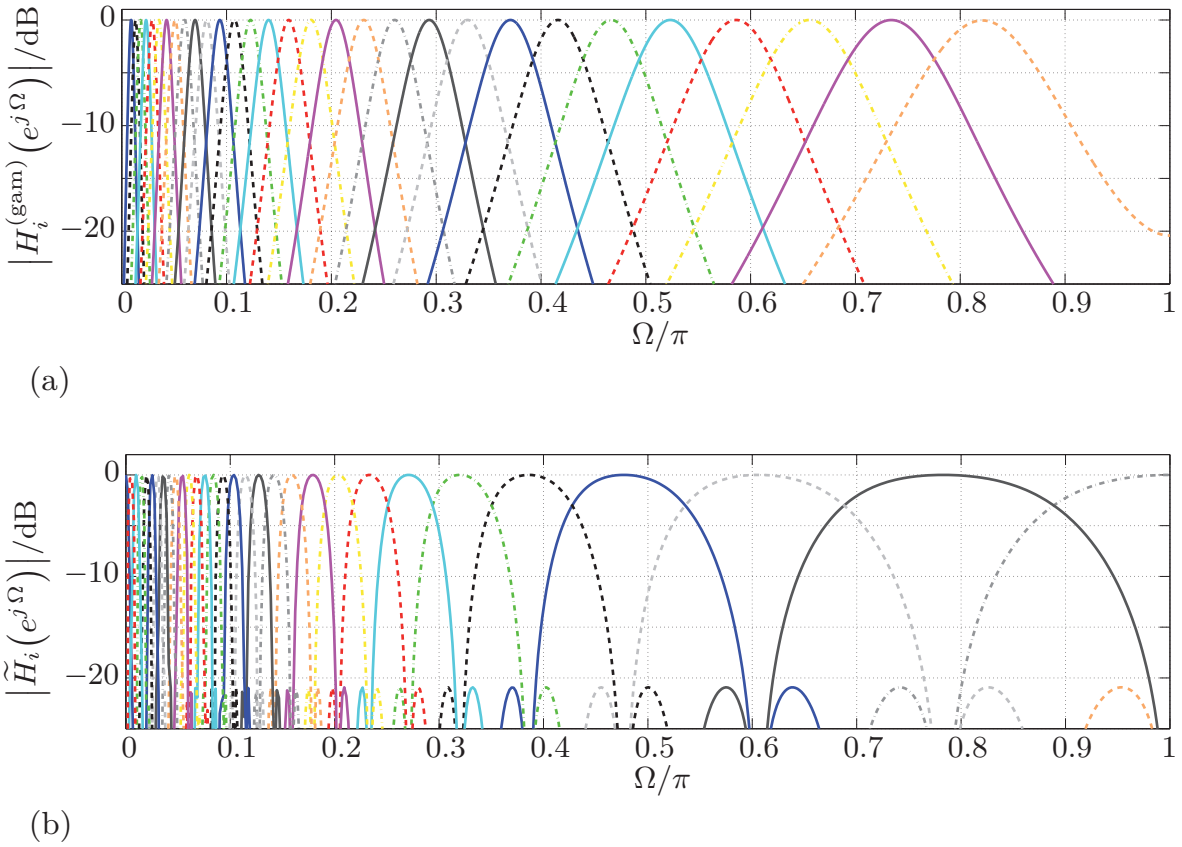

Figure C.3: *Magnitude responses of analysis filter-banks with approximately ERB-scaled frequency bands:*
(a) *gammatone filter-bank with* 30 *channels according to [Hoh02]*
(b) *allpass transformed DFT filter-bank with* 60 *channels* ($a = 0.7435$).

signals of the analysis filters are now further decomposed by means of a lowpass (LP) and highpass (HP) filter. This step can be repeated successively until the desired frequency resolution is (approximately) achieved. This procedure leads to different signal delays for the subband signals, which can be compensated by adequate delay elements. The signal reconstruction is performed by a corresponding synthesis filter-bank (tree) as shown in Figure C.4-b. The signal delay of such a tree-structured AS FB amounts to

$$D_{\mathrm{o}}^{\mathrm{tree}} = \left(2^{J_{\mathrm{s}}} - 1\right) \cdot D_{\mathrm{o}}^{\mathrm{qmfb}} \tag{C.10}$$

input sample instants with J_{s} marking the number of stages and $D_{\mathrm{o}}^{\mathrm{qmfb}}$ denoting the signal delay of the underlying two-channel QMF-bank. For a para-unitary QMF-bank which fulfills Eq. (C.7), this delay amounts to

$$D_{\mathrm{o}}^{\mathrm{qmfb}} = L - 1 \tag{C.11}$$

sample instants. Thus, the signal delay of a tree-structured filter-bank grows exponentially with the number of stages, which can become problematic for applications with demanding signal delay constraints.

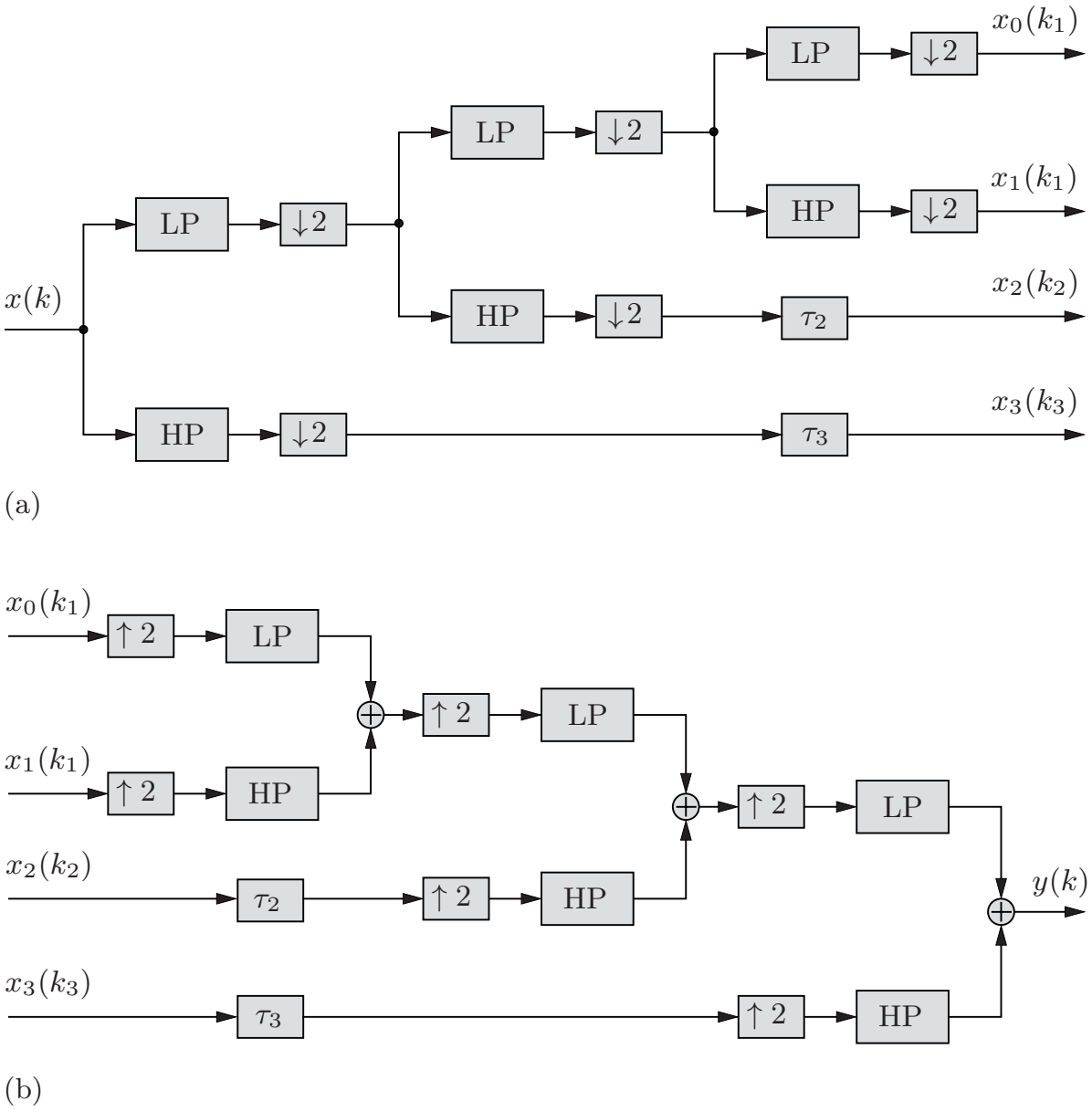

Figure C.4: *Tree-structured filter-bank with $J_s = 3$ stages:*
(a) *analysis filter-bank*
(b) *synthesis filter-bank.*

Instead of a pair of quadrature-mirror filters (QMFs), the closely related wavelets can also used as basis, cf., Sec. C.1. The resulting tree-structured filter-bank is termed as *wavelet packets*, e.g., [BGG98, VK95]. The choice for the nodes where the subband signals are further split determines the bandwidths of the analysis filters. By this, it is possible to obtain a filter-bank with octave bands, e.g., [Vai93]. Another option are tree-structured filter-banks with *Bark-scaled* frequency bands, which are of interest for speech coding as well as speech enhancement [Eng98, GEH98, CD99, Coh01, KKP07].

The magnitude responses of such a Bark-scaled analysis filter-bank are plotted in Figure C.5 and contrasted to those of a comparable allpass transformed DFT filter-bank. The decomposition of the tree-structured filter-bank is performed for a sampling

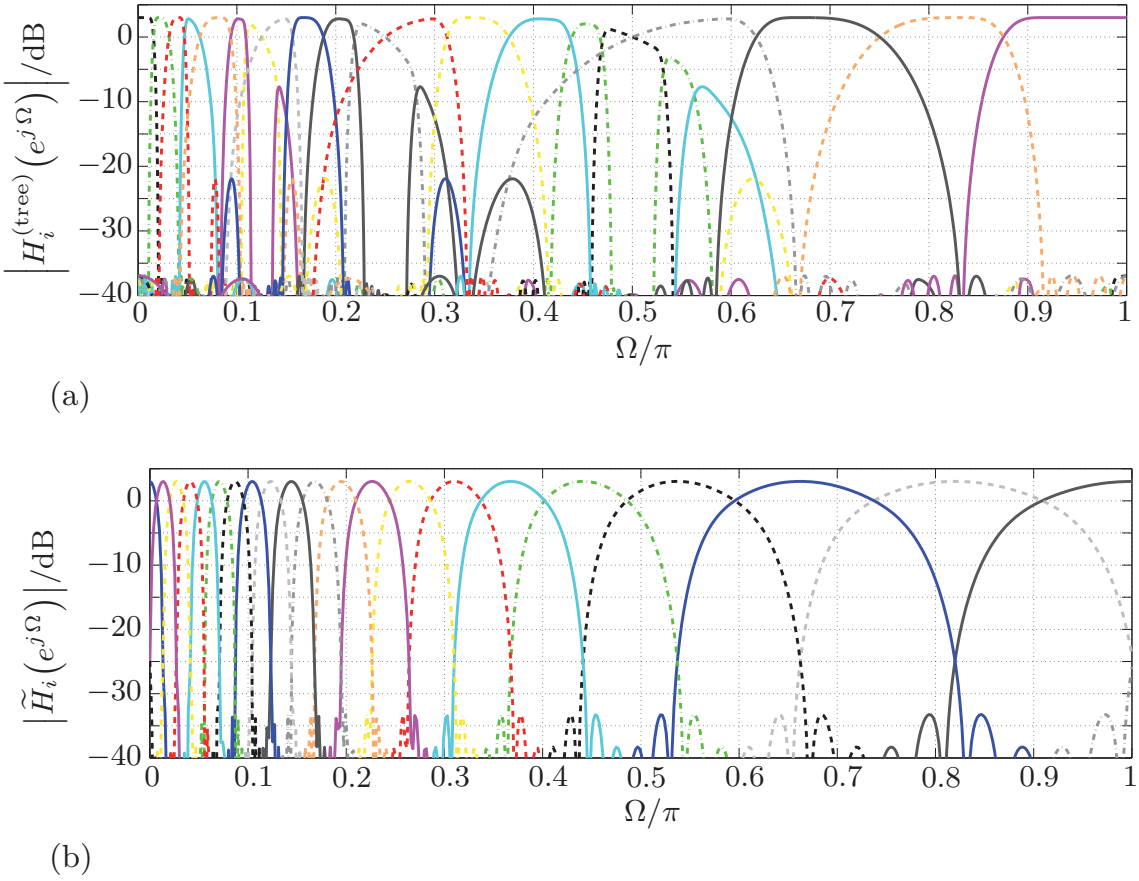

Figure C.5: *Magnitude responses of analysis filter-banks with approximately Bark-scaled frequency bands:*
(a) *tree-structured QMF-bank with* 20 *channels*
(b) *allpass transformed DFT filter-bank with* 40 *channels* ($a = 0.577$).

frequency of $f_\text{s} = 16\,\text{kHz}$ according to [CD99]. This results in an (approximately) Bark-scaled filter-bank with $J = 6$ stages and $M = 20$ channels. Para-unitary QMFs with filter length $L = 16$ are employed, which are constructed by the design of [SB84] (briefly described in App. C.1). The allpass transformed DFT analysis filter-bank possesses $M = 40$ channels.[4] It uses as prototype lowpass filter a root-raised-cosine filter of length $L = 4\,M$ with a roll-off factor of one (cf., [Fli93]) in order to achieve a similar stopband attenuation as the tree-structured filter-bank. An allpass coefficient of $a = 0.5755$ is taken, which provides a very good approximation of the Bark scale for a sampling frequency of 16 kHz according to Eq. (4.7).

Figure C.5 reveals that the magnitude responses of the warped analysis filter-bank are much more 'regular' and exhibit much less interfering sidelobes in comparison to the analysis filters of the tree-structured filter-bank. A similar observation can also be

[4] The analysis filters of a QMF-bank as well as a DCT filter-bank have real-valued impulse responses such that their magnitude responses are symmetric to $\Omega = \pi$. A DFT filter-bank with M channels has $M - 2$ subband filters with complex impulse responses where this symmetry does not hold. Therefore, a DFT filter-bank with twice the number of channels has to be taken to obtain analysis filters with comparable bandwidths.

made for other QMFs or wavelets. For example, the use of a Daubechies wavelet with 16 coefficients yields a higher transition bandwidth and higher stopband attenuation, but the course of the magnitude responses and its sidelobes is rather similar to that of Figure C.5-a.

The considered tree-structured QMF-bank exhibits a signal delay of 945 samples according to Eq. (C.10). In contrast, the delay of a comparable allpass transformed AS FB of first order lies roughly between $3\,L \leq D_{\mathrm{o}} \leq 4\,L$ samples dependent on the design and the tolerated reconstruction error, cf., Chap. 4. Therefore, the warped AS FB has a signal delay which is only about 1/2 or at least 2/3 of the delay caused by the considered tree-structured AS FB.

Hence, an advantage of tree-structured filter-banks is that they achieve perfect reconstruction, if the underlying two-channel filter-bank achieves perfect reconstruction, which simplifies the design. In addition, critical subsampling can be performed, which makes such filter-banks of special interest for subband coding, e.g., [VK95, CD99, KKP07]. In contrast, allpass transformed AS FB have (usually) a lower signal delay and are more suitable for applications with non-critical subsampling such as speech enhancement. Such different applications for tree-structured and allpass transformed filter-banks are discussed in Chap. 6.

Appendix D

Error Norms and Optimization Methods

A frequent design problem is to find the *optimal* filter coefficients according to a given optimization criterion. To solve this problem, an appropriate error criterion is needed as well as a method to find the optimal solution. This section describes briefly the errors norms and mathematical programs which are used in this work for the design of filters and filter-banks, respectively.

D.1 Error Norms

A common design problem is to find an approximation for a desired function $f_{\mathrm{des}}(\Omega)$ which minimizes the weighted error over a set of (normalized) frequencies $\mathcal{F}$:

$$\Delta f(\Omega) = \Upsilon(\Omega) \cdot [f(\Omega) - f_{\mathrm{des}}(\Omega)] \quad \text{with} \quad \Upsilon(\Omega) \in \mathbb{R}_+ \,. \tag{D.1}$$

All functions are assumed to be continuous and differentiable for $\Omega \in \mathcal{F}$. The considered function $f(\Omega)$ has K_c unknown coefficients. These coefficients should be determined in such a manner that the *norm* of the weighted error of Eq. (D.1) is minimized. The $\mathcal{L}_p$-norm of the approximation error function $\Delta f(\Omega)$ over the set $\mathcal{F}$ is given for a continuous function by

$$\|\Delta f(\Omega)\|_p = \left[\int_{\Omega \in \mathcal{F}} |\Delta f(\Omega)|^p \; \mathrm{d}\,\Omega \right]^{\frac{1}{p}} \quad \text{for} \quad p \in \{\, 1, 2, \ldots, \infty \,\} \,. \tag{D.2}$$

For a finite set of discrete frequencies, the $\mathcal{L}_p$-norm of the approximation error is given by

$$\|\Delta f(\Omega_n)\|_p = \left[\sum_{\Omega_n \in \mathcal{F}} |\Delta f(\Omega_n)|^p \right]^{\frac{1}{p}} \,. \tag{D.3}$$

In this work, the $\mathcal{L}_1$-norm, the $\mathcal{L}_2$-norm (LS error norm) and the $\mathcal{L}_\infty$-norm, which is also termed as Chebyshev norm or infinity norm, are considered. The Chebyshev norm features the property

$$\|\Delta f(\Omega)\|_\infty = \max_{\Omega \in \mathcal{F}} \{|\Delta f(\Omega)|\} \,. \tag{D.4}$$

A Chebyshev solution for an approximation problem follows from the *alternation theorem*, which can be briefly formulated as follows:[1]

For an appropriate set of functions $f(\Omega)$ with $\Omega \in \mathcal{F}$, a necessary and sufficient condition that the function $f(\Omega)$ is a unique, best weighted Chebyshev approximation to a given continuous function $f_{\mathrm{des}}(\Omega)$ is that the weighted error of Eq. (D.1) exhibits at least $K_c + 2$ extrema at the extremal points $\Omega_0 < \Omega_1, \ldots, < \Omega_{K_c+1}$ such that

$$\Delta f(\Omega_n) = -\Delta f(\Omega_{n+1}); \quad n = 0, 1, \ldots, K_c \tag{D.5a}$$

$$\text{and} \quad |\Delta f(\Omega_n)| = \max_{\Omega \in \mathcal{F}} \{|\Delta f(\Omega)|\} = \|\Delta f(\Omega)\|_\infty \,. \tag{D.5b}$$

The alternating extrema of the residual error $\Delta f(\Omega)$ are termed as *alternate*. Due to the alternation theorem, the error between desired and approximated function shows an equiripple behavior. Therefore, filters designed by this criterion are also denoted as *equiripple filters*. An algorithm to find the extremal frequencies is given by the Remez-Exchange algorithm, e.g., [PB87, Lan93]. An advantage of a Chebyshev approximation is that the maximal deviation from the desired function is considered rather than the sum or integral of all squared deviations as for an LS error solution.

D.2 Convex Programs

This section gives an overview of the different convex optimization problems considered in this work. A more comprehensive treatment of convex optimization methods can be found in various textbooks such as [WSV00, BV04, AL07]. It should be noted that the different optimization problems (or programs) are formulated in this section in a generic way, which means that the used notation for vectors, matrices and functions is not related to the notation used for the numerical filter-bank designs (and hence not listed in App. A).

In general, a *convex optimization problem* is of the form

$$\underset{\boldsymbol{x}}{\text{minimize}} \; f_0(\boldsymbol{x}) \tag{D.6a}$$

$$\text{subject to } f_k(\boldsymbol{x}) \leq 0 \quad \text{for} \quad k = 1, 2, \ldots, K_{\mathrm{u}} \tag{D.6b}$$

$$\boldsymbol{a}_k^T \, \boldsymbol{x} = \boldsymbol{b}_k \quad \text{for} \quad k = 1, 2, \ldots, K_{\mathrm{e}} \tag{D.6c}$$

where the equality constraints are affine. The real objective function $f_0(\boldsymbol{x})$ and the real inequality constraint functions $f_1(\boldsymbol{x})$ to $f_{K_{\mathrm{u}}}(\boldsymbol{x})$ are convex. A real function $f(\boldsymbol{x})$ is convex, if for two arbitrary arguments $\boldsymbol{x}_1$ and $\boldsymbol{x}_2$:

$$f(\mu \, \boldsymbol{x_1} + (1 - \mu) \, \boldsymbol{x_2}) \leq \mu \, f(\boldsymbol{x_1}) + (1 - \mu) \, f(\boldsymbol{x_2}) \quad \text{for} \quad 0 \leq \mu \leq 1 \,. \tag{D.7}$$

[1] A more precise formulation and discussion of this theorem can be found in [Lan93] where the appropriate set of functions for which this theorem applies is exactly specified. However, this shortened (informal) formulation of the alternation theorem is sufficient for the treatment in Sec. 3.3.4 where Eq. (D.5) is used to characterize the derived expressions for different approximation errors.

The function is strictly convex, if Eq. (D.7) is a strict inequality whenever $\boldsymbol{x}_1 \neq \boldsymbol{x}_2$ and $0 < \mu < 1$. An important example for a convex function is the *norm* of a vector $f(\boldsymbol{x}) = \|\boldsymbol{x}\|_p$ (see also App. D.1). The *feasible set* of vectors fulfills the constraints of Eq. (D.6b) and Eq. (D.6c) and is a convex set. The vector $\hat{\boldsymbol{x}}$, which solves the optimization problem of Eq. (D.6), is *optimal*, if the problem is feasible. The problem is *infeasible*, if $f_0(\hat{\boldsymbol{x}}) = -\infty$. For the sake of simplicity, only real vectors and matrices are considered in the following, but the listed mathematical programs can also be applied to complex variables (as demonstrated in Chap. 4).

A special case of the general convex optimization problem of Eq. (D.6) is a *semi-definite program* (SDP), which can be formulated as follows[2]

$$\underset{\boldsymbol{x}}{\text{minimize}}\ \boldsymbol{y}^T\boldsymbol{x} \tag{D.8a}$$

$$\text{subject to}\ \boldsymbol{C}_0^{(k)} + \sum_{n=1}^{N} x_n \cdot \boldsymbol{C}_n^{(k)} \succeq 0 \quad \text{for} \quad k = 1, 2, \ldots, K_\mathrm{u} \tag{D.8b}$$

$$\boldsymbol{B}\,\boldsymbol{x} \succeq \boldsymbol{h} \tag{D.8c}$$

$$\boldsymbol{F}\,\boldsymbol{x} = \boldsymbol{b} \tag{D.8d}$$

where $\boldsymbol{x} = [x_1, x_2, \ldots, x_N]^T \in \mathbb{R}^N$, $\boldsymbol{b} \in \mathbb{R}^M$ and $\boldsymbol{y}, \boldsymbol{h} \in \mathbb{R}^N$. The real matrices $\boldsymbol{B}$ and $\boldsymbol{C}_n^{(k)}$ for $k = 0, 1, \ldots, K_\mathrm{u}$ are symmetric and $\boldsymbol{F} \in \mathbb{R}^{M \times N}$ with $M > N$.

A special case of an SDP is a *second order cone program* (SOCP)

$$\underset{\boldsymbol{x}}{\text{minimize}}\ \boldsymbol{y}^T\boldsymbol{x} \tag{D.9a}$$

$$\text{subject to}\ \|\boldsymbol{A}_k\,\boldsymbol{x} + \boldsymbol{b}_k\|_2 \leq \boldsymbol{c}_k^T\boldsymbol{x} + d_k \quad \text{for} \quad k = 1, 2, \ldots, K_\mathrm{u} \tag{D.9b}$$

$$\boldsymbol{F}\,\boldsymbol{x} = \boldsymbol{b} \tag{D.9c}$$

with $d_k \in \mathbb{R}$, $\boldsymbol{c}_k \in \mathbb{R}^N$, $\boldsymbol{b}_k \in \mathbb{R}^{M_k}$ and $\boldsymbol{A}_k \in \mathbb{R}^{M_k \times N}$ where $M_k > N$.

The special case $\boldsymbol{c}_k = \boldsymbol{0}_N$ for $k = 1, 2, \ldots, K_\mathrm{u}$ leads to a *quadratically constrained quadratic program* (QCQP)

$$\underset{\boldsymbol{x}}{\text{minimize}}\ \frac{1}{2}\,\boldsymbol{x}^T\boldsymbol{P}_0\,\boldsymbol{x} + \boldsymbol{q}_0^T\,\boldsymbol{x} + r_0 \tag{D.10a}$$

$$\text{subject to}\ \frac{1}{2}\,\boldsymbol{x}^T\boldsymbol{P}_k\,\boldsymbol{x} + \boldsymbol{q}_k^T\,\boldsymbol{x} + r_k \leq 0 \quad \text{for} \quad k = 1, 2, \ldots, K_\mathrm{u} \tag{D.10b}$$

$$\boldsymbol{F}\,\boldsymbol{x} = \boldsymbol{b} \tag{D.10c}$$

where the matrices $\boldsymbol{P}_k \in \mathbb{R}^{N \times N}$ for $k = 0, 1, \ldots, K_\mathrm{u}$ are positive semi-definite.

A *linearly constrained quadratic program* (LCQP) is obtained, if the matrix $\boldsymbol{P}_k$ is a zero-matrix for $k = 1, 2, \ldots, K_\mathrm{u}$:

$$\underset{\boldsymbol{x}}{\text{minimize}}\ \frac{1}{2}\,\boldsymbol{x}^T\boldsymbol{P}_0\,\boldsymbol{x} + \boldsymbol{q}_0^T\,\boldsymbol{x} + r_0 \tag{D.11a}$$

$$\text{subject to}\ \boldsymbol{q}_k^T\,\boldsymbol{x} + r_k \leq 0 \quad \text{for} \quad k = 1, 2, \ldots, K_\mathrm{u} \tag{D.11b}$$

$$\boldsymbol{F}\,\boldsymbol{x} = \boldsymbol{b}\,. \tag{D.11c}$$

[2] This inequality form is not the general standard form being mostly used, but more convenient for the treatment in this work.

Solving Eq. (D.10) without constraints is equivalent to an (unconstrained) LS error minimization of the form

$$\underset{\boldsymbol{x}}{\text{minimize}} \ \|\boldsymbol{A}\,\boldsymbol{x} + \boldsymbol{b}\|_2^2 \tag{D.12}$$

with $\boldsymbol{A} \in \mathbb{R}^{M \times N}$ and $\boldsymbol{b} \in \mathbb{R}^{M}$ where $M > N$.

Another special case of an SOCP is a *linear program*

$$\underset{\boldsymbol{x}}{\text{minimize}} \ \boldsymbol{y}^T \boldsymbol{x} \tag{D.13a}$$

$$\text{subject to } \boldsymbol{G}\,\boldsymbol{x} \succeq \boldsymbol{d} \tag{D.13b}$$

$$\boldsymbol{F}\,\boldsymbol{x} = \boldsymbol{b} \tag{D.13c}$$

with $\boldsymbol{G} \in \mathbb{R}^{K_\mathrm{e} \times N}$ and $\boldsymbol{d} \in \mathbb{R}^{K_\mathrm{e}}$ where $K_\mathrm{e} > N$.

There exist different operations which allow to transform a convex optimization problem into another convex problem. In this work, the conversion of a convex problem into the *epigraph form* is of special importance. The epigraph of a real function is the parameter set $(\boldsymbol{x}, \rho)$ for which $f(\boldsymbol{x}) \leq \rho$ where ρ is denoted as 'epigraph variable' in this work. For example, the convex optimization problem

$$\underset{\boldsymbol{x}}{\text{minimize}} \ f(\boldsymbol{x}) \tag{D.14}$$

can be expressed in the epigraph form

$$\underset{\boldsymbol{x},\,\rho}{\text{minimize}} \ \rho \tag{D.15a}$$

$$\text{subject to } f(\boldsymbol{x}) \leq \rho\,. \tag{D.15b}$$

Since $f(\boldsymbol{x})$ is convex, the function $f(\boldsymbol{x}) - \rho$ and hence the problem in the epigraph form are also convex.

Appendix E

Instrumental Measures for Speech Enhancement Systems

Instrumental quality measures are used in Sec. 6.2.1 to compare the performance of different filter-banks used for noise reduction. The investigated noise reduction systems are judged based on listener's impression *and* instrumental measures. This is important since disturbing artifacts as, for instance, musical noise are only insufficiently represented by (most) instrumental measures. With this in mind, the following measures are used according to [Gus99, VHH98].

In a simulation, the clean speech $s(k)$ and the additive background noise $u(k)$ can be filtered separately with coefficients adapted for the noisy speech $x(k) = s(k) + u(k)$. This provides the filtered speech $\breve{s}(k)$ and filtered noise $\breve{u}(k)$ separately where

$$y(k) = \hat{s}(k) = \breve{s}(k) + \breve{u}(k) \,. \tag{E.1}$$

The algorithmic *signal delay* of systems with a non-linear phase response is determined here by the maximum of the cross-correlation between the clean speech $s(k)$ and the processed speech $\breve{s}(k)$ according to

$$D_\mathrm{o} = \arg\left\{ \max_{\kappa} \left\{ \mathrm{corr}\left\{ s(k-\kappa), \breve{s}(k) \right\} \right\} \right\} \,. \tag{E.2}$$

A common *time-domain* measure for the quality of the enhanced speech $y(k) = \hat{s}(k)$ is given by the *segmental SNR*

$$\frac{\mathrm{SNR}_\mathrm{seg}}{\mathrm{dB}} = \frac{10}{\mathcal{C}(\mathbb{F}_\mathrm{s})} \sum_{m \in \mathbb{F}_\mathrm{s}} \log_{10} \left(\frac{\sum_{\mu=0}^{M_\mathrm{m}-1} s^2(m\,M_\mathrm{m} + \mu - D_\mathrm{o})}{\sum_{\mu=0}^{M_\mathrm{m}-1} \left(\hat{s}(m\,M_\mathrm{m} + \mu) - s(m\,M_\mathrm{m} + \mu - D_\mathrm{o}) \right)^2} \right) \,. \tag{E.3}$$

The calculation comprises only frames with speech activity ($m \in \mathbb{F}_\mathrm{s}$) whose total number is denoted by $\mathcal{C}(\mathbb{F}_\mathrm{s})$.

The achieved *segmental noise attenuation* is calculated by the expression

$$\frac{\mathrm{NA_{seg}}}{\mathrm{dB}} = \frac{10}{\mathcal{C}(\mathbb{F})} \sum_{m \in \mathbb{F}} \log_{10} \left(\frac{\sum_{\mu=0}^{M_\mathrm{m}-1} u^2(m\,M_\mathrm{m} + \mu - D_\mathrm{o})}{\sum_{\mu=0}^{M_\mathrm{m}-1} \breve{u}^2(m\,M_\mathrm{m} + \mu)} \right) \tag{E.4}$$

where $\mathbb{F}$ marks the set of all frame indices including speech pauses and $\mathcal{C}(\mathbb{F})$ denotes the total number of frames.

A *frequency-domain* measure for the quality of the enhanced speech is given by the *cepstral distance* (CD). The real cepstrum of a signal $s(k)$ is considered. The cepstral coefficients of $s(k)$ with frame index m are given by

$$C_s(m\,M + i) = \mathrm{IDFT}_M \Big\{ \ln \Big| \mathrm{DFT}_M \{ s(m\,M + k) \} \Big| \Big\} \tag{E.5}$$

for $i \in \{\,0, 1, \ldots, M-1\,\}$. Here, only a relatively coarse description of the spectrum with $M_{CD} < M$ coefficients is needed. The (mean) CD value[1] between the filtered and original speech is calculated by averaging the cepstral distance per frame $\mathrm{CD}(m)$ over all frames with speech activity

$$\mathrm{CD} = \frac{1}{\mathcal{C}(\mathbb{F}_\mathrm{s})} \sum_{m \in \mathbb{F}_\mathrm{s}} \frac{10}{\ln(10)} \mathrm{CD}(m) \tag{E.6}$$

with

$$\mathrm{CD}(m) = \sqrt{\Big[C_s(m\,M - D_\mathrm{o}) - C_{\breve{s}}(m\,M)\Big]^2 + 2 \sum_{\mu=1}^{M_{CD}-1} \Big[C_s(m\,M - D_\mathrm{o} + \mu) - C_{\breve{s}}(m\,M + \mu)\Big]^2}. \tag{E.7}$$

A value of $M_{CD} = 40$ coefficients is taken for this work. A high CD indicates a strong distortion. As a consequence of the logarithmic spectrum and the reduced number of cepstral coefficients M_{CD}, the cepstral difference emphasizes differences in strong speech components where differences in weak components or in the fine structure of the spectrum are weighted less.

[1] The CD always refers to the mean CD value in this work.

Appendix F

Deutschsprachige Zusammenfassung

Digitale Signalverarbeitungssysteme haben analoge Systeme in den letzten Jahrzehnten sukzessive ersetzt und sind heutzutage in einer Vielzahl von unterschiedlichen Geräten, wie z.B. Mobilfunktelefonen, Unterhaltungselektronik oder Hörgeräten zu finden. Ein entscheidender Vorteil der digitalen Signalverarbeitung besteht u.a. darin, dass damit auch Systeme realisiert werden können, die mit analoger Signalverarbeitung nicht oder nur sehr aufwendig zu realisieren sind.

Ein wichtiger Bestandteil vieler Systeme zur digitalen Signalverarbeitung sind Filter und deren Kombination zu Filterbänken. In vielen Fällen ist es notwendig oder zumindest vorteilhaft, ein Signal im Frequenzbereich anstatt im Zeitbereich zu verarbeiten. Dies kann man mit Hilfe einer *Analyse-Synthese-Filterbank* bewerkstelligen, wie sie in Abbildung F.1 dargestellt ist. Das digitale Eingangssignal $x(k)$ wird durch Analysefilter in verschiedene Teilbandsignale zerlegt. Diese sind bandbegrenzt und können daher mit der Rate R unterabgetastet werden, d.h. mit einer geringeren Abtastrate verarbeitet werden als das Eingangssignal. Die Teilbandsignale werden nach der Teilbandverarbeitung zuerst mit der Rate R hochgetastet und dann nach der Filterung mit den entsprechenden Synthesefiltern aufaddiert, was schließlich das Ausgangssignal $y(k)$ liefert. Falls keine Teilbandverarbeitung durchgeführt wird, soll die Synthese-Filterbank

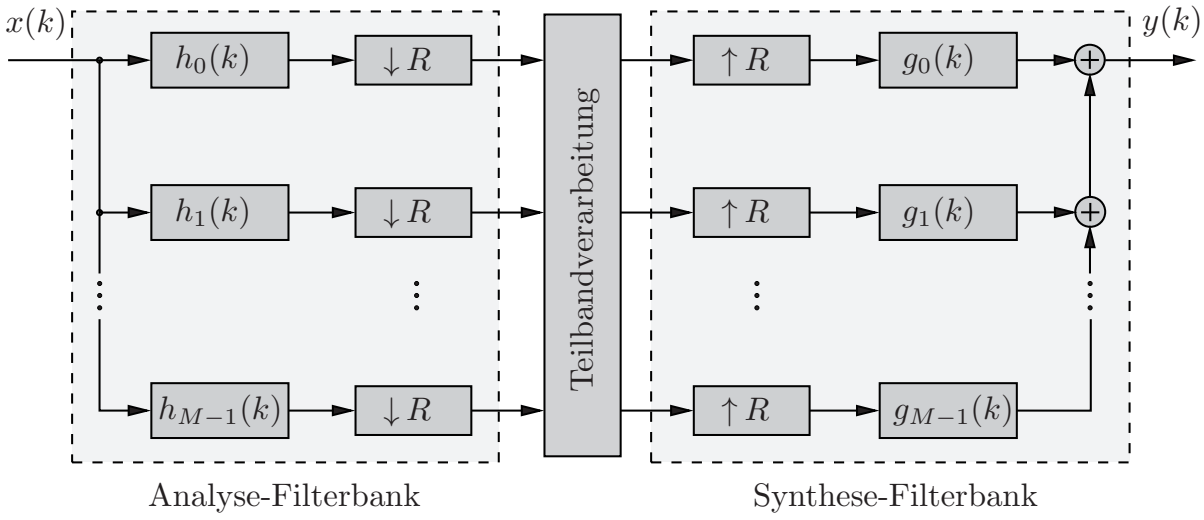

Abbildung F.1: *Digitale Analyse-Synthese-Filterbank mit M Teilbändern und einheitlicher Unterabtastrate R.*

eine *perfekte Rekonstruktion* (PR) oder zumindest eine *nahezu perfekte Rekonstruktion* (NPR) des Eingangssignals erreichen.

Die Unterabtastung der Teilbandsignale ermöglicht eine effiziente Realisierung von Filterbänken, aber sie führt auch zu einer Überlagerung von Spektralkomponenten, dem sog. Aliasing-Effekt. Dieser kann zu Signalverzerrungen führen und muss daher durch die Synthese-Filterbank mittels einer *Aliasing-Cancellation* kompensiert werden.

Analyse-Synthese-Filterbänke (mit Unterabtastung) werden für eine Vielzahl von Aufgaben benutzt, wie z.B. zur Teilbandcodierung von Sprach-, Audio- und Videosignalen oder zur adaptiven Filterung von Signalen im Frequenzbereich. Die vielfältigen Einsatzmöglichkeiten von Filterbänken haben zur Entwicklung von unterschiedlichen Klassen geführt.

Am häufigsten werden Analyse-Synthese-Filterbänke mit einer *gleichförmigen* Zeit-Frequenzauflösung eingesetzt. Gleichförmige Filterbänke bieten den Vorteil, dass sie sehr effizient realisiert werden können. Es handelt sich dabei meistens um modulierte Filterbänke, die auf einer Diskreten Fourier Transformation (DFT) oder Diskreten Cosinus Transformation (DCT) beruhen und daher sehr effizient mittels eines sog. *Polyphasennetzwerks* implementiert werden können. Für die Analyse- und Synthesefilter werden meist *nichtrekursive* Filter benutzt, die eine begrenzte Impulsantwort (*Finite Impulse Response*, FIR) besitzen.

Ein Vorteil von FIR-Teilbandfiltern ist, dass eine Filterbank mit linearphasigen Filtern oder perfekter Signalrekonstruktion einfacher zu entwerfen und realisieren ist als mit rekursiven Filtern, die eine unbegrenzte Impulsantwort (*Infinite Impulse Response*, IIR) aufweisen. Dementsprechend wird der Entwurf bzw. das Design von FIR-Filterbänken in der Literatur stärker behandelt als von IIR-Filterbänken.

Ein Vorteil von *rekursiven* Filterbänken ist hingegen, dass sie mit einem deutlich geringerem Filtergrad eine vergleichbare Frequenzselektivität wie FIR-Filterbänke erreichen können, was eine geringere Signalverzögerung und Komplexität impliziert. Darüber hinaus ist es nicht immer notwendig eine Filterbank mit linearphasigen Teilbandfiltern oder perfekter Signalrekonstruktion zu entwerfen. Bei der Sprach- und Audiosignalverarbeitung können beispielsweise leichte Signalverzerrungen toleriert werden, da diese vom menschlichen Gehör in der Regel nicht wahrgenommen werden. Die Tolerierung eines Rekonstruktionsfehlers liefert im Gegenzug zusätzliche Freiheitsgrade für den Entwurf der Filterbank. Daher sind rekursive Filterbänke eine attraktive Alternative zu nichtrekursiven Filterbänken.

In dieser Arbeit werden der Entwurf und die Anwendung von rekursiven Filterbänken behandelt, die mit Hilfe von *Allpassfiltern* realisiert werden. Die betrachteten allpass-basierten Filterbänke teilen sich in zwei wesentliche Klassen auf.

Zum einen werden allpass-basierte zweikanalige *Quadrature-Mirror-Filterbänke* (QMF-Bänke) und deren Erweiterung zu mehrkanaligen Pseudo-QMF-Bänken betrachtet. Diese rekursiven Filterbänke besitzen eine gleichförmige Frequenzauflösung und führen eine sog. kritische Unterabtastung durch, was diese u.a. für die Teilbandcodierung von Signalen attraktiv macht. QMF-Bänke und Pseudo-QMF-Bänke sind modulierte Filterbänke, die mittels eines Polyphasennetzwerks sehr effizient realisiert werden können. Die Polyphasenkomponenten der in dieser Arbeit betrachteten rekursiven Filterbänke bestehen dabei aus Allpassfiltern.

Die zweite Klasse bilden *allpass-transformierte* Analyse-Synthese-Filterbänke. Diese entstehen aus einer gleichförmigen Filterbank indem deren Verzögerungselemente durch Allpassfilter ersetzt werden. Diese sog. Allpass-Transformation erlaubt den Entwurf einer *ungleichförmigen* Filterbank dessen (ungleichförmige) Zeit-Frequenzauflösung an die des menschlichen Gehörs angepasst werden kann. Daher sind allpass-transformierte Filterbänke von besonderem Interesse für die Sprach- und Audiosignalverarbeitung.

Ein Problem bei beiden Klassen von allpass-basierten Filterbänken ist es, die nichtlinearen Phasenverzerrungen durch die rekursive Analyse-Filterbank syntheseseitig zu kompensieren, was deren gemeinsame Betrachtung motiviert.

Frühere Arbeiten & Offene Probleme

Die in dieser Arbeit betrachteten allpass-basierten Filterbänke wurden bereits in verschiedenen Dissertationen, sowie zahlreichen anderen Veröffentlichungen behandelt. Der Entwurf derartiger Filterbänke stellt jedoch eine anspruchsvolle Aufgabe dar, und es gibt immer noch eine Reihe von Problemen und Fragestellungen, die in bisherigen Arbeiten nicht oder nur teilweise gelöst wurden.

In der Dissertation von E. Galijašević (2002) wurde der Entwurf von allpass-basierten QMF-Bänken und Pseudo-QMF-Bänken sowie allpass-transformierten DFT-Filterbänken mit nahezu perfekter Rekonstruktion behandelt. Es wurde u.a. ein FIR-Phasenequalizer vorgestellt, der in beiden Fällen für die Konstruktion der Synthese-Filterbänke eingesetzt wird. Ein Vorteil dieses Verfahrens ist, dass der Phasenequalizer, und somit die Filterbank, durch geschlossene Formeln konstruiert wird, was zu recht einfachen Entwurfsverfahren führt. Ein Nachteil ist jedoch, dass der vorgeschlagene Phasenequalizer im Falle einer allpass-transformierten Filterbank eine recht hohe Signalverzögerung verursacht. Dies motiviert eine genauere Untersuchung von bekannten und neuen Ansätzen zur Lösung des Phasenkomensationsproblems bei allpass-basierten Filterbänken. Die Betrachtung dieses speziellen Problems ermöglicht dabei besser angepasste bzw. einfachere Lösungsansätze, als sie durch den Einsatz von allgemeinen Phasenequalizern, deren numerischer Entwurf in der Literatur relativ ausführlich behandelt wird, erreicht werden können.

Der Entwurf von allpass-transformierten DFT-Filterbänken wurde in der Dissertation von M. Kappelan (1998) ausführlich behandelt. Es wurde u.a. gezeigt, dass Filterbänke auch mittels einer Allpass-Transformation höherer Ordnung konstruiert werden können, wobei die Verzögerungselemente der zugrunde liegenden gleichförmigen Analyse-Filterbank durch Allpassfilter höherer Ordnung ersetzt werden. Dies ermöglicht gegenüber einer Allpass-Transformation erster Ordnung eine erhöhte Flexibilität für die Einstellung der Zeit-Frequenzauflösung. Für den Spezialfall einer Allpass-Transformation erster Ordnung wurde erstmals gezeigt, dass eine perfekte Signalrekonstruktion erreicht werden kann. Die in der Dissertation von Kappelan vorgestellte Synthese-Filterbank hat den Vorteil, dass sie durch geschlossene Formeln bestimmt wird und nur eine geringe Signalverzögerung und Komplexität aufweist. Ein gravierender Nachteil ist jedoch, dass die Synthesefilter keine Bandpasscharakteristik aufweisen. Dies kann zu starken Signalverzerrungen führen, falls eine Teilbandverarbeitung stattfindet, und schränkt damit die praktischen Einsatzmöglichkeiten einer

derartigen Filterbank sehr stark ein. Ein anderes ungelöstes Problem ist, ob es möglich ist eine stabile *und* frequenzselektive Synthese-Filterbank zu entwerfen, die eine perfekte Rekonstruktion im Falle einer Allpass-Transformation erster sowie höherer Ordnung ermöglicht.

Es gibt neben den geschlossenen Entwurfsmethoden für allpass-transformierte Analyse-Synthese Filterbänke auch numerische Entwurfsverfahren, die u.a. in der Dissertation von M. de Haan (2004) entwickelt wurden. Die Analyse- und Synthese-Filterbank wird dabei jeweils einer Allpass-Transformation erster Ordnung unterzogen. Der erhöhte Signalrekonstruktionsfehler, der sich dadurch ergibt, wird durch dedizierte numerische Entwurfsverfahren für die Prototypfilter der Analyse- und Synthese-Filterbank reduziert. Dieser Ansatz bietet den Vorteil, dass damit die Signallaufzeit und Komplexität der ursprünglichen, allpass-transformierten Analyse-Synthese-Filterbank nicht nennenswert verändert wird, so dass eine derartige Filterbank eine vergleichsweise geringe Latenz aufweist. Ein Nachteil ist jedoch, dass sich mit dieser Methode keine allpass-transformierte Analyse-Synthese-Filterbank konstruieren lässt, die eine (nahezu) perfekte Aliasing-Cancellation oder sogar eine perfekte Signalrekonstruktion aufweist. Dies wirft die Frage auf, ob eine allpass-transformierte Analyse-Synthese-Filterbank mit derartigen Eigenschaften mittels eines numerischen Entwurfsverfahrens überhaupt konstruiert werden kann.

Die Anwendung von allpass-transformierten Filterbänken sowie Wavelet-Filterbänken für die Verbesserung von akustisch gestörten Sprachsignalen wurde in den Dissertationen von A. Engelsberg (1998) sowie T. Gülzow (2001) erstmals ausführlich behandelt. In diesen Arbeiten wurden die Vorteile von derartigen ungleichförmigen Filterbänken für die Störgeräuschreduktion aufgezeigt und untersucht. Ein Nachteil der vorgestellten (ungleichförmigen) Analyse-Synthese-Filterbänke ist jedoch deren recht hohe Signallaufzeit. Daher sind diese Filterbänke weniger geeignet für Sprachverbesserungssysteme, die nur eine geringe Latenz aufweisen dürfen. Es stellt sich daher die grundlegende Frage, ob die Vorteile einer allpass-transformierten Filterbank mit ungleichmäßiger Frequenzauflösung bei der adaptiven Teilbandfilterung ausgenutzt werden können, ohne dabei eine übermäßig hohe Signallaufzeit in Kauf nehmen zu müssen.

In dieser Dissertation werden die aufgezeigten Fragestellungen und Probleme beim Entwurf allpass-basierter Filterbänke behandelt und durch neue Entwurfsmethoden gelöst. Darüber hinaus wird die Anwendung der eingeführten Filterbänke anhand von ausgewählten Beispielen diskutiert. Die wichtigsten Ergebnisse werden im Folgenden kurz dargestellt.

Rekursive QMF-Bänke

In dieser Arbeit werden unterschiedliche Entwurfsverfahren für allpass-basierte QMF-Bänke entwickelt. Bei all den vorgeschlagenen QMF-Bänken bestehen dabei die Polyphasenkomponenten der Analyse- *und* Synthese-Filterbank aus Allpassfiltern. Die Allpassfilter der Synthese-Filterbank agieren dabei als *Phasenequalizer*, die die nichtlinearen Phasenverzerrungen, die durch die rekursiven Analysefilter entstehen, ausgleichen. Diese Equalizer werden mittels einfacher geschlossener Formel entworfen, was es

erlaubt den Zielkonflikt zwischen Rekonstruktionsfehler und Signallaufzeit in einfacher Weise zu kontrollieren.

Ein erstes QMF-Bank-Design erreicht eine Minimierung der Amplituden-, Phasen- und Aliasingverzerrungen der Filterbank in Abhängigkeit vom Grad der eingesetzten Synthese-Polyphasenfilter (Allpassfilter). Das zweite vorgeschlagene QMF-Bank-Design hat eine größere Komplexität und Signalverzögerung als das erste, ermöglicht dafür aber eine komplette Aliasing-Cancellation und verursacht keine Betragsverzerrungen (falls keine Teilbandverarbeitung stattfindet). Es wird auch gezeigt, wie die vorgestellten Designs für zweikanalige QMF-Bänke auf mehrkanalige Pseudo-QMF-Bänke erweitert werden können.

Die neu vorgestellten, allpass-basierten IIR/IIR-QMF-Bänke unterscheiden sich von vergleichbaren FIR/FIR- und IIR/FIR-QMF-Bänken dadurch, dass sie höhere Phasenverzerrungen verursachen, aber dafür keine Betragsverzerrungen aufweisen und eine geringere Komplexität besitzen. Aufgrund dieser Eigenschaften sind die vorgeschlagenen allpass-basierten IIR/IIR-QMF-Bänke von besonderem Interesse für die Sprach- und Audioverarbeitung, da das menschliche Gehör relativ unempfindlich gegenüber Phasenverzerrungen ist.

Das neue, rein allpass-basierte QMF-Bank-Design mit perfekter Aliasing-Cancellation ist Bestandteil eines neuen Sprach- und Audiocodecs, der als Kandidat im Rahmen einer ITU-T Standardisierung vorgeschlagen wurde. Die neue IIR/IIR-QMF-Bank wird im vorgeschlagenen Codec dafür eingesetzt ein Signal in zwei Teilbandsignale der halben Abtastrate zu zerlegen. Diese Teilbandsignale werden dann separat codiert um einen hierarchischen Datenstrom (Bitstream) zu generieren, so dass je nach Übertragungskapazität des Kanals bzw. Netzwerks Teile des Bitstreams verworfen werden können. Es wird gezeigt, dass der Einsatz der neuen rekursiven QMF-Bank eine geringere Signallaufzeit und Komplexität verursacht als eine vergleichbare nichtrekursive FIR/FIR-QMF-Bank, wie sie beispielsweise im bestehenden G.729.1 Codec eingesetzt wird.

Phasenkomensation für Allpass-Basierte Filterbänke

Ein zentrales Problem beim Entwurf von allpass-basierten Filterbänken ist es, die nichtlinearen Phasenverzerrungen durch die allpass-basierte Analyse-Filterbank mittels einer Phasenkompensation (*Phase Equalization*) syntheseseitig zu korrigieren. Deshalb werden unterschiedliche Ansätze zur Lösung dieses Problem in dieser Arbeit näher untersucht.

Einen perfekten Phasenausgleich kann man durch inverse Allpassfilter erreichen, die jedoch ein nichtkausales System darstellen. Es gibt Ansätze derartige nichtkausale Filter mittels einer Pufferung von Werten praktisch zu realisieren, deren Einsatz für allpass-basierte Filterbänke jedoch mit Problemen verbunden ist. Es wird gezeigt, dass die resultierenden Filterbänke entweder empfindlich gegenüber einer Teilbandverarbeitung sind oder aber zusätzliche Aliasing-Verzerrungen verursachen können.

Diese Probleme treten nicht auf bei kausalen FIR- oder IIR-Phasenequalizern, die ein lineares, zeitinvariantes System darstellen und auf eine nahezu perfekte Phasenkompensation abzielen. Im Falle von allpass-basierten Filterbänken können die benö-

tigten Phasenequalizer mittels einfacher geschlossener Formel bestimmt werden und müssen nicht notwendigerweise durch ein (aufwendiges) numerisches Design entworfen werden. Für den FIR-Phasenequalizer, der in der Dissertation von E. Galijašević für den Entwurf von allpass-basierten Filterbänken vorgestellt wurde, wird gezeigt, dass dieser einen Equiripple-Approximationsfehler für die gewünschte Gruppenlaufzeit, Phasen- und Betragsantwort bei der Phasenkompensation von Allpassketten erreicht, weshalb die Bezeichnung als *Equiripple-FIR-Phasenequalizer* eingeführt wird. Der in dieser Arbeit vorgestellte Allpass-Phasenequalizer erzielt ebenso einen Equiripple-Approximationsfehler für die gewünscht Phasenantwort und Gruppenlaufzeit. Die Phasenverzerrungen dieses *Equiripple-Allpass-Phasenequalizers* sind größer als für den Equiripple-FIR-Phasenequalizer, wobei der Allpass-Phasenequalizer jedoch keine Betragsverzerrungen verursacht und in der Regel eine geringere Komplexität aufweist. Damit ist der vorgestellte Allpass-Phasenequalizer von besonderem Interesse für die Sprach- und Audioverarbeitung, bei der Phasenverzerrungen weniger problematisch sind.

Im Falle einer allpass-transformierten Filterbank tritt das Problem auf, dass die Phasenantwort von zum Teil recht langen Allpassketten kompensiert werden muss. Es wird gezeigt, dass ein sog. *Least-Squares* (LS) FIR-Phasenequalizer besonders gut dafür geeignet ist. Dessen Koeffizienten erhält man dadurch, dass man die unendliche, nichtkausale Impulsantwort eines inversen Allpassfilters begrenzt und zeitlich verschiebt, was einer Least-Squares-Fehlerapproximation des 'idealen', nichtkausalen Phasenequalizers entspricht.

Allpass-Transformierte Filterbänke

In dieser Arbeit werden verschiedene Entwurfsverfahren für allpass-transformierte DFT-Analyse-Synthese-Filterbänke entwickelt, die unterschiedlichen Anforderungen genügen.

Die Synthese-Filterbank für eine allpass-transformierte Analyse-Filterbank kann, wie zuvor erwähnt, mit Hilfe von Phasenequalizern konstruiert werden. Es wird gezeigt, dass der Einsatz des o.g. LS-FIR-Phasenequalizers für diesen Zweck deutliche Vorteile gegenüber dem Equiripple-FIR-Phasenequalizer bietet, der in früheren Arbeiten vorgeschlagen wurde: Die mit dem neuen Verfahren entworfene Filterbank erreicht bei gleicher Signallaufzeit und vergleichbarer Komplexität einen deutlich geringeren Rekonstruktionsfehler und eine bessere Bandpasscharakteristik für die Synthesefilter als das bisherige Verfahren.

Ein Vorteil der vorgestellten geschlossenen Entwurfsverfahren ist deren Einfachheit, da die Synthese-Filterbank mittels geschlossener analytischer Formeln konstruiert werden kann. Hierdurch kann der Zielkonflikt zwischen Signalverzögerung und Rekonstruktionsfehler der Filterbank recht einfach kontrolliert werden. Andererseits ist es mit diesen Ansätzen schwierig, zusätzliche Entwurfskriterien zu berücksichtigen. Dieses Problem wird durch eine neue *numerische* Entwurfsmethodik angegangen. Sie basiert auf einer neuen Matrixbeschreibung für allpass-transformierte Filterbänke aus der unterschiedliche Entwurfsverfahren abgeleitet werden.

Das erste daraus abgeleitete Design ist eine Verallgemeinerung des geschlossenen Designs mit LS-FIR-Phasenequalizern. Die FIR-Synthesefilter werden durch numeri-

sche Optimierung mittels eines *Linearly Constrained Quadratic Program* (LCQP) bestimmt.[1] Dabei werden die Phasenverzerrungen minimiert mit der zusätzlichen Bedingung für eine perfekte Aliasing-Cancellation. Dieser Ansatz wird in einem zweiten Schritt verallgemeinert, so dass man einen begrenzten Fehler für die Aliasing-Kompensation zulassen kann, um dadurch im Gegenzug die linearen Signalverzerrungen stärker reduzieren zu können. Die Koeffizienten der Synthese-Filterbank können in diesem Fall durch ein *Semi-Definite Program* (SDP) bestimmt werden.

Eine andere Erweiterung dieses Entwurfsverfahrens zielt auf ein sog. *sparse Design* ab. Dabei wird die Anzahl der Synthesefilterkoeffizienten die ungleich Null sind minimiert, um die Komplexität der Filterbank zu reduzieren. Dieses kann beispielsweise von Vorteil für eine Hardwarerealisierung sein, um dadurch die Anzahl der benötigten Schaltelemente zu reduzieren. Das hergeleitete Entwurfs- bzw. Optimierungsverfahren für die Synthese-Filterbank beruht auf einem *Second Order Cone Program* (SOCP). Dabei kann der Trade-Off zwischen Rekonstruktionsfehler der Filterbank und Komplexitätsreduktion durch ein Gewichtungsfaktor in einfacher Weise beeinflusst werden.

Es wird auch gezeigt, dass eine allpass-transformierte Filterbank mit *perfekter Rekonstruktion* mittels eines numerischen Verfahrens konstruiert werden kann. Bei einem ersten Entwurfsverfahren ohne Nebenbedingung werden die Koeffizienten der Synthesefilter durch ein einfaches lineares Gleichungssystem *(Linear Program)* bestimmt. Ein zweites Entwurfsverfahren mit Nebenbedingung strebt auch nach einer perfekte Rekonstruktion, optimiert dabei aber zusätzlich die Bandpasscharakteristik der Synthesefilter, dessen Koeffizienten in diesem Fall durch ein Linearly Constrained Quadratic Program bestimmt werden.

Die eingeführten numerischen Designs haben deutliche Vorteile gegenüber bekannten Designs für perfekte Rekonstruktion, die auf geschlossen lösbaren Entwurfsverfahren beruhen. Die neuen numerischen Entwurfsmethoden liefern auch im Falle einer Allpass-Transformation höherer Ordnung stabile Synthesefilter mit einer ausgeprägten Bandpasscharakteristik. Darüber hinaus können sie auch auf Filterbänke angewendet werden, bei denen der Filtergrad der Analysefilter größer ist als die Kanalzahl, was eine erhöhte Frequenzselektivität der Teilbandfilter ermöglicht.

Die neu vorgestellten numerischen Entwurfsverfahren können alle durch Semi-Definite Programmierung oder Spezialfälle davon gelöst werden. Derartige *konvexe Optimierungsprobleme* liefern ein globales Optimum und können, im Vergleich zu nicht-konvexen Optimierungsproblemen, relativ einfach gelöst. Im Gegensatz zu früheren numerischen Designs für allpass-transformierte Filterbänke können die neuen Ansätze eine perfekte Aliasing-Cancellation oder sogar eine perfekte Rekonstruktion erreichen. Darüber hinaus beziehen die neuen Verfahren auch explizit den allgemeineren Fall einer Allpass-Transformation höherer Ordnung mit ein, was zusätzliche Freiheitsgrade bei der Einstellung der Zeit-Frequenzauflösung der Filterbank erlaubt. Nicht zuletzt können all die in dieser Arbeit vorgeschlagenen Synthese-Filterbänke durch ein Polyphasennetzwerk effizient implementiert werden.

Eine Übersicht über die neuen Designs für allpass-transformierte Analyse-Synthese-Filterbänke liefert Tabelle F.1. Es werden dabei aus Gründen der Konsistenz die in

[1] Der englische Begriff *Program* wird hier ausschließlich im mathematischen Sinne verwendet und bezieht sich auf ein (numerisch zu lösendes) Optimierungsproblem.

Entwurfsverfahren	Abschnitt	Optimierungs-methode	Besondere Eigenschaft
NPR Design mittles Phase Equalization	4.2.2	geschlossene Lösung	minimierte Phasenverzerrungen
Constrained NPR Design	4.3.3	LCQP	perfekte Aliasing Cancellation
Generalized Constrained NPR design	4.3.3	SDP	kontrollierbarer Aliasingfehler
Sparse NPR Design	4.3.4	SOCP	Filterbank mit geringer Komplexität
Unconstrained PR Design	4.3.5	lineares Gleichungssystem	einfaches Optimierungsproblem
Constrained PR Design	4.3.6	LCQP	optimierte Bandpasscharakteristik

Tabelle F.1: *Übersicht über die in dieser Arbeit entwickelten Entwurfsverfahren für allpass-transformierte DFT-Analyse-Synthese-Filterbänke.*

dieser Arbeit eingeführten englischen Bezeichnungen und Abkürzungen benutzt. Die verschiedenen Verfahren verfolgen unterschiedliche Entwurfsziele, so dass es von der beabsichtigten Anwendung abhängt welches Verfahren zu bevorzugen ist.

Filterbank-Entwurf mit geringer Signallaufzeit

In der Praxis benötigt man oft Filterbänke mit einer geringen Signallaufzeit. Beispiele dafür sind Sprachverarbeitungssysteme, wie sie u.a. in Mobilfunktelefonen oder digitalen Hörgeräten eingesetzt werden. Für derartige Anwendungsfälle wird das Konzept des *Filter-Bank Equalizers* (FBEs) in dieser Arbeit entwickelt. Dieses System erlaubt die adaptive Teilbandverarbeitung von Signalen mit gleichförmiger als auch ungleichförmiger Frequenzauflösung sowie einer gleichzeitig geringen Signalverzögerung. Der FBE ist eine effiziente Implementierung der sog. Filterbank-Summationsmethode, die als Spezialfall einer Analyse-Synthese-Filterbank ohne Unterabtastung betrachtet werden kann.

Das Prinzip des FBEs ist in Abbildung F.2 dargestellt. Das Eingangssignal wird mittels einer gleichförmigen oder allpass-transformierten Analyse-Filterbank in den Frequenzbereich transformiert. Die im Frequenzbereich adaptiv berechneten Koeffizienten werden mittels einer Spektraltransformation, wie z.B. der generalisierten diskreten Fourier Transformation (GDFT), in den Zeitbereich transformiert und zur Filterung des Eingangssignal im Zeitbereich verwendet. Im Falle des allpass-transformierten FBEs werden eine allpass-transformierte Analyse-Filterbank und ein allpass-transformiertes Zeitbereichsfilter verwendet. Die in diesem Fall auftretenden Phasenverzerrungen können durch einen nachgeschalteten Phasenequalizer am Ausgang kompensiert werden.

Ein Vorteil des gleichförmigen und allpass-transformierten FBEs gegenüber vergleichbaren Analyse-Synthese-Filterbänken mit Unterabtastung ist neben der geringe-

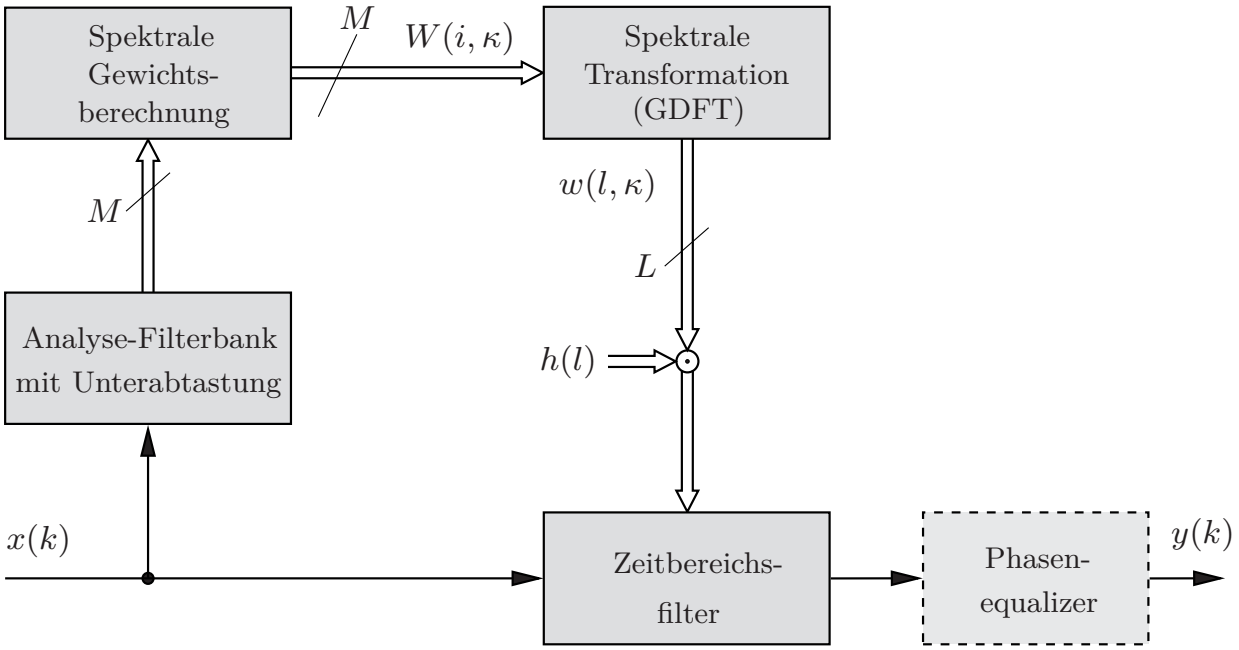

Abbildung F.2: *Prinzip des Filter-Bank Equalizers (FBEs). Der Phasenequalizer am Ausgang wird nur im Fall des allpass-transformierten FBEs benötigt.*

ren Signalverzögerung auch die Eigenschaft, dass eine perfekte bzw. nahezu perfekte Signalrekonstruktion mit einem deutlich geringerem Aufwand erzielt werden kann.

Die Implementierung des FBEs in der direkten Filterform, sowie der transponiert direkten Filterform wird untersucht. Die Realisierung mittels der transponiert direkten Form hat den Vorteil, dass die zeitveränderlichen Filterkoeffizienten des Zeitbereichsfilters stärker geglättet werden, was zur Vermeidung von hörbaren Artefakten durch das Umschalten der Filterkoeffizienten beiträgt. Die direkte Form hat hingegen den Vorteil, dass die Adaption der Koeffizienten im Frequenzbereich und die Filterung im Zeitbereich ohne eine zeitliche Verschiebung erfolgt wie bei der transponiert direkten Form. Mögliche Artefakte durch die zeitveränderliche Filterung im Zeitbereich können durch eine spezielle Glättung (*Cross-Fading*) vermieden werden.

Der FBE kann mittels eines Polyphasennetzwerks effizient realisiert werden. Der FBE mit gleichförmiger Frequenzauflösung hat dabei in der Regel eine höhere Komplexität als eine gleichförmige Analyse-Synthese-Filterbank mit Unterabtastung, wohingegen der allpass-transformierte FBE in der Regel eine geringere Komplexität als eine vergleichbare allpass-transformierte Analyse-Synthese-Filterbank aufweist. In beiden Fällen hat der FBE jedoch eine deutlich geringere Signallaufzeit als eine entsprechende Analyse-Synthese-Filterbank. Es wird auch gezeigt, wie die Phasenantwort des FBEs trotz der zeitveränderlichen Koeffizienten zeitinvariant bleiben kann, was z.B. für den Einsatz in mehrkanaligen Signalverarbeitungssystemen von Vorteil sein kann.

Das neu vorgestellte Konzept des *Low Delay Filters* ist eine Erweiterung des FBEs. Hierbei wird das ursprüngliche Zeitbereichsfilter des FBEs durch ein Filter geringeren Grades approximiert. Dies ermöglicht die Signallaufzeit und Komplexität des Systems

in einfacher und flexibler Art und Weise weiter zu reduzieren, ohne dabei die Adaption der Koeffizienten im Frequenzbereich anpassen zu müssen. Die Approximation des ursprünglichen Filters kann durch ein nichtrekursives *Moving-Average* (MA) Filter oder ein rekursives *Auto-Regressive* (AR) Filter erfolgen. Die Approximation mittels eines gleichförmigen oder allpass-transformierten MA-Filters erlaubt es, eine zeitinvariante oder sogar nahezu lineare Phasenantwort zu erhalten, was beispielsweise für eine binaurale Sprachverarbeitung in Hörgeräten von Interesse sein kann. Das gleichförmige und allpass-transformierte AR-Filter ist ein minimalphasiges System und kann eine Signalverzögerung von nur wenigen Abtastwerten erreichen. Eine derartige Eigenschaft ist von Interesse für Anwendungen, die nur eine sehr geringe Latenz erlauben.

Die Anwendung des FBEs zur Verbesserung akustisch gestörter Sprachsignale, sowie zur Sprachverständlichkeitsverbesserung in gestörten Umgebungen wird behandelt. Es wird gezeigt, dass der FBE mit gleichförmiger oder ungleichförmiger Frequenzauflösung die gleiche subjektive und objektive Sprachqualität erreichen kann wie eine vergleichbare Analyse-Synthese-Filterbank mit Unterabtastung, dabei jedoch eine deutlich geringere Signalverzögerung verursacht. Der Einsatz einer allpass-transformierten Filterbank kann entweder erfolgen um eine verbesserte Sprachqualität im Gegensatz zu einer Filterbank mit gleichförmiger Frequenzauflösung zu erreichen, oder aber um eine Teilbandfilterung mit einer geringeren Anzahl von Frequenzbändern durchzuführen. Der Einsatz des Low Delay Filters erlaubt es dabei, die Signallaufzeit des FBEs weiter zu reduzieren, ohne dabei eine deutlich wahrnehmbare Verschlechterung der Sprachqualität in Kauf nehmen zu müssen.

Die Anwendung der neuen Filterbänke für die Sprach- und Audiosignalverarbeitung wird in dieser Arbeit primär betrachtet, aber die neu vorgestellten Verfahren und Systeme sind auch für andere Anwendungen von Interesse.

Bibliography

[AGK09] D. Alfsmann, H. G. Göckler, and T. Kurbiel. "Filter Banks for Hearing Aids Applying Subband Amplification: A Comparison of Different Specification and Design Approaches". *Proceedings of European Signal Processing Conference (EUSIPCO)*, pp. 2663–2667, Glasgow, UK, August 2009.

[AL85] R. Ansari and B. Liu. "A Class of Low-Noise Computationally Efficient Recursive Digital Filters with Applications to Sampling Rate Alterations". *IEEE Transactions on Acoustics, Speech, and Signal Processing*, vol. 33, no. 1, pp. 90–97, February 1985.

[AL07] A. Antoniou and W.-S. Lu. *Practical Optimization: Algorithms and Engineering Applications*. Springer, Berlin, New York, 2007.

[ALM10] F. Altenbach, H. W. Löllmann, and R. Mathar. "Robust Equalizer Design for Allpass Transformed DFT Filter Banks with LTI Property". *Proceedings of International Symposium on Personal, Indoor and Mobile Radio Communications (PIMRC)*, pp. 846–850, Istanbul, Turkey, September 2010.

[ANS97] ANSI. "Methods for the Calculation of the Speech Intelligibility Index". American National Standards Institute (ANSI) S3.5-1997, 1997.

[AR79] S. S. Ahuja and S. C. D. Roy. "Linear Phase Variable Digital Bandpass Filters". *Proceedings of the IEEE*, vol. 67, no. 1, pp. 173–174, January 1979.

[AT00] J. Agnew and J. M. Thornton. "Just Noticeable and Objectionable Group Delays in Digital Hearing Aids". *Journal of the American Academy of Audiology*, vol. 11, no. 6, pp. 330–336, June 2000.

[AV99] S. Akkarakaran and P. P. Vaidyanathan. "New Results and Open Problems on Nonuniform Filter-Banks". *Proceedings of International Conference on Acoustics, Speech, and Signal Processing (ICASSP)*, pp. 1314–1318, Phoenix (Arizona), USA, March 1999.

[AZ03] M. Abo-Zahhad. "Current State and Future Directions of Multirate Filter Banks and Their Applications". *Digital Signal Processing*, vol. 13, no. 3, pp. 495–518, July 2003.

[BBC76] M. G. Bellanger, G. Bonnerot, and M. Coudreuse. “Digital Filtering by Polyphase Network: Application to Sample-Rate Alteration and Filter Banks”. *IEEE Transactions on Acoustics, Speech, and Signal Processing*, vol. 24, no. 2, pp. 109–114, April 1976.

[Bea75] K. G. Beauchamp. *Walsh Functions And Their Applications*. Academic Press, London, UK, 1975.

[Ber92] J. P. Berns. “Untersuchung digitaler Filterbänke mit ungleichmäßiger Frequenzauflösung”. diploma thesis, RWTH Aachen University, Aachen, Germany, 1992. (in German).

[BGG98] C. S. Burrus, R. A. Gopinath, and H. Guo. *Introduction to Wavelets and Wavelet Transforms: A Primer*. Prentice-Hall, Upper Saddle River, New Jersey, 1998.

[BMC05] J. Benesty, S. Makino, and J. Chen, editors. *Speech Enhancement*. Springer, Berlin, Heidelberg, 2005.

[BO74] C. Braccini and A. V. Oppenheim. “Unequal Bandwidth Spectral Analysis using Digital Frequency Warping”. *IEEE Transactions on Acoustics, Speech, and Signal Processing*, vol. 22, no. 4, pp. 236–244, August 1974.

[Boa03] B. Boashash, editor. *Time Frequency Signal Analysis and Processing: A Comprehensive Reference*. Elsevier, Amsterdam, 2003.

[Bor06] B. Borchers. “CSDP 2.3 User’s Guide”. New Mexico Tech, Socorro, New Mexico, USA, November 2006. (`https://projects.coin-or.org/Csdp/`).

[BP99] K. Bielawski and A. Petrovsky. “Speech Enhancement System for Hands-Free Telephone Based on the Psychoacoustically Motivated Filter Bank with Allpass Frequency Transformation”. *Proceedings of European Conference on Speech Communication and Technology (EUROSPEECH)*, pp. 2555–2558, Budapest, Hungary, September 1999.

[BPP06] A. Borowicz, M. Parfieniuk, and A. Petrovsky. “An Application of the Warped Discrete Fourier Transform in the Perceptual Speech Enhancement”. *Speech Communications*, vol. 48, pp. 1024–1036, 2006.

[Bre03] R. Bregović. *Optimal Design of Perfect-Reconstruction and Nearly Perfect-Reconstruction Multirate Filter Banks*. PhD thesis, Tampere University of Technology, Tampere, Finnland, 2003.

[BTN98] A. Ben-Tal and A. Nemirovski. “Robust Convex Optimization”. *Mathematics of Operations Research*, vol. 23, no. 4, pp. 769–805, November 1998.

[BV04] S. Boyd and L. Vandenberghe. *Convex Optimization*. Cambridge University Press, Cambridge, UK, 2004.

[BY05] S. J. Benson and Y. Ye. "DSDP5 User Guide: Software for Semidefinite Programming". Technical Report ANL/MCS-TM-277, Argonne National Laboratory, Argonne, Illinois, USA, September 2005. (`www.mcs.anl.gov/hs/software/DSDP/`).

[CD99] B. Carnero and A. Drygajlo. "Perceptual Speech Coding and Enhancement Using Frame-Synchronized Fast Wavelet Packet Transform Algorithms". *IEEE Transactions on Signal Processing*, vol. 47, no. 6, pp. 1622–1635, June 1999.

[CEG76] A. Croisier, D. Esteban, and C. Galand. "Perfect Channel Splitting by Use of Interpolation/ Decimation/ Tree Decomposition Techniques". *Proceedings of International Symposium on Information, Circuits and Systems*, Patras, Greece, 1976.

[CJ03] Z. Cvetković and J. D. Johnston. "Nonuniform Oversampled Filter Banks for Audio Signal Processing". *IEEE Transactions on Speech and Audio Processing*, vol. 11, no. 5, pp. 393–399, September 2003.

[CL94] C.-K. Chen and J.-H. Lee. "Design of Digital All-Pass Filters Using a Weighted Least Squares Approach". *IEEE Transactions on Circuits and Systems II*, vol. 41, no. 5, pp. 346–351, May 1994.

[CM96] C. D. Creusere and S. K. Mitra. "Efficient Audio Coding Using Perfect Reconstruction Noncausal IIR Filter Banks". *IEEE Transactions on Speech and Audio Processing*, vol. 4, no. 2, pp. 115–123, March 1996.

[CMH00] S. C. Chan, J. S. Mao, and K. L. Ho. "A New Design Method for Two-Channel Perfect Reconstruction IIR Filter Banks". *IEEE Signal Processing Letters*, vol. 7, no. 8, pp. 221–223, August 2000.

[Coh01] I. Cohen. "Enhancement of Speech Using Bark-Scaled Wavelet Packet Decomposition". *Proceedings of European Conference on Speech Communication and Technology (EUROSPEECH)*, pp. 1933–1936, Aalborg, Denmark, September 2001.

[Con67] A. G. Constantinides. "Frequency Transformation for Digital Filters". *Electronic Letters*, vol. 3, no. 11, pp. 487–489, November 1967.

[Con68] A. G. Constantinides. "Frequency Transformations for Digital Filters". *Electronic Letters*, vol. 4, no. 7, pp. 115–116, April 1968.

[Con70] A. G. Constantinides. "Spectral Transformations for Digital Filters". *Proceedings of the Institution of Electrical Engineers*, vol. 117, no. 8, pp. 1585–1590, August 1970.

[CR76] R. E. Crochiere and L. R. Rabiner. "On the Properties of Frequency Transformations for Variable Cutoff Linear Phase Digital Filters". *IEEE Transactions on Circuits and Systems*, vol. 23, no. 11, pp. 684–686, November 1976.

[CR83] R. E. Crochiere and L. R. Rabiner. *Multirate Digital Signal Processing*. Prentice-Hall, Englewood Cliffs, New Jersey, 1983.

[Cro80] R. E. Crochiere. "A Weighted Overlap-Add Method of Short-Time Fourier Analysis/Synthesis". *IEEE Transactions on Acoustics, Speech, and Signal Processing*, vol. 28, no. 1, pp. 99–102, February 1980.

[CV92] T. Chen and P. P. Vaidyanathan. "General Theory of Time-Reversed Inversion for Perfect Reconstruction Filter Banks". *Proceedings of Asilomar Conference on Signals, Systems, and Computers*, vol. 2, pp. 821–825, Pacific Grove (California), USA, October 1992.

[CV93] T. Chen and P. P. Vaidyanathan. "Time-Reversed Inversion for Time-Varying Filter-Banks". *Proceedings of Asilomar Conference on Signals, Systems, and Computers*, vol. 1, pp. 55–59, Pacific Grove (California), USA, November 1993.

[CWF76] R. E. Crochiere, S. A. Webber, and J. L. Flanagan. "Digital Coding of Speech in Sub-Bands". *Proceedings of International Conference on Acoustics, Speech, and Signal Processing (ICASSP)*, pp. 233–236, Philadelphia (Pennsylvania), USA, April 1976.

[Cza82] R. Czarnach. "Recursive Processing by Noncausal Digital Filters". *IEEE Transactions on Acoustics, Speech, and Signal Processing*, vol. 30, no. 3, pp. 363–370, June 1982.

[DBSN06] B. Dumitrescu, R. Bregović, T. Saramäki, and R. Niemistö. "Low-Delay Nonuniform Oversampled Filterbanks for Acoustic Echo Control". *Proceedings of European Signal Processing Conference (EUSIPCO)*, Florence, Italy, September 2006.

[dH04] J. M. de Haan. *Filter Bank Design for Digital Speech Signal Processing*. PhD thesis, Blekinge Institute of Technology, Ronneby, Sweden, 2004.

[dHCG03] J. M. de Haan, I. Claesson, and H. Gustafsson. "Least Squares Design of Nonuniform Filter Banks with Evaluation in Speech Enhancement". *Proceedings of International Conference on Acoustics, Speech, and Signal Processing (ICASSP)*, vol. 6, pp. 109–112, Hong Kong, China, April 2003.

[dHGCN02] J. M. de Haan, N. Grbić, I. Claesson, and S. Nordholm. "Design and Evaluation of Nonuniform DFT Filter Banks in Subband Microphone Arrays". *Proceedings of International Conference on Acoustics, Speech, and Signal Processing (ICASSP)*, vol. 2, pp. 1173–1176, Orlando (Florida), USA, May 2002.

[DMFB07] Y. Deng, V. J. Mathews, and B. Farhang-Boroujeny. "Low-Delay Nonuniform Pseudo-QMF Banks With Application to Speech Enhancement". *IEEE Transactions on Signal Processing*, vol. 55, no. 5, pp. 2110–2121, May 2007.

[Dob91] G. Doblinger. "An Efficient Algorithm for Uniform and Nonuniform Digital Filter Banks". *Proceedings of International Symposium on Circuits and Systems (ISCAS)*, vol. 1, pp. 646–649, Singapore, June 1991.

[DS98] I. Daubechies and W. Sweldens. "Factoring Wavelet Transforms into Lifting Steps". *Journal of Fourier Analysis and Applications*, vol. 4, no. 3, pp. 247–269, May 1998.

[DZ96] G. Doblinger and T. Zeitlhofer. "Improved Design of Uniform and Nonuniform Modulated Filter Banks". *Proceedings of IEEE Nordic Signal Processing Symposium (NORSIG)*, pp. 327–330, Helsinki, Finland, September 1996.

[EG77] D. Esteban and C. Galand. "Application of Quadrature Mirror Filters to Split Band Voice Coding Schemes". *Proceedings of International Conference on Acoustics, Speech, and Signal Processing (ICASSP)*, vol. 2, pp. 191–195, Hartford (Connecticut), USA, May 1977.

[EG97] A. Engelsberg and T. Gülzow. "Comparison of a Wavelet Transform and a Nonuniform Polyphase Filterbank Applied to Spectral Subtraction". *Proceedings of International Workshop on Acoustic Echo and Noise Control (IWAENC)*, pp. 124–127, London, UK, September 1997.

[EM84] Y. Ephraim and D. Malah. "Speech Enhancement Using a Minimum Mean-Square Error Short-Time Spectral Amplitude Estimator". *IEEE Transactions on Acoustics, Speech, and Signal Processing*, vol. 32, no. 6, pp. 1109–1121, December 1984.

[EM85] Y. Ephraim and D. Malah. "Speech Enhancement Using a Minimum Mean-Square Error Log-Spectral Amplitude Estimator". *IEEE Transactions on Acoustics, Speech, and Signal Processing*, vol. 33, no. 2, pp. 443–445, April 1985.

[Eng98] A. Engelsberg. *Transformationsbasierte Systeme zur einkanaligen Störunterdrückung bei Sprachsignalen*. PhD thesis, Christian-Albrechts-Universität zu Kiel, Kiel, Germany, 1998. (in German).

[FK03] C. Feldbauer and G. Kubin. "Critically Sampled Frequency-Warped Perfect Reconstruction Filterbank". *Proceedings of European Conference on Circuit Theory and Design (ECCTD)*, vol. 3, pp. 109–112, Cracow, Poland, September 2003.

[FKK05] C. Feldbauer, G. Kubin, and W. B. Kleijn. "Anthropomorphic Coding of Speech and Audio: A Model Inversion Approach". *EURASIP Journal on Applied Signal Processing*, vol. 2005, no. 9, pp. 1334–1349, 2005.

[FKNY04] K. Fujisaway, M. Kojima, K. Nakata, and M. Yamashitaz. "SDPA (SemiDefinite Programming Algorithm) User's Manual (Version 6.2.0)". Research Reports on Mathematical and Computing Sciences, Tokyo Institute of Technology, Tokyo, Japan, 2004. (`http://sdpa.indsys.chuo-u.ac.jp/sdpa/`).

[Fli93] N. Fliege. *Multiraten-Signalverarbeitung*. B. G. Teubner, Stuttgart, 1993. (in German).

[FMD03] S. Franz, S. K. Mitra, and G. Doblinger. "Frequency Estimation Using Warped Discrete Fourier Transform". *Signal Processing*, vol. 83, no. 8, pp. 1661–1671, August 2003.

[FMSD02] S. Franz, S. K. Mitra, J. C. Schmidt, and G. Doblinger. "Warped Discrete Fourier Transform: A New Concept in Digital Signal Processing". *Proceedings of International Conference on Acoustics, Speech, and Signal Processing (ICASSP)*, vol. 2, pp. 1205–1208, Orlando (Florida), USA, May 2002.

[Gal02] E. Galijašević. *Allpass-Based Near-Perfect-Reconstruction Filter Banks*. PhD thesis, Christian-Albrechts-Universität zu Kiel, Kiel, Germany, 2002.

[GB09] M. Grant and S. Boyd. *CVX: Matlab Software for Disciplined Convex Programming*. Austin, Texas, USA, June 2009. (`http://cvxr.com/`).

[GEH98] T. Gülzow, A. Engelsberg, and U. Heute. "Comparison of a Discrete Wavelet Transformation and a Nonuniform Polyphase Filterbank applied to Spectral-Subtraction Speech Enhancement". *Signal Processing*, vol. 64, no. 1, pp. 5–19, January 1998.

[GG04] H. G. Göckler and A. Groth. *Multiratensysteme: Abtastratenumsetzung und digitale Filterbänke*. J. Schlembach Fachverlag, Wilburgstetten, 2004. (in German).

[GJV+07] B. Geiser, P. Jax, P. Vary, H. Taddei, S. Schandl, M. Gartner, C. Guillaumé, and S. Ragot. "Bandwidth Extension for Hierarchical Speech and Audio Coding in ITU-T Rec. G.729.1". *IEEE Transactions on Audio, Speech, and Language Processing*, vol. 15, no. 8, pp. 2496–2509, November 2007.

[GK00] E. Galijašević and J. Kliewer. "Non-Uniform Near-Perfect-Reconstrucktion Oversampled DFT Filter Banks based on Allpass-Transforms". *Proceedings of IEEE DSP Workshop*, Hunt (Texas), USA, October 2000.

[GK01a] E. Galijašević and J. Kliewer. "On the Design of Near-Perfect-Reconstruction IIR QMF Banks Using FIR Phase-Compensation Filters". *Proceedings of International Symposium on Image and Signal Processing and Analysis (ISPA)*, pp. 530–534, Pula, Croatia, June 2001.

[GK01b] E. Galijašević and J. Kliewer. "Design of Maximally Decimated Near-Perfect-Reconstruction DFT Filter Banks with Allpass-Based Analysis Filters". *Proceedings of Asilomar Conference on Signals, Systems, and Computers*, vol. 1, pp. 577–581, Pacific Grove (California), USA, November 2001.

[GK02] E. Galijašević and J. Kliewer. "Design of Allpass-Based Non-Uniform Oversampled DFT Filter Banks". *Proceedings of International Conference on Acoustics, Speech, and Signal Processing (ICASSP)*, vol. 2, pp. 1181–1184, Orlando (Florida), USA, May 2002.

[GKL+09] B. Geiser, H. Krüger, H. W. Löllmann, P. Vary, D. Zhang, H. Wan, H. T. Li, and L. B. Zhang. "Candidate Proposal for ITU-T Super-Wideband Speech and Audio Coding". *Proceedings of International Conference on Acoustics, Speech, and Signal Processing (ICASSP)*, pp. 4121–4124, Taipei, Taiwan, April 2009.

[GL97] L. E. Ghaoui and H. Lebert. "Robust Solutions to Least-Squares Problems with Uncertain Data". *SIAM Journal on Matrix Analysis and Applications*, vol. 18, no. 4, pp. 1035–1064, 1997.

[GLH03] T. Gülzow, T. Ludwig, and U. Heute. "Spectral-Subtraction Speech Enhancement in Multirate Systems with and without Non-Uniform and Adaptive Bandwidths". *Signal Processing*, vol. 83, no. 8, pp. 1613–1631, August 2003.

[Glu93] R. Gluth. *Beiträge zur Beschreibung und Realisierung digitaler, nichtrekursiver Filterbänke auf der Grundlage linearer diskreter Transformationen*. PhD thesis, Ruhr-Universität Bochum, Bochum, Germany, 1993. (in German).

[GNC01] H. Gustafsson, S. E. Nordholm, and I. Claesson. "Spectral Subtraction Using Reduced Delay Convolution and Adaptive Averaging". *IEEE Transactions on Speech and Audio Processing*, vol. 9, no. 8, pp. 799–807, November 2001.

[GRV10] B. Geiser, M. Roggendorf, and P. Vary. "Multi-Band Pre-Echo Control Using a Filterbank Equalizer". *Proceedings of European Signal Processing Conference (EUSIPCO)*, Aalborg, Denmark, August 2010.

[Gül01] T. Gülzow. *Verbesserung der Qualität stark gestörter Sprachsignale: Detektion eines Trägerversatzes und Unterdrückung additiver Störungen*. PhD thesis, Christian-Albrechts-Universität zu Kiel, Kiel, Germany, 2001. (in German).

[Gus99] S. Gustafsson. *Enhancement of Audio Signals by Combined Acoustic Echo Cancellation and Noise Reduction*. PhD thesis, RWTH Aachen University, Aachen, Germany, 1999.

[Gv96] G. H. Golub and C. F. van Loan. *Matrix Computations*. The Johns Hopkins University Press, Baltimore, Maryland, 3rd edition, 1996.

[GW77] R. C. Gonzalez and P. Wintz. *Digital Image Processing*. Addison-Wesley Publishing Company, London, 1977.

[Hab07] E. A. P. Habets. *Single- and Multi-Microphone Speech Dereverberation using Spectral Enhancement*. PhD thesis, Eindhoven University, Eindhoven, The Netherlands, 2007.

[Här98] A. Härmä. "Implementation of Recursive Filters Having Delay Free Loops". *Proceedings of International Conference on Acoustics, Speech, and Signal Processing (ICASSP)*, vol. 3, pp. 1261–1264, Seattle (Washington), USA, May 1998.

[Här00] A. Härmä. "Implementation of Frequency-Warped Recursive Filters". *Signal Processing*, vol. 80, no. 3, pp. 543–548, March 2000.

[Hil08] M. Hildenbrand. "Konzepte für die Audio Teilband-Codierung mit geringer Signallaufzeit". diploma thesis, IND, RWTH Aachen University, Aachen, Germany, May 2008. (in German).

[HL06] Y. Hu and P. C. Loizou. "Subjective Comparison of Speech Enhancement Algorithms". *Proceedings of International Conference on Acoustics, Speech, and Signal Processing (ICASSP)*, vol. 1, pp. 153–156, Toulouse, France, May 2006.

[Hoh02] V. Hohmann. "Frequency Analysis and Synthesis Using a Gammatone Filterbank". *ACTA Acoustica United with Acoustica*, vol. 88, pp. 433–442, 2002.

[HR90] J. H. Husøy and T. A. Ramstad. "Application of an Efficient Parallel IIR Filter Bank to Image Subband Coding". *Signal Processing*, vol. 20, no. 4, pp. 279–292, August 1990.

[HV89] P.-Q. Hoang and P. P. Vaidyanathan. "Non-Uniform Multirate Filter Banks: Theory and Design". *Proceedings of International Symposium on Circuits and Systems (ISCAS)*, vol. 1, pp. 371–374, Portland (Oregon), USA, May 1989.

[ITK94] M. Ikehara, H. Tanaka, and H. Kuroda. "Design of IIR Digital Filters Using All-Pass Networks". *IEEE Transactions on Circuits and Systems II*, vol. 41, no. 3, pp. 231–235, March 1994.

[ITU88] ITU-T Rec. G.722. "7 kHz Audio Coding within 64 kbit/s". Blue Book, vol. Fascicle III.4, pp. 269-341, 1988.

[ITU96] ITU-T Rec. G.729. "Coding of Speech at 8 kbit/s Using Conjugate Structure Algebraic Code Excitated Linear Prediction (CS-ACELP)", March 1996.

[ITU01] ITU-T Rec. P.862. "Perceptual Evaluation of Speech Quality (PESQ): An Objective Method for End-To-End Speech Quality Assessment of Narrow-Band Telephone Networks and Speech Codecs", February 2001.

[ITU05] ITU-T Rec. G.191. "Software Tools for Speech and Audio Coding Standardization", 2005.

[ITU06] ITU-T Rec. G.729.1. "G.729 based Embedded Variable Bit-Rate Coder: An 8-32 kbit/s Scalable Wideband Coder Bitstream Interoperable with G.729", March 2006.

[ITU08] ITU-T. "Terms of reference and time schedule for the joint qualification phase of SWB extension of G.EV-VBR and G.729.1". ITU-T SG16 temp. doc Q23/16 TD358-WP3, Annex Q23B and Annex Q23C, April 2008.

[Jac96] L. B. Jackson. *Digital Filters and Signal Processing*. Kluwer Academic Publishers, Boston, Massachusetts, 3rd edition, 1996.

[JLV10] M. Jeub, H. W. Löllmann, and P. Vary. "Blind Dereverberation for Hearing Aids with Binaural Link". *Proceedings of ITG Conference on Speech Communication*, Bochum, Germany, October 2010.

[Joh80] J. D. Johnston. "A Filter Family Designed for Use in Quadrature Mirror Filter Banks". *Proceedings of International Conference on Acoustics, Speech, and Signal Processing (ICASSP)*, vol. 5, pp. 291–294, Denver (Colorado), USA, April 1980.

[KA05] J. M. Kates and K. H. Arehart. "Multichannel Dynamic-Range Compression Using Digital Frequency Warping". *EURASIP Journal on Applied Signal Processing*, vol. 2005, no. 18, pp. 3003–3014, October 2005.

[Kap98] M. Kappelan. *Eigenschaften von Allpaß-Ketten und ihre Anwendung bei der nicht-äquidistanten spektralen Analyse und Synthese*. PhD thesis, RWTH Aachen University, Aachen, Germany, 1998. (in German).

[KB06] J. Kliewer and E. Brka (Galijašević). "Near-Perfect-Reconstruction Low-Complexity Two-Band IIR/FIR QMF Banks with FIR Phase-Compensation Filters". *Signal Processing*, vol. 86, no. 1, pp. 171–181, January 2006.

[KD02] A. Klouche-Djedid. "Design of Mixed IIR/FIR Two-Channel QMF Bank". *Signal Processing*, vol. 82, no. 3, pp. 507–520, March 2002.

[KDL00] A. Klouche-Djedid and S. S. Lawson. "A General Design of Mixed IIR-FIR Two-Channel QMF Bank". *Proceedings of International Symposium on Circuits and Systems (ISCAS)*, vol. 1, pp. 559–562, Geneva, Switzerland, May 2000.

[KK98] K. D. Kammeyer and K. Kroschel. *Digitale Signalverarbeitung*. B. G. Teubner, Stuttgart, 4th edition, 1998. (in German).

[KKP07] A. Karmakar, A. Kumar, and R. K. Patney. "Design of Optimal Wavelet Packet Trees Based on Auditory Perception Criterion". *IEEE Signal Processing Letters*, vol. 14, no. 4, pp. 240–243, April 2007.

[Kli99] J. Kliewer. *Beiträge zum Entwurf modulierter Filterbänke für verschiedene Teilbandabtastraten*. PhD thesis, Christian-Albrechts-Universität zu Kiel, Kiel, Germany, 1999. (in German).

[KM97] T. Karp and A. Mertins. "Lifting Schemes for Biorthogonal Modulated Filter Banks". *Proceedings of International Conference on Digital Signal Processing (DSP)*, vol. 1, pp. 443–446, Santorini, Greece, July 1997.

[KM98] J. Kliewer and A. Mertins. "Oversampled Cosine-Modulated Filter Banks with Arbitrary System Delay". *IEEE Transactions on Signal Processing*, vol. 46, no. 4, pp. 941–955, April 1998.

[KMS01] T. Karp, A. Mertins, and G. Schuller. "Efficient Biorthogonal Cosine-Modulated Filter Banks". *Signal Processing*, vol. 81, no. 5, pp. 997–1016, May 2001.

[KSV96] M. Kappelan, B. Strauß, and P. Vary. "Flexible Nonuniform Filter Banks Using Allpass Transformation of Multiple Order". *Proceedings of European Signal Processing Conference (EUSIPCO)*, vol. 3, pp. 1745–1748, Trieste, Italy, September 1996.

[LA84] T.-Y. Leou and J. K. Aggarwal. "Recursive Implementation of LTV Filters - Frozen-Time Transfer Function Versus Generalized Transfer Function". *Proceedings of the IEEE*, vol. 72, no. 7, pp. 980–981, July 1984.

[LA00] W.-S. Lu and A. Antoniou. "Design of Digital Filters and Filter Banks by Optimization: A State of the Art Review". *Proceedings of European Signal Processing Conference (EUSIPCO)*, vol. 1, pp. 351–354, Tampere, Finnland, August 2000.

[Lan92] M. Lang. "Optimal Weighted Phase Equalization according to the L_∞-Norm". *Signal Processing*, vol. 27, no. 1, pp. 87–98, April 1992.

[Lan93] M. Lang. *Ein Beitrag zur Phasenapproximation mit Allpässen*. PhD thesis, University of Erlangen-Nuremberg, Erlangen-Nuremberg, Germany, 1993. (in German).

[Lan98] M. Lang. "Allpass Filter Design and Applications". *IEEE Transactions on Signal Processing*, vol. 46, no. 9, pp. 2505–2514, September 1998.

[LBD01] K. Lebart, J. M. Boucher, and P. N. Denbigh. "A New Method Based on Spectral Subtraction for Speech Dereverberation". *acta acoustica - ACOUSTICA*, vol. 87, no. 3, pp. 359–366, 2001.

[LDV08a] H. W. Löllmann, G. Dartmann, and P. Vary. "Design of Multiple Order Allpass Transformed DFT Filter-Banks with Aliasing-Free Signal Reconstruction by Linear Programming". *Proceedings of ITG Conference on Speech Communication*, Aachen, Germany, October 2008.

[LDV08b] H. W. Löllmann, G. Dartmann, and P. Vary. "Least-Squares Design of Subsampled Allpass Transformed DFT Filter-Banks with LTI Property". *Proceedings of International Conference on Acoustics, Speech, and Signal Processing (ICASSP)*, pp. 3529–3532, Las Vegas (Nevada), USA, April 2008.

[LDV09] H. W. Löllmann, G. Dartmann, and P. Vary. "General Least-Squares Design of Allpass Transformed DFT Filter-Banks". *Proceedings of European Signal Processing Conference (EUSIPCO)*, pp. 2653–2657, Glasgow, UK, August 2009.

[LJW00] P. Löwenborg, H. Johansson, and L. Wanhammar. "A Class of Two-Channel IIR/FIR Filter Banks". *Proceedings of European Signal Processing Conference (EUSIPCO)*, pp. 1897–1900, Tampere, Finland, September 2000.

[LL94] M. Lang and T. I. Laakso. "Simple and Robust Method for the Design of Allpass Filters Using Least-Squares Phase Error Criterion". *IEEE Transactions on Circuits and Systems II*, vol. 41, no. 1, pp. 40–48, January 1994.

[LNT97] J. Li, T. Q. Nguyen, and S. Tantaratana. "A Simple Design for Near-Perfect-Reconstruction Nonuniform Filter Banks". *IEEE Transactions on Signal Processing*, vol. 45, no. 8, pp. 2105–2109, August 1997.

[Loi07] P. C. Loizou. *Speech Enhancement*. Taylor & Francis, New York, 2007.

[Lot04] T. Lotter. *Single and Multimicrophone Speech Enhancement for Hearing Aids*. PhD thesis, RWTH Aachen University, Aachen, Germany, 2004.

[LV04a] H. W. Löllmann and P. Vary. "Speech Enhancement for Mobile Communication Infrastructure: Investigation of Alternative Approaches". project report for Siemens ICM, IND, RWTH Aachen University, January 2004.

[LV04b] H. W. Löllmann and P. Vary. "New Concepts for Robust Noise Suppression ". project report for Siemens Com, IND, RWTH Aachen University, November 2004.

[LV05a] H. W. Löllmann and P. Vary. "Efficient Non-Uniform Filter-Bank Equalizer". *Proceedings of European Signal Processing Conference (EUSIPCO)*, Antalya, Turkey, September 2005.

[LV05b] H. W. Löllmann and P. Vary. "Generalized Filter-Bank Equalizer for Noise Reduction with Reduced Signal Delay". *Proceedings of European Conference on Speech Communication and Technology (Interspeech)*, pp. 2105–2108, Lisbon, Portugal, September 2005.

[LV05c] H. W. Löllmann and P. Vary. "Low Delay Filter for Adaptive Noise Reduction". *Proceedings of International Workshop on Acoustic Echo and Noise Control (IWAENC)*, pp. 205–208, Eindhoven, The Netherlands, September 2005.

[LV05d] T. Lotter and P. Vary. "Speech Enhancement by MAP Spectral Amplitude Estimation Using a Super-Gaussian Speech Model". *EURASIP Journal on Applied Signal Processing*, vol. 2005, no. 7, pp. 1110–1126, January 2005.

[LV06a] H. W. Löllmann and P. Vary. "Integrated Beamforming and Post-Filtering". project report for GN ReSound, IND, RWTH Aachen University, February 2006.

[LV06b] H. W. Löllmann and P. Vary. "A Filter Structure for Low Delay Noise Suppression". *Proceedings of ITG Conference on Speech Communication*, Kiel, Germany, April 2006.

[LV06c] H. W. Löllmann and P. Vary. "A Warped Low Delay Filter for Speech Enhancement". *Proceedings of International Workshop on Acoustic Echo and Noise Control (IWAENC)*, Paris, France, September 2006.

[LV06d] H. W. Löllmann and P. Vary. "Parametric Phase Equalizers for Warped Filter-Banks". *Proceedings of European Signal Processing Conference (EUSIPCO)*, Florence, Italy, September 2006.

[LV07a] H. W. Löllmann and P. Vary. "Post-Filters for Speech Enhancement in Hearing-Aids". project report for GN ReSound, IND, RWTH Aachen University, January 2007.

[LV07b] H. W. Löllmann and P. Vary. "Uniform and Warped Low Delay Filter-Banks for Speech Enhancement". *Speech Communications, Special Issue on Speech Enhancement*, vol. 49, no. 7-8, pp. 574–587, July 2007.

[LV07c] H. W. Löllmann and P. Vary. "Improved Design of Oversampled Allpass Transformed DFT Filter-Banks with Near-Perfect Reconstruction". *Proceedings of European Signal Processing Conference (EUSIPCO)*, pp. 50–54, Poznan, Poland, September 2007.

[LV07d] H. W. Löllmann and P. Vary. "Post-Filter Design for Superdirective Beamformers with Closely Spaced Microphones". *Proceedings of IEEE Workshop on Applications of Signal Processing to Audio and Acoustics (WASPAA)*, pp. 291–294, New Paltz (New York), USA, October 2007.

[LV08a] H. W. Löllmann and P. Vary. "Low Delay Filter-Banks for Speech and Audio Processing". E. Hänsler and G. Schmidt, editors, *Speech and Audio Processing in Adverse Environments*, chapter 2, pp. 13–61. Springer, Berlin, Heidelberg, 2008.

[LV08b] H. W. Löllmann and P. Vary. "Speech Enhancement for Hearing Aids". project report for GN ReSound, IND, RWTH Aachen University, August 2008.

[LV08c] H. W. Löllmann and P. Vary. "Design of IIR QMF Banks with Near-Perfect Reconstruction and Low Complexity". *Proceedings of International Conference on Acoustics, Speech, and Signal Processing (ICASSP)*, pp. 3521–3524, Las Vegas (Nevada), USA, April 2008.

[LV08d] H. W. Löllmann and P. Vary. "Estimation of the Reverberation Time in Noisy Environments". *Proceedings of International Workshop on Acoustic Echo and Noise Control (IWAENC)*, Seattle (Washington), USA, September 2008.

[LV08e] H. W. Löllmann and P. Vary. "A Blind Algorithm for Joint Noise Suppression and Dereverberation". *Proceedings of ITG Conference on Speech Communication*, Aachen, Germany, October 2008.

[LV09a] H. W. Löllmann and P. Vary. "Low Delay Noise Reduction and Dereverberation for Hearing Aids". *EURASIP Journal on Applied Signal Processing*, vol. 2009, pp. 1–9, 2009.

[LV09b] H. W. Löllmann and P. Vary. "IIR QMF-Bank Design for Speech and Audio Subband Coding". *Proceedings of IEEE Workshop on Applications of Signal Processing to Audio and Acoustics (WASPAA)*, pp. 269–272, New Paltz (New York), USA, October 2009.

[LV09c] H. W. Löllmann and P. Vary. "Reverberation Time Estimation for Speech Processing Applications". *International Conference on Acoustics, including the 35th German Annual Conference on Acoustics (DAGA)*, vol. 3, pp. 1655–1658, Rotterdam, The Netherlands, March 2009.

[LV09d] H. W. Löllmann and P. Vary. "A Blind Speech Enhancement Algorithm for the Suppression of Late Reverberation and Noise". *Proceedings of International Conference on Acoustics, Speech, and Signal Processing (ICASSP)*, pp. 3989–3992, Taipei, Taiwan, April 2009.

[LV09e] H. W. Löllmann and P. Vary. "Design of Critically Subsampled DFT Filter-Banks with Allpass Polyphase Filters and Near-Perfect Reconstruction". *Proceedings of International Conference on Acoustics, Speech, and Signal Processing (ICASSP)*, pp. 3185–3188, Taipei, Taiwan, April 2009.

[LV10] H. W. Löllmann and P. Vary. "Least-Squares Design of DFT Filter-Banks based on Allpass Transformation of Higher Order". *IEEE Transactions on Signal Processing*, vol. 58, no. 4, pp. 2393–2398, April 2010.

[LV11] H. W. Löllmann and P. Vary. "Estimation of the Frequency Dependent Reverberation Time by Means of Warped Filter-Banks". *Proceedings of International Conference on Acoustics, Speech, and Signal Processing (ICASSP)*, Prague, Czech Republic, May 2011.

[LY06] Z.-Q. Luo and W. Yu. "An Introduction to Convex Optimization for Communications and Signal Processing". *IEEE Journal on Selected Areas in Communications*, vol. 24, no. 8, pp. 1426–1438, August 2006.

[LYJV10] H. W. Löllmann, E. Yilmaz, M. Jeub, and P. Vary. "An Improved Algorithm for Blind Reverberation Time Estimation". *Proceedings of International Workshop on Acoustic Echo and Noise Control (IWAENC)*, Tel Aviv, Israel, August 2010.

[Mal92] H. S. Malvar. *Signal Processing with Lapped Transforms*. Artech House, Boston, Massachusetts, 1992.

[Mar01] R. Martin. "Noise Power Spectral Density Estimation Based on Optimal Smoothing and Minimum Statistics". *IEEE Transactions on Speech and Audio Processing*, vol. 9, no. 5, pp. 504–512, July 2001.

[MCA99] D. Malah, R. V. Cox, and A. J. Accardi. "Tracking Speech-Presence Uncertainty to Improve Speech Enhancement in Non-Stationary Noise Environments". *Proceedings of International Conference on Acoustics, Speech, and Signal Processing (ICASSP)*, vol. 2, pp. 789–792, Phoenix (Arizona), USA, March 1999.

[MCB92] S. K. Mitra, C. D. Creusere, and H. Babic. "A Novel Implementation of Perfect Reconstruction QMF Banks Using IIR Filters for Infinite Length Signals". *Proceedings of International Symposium on Circuits and Systems (ISCAS)*, vol. 5, pp. 2312–2315, San Diego (California), USA, May 1992.

[MG96] B. C. J. Moore and B. R. Glasberg. "A Revision of Zwicker's Loudness Model". *Acta Acustica United With Acustica*, vol. 82, no. 2, pp. 335–345, April 1996.

[MI03] T. Matsunaga and M. Ikehara. "Group Delay Approximation of Allpass Digital Filters by Transforming the Desired Response". *Proceedings of International Conference on Acoustics, Speech, and Signal Processing (ICASSP)*, vol. 6, pp. 393–396, Hong Kong, China, March 2003.

[Min85] F. Mintzer. "Filters for Distortion-Free Two-Band Multirate Filter Banks". *IEEE Transactions on Acoustics, Speech, and Signal Processing*, vol. 33, no. 3, pp. 626–630, June 1985.

[Mit98] S. K. Mitra. *Digital Signal Processing: A Computer-Based Approach*. McGraw-Hill, New York, 1998.

[MM01] A. Makur and S. K. Mitra. "Warped Discrete Fourier Transform: Theory and Application". *IEEE Transactions on Circuits and Systems I*, vol. 48, no. 9, pp. 1086–1093, September 2001.

[MM07] D. Mauler and R. Martin. "A Low Delay, Variable Resolution, Perfect Reconstruction Spectral Analysis-Synthesis System for Speech Enhancement". *Proceedings of European Signal Processing Conference (EUSIPCO)*, pp. 222–226, Poznan, Poland, September 2007.

[Moo97] B. C. J. Moore. *An Introduction to the Psychology of Hearing*. Academic Press, London, UK, 4th edition, 1997.

[MPH02] D. Mattera, F. Palmieri, and S. Haykin. "Efficient Sparse FIR Filter Design". *Proceedings of International Conference on Acoustics, Speech, and Signal Processing (ICASSP)*, vol. 2, pp. 1537–1540, Orlando (Florida), USA, May 2002.

[MT95] D. R. Morgan and J. C. Thi. "A Delayless Subband Adaptive Filter Architecture". *IEEE Transactions on Signal Processing*, vol. 43, no. 8, pp. 1819–1830, August 1995.

[NBS94] K. Nayebi, T. P. Barnwell, and M. J. T. Smith. "Low Delay FIR Filter Banks: Design and Evaluation". *IEEE Transactions on Signal Processing*, vol. 42, no. 11, pp. 24–31, January 1994.

[NLK94] T. Q. Nguyen, T. I. Laakso, and R. D. Koilpillai. "Eigenfilter Approach for the Design of Allpass Filters Approximating a Given Phase Response". *IEEE Transactions on Signal Processing*, vol. 42, no. 9, pp. 2257–2263, September 1994.

[OJ72] A. V. Oppenheim and D. H. Johnson. "Discrete Representation of Signals". *Proceedings of the IEEE*, vol. 60, no. 6, pp. 681–691, June 1972.

[OJS71] A. V. Oppenheim, D. Johnson, and K. Steiglitz. "Computation of Spectra with Unequal Resolution Using the Fast Fourier Transform". *Proceedings of the IEEE*, vol. 59, no. 2, pp. 299–301, February 1971.

[OMM76] A. V. Oppenheim, W. F. G. Mecklenbräuker, and R. M. Mersereau. "Variable Cutoff Linear Phase Digital Filters". *IEEE Transactions on Circuits and Systems*, vol. 23, no. 4, pp. 199–203, April 1976.

[OSB99] A. V. Oppenheim, R. W. Schafer, and J. R. Buck. *Discrete-Time Signal Processing*. Prentice-Hall, Upper Saddle River, New Jersey, 2nd edition, 1999.

[Pau96] J. Paulus. *Codierung breitbandiger Sprachsignale bei niedriger Datenrate*. PhD thesis, RWTH Aachen University, Aachen, Germany, 1996. (in German).

[PB87] T. W. Parks and C. S. Burrus. *Digital Filter Design*. John Wiley & Sons, Chichester, UK, 1987.

[PdL99] P. Philippe, F. M. de Saint-Martin, and M. Lever. "Wavelet Packet Filterbanks for Low Time Delay Audio Coding". *IEEE Transactions on Speech and Audio Processing*, vol. 7, no. 3, pp. 310–322, May 1999.

[PKVA95] S.-M. Phoong, C. W. Kim, P. P. Vaidyanathan, and R. Ansari. "A New Class of Two-Channel Biorthogonal Filter Banks and Wavelet Bases". *IEEE Transactions on Signal Processing*, vol. 43, no. 3, pp. 649–665, March 1995.

[PM96] J. G. Proakis and D. G. Manolakis. *Digital Signal Processing: Principles, Algorithms, and Applications*. Prentice-Hall, Upper Saddle River, New Jersey, 3rd edition, 1996.

[PP03a] M. Parfieniuk and A. Petrovsky. "Reduced Complexity Synthesis Part of Non-Uniform Near-Perfect-Recontruction DFT Filter Bank Based on All-Pass Transformation". *Proceedings of European Conference on Circuit Theory and Design (ECCTD)*, vol. 3, pp. 5–8, Cracow, Poland, September 2003.

[PP03b] M. Parfieniuk and A. Petrovsky. "Simple Rule of Selection of Subsampling Ratios for Warped Filter Banks". *Proceedings of International Conference 'Modern Communication Systems'*, pp. 130–134, Naroch, Belarus, September 2003.

[PP08] M. Parfieniuk and A. Petrovsky. "Approximating the Critical Bands Using Warped Filter Banks Based on Multiplierless Allpass Chains". *Proceedings of International Conference on Signals and Electronic Systems (ICSES)*, pp. 351–354, Cracow, Poland, September 2008.

[PPB04] A. Petrovsky, M. Parfieniuk, and A. Borowicz. "Warped DFT Based Perceptual Noise Reduction System". *Convention Paper of Audio Engineering Society*, pp. 1–16, Berlin, Germany, May 2004.

[PPW08] M. Parfieniuk, A. Petrovsky, and W. Wan. "Frequency Warping and Subband Merging for Approximating the Critical Bands with Cosine-Modulated Filter Banks". *Proceedings of International Conference on Audio, Language and Image Processing ICALIP)*, pp. 1159 – 1166, Shanghai, China, July 2008.

[PRH+92] R. D. Patterson, K. Robinson, J. Holdsworth, D. McKeown, C. Zhang, and M. Allerhand. "Complex Sounds and Auditory Images". Y. Cazals, L. Demany, and K. Horner, editors, *Auditory Physiology and Perception*, vol. 83

of *Advances in the Biosciences Series*, pp. 429–446. Pergamon Press, Oxford, UK, 1992.

[Pri95] J. Princen. "The Design of Nonuniform Modulated Filterbanks". *IEEE Transactions on Signal Processing*, vol. 43, no. 11, pp. 2550–2560, November 1995.

[PTVF92] W. H. Press, S. A. Teukolsky, W. T. Vetterling, and B. P. Flannery. *Numerical Recipes in C*. Cambridge University Press, Cambridge, UK, 2nd edition, 1992.

[Rad70] C. Rader. "An Improved Algorithm for High-Speed Autocorrelation with Application to Spectral Estimation". *IEEE Transactions on Audio and Electroacoustics*, vol. 18, no. 4, pp. 439–441, December 1970.

[Ram88] T. A. Ramstad. "IIR Filterbank for Subband Coding of Images'". *Proceedings of International Symposium on Circuits and Systems (ISCAS)*, vol. 1, pp. 827–830, Espoo, Finnland, June 1988.

[Rao98] B. D. Rao. "Signal Processing with the Sparseness Constraint". *Proceedings of International Conference on Acoustics, Speech, and Signal Processing (ICASSP)*, vol. 3, pp. 1861–1864, Seattle (Washington), USA, May 1998.

[RF80] T. A. Ramstad and O. Foss. "Sub-Band Coder Design Using Recursive Quadrature Mirror Filters". *Short Communication Digest of European Signal Processing Conference (EUSIPCO)*, pp. 747–752, Lausanne, Switzerland, September 1980.

[RKT+07] S. Ragot, B. Kövesi, R. Trilling, D. Virette, N. Duc, D. Massaloux, S. Proust, B. Geiser, M. Gartner, S. Schandl, H. Taddei, Y. Gao, E. Shlomot, H. Ehara, K. Yoshida, T. Vaillancourt, R. Salami, M. S. Lee, and D. Y. Kim. "ITU-T G.729.1: An 8-32 kbit/s Scalable Coder Interoperable with G.729 for Wideband Telephony and Voice Over IP". *Proceedings of International Conference on Acoustics, Speech, and Signal Processing (ICASSP)*, vol. 4, pp. 529–532, Honolulu (Hawaii), USA, April 2007.

[RMV88] P. A. Regalia, S. K. Mitra, and P. P. Vaidyanathan. "The Digital All-Pass Filter: A Versatile Signal Processing Building Block". *Proceedings of the IEEE*, vol. 76, no. 1, pp. 19–37, January 1988.

[RNM86] M. Renfors, Y. Neuvo, and S. K. Mitra. "A New Class of Uniform Filter Banks Based on Recursive Nth-Band Filters". *Proceedings of International Conference on Acoustics, Speech, and Signal Processing (ICASSP)*, vol. 11, pp. 2555–2558, Tokyo, Japan, April 1986.

[Rot83] J. H. Rothweiler. "Polyphase Quadrature Filters - A New Subband Coding Technique". *Proceedings of International Conference on Acoustics, Speech, and Signal Processing (ICASSP)*, vol. 8, pp. 1280–1283, Boston (Massachusetts), USA, April 1983.

[RS87] M. Renfors and T. Saramäki. "Recursive Nth-Band Digital Filters-Part I: Design and Properties". *IEEE Transactions on Circuits and Systems*, vol. 34, no. 1, pp. 24–39, January 1987.

[RY90] K. R. Rao and P. Yip. *Discrete Cosine Transform: Algorithms, Advantages, Applications*. Academic Press, New York, 1990.

[SA99] J. O. Smith and J. S. Abel. "Bark and ERB Bilinear Transforms". *IEEE Transactions on Speech and Audio Processing*, vol. 7, no. 6, pp. 697–708, November 1999.

[Sar85] T. Saramäki. "On the Design of Digital Filters as a Sum of Two All-Pass Filters". *IEEE Transactions on Circuits and Systems*, vol. 32, no. 11, pp. 1191–1193, November 1985.

[SB84] M. Smith and T. Barnwell III. "A Procedure for Designing Exact Reconstruction Filter Banks for Tree-Structured Subband Coders". *Proceedings of International Conference on Acoustics, Speech, and Signal Processing (ICASSP)*, vol. 9, pp. 421–424, San Diego (California), USA, March 1984.

[SB02] T. Saramäki and R. Bregović. "Multirate Systems and Filter Banks". G. Jonanovic-Dolecek, editor, *Multirate Systems: Design & Application*, chapter 2, pp. 27–85. Idea Group Publishing, Hershey, Pennsylvania, 2002.

[SBS+06] M. Schönle, C. Beaugeant, K. Steinert, H. W. Löllmann, B. Sauert, and P. Vary. "Hands-Free Audio and Its Application to Telecommunication Terminals". *Proceedings of International Conference on Audio for Mobile and Handheld Devices (AES)*, Seoul, Korea, September 2006.

[Sch68] H. W. Schüßler. "Zur Allgemeinen Theorie der Verzweigungsnetzwerke". *Archiv für Elektronik und Übertragungstechnik (AEÜ), Electronics and Communications*, vol. 22, pp. 361–369, 1968. (in German).

[Sch75] H. W. Schüßler. "On the Desin of General Combfilters". *Proceedings of International Symposium on Circuits and Systems (ISCAS)*, pp. 400–403, 1975.

[Sch08] H. W. Schüßler. *Digitale Signalverarbeitung 1: Analyse diskreter Signale und Systeme*. Springer, Berlin, Heidelberg, 5th edition, 2008. (in German).

[Sha00] B. Shankar M. R. "IIR Perfect Reconstruction Filter Banks with Warped Delay Chain and their use in Design of Correlating Filter Banks". Master's thesis, Indian Institute of Science, Bangalore, Indian, January 2000.

[SK00] G. D. T. Schuller and T. Karp. "Modulated Filter Banks with Arbitrary System Delay: Efficient Implementation and the Time-Varying Case". *IEEE Transactions on Signal Processing*, vol. 48, no. 3, pp. 737–748, March 2000.

[SL97] Y.-S. Song and Y. H. Lee. "Design of Sparse FIR Filters Based on Branch-and-Bound Algorithm". *Proceedings of Midwest Symposium on Circuits and Systems (MWSCAS)*, vol. 2, pp. 1445–1448, Sacramento (California), USA, August 1997.

[Sla93] M. Slany. "An Efficient Implementation of the Patterson Holdsworth Auditory Filter Bank". Technical report, Apple Computer, New York, 1993.

[SLV08] B. Sauert, H. W. Löllmann, and P. Vary. "Near End Listening Enhancement by Means of Warped Low Delay Filter-Banks". *Proceedings of ITG Conference on Speech Communication*, Aachen, Germany, October 2008.

[SM02a] B. Shankar M. R. and A. Makur. "Allpass Delay Chain-Based IIR PR Filterbank and Its Application to Multiple Description Subband Coding". *IEEE Transactions on Signal Processing*, vol. 50, no. 4, pp. 814–823, April 2002.

[SM02b] M. A. Stone and B. C. J. Moore. "Tolerable Hearing Aid Delays II: Estimation of Limits Imposed During Speech Production". *Ear and Hearing*, vol. 23, no. 4, pp. 325–338, 2002.

[SM05] P. Stoica and R. Moses. *Spectral Analysis of Signals*. Prentice Hall, Upper Saddle River, New Jersey, 2005.

[SPA07] A. Spanias, T. Painter, and V. Atti. *Audio Signal Processing and Coding*. Wiley, Hoboken, New Jersy, 2007.

[SS90] H. W. Schüßler and P. Steffen. "On the Design of Allpasses with Prescribed Group Delay". *Proceedings of International Conference on Acoustics, Speech, and Signal Processing (ICASSP)*, vol. 3, pp. 1313–1316, Albuquerque (New Mexico), USA, April 1990.

[SSBF08] K. Steinert, M. Schönle, C. Beaugeant, and T. Fingscheidt. "Hands-Free System with Low-Delay Subband Acoustic Echo Control and Noise Reduction". *Proceedings of International Conference on Acoustics, Speech, and Signal Processing (ICASSP)*, pp. 1521–1524, Las Vegas (Nevada), USA, March 2008.

[ST93] D. Sinha and A. H. Tewfik. "Low Bit Rate Transparent Audio Compression Using Adapted Wavelets". *IEEE Transactions on Signal Processing*, vol. 41, no. 12, pp. 3463–3479, December 1993.

[Ste80] K. Steiglitz. "A Note on Variable Recursive Digital Filters". *IEEE Transactions on Acoustics, Speech, and Signal Processing*, vol. 28, no. 1, pp. 111–112, February 1980.

[Stu99] J. Sturm. "Using SeDuMi 1.02: A MATLAB Toolbox for Optimization over Symmetric Cones". Tilburg University, Tilburg, The Netherlands, 1999.

[SV06] B. Sauert and P. Vary. "Near End Listening Enhancement: Speech Intelligibility Improvement in Noisy Environments". *Proceedings of International Conference on Acoustics, Speech, and Signal Processing (ICASSP)*, pp. 493–496, Toulouse, France, April 2006.

[SW70] H. W. Schüßler and W. Winkelnkemper. "Variable Digital Filters". *Archiv für Elektronik und Übertragungstechnik (AEÜ), Electronics and Communications*, vol. 24, no. 11, pp. 524–525, 1970.

[Swe96] W. Sweldens. "The Lifting Scheme: A Custom-Design Construction of Biorthogonal Wavelets". *Applied and Computational Harmonic Analysis*, vol. 3, no. 2, pp. 186–200, April 1996.

[TM09] I. The MathWorks. "MATLAB Reference". Version 7.9.0.529 (R2009b), August 2009.

[TN95] T. E. Tuncer and T. Q. Nguyen. "General Analysis of Two-Band QMF Banks". *IEEE Transactions on Signal Processing*, vol. 43, no. 2, pp. 544–548, February 1995.

[TTT06] K. Toh, R. H. Tütüncü, and M. J. Todd. "On the Implementation and Usage of SDPT3: A Matlab Software Package for Semidefinite-Quadratic-Linear Programming (Version 4.0)". Department of Mathematics, National University of Singapore, Singapore, July 2006. (`www.math.nus.edu.sg/~mattohkc/sdpt3.html`).

[Vai90] P. P. Vaidyanathan. "Multirate Digital Filters, Filter Banks, Polyphase Networks, and Applications: A Tutorial". *Proceedings of the IEEE*, vol. 78, no. 1, pp. 56–93, January 1990.

[Vai93] P. P. Vaidyanathan. *Multirate Systems and Filter Banks*. Prentice-Hall, Upper Saddle River, New Jersey, 1993.

[Var78] P. Vary. *Ein Beitrag zur Kurzzeitspektralanalyse mit digitalen Systemen*. PhD thesis, University of Erlangen-Nuremberg, Erlangen-Nuremberg, Germany, 1978. (in German).

[Var79] P. Vary. "On the Design of Digital Filter Banks Based on a Modified Principle of Polyphase". *Archiv für Elektronik und Übertragungstechnik (AEÜ), Electronics and Communications*, vol. 33, pp. 293–300, 1979.

[Var80] P. Vary. "Digital Filter Banks with Unequal Resolution". *Short Communication Digest of European Signal Processing Conference (EUSIPCO)*, pp. 41–42, Lausanne, Switzerland, September 1980.

[Var85] P. Vary. "Noise Suppression by Spectral Magnitude Estimation - Mechanism and Theoretical Limits -". *Signal Processing*, vol. 8, no. 4, pp. 387–400, July 1985.

[Var06] P. Vary. "An Adaptive Filter-Bank Equalizer for Speech Enhancement". *Signal Processing, Special Issue on Applied Signal and Audio Processing*, vol. 86, no. 6, pp. 1206–1214, June 2006.

[VB96] L. Vandenberghe and S. Boyd. "Semidefinite Programming". *SIAM Review*, vol. 38, no. 1, pp. 49–95, March 1996.

[VH88] P. P. Vaidyanathan and P. Q. Hoang. "Lattice Structures for Optimal Design and Robust Implementation of Two-Channel Perfect-Reconstruction QMF Banks". *IEEE Transactions on Acoustics, Speech, and Signal Processing*, vol. 36, no. 1, pp. 81–94, January 1988.

[VHH98] P. Vary, U. Heute, and W. Hess. *Digitale Sprachsignalverarbeitung*. B. G. Teubner, Stuttgart, 1998. (in German).

[VK95] M. Vetterli and J. Kovačević. *Wavelets and Subband Coding*. Prentice-Hall, Upper Saddle River, New Jersey, 1995.

[VM06] P. Vary and R. Martin. *Digital Speech Transmission: Enhancement, Coding and Error Concealment*. Wiley, Chichester, UK, 2006.

[VMN86] P. P. Vaidyanathan, S. K. Mitra, and Y. Neuvo. "A New Approach to the Realization of Low-Sensitivity IIR Digital Filters". *IEEE Transactions on Acoustics, Speech, and Signal Processing*, vol. 34, no. 2, pp. 350–361, April 1986.

[VN03] B. Vo and S. Nordholm. "Non-Uniform DFT Filter Bank Design with Semi-Definite Programming". *Proceedings of International Symposium on Signal Processing and Information Technology (ISSPIT)*, pp. 42–45, Darmstadt, Germany, December 2003.

[VP06] R. Venkataramanan and K. M. M. Prabhu. "Estimation of Frequency Offset Using Warped Discrete-Fourier Transform". *Signal Processing*, vol. 86, no. 2, pp. 250–256, February 2006.

[VW83] P. Vary and G. Wackersreuther. "A Unified Approach to Digital Polyphase Filter Banks". *Archiv für Elektronik und Übertragungstechnik (AEÜ), Electronics and Communications*, vol. 37, no. 1/2, pp. 29–34, 1983.

[Wac86] G. Wackersreuther. "Some New Aspects of Filters for Filter Banks". *IEEE Transactions on Acoustics, Speech, and Signal Processing*, vol. 34, no. 5, pp. 1182–1200, October 1986.

[WdDC03] N. Westerlund, J. M. de Haan, M. Dahl, and I. Claesson. "Low Distortion SNR-Based Speech Enhancement Employing Critical Band Filter Banks". *Proceedings of the Fourth International Conference on Information, Communication and Signal Processing and the Fourth Pacific Rim Conference on Multimedia (ICICS-PCM)*, vol. 1, pp. 129–133, Singapore, December 2003.

[Weg79] W. Wegener. "Wave Digital Directional Filters with Reduced Number of Mulitiplications and Adders". *Archiv für Elektronik und Übertragungstechnik (AEÜ), Electronics and Communications*, vol. 33, pp. 239–243, June 1979.

[WM93] J. L. H. Webb and D. C. Munson. "Design of Sparse FIR Filters Using Linear Programming". *Proceedings of International Symposium on Circuits and Systems (ISCAS)*, vol. 1, pp. 339–342, Chicago (Illinois), USA, May 1993.

[WM96] J. L. H. Webb and D. C. Munson. "Chebyshev Optimization of Sparse FIR Filters Using Linear Programming with an Application to Beamforming". *IEEE Transactions on Signal Processing*, vol. 44, no. 8, pp. 1912–1992, August 1996.

[Wri97] S. J. Wright. *Primal-Dual Interior-Point Methods*. SIAM, Philadelphia, Pennsylvania, 1997.

[WSV00] H. Wolkowicz, R. Saigal, and L. Vandenberghe, editors. *Handbook of Semidefinite Programming: Theory, Algorithms and Applications*. Springer, Berlin, New York, 2000.

[Ye97] Y. Ye. *Interior Point Algorithms: Theory and Analysis*. Wiley, Chichester, UK, 1997.

[YIEB10] C. Yemdji, M. M. Idrissa, N. W. D. Evans, and C. Beaugeant. "Efficient Low Delay Filtering for Residual Echo Suppression". *Proceedings of European Signal Processing Conference (EUSIPCO)*, pp. 16–20, Aalborg, Denmark, August 2010.

[ZAS98] W.-P. Zhu, M. O. Ahmad, and M. N. S. Swamy. "An Efficient Approach for the Design of Nearly Perfect-Reconstruction QMF Banks". *IEEE Transactions on Circuits and Systems II*, vol. 45, no. 8, pp. 1161–1165, August 1998.

[ZF99] E. Zwicker and H. Fastl. *Psychoacoustics: Facts and Models*. Springer, Berlin, New York, 2nd edition, 1999.

[ZI95] X. Zhang and H. Iwakura. "Design of QMF Banks Using Allpass Filters". *Electronic Letters*, vol. 31, no. 3, pp. 172–174, February 1995.

[ZY99] X. Zhang and T. Yoshikawa. "Design of Orthonormal IIR Wavelet Filter Banks using Allpass Filters". *Signal Processing*, vol. 78, no. 1, pp. 91–100, October 1999.